



## **THÈSE de doctorat**

Pour obtenir le grade de Docteur délivré par

**Université de Lille**

**École Doctorale Sciences de la Matière, du Rayonnement et de l'Environnement**

**Spécialité : Chimie Organique**

Présentée et soutenue publiquement par

**Manal RIDANY**

Le 14 Décembre 2023

**Radicaux phénoxy impliqués dans la biosynthèse de la lignine :  
photo-génération en conditions de chimie en flux, formation et  
piégeage par la peroxydase de raifort.**

Dr Christian ROLANDO	Directeur de recherche émérite au CNRS, Université de Lille	Co-Directeur de thèse
Pr Youssef BAKKOUR	Professeur, Université Libanaise	Directeur de thèse
Pr Ahmed MAZZAH	Professeur, Université de Lille	Directeur de thèse
Pr Stéphanie BAUMBERGER	Professeur, AgroParisTech	Rapportrice
Pr Axel MARCHAL	Professeur, Université de Bordeaux	Rapporteur (Président)
Pr Stéphanie OGNIER	Maître de conférences, Chimie ParisTech	Examinatrice

## **OUTLINE**

The goal of this work is to demonstrate the synthesis of lignin utilizing a variety of methods (photochemistry in a flow system or enzymatically using peroxidase), with an emphasis on the fundamental principles of green chemistry.

**Chapter 1.** Provides a general introduction to the synthesis and biosynthesis of lignin. It illuminates the initiatives that contributed in obtaining a comprehensive understanding of its structure and chemical composition. Also discusses the various photochemical pathways for the phenoxy radical production and microflow technology.

**Chapter 2.** Involve the use of riboflavin as a photo-sensitizer in an anaerobic environment to carry out the dimerization of lignin phenolic derivatives using a microflow system.

**Chapter 3.** Investigates the oxidation of vanillin using chemical and enzymatic methods. It provides a new method using immobilized HRP for the in vitro synthesis of lignin model.

**Chapter 4.** Focuses on the effects of the phenoxy radical attack on the peroxidases. It also presents a unique method based on the combination of two approaches, HRP-proximity dependent labeling and click chemistry, to identify or inhibit plant peroxidases involved in lignification. It also provides novel perspectives for lignin research.

**Chapter 5.** Aims at applying an actinometric protocol with a synthetic water-soluble azobenzene derivative in a photo-microfluidic reactor in order to measure accurately the photon flux of an UV lamp irradiating a blood bag.

**Chapter 6.** Outlines the key conclusions reached in this investigation.

## **ACKNOWLEDGEMENT**

First and foremost, praise and appreciation to God, the Almighty, for his showers of blessings which enabled me to successfully complete this research.

This work would not have been accomplished without many people whom I would like to thank.

I would like to express my deep and sincere gratitude to my co-supervisor **Professor Christian ROLANDO**, for his supervision, motivation and everyday discussion. He helped me to conduct research and present my work in the simplest and most professional way. I appreciate his trust in me since the first day I was accepted in his research group! You really listened to me, encouraged me, and guided me throughout my thesis, which helped me stay motivated. I sincerely appreciate everything you've done to help me become a better chemist.

Special thanks to my supervisor, **Professor Ahmed MAZZAH**. I appreciate your ongoing assistance and guidance. Thank you for your invaluable advices, continuous support, and patience.

I would like to thank my Lebanese supervisor, **Professor Youssef BAKKOUR**, for allowing me to pursue my doctorate studies under his supervision. Thank you for your efforts.

I am very grateful to Professor **Stéphanie BAUMBERGER** and Professor **Axel MARCHAL** for accepting to review this work. Special thanks also to Professor **Stéphanie OGNIER**. Thank you for devoting your valuable time to evaluating this work. I am grateful to have such brilliant scientists on my dissertation committee.

I would also like to express my thanks to **MSAP team**: Stephanie, Fabrice, Melanie, Elise, Mael, Matthieu, Françoise, Nicolas, Marc and especially Marie, Ziad and Bayan.

Additionally, thanks to all the Bachelor's, Masters or Engineers trainees that participated in this work: Ségolène LEDUCQ, Sonia MIDALI, Lilian ESTAQUE, Clara DESGARDIN, Mathieu SAVIGNY, Baptiste GUILLOTEAU, Elisa LECOMPTE, Philemon GAMACHE, and Xavier HEINEN.

Thanks to the girl I have spent with her a very happy and funny moments; Wissal Adhami thanks for all your support.

I would like to thank my friends, laboratory mates and research partners Ranin DABBOUSY and Lamis ELWENNI for the cherished time we spent together both inside and outside the laboratory.

The two girls who were always there for discussions on anything that I was unsure of, and who offered all the help that I needed at any time. I would like also to thank them for their encouragement and support throughout my study. A big Thanks for you both.

I am extremely grateful to my parents Tarek & Hiam for their love, prayers, care, and sacrifices in teaching and preparing me for the future. I am grateful to my father for encouraging me to pursue my PhD; regardless of the distance, you were always close to me, listening to my problems and showing me love and patience. Thank you for every second you spend motivating me to be a strong woman amid my loneliness in France. My enormous family, the perpetual love of my life, are people who no one can compare to; sisters and brothers.

A very special thanks to my wonderful husband "Ali," whom without his tremendous understanding, sacrifices, and encouragement over the last few years to help me achieve my dream, it would have been impossible for me to finish my studies. You are the best in my life.

Finally, I cannot forget my Baby "Taline"; despite the fact that I became pregnant during the final tough year of my PhD and that I faced the most unbearable pressures at that time, you were my sole hope of completing this route. My twinkle little star, I wish to be an excellent mommy to you.

To my dad "Abou Jalal"

# Table of Contents

<b>OUTLINE</b> .....	<b>ii</b>
<b>ACKNOWLEDGEMENT</b> .....	<b>iii</b>
<b>List of figures</b> .....	<b>x</b>
<b>List of tables</b> .....	<b>xv</b>
<b>List of abbreviations</b> .....	<b>xvi</b>
<b>Abstract</b> .....	<b>xix</b>
<b>Résumé</b> .....	<b>xx</b>
<b>Introduction</b> .....	<b>1</b>
<b>1. CHAPTER ONE: LITERATURE OVERVIEW</b> .....	<b>3</b>
1.1. Lignin .....	3
1.1.1. Chemical nature and composition .....	3
1.1.2. Lignin sources .....	4
1.1.3. Lignin and biorefineries .....	5
1.1.4. Lignin biosynthesis-derived linkages .....	6
1.2. Platform of molecules derived from lignin.....	10
1.3. Synthesis of lignin models .....	11
1.4. Chromatography techniques.....	12
1.5. Overview of proximity dependent labeling technologies .....	12
1.5.1. HRP-based proximity labeling .....	13
1.5.2. Strategies for detecting biotinylated proteins .....	13
1.6. Click chemistry.....	15
1.7. Different routes for peroxidase inactivation during the oxidation of phenolic substances .	15
1.8. Phenols probes .....	16
1.9. Photochemistry .....	18
1.9.1. Photochemical oxidation for organic synthesis.....	18
1.9.2. Microreactor technology.....	20
1.9.3. Continuous Flow system.....	21
1.9.4. Materials for the construction of microreactors.....	22
1.9.5. Why Should Photochemistry Be Used in Flow? .....	24
1.9.6. Models of Photochemistry Reactions developed in Continuous Flow.....	26
1.10. Advantages and limitations of microflow reactor.....	28
1.11. Phenoxy radicals: generalities and reactivity .....	28
1.11.1. Ways to generate phenoxy radicals .....	29

<b>2. CHAPTER TWO: HIGH RIBOFLAVIN SELECTIVITY FLOW PHOTO-OXIDATION OF PHENOLIC COMPOUNDS DERIVED FROM LIGNIN IN ANAEROBIC ENVIRONMENT.....</b>	<b>35</b>
2.1. Introduction.....	35
2.2. Methods used for the dimerization of phenols.....	36
2.3. Generality on Riboflavin.....	38
2.4. Mechanism of riboflavin.....	39
2.5. Flow chemistry.....	42
2.6. Objective.....	42
2.7. Experimental part.....	43
2.7.1. Chemicals.....	43
2.7.2. Microfluidic system.....	44
2.7.3. Riboflavin purification.....	44
2.7.4. Analysis of riboflavin consumption by FT-ICR.....	45
2.7.5. MALDI FT-ICR (Matrix assisted laser desorption ionisation- Fourier transform ion cyclotron resonance mass spectrometry).....	45
2.7.6. Matrix-assisted laser desorption Time of Flight (MALDI-TOF) mass spectrometry.....	45
2.7.7. NMR measurements.....	46
2.7.8. Column Chromatography.....	46
2.7.9. General dimerization procedure of lignin phenolic derivatives.....	47
2.7.10. Synthesis of the methyl ester of sinapic acid.....	47
2.8. Results and discussion.....	47
2.8.1. Oxidation of phenols mediated by RF photoreactions.....	47
2.8.2. Mechanism of riboflavin.....	50
2.8.3. Analysis of purified riboflavin consumption by FT-ICR.....	51
2.8.4. Flow photo-oxidation of vanillyl alcohol.....	53
2.8.5. Reaction conditions studied on vanillyl alcohol.....	58
2.8.6. Substrate screening.....	58
2.9. Conclusion.....	73
<b>3. CHAPTER THREE: C-O COUPLED-POLYVANILLIN BY DEHYDROGENATIVE POLYMERIZATION OF VANILLIN USING IMMOBILIZED HORSERADISH PEROXIDASE.....</b>	<b>75</b>
3.1. New possibility for lignin models based on vanillin.....	75
3.1.1. Vanillin and its extraction.....	76
3.1.2. Vanillin as a model for lignin.....	76
3.1.3. Divanillin.....	76
3.2. Polymerization triggered by peroxidase.....	78

3.4.	Experimental part.....	79
3.4.1.	Chemicals.....	79
3.4.2.	C-C vanillin dimerization by chemical way .....	80
3.4.3.	C-C vanillin dimerization using HRP type I/II .....	80
3.4.4.	C-C vanillin dimerization using laccases .....	81
3.4.5.	Divanillin reduction to Divanillyl alcohol.....	81
3.4.6.	Vanillin or vanillyl alcohol derivatization using different bases.....	82
3.4.7.	Functionalization of 5-5' dehydrodivanillin.....	83
3.4.8.	Purification of derivatized polyvanillin.....	84
3.4.9.	Polyvanillin synthesis on HRP immobeads®150P.....	84
3.4.10.	Derivatization of polyvanillin using iodoacetamide in basic medium (amidation reaction) 84	
3.4.11.	Derivatization of polyvanillin using acetic anhydride (acylation reaction) .....	85
<b>3.5.</b>	<b>Results and discussion.....</b>	<b>85</b>
3.5.1.	Different routes for vanillin oxidation.....	85
3.5.2.	Amidation of vanillin/ divanillin using iodoacetamide.....	87
3.5.3.	Polyvanillin oxidation using immobilized oxidoreductases.....	92
3.6.	Conclusion .....	98
<b>4.</b>	<b>CHAPTER FOUR: SYNTHESIS OF SUICIDE INHIBITORS OF LIGNIFICATION .....</b>	<b>100</b>
4.1.	Introduction.....	100
4.2.	Horseradish peroxidase (HRP): A versatile enzyme .....	101
4.3.	Several routes by which peroxidase is inactivated during the oxidation of phenolic substances.....	102
4.4.	Click chemistry.....	104
4.5.	Azide-alkyne cycloaddition process catalyzed by copper (I) (CuAAC).....	104
4.6.	CuAAC reaction mechanism .....	104
4.7.	Adding reactive handles (such as azide or alkyne) to biological compounds.....	105
4.8.	Inhibitor of lignification.....	105
4.9.	Objective.....	106
4.10.	Experimental part.....	107
4.10.1.	Chemicals.....	107
4.10.2.	Fisher esterification of phenols .....	107
4.10.3.	Functionalization of ferulic ester with propargyl bromide .....	108
4.10.4.	Bifunctionalization of ferulic acid.....	108
4.10.5.	Deuterated propargylated ferulic acid .....	109

4.10.6.	Coniferyl alcohol analogue .....	110
4.10.7.	Purification on column chromatography .....	111
4.10.8.	Summary of all inhibitors synthesized .....	111
4.10.9.	Self-labeling of HRP with alkyne-lignin monomer probes.....	113
4.10.10.	CuAAC reaction of biotin-PEG3-azide with alkyne handles.....	113
4.10.11.	Kinetic study of HRP inactivation .....	113
4.10.12.	Acetone precipitation of HRP .....	114
4.10.13.	HRP subjected to protein digestion.....	114
4.11.	Results and Discussion .....	116
4.11.1.	Synthesis of the coniferyl alcohol derivative.....	116
4.11.2.	Ferulic acid derivative.....	116
4.11.3.	Extension to other lignin acids .....	117
4.11.4.	Coniferyl alcohol etherification .....	119
4.11.5.	Bifunctional phenols.....	120
4.11.6.	HRP self-labelling is being developed using lignin monomer tags .....	122
4.11.7.	A "click" technique is used to bind acetylene-containing monomers to biotin with an azide terminus .....	124
4.11.1.	Peroxidase inactivation mechanism during phenol oxidation .....	126
4.11.2.	HRP is rendered inactive by the oxidation of its aromatic substrates .....	127
4.11.3.	HRP polypeptide chain modification.....	132
4.12.	Conclusion .....	133
<b>5.</b>	<b>CHAPTER FIVE: CHEMICAL ACTINOMETRY .....</b>	<b>134</b>
5.1.	Introduction.....	134
5.2.	Determining the exact amount of light necessary to inactivate a blood component .....	135
5.3.	Chemical actinometers.....	136
5.4.	Overview of chemical actinometers examples .....	137
5.5.	Azobenzene .....	138
5.6.	MSAP laboratory state-of-the-art: Nassim El Achi's PhD thesis.....	138
5.7.	The target of azobenzene.....	140
5.8.	Isomerization of water soluble azobenzene .....	142
5.9.	Preliminary photochemistry experiments.....	142
5.9.1.	Importance of mixing .....	142
5.10.	Materials and methods .....	143
5.10.1.	Materials.....	143
5.10.2.	Photo microfluidic reaction of (E)-Azobenzene .....	144
5.10.3.	NMR measurements.....	144

5.10.4.	Synthesis of derivateed fluorinated azobenzene .....	144
5.10.5.	Experimental Actinometric Measurements .....	147
5.11.	Results and discussions .....	149
5.11.1.	Actinometric protocol for the azobenzene .....	149
5.11.2.	Calculation of Photon Flux emitted by the UV LEDs .....	151
5.11.3.	Water soluble azobenzene .....	152
5.11.4.	Actinometric protocol for the water soluble azobenzene .....	153
5.11.5.	Pyridine actinometre .....	158
5.12.	Conclusion .....	163
<b>6.</b>	<b>GENERAL CONCLUSION.....</b>	<b>164</b>
<b>7.</b>	<b>LIST OF REFERENCES .....</b>	<b>166</b>

## List of figures

Figure 1-1: Typical lignocellulosic biomass composition .....	3
Figure 1-2: The three main monolignols of lignin .....	4
Figure 1-3: The monomer structures of lignin [14].....	4
Figure 1-4: The potential use of lignin as a platform in biorefineries.....	6
Figure 1-5: Different linkages constitute lignin [24].....	7
Figure 1-6: Transport of monolignols in plant cells.....	8
Figure 1-7: Mechanism of lignin polymerization catalyzed by HRP [35].....	9
Figure 1-8: Laccase-catalyzed oxidative coupling of vanillyl alcohol.....	9
Figure 1-9: Selected phenolic compounds commonly found in bio-oil .....	10
Figure 1-10: $\beta$ -O-4 and $\beta$ - $\beta'$ dimers resulting from the oxidative dimerization of sinapic acid [54]. .....	11
Figure 1-11: Biotinylation site identification strategy [71].....	14
Figure 1-12: CuAAC reaction .....	15
Figure 1-13: Chemical structures of several monolignols probes .....	17
Figure 1-14: Lamps used for photochemical syntheses .....	19
Figure 1-15: (a) Immersion well irradiation apparatus; (b) a refrigerated apparatus for conducting reactions at low temperature.....	20
Figure 1-16: Set-up of a photo-microreactor.....	22
Figure 1-17: Photographs of microchannels in plate-type microflow reactors; (a) KeyChem-Lumino (YMC) and (b) Dwell Device. (c) Photographs of the flow channel in FEP tubing equipped with an Hg lamp [114].....	23
Figure 1-18: Mechanical pumps: (a) syringe pump; (b) peristaltic pump; (c) HPLC pump [117]. .....	23
Figure 1-19: [2+2] Intramolecular photocycloaddition reactions of simple alkene- linked coumarins. ....	26
Figure 1-20: Metal-free photocatalytic aerobic oxidation of thiols. ....	27
Figure 1-21: Photocatalytic reductive halogenation reactions of halocarbonyl compounds. ..	27
Figure 1-22: Generation of guaiacoxy radical.....	29
Figure 1-23: Photogeneration of phenoxy radicals with Eosin Y .....	31
Figure 1-24: Photogeneration of phenoxy radicals with AIBN and Cupper Complex .....	32
Figure 1-25: Generation of o,o'- dityrosine with Pterin or folic acid .....	32

Figure 1-26: generation of dityrosine using riboflavin .....	<b>Error! Bookmark not defined.</b>
Figure 2-1: Laccase-catalyzed synthesis of poly(2,6-dimethyl-1,4-oxyphenylene) and 3,5,3',5'-tetramethyl-4,4'-diphenoquinone from 2,6-dimethylphenol.....	36
Figure 2-2: Ferulic acid oxidative coupling .....	37
Figure 2-3: $\beta$ - $\beta'$ dimerization of ethyl sinapate.....	38
Figure 2-4 Proposed mechanism of riboflavin under anaerobic conditions H2A stands for ascorbic acid, HA for the monodehydroascorbic acid and A for dehydroascorbic acid .....	39
Figure 2-5 Proposed mechanism of riboflavin under anaerobic conditions.....	40
Figure 2-6 Anaerobic photooxidation of riboflavin .....	41
Figure 2-7: The mechanism of photo-oxidation of riboflavin and tryptophan.....	41
Figure 2-8: Advantages of continuous flow micro-reactor .....	42
Figure 2-9: Lignin phenolic derivatives and unsaturated phenolic compounds used in this work .....	43
Figure 2-10: Continuous recycle microflow reactor .....	44
Figure 2-11: Proposed mechanism for dimer and trimer formation from phenol induced by RF photoreactions .....	51
Figure 2-12: MALDI-FT-ICR of non-purified riboflavin.....	52
Figure 2-13: Purified riboflavin's FT-ICR spectra after exposure to UV light at various times .....	53
Figure 2-14: The general mechanism for the recombination of lignin phenolic substrates. ....	54
Figure 2-15: The products that were previously reported in the laccase-catalyzed oxidation of vanillic alcohol [43, 196, 197]. .....	54
Figure 2-16: $^1\text{H}$ NMR of vanillyl alcohol (a) and divanillyl alcohol (b) .....	56
Figure 2-17: $^{13}\text{C}$ NMR spectra of divanillyl alcohol.....	56
Figure 2-18: HSQC NMR for divanillyl alcohol .....	57
Figure 2-19: MALDI-TOF spectrum of C-C coupled divanillyl alcohol.....	57
Figure 2-20: $^1\text{H}$ NMR of (a) eugenol and (b)dieugenol .....	59
Figure 2-21: MALDI-TOF of dieugenol .....	60
Figure 2-22: $^1\text{H}$ NMR of di-isogeunol .....	61
Figure 2-23: MALDI-TOF of di-isogeunol.....	61
Figure 2-24: $^1\text{H}$ NMR spectra of methyl ester of sinapic acid (6) .....	62
Figure 2-25: mechanism of the mesomeric forms I–V of the phenoxy radical.....	62
Figure 2-26: Possible combination of phenoxide radicals of 4-hydroxypropanoids. The resulting primary bond is shown in the purple color.....	63

Figure 2-27: <sup>1</sup> H NMR spectra of sinapic acid (5) and of sinapic acid β-β coupling dimer.....	64
Figure 2-28: <sup>1</sup> H NMR spectra of sinapic acid (5) and of purified sinapic acid β-β coupling dimer .....	64
Figure 2-29: MALDI-TOF of β-β' dimer resulting from the oxidative dimerization of sinapic acid (5).....	65
Figure 2-30: <sup>1</sup> H NMR of methyl ester dimer of sinapic acid .....	66
Figure 2-31: MALDI-TOF spectrum of the dimer of methyl ester of sinapic acid (6).....	66
Figure 2-32: <sup>1</sup> H NMR spectra of caffeic acid (7).....	67
Figure 2-33: MALDI-TOF spectrum of caffeic acid (7).....	67
Figure 2-34: <sup>1</sup> H NMR spectra of ferulic acid (8) .....	68
Figure 2-35: MALDI-TOF of ferulic acid dimer (8).....	68
Figure 2-36: <sup>1</sup> H NMR spectrum of coniferyl alcohol .....	69
Figure 2-37: <sup>1</sup> H NMR spectrum of di-coniferyl alcohol coupled by C-O linkage.....	70
Figure 2-38: <sup>1</sup> H NMR spectrum of di-coniferyl alcohol coupled by C-C linkage.....	70
Figure 2-39: <sup>1</sup> H NMR of 4-hydroxybenzyl alcohol .....	71
Figure 2-40: <sup>1</sup> H NMR of 4-hydroxybenzyl alcohol dimer coupled by C-C linkage.....	72
Figure 3-1: Mechanism of phenol polymerization by peroxidase. A. Phenoxy radicals first form. B. a radical combination. C. polymerization and radical transfer [234]. .....	79
Figure 3-2: <sup>1</sup> H NMR of vanillin in DMSO .....	86
Figure 3-3: <sup>13</sup> C NMR of vanillin .....	86
Figure 3-4: <sup>1</sup> H NMR of divanillin .....	87
Figure 3-5: <sup>1</sup> H NMR of derivatized vanillin .....	89
Figure 3-6: <sup>1</sup> H NMR of divanillyl alcohol .....	90
Figure 3-7: <sup>1</sup> H NMR of derivatized divanillin .....	91
Figure 3-8: MALDI-TOF of derivatized divanillin.....	91
Figure 3-9: FT-ICR MALDI spectrum of C-C coupled derivatized divanillin .....	91
Figure 3-10: oligomers produced by immobilized HRP following vanillin oxidation. ....	93
Figure 3-11: Oligomer produced following DCM/water treatment. ....	94
Figure 3-12: polyvanillin derivatized using iodoacetamide. ....	95
Figure 3-13: polyvanillin derivatized in acidic medium. ....	97
Figure 3-14: Polyvanillin's suggested structures .....	98
Figure 4-1: Process of lignification peroxidases' deactivation during the oxidation of specific lignin monomers.....	101
Figure 4-2: Peroxidase catalytic cycle [254]......	102

Figure 4-3: Peroxidase's full catalytic cycle displaying the two side reactions. Compounds I, II, and III each have a ground state identified by the letters Ei, Eii, and Eiii, respectively. AH <sub>2</sub> and A.P-670, also known as verdohaemoprotein, is the inactive form of peroxidase [260].	103
Figure 4-4: The several mechanisms by which phenoxyl radicals inactivate peroxidases.	103
Figure 4-5: The CuAAC reaction's postulated mechanism by Kolb et al.[72].	105
Figure 4-6: Functionalization of for pull-down of lignification peroxidase by a bait and prey strategy	107
Figure 4-7: synthesis of propargylated phenols	116
Figure 4-8: <sup>1</sup> H NMR of ferulic acid and propargylated ferulic acid	117
Figure 4-9: <sup>1</sup> H NMR of propargyl sinapate	118
Figure 4-10: <sup>1</sup> H NMR of propargyl coumarate	119
Figure 4-11: Protected coniferyl alcohol and protected coniferyl alcohol etherified	120
Figure 4-12: Bifunctionalization of ferulic ester with triple bond	121
Figure 4-13: Synthesis of PMF	121
Figure 4-14: <sup>1</sup> H NMR of PMF	121
Figure 4-15: Synthesis mechanism and <sup>1</sup> H NMR of PMC	122
Figure 4-16: Novel clickable lignin monomers	122
Figure 4-17: MALDI-TOF spectrum of PC linked to biotin-azide by click reaction.	125
Figure 4-18: MALDI-TOF spectrum of PF linked to biotin-azide by click reaction.	125
Figure 4-19: MS/MS spectrum revealing the labeling of KZWW6 isoform of HRP with PC. Peaks in magenta ( <i>m/z</i> 366.12 Da) corresponds to immonium ion of the labeled tyrosine.	126
Figure 4-20: Inhibition of HRP under optimized proximity conditions	127
Figure 4-21: % Residual activity after treatment with PC, PF, PMC, PF, and H <sub>2</sub> O <sub>2</sub> at a ratio of 1:17×10 <sup>3</sup> for HRP to substrate.	129
Figure 4-22: Modified lignin monomers	130
Figure 4-23: Residual activity of HRP (0.1 mM) after being exposed to coumaric acid derivatives PC/MC/PMC/MPC (0.1 M) in 0.45 mL PBS, pH 7.4 in the presence of H <sub>2</sub> O <sub>2</sub> (0.1 M).	131
Figure 4-24: MS/MS spectrum showing PC tagging of the HRP KZWW6 isoform. Magenta-colored peaks ( <i>m/z</i> 366.12 Da) represent immonium ions from the tagged tyrosine.	132
Figure 5-1: Machine for UV blood irradiation from Macopharma [289]	136
Figure 5-2: The structure of E and Z azobenzene	138
Figure 5-3: Azobenzene isomerization reaction	138
Figure 5-4: Evolution of the E and Z isomers during the radiation period [300]	139

Figure 5-5: Graph of $\ln(Z_{PSS}-Z_t)$ vs time (s).....	140
Figure 5-6: Molecule of interest 1 and 3 .....	141
Figure 5-7: Isomerization reaction of the Water soluble Azobenzene .....	142
Figure 5-8: difference irradiation according to the nature of the flow .....	143
Figure 5-9: Set-up for photo microfluidic reaction .....	144
Figure 5-10: Synthesis of (E)-1-(2,6-difluorophenyl)-2-(4-methoxyphenyl) diazene .....	145
Figure 5-11: Synthesis of (E)-4-((2,6-difluorophenyl) diazenyl) phenol.....	145
Figure 5-12: Synthesis of (E)-1-(2,6-difluorophenyl)-2-(4-methoxyphenyl) diazene .....	146
Figure 5-13: synthesis of (E)-1-(2,6-difluorophenyl)-2-(4-methoxyphenyl) diazene.....	147
Figure 5-14: Graph of $\ln(Z_{PSS} - Z_t)$ vs time (s) following the irradiation.....	151
Figure 5-15: $^1\text{H}$ NMR of water soluble azobenzene .....	153
Figure 5-16: $^{19}\text{F}$ NMR of water soluble azobenzene.....	153
Figure 5-17: $^1\text{H}$ NMR of WSA under $\lambda=365$ nm.....	155
Figure 5-18: Graph of $Z_{PSS}$ vs radiant energy (J) following the irradiation of $6.4 \times 10^{-5}$ M WSA in ethanol/water .....	158
Figure 5-19: Pyridine concentration dependence of PNA-Pyr photolysis quantum yield .....	159
Figure 5-20: Reaction between pyridine and FNB.....	160
Figure 5-21: Proposed mechanism for nucleophilic substitution of halogen atoms and nitro group in nitroarenes [311] .....	161
Figure 5-22: Graph of $\log$ FNB vs time (s) following the irradiation.....	162
Figure 5-23: Graph of $\log$ standard vs time (s) following the irradiation .....	162

## List of tables

Table 2-1: Types of couplings and yields of phenolic derivatives-dimerization products formed by continuous photooxidation.....	48
Table 3-1: Summary of the conditions for the derivatization reaction of vanillin and vanillyl alcohol. ....	88
Table 3-2: Summary of the conditions for the derivatization reaction of 5,5' dehydrodivanillin and polyvanillin. ....	89
Table 3-3: a summary of the three series of polyvanillin in basic medium .....	95
Table 3-4: a summary of the three series of polyvanillin in acidic medium .....	97
Table 4-1: Summary of all modified lignin monomers synthesized in this work .....	111
Table 4-2: List of the phenolic compounds used in the HRP labeling experiment. The modifications and the signature ions used in mass spectrometry are also provided. ....	<b>Error!</b>
<b>Bookmark not defined.</b>	
Table 5-1: Spectral and photochemical characteristics of several azobenzene types .....	141
Table 5-2: Summary of the experiments done for the chemical actinometric assessment....	148
Table 5-3: Physical constants used for calculations .....	149
Table 5-4: Results for the conversion (Z) – Azobenzene.....	149
Table 5-5: Irradiation of E – Azobenzene for different durations.....	150
Table 5-6: Results for the conversion (Z)-WSA .....	154
Table 5-7: Evolution (Z)-WSA after rest time .....	154
Table 5-8: Results for the conversion (Z) in the plastic bag .....	155
Table 5-9: Results for the conversion (Z) in the blood bag.....	156
Table 5-10: Results for the conversion (Z) in the blood bag ( second trial ) .....	157
Table 5-11: summary of experiments performed for PNA-pyr actinometer.....	160
Table 5-12: Results for the irradiation solutions for different durations.....	161

## List of abbreviations

ACN	Acetonitrile
DMSO	Dimethylsulfoxide
CuAAC	Copper (I)-catalyzed azide-alkyne cycloaddition reaction
DCM	Dichloromethane
DMF	Dimethylformamide
EtOAc	Ethyl acetate
FT-ICR	Fourrier transform ion cyclotron resonance
H <sub>2</sub> O <sub>2</sub>	Hydrogen peroxide
HCCA	$\alpha$ -cyano-4-hydroxycinnamic acid
HCl	Hydrochloric acid
HPLC	High performance liquid chromatography
HRP	Horseradish peroxidase
K <sub>2</sub> CO <sub>3</sub>	Potassium carbonate
LC-MS/MS	Liquid chromatography-tandem mass spectrometry
MALDI TOF/TOF	Matrix laser assisted desorption-time of flight/ time of flight
MALDI-FT-ICR	Matrix assisted laser desorption ionisation- Fourrier transform ion cyclotron resonance
MALDI-TOF	Matrix assisted laser desorption-Time of flight
MC	Methyl trans- <i>p</i> -coumarate
MeOH	Methanol
MgSO <sub>4</sub>	Magnesium sulfate
MPC	Methyl propargylcoumarate
Mr	Molecular mass
MS	Mass spectrometry
MS/MS	Tandem mass spectrometry
<i>MtL</i>	<i>Mycelio thermophila</i> lacase

LED	Light Emitting Diode
Na <sub>2</sub> S <sub>2</sub> O <sub>8</sub>	Sodium persulfate
NaCl	Sodium chloride
NaHCO <sub>3</sub>	Sodium bicarbonate
NaOAc	Sodium acetate
NaOH	Sodium hydroxide
NH <sub>4</sub> HCO <sub>3</sub>	Ammonium bicarbonate
NHS	N-hydroxysuccinimide
NMR	Nuclear magnetic resonance
PC	Propargyl coumarate
PDB	Proximity dependent biotinylation
PEG	Polyethylene glycol
rpm	Rotation per minute
PL	Proximimty labeling
PMC	Propargyl methyl coumarate
MS	Mass Spectrometry
TFA	Trifluoroacetic acid
TLC	Thin layer chromatography
PMF	Propargyl methyl ferulate
PS	Propargyl sinapate
TMS	Tetramethylsilane
Tyr	Tyrosine
THF	Tetrahydrofuran
Eq.	Equivalent
PSS	Photo Stationary State
PTSA	Paratoluene sulfonic acid
CA	Coniferyl alcohol
AgNO <sub>3</sub>	Silver nitrate
Ag <sub>2</sub> O	Silver(I) oxide
NaBH <sub>4</sub>	Sodium borohydride
BioID	proximity-dependent biotin identification
APEX	HRP-based proximity labeling; ascorbate peroxidase - based proximity labeling

ABC	Ammonium bicarbonate
ATP	Adenosine triphosphate
PbO <sub>2</sub>	Lead dioxide
HgO	Mercuric oxide
MnO <sub>2</sub>	Manganese(IV) oxide
AIBN	2,2'-azobisisobutyronitrile
RF	Riboflavin
TFA	Trifluoroacetic acid
CD <sub>3</sub> SOCD <sub>3</sub>	Deuterated dimethylsulfoxide
CDCl <sub>3</sub>	Deuterated chloroform
FA	Formic acid
NaHCO <sub>3</sub>	Sodium bicarbonate
Na <sub>2</sub> SO <sub>4</sub>	Sodium sulfate
NaOH	Sodium hydroxide
FeCl <sub>3</sub>	iron (II) chloride
DIPEA	<i>N,N</i> -Diisopropylethylamine
MOMBr	Bromomethyl methyl ether
ABTS	2,2'-azino-bis(3-ethylbenzothiazoline-6-sulfonic acid
CHCl <sub>3</sub>	Chloroform
NaH	Sodium hydride
ETOH	Ethanol
PBS	Phosphate-Buffered saline
HCl	Hydrogen chloride
NaCl	Sodium chloride
WSA	Water soluble azobenzene
PNA-pyr	p-nitroanisole/pyridine
FNB	1-fluoro-4-nitrobenzene

## **Abstract**

Lignin is the second most abundant biopolymer on the planet, although its creation mechanism and structures remain unknown. In this study, lignin and lignification were investigated using three different approaches. The first technique was developed to study the different linkages constitute lignin by radical coupling to form a dimer in presence of riboflavin as a photosensitizer under UV-light (395 nm), using continuous-flow photochemistry in micro-reactors. The second technique was devised to investigate the lignin interunit connections created by a simple lignin monomeric molecule, meaning immobilized enzymes that allowed for the simulation of the hydrophobic environment for lignin production. The third technique, which involved the use of alkyne-containing monolignols, allowed researchers to investigate the behavior of peroxidases during the oxidation of lignin monomers. It also enabled researchers to investigate lignification by analyzing the deactivation or identification of lignification peroxidases via click-chemistry processes.

The first strategy consisted of the dimerization of different monomers of natural lignin. High dimerization yield of all coupled dimers was achieved including C-C, C-O or  $\beta$ - $\beta'$  linkages. Immobilized enzymes were employed in the second strategy to investigate vanillin polymerization as a lignin template. After derivatization in either acidic or basic solution, the oxidation reaction of vanillin catalyzed by immobilized HRP resulted in the synthesis of polyvanillin with up to 15 units, primarily linked by carbon-oxygen bonds, as demonstrated by MALDI-FT-ICR studies. In the third strategy the modulation of HRP activity during oxidation of its substrates was explored utilizing modified monolignols bearing alkyne tags. In the presence of H<sub>2</sub>O<sub>2</sub>, HRP creates phenoxyl radicals during phenol oxidation. These radicals react with HRP, changing its heme or apoprotein via several routes. Coumaric acid-derived compounds inhibited HRP with varying effectiveness and specificity across the lignification probes utilized in this work. A kinetic analysis demonstrated that two probes, propargyl coumarate and methyl coumarate, were responsible for the full loss of HRP activity.

## Résumé

La lignine est le deuxième biopolymère le plus abondant sur la planète, bien que son mécanisme de création et ses structures restent inconnus. Dans cette étude, la lignine et la lignification ont été étudiées en utilisant trois différentes approches. La première technique a été développée pour étudier les différentes liaisons constituant la lignine par couplage radicalaire pour former un dimère en présence de riboflavine comme photosensibilisateur sous lumière UV (395 nm), en utilisant la photochimie en flux continu dans des micro-réacteurs. La deuxième technique a été conçue pour étudier les connexions interunités de la lignine, créées par une simple molécule monomère de lignine, c'est-à-dire des enzymes immobilisées permettant la simulation de l'environnement hydrophobe pour la production de lignine. La troisième technique, qui impliquait l'utilisation de monolignols contenant des alcynes, a permis aux chercheurs d'étudier le comportement des peroxydases lors de l'oxydation des monomères de lignine. Il a également permis aux chercheurs d'étudier la lignification en analysant la désactivation ou l'identification des peroxydases de lignification via des processus de chimie de clic.

La première stratégie consistait la dimérisation de différents monomères de la lignine naturelle. Un rendement de dimérisation élevé de tous les dimères couplés a été obtenu, y compris les liaisons C-C, C-O ou  $\beta$ - $\beta'$ . Des enzymes immobilisées ont été utilisées dans la deuxième stratégie pour étudier la polymérisation de la vanilline en tant que matrice de lignine. Après marquage en solution acide ou basique, la réaction d'oxydation de la vanilline catalysée par HRP immobilisé a entraîné la synthèse de polyvanilline jusqu'à 15 unités, principalement liées par des liaisons C-O, comme les études MALDI-FT-ICR démontrent. Dans la troisième stratégie, la modulation de l'activité HRP lors de l'oxydation de ses substrats a été explorée en utilisant des monolignols modifiés portant des étiquettes alcynes. En présence de H<sub>2</sub>O<sub>2</sub>, HRP crée des radicaux phénoxys lors de l'oxydation du phénol. Ces radicaux réagissent avec HRP, changeant son hème ou apoprotéine par plusieurs voies. Les composés dérivés de l'acide coumarique ont inhibé la HRP avec une efficacité et une spécificité, variables selon les sondes de lignification utilisées dans ce travail. Une analyse cinétique a démontré que deux sondes, le coumarate de propargyle et le coumarate de méthyle, étaient responsables de la perte complète de l'activité HRP.



## **Introduction**

The focus of this thesis is the examination of lignin polymerization from several angles. Higher plants contain the biopolymer lignin. One of the most prevalent polymers on the world is this one. Yet, lignin poses an issue on a global scale since it is produced in large quantities and even though it is a resource that is environmentally friendly and sustainable and plays important roles in a variety of industries, it is still underutilized. This is due to the fact that lignin is still not fully understood, despite years of rigorous research into its structure and the processes that lead to its synthesis. The complexity of mechanisms influencing lignin production, which leads to a polymer with a highly variable composition and structure, is the root cause of the issue. Thus, it is essential to comprehend all of the biosynthetic processes that underlie the formation of lignin polymers. The manufacture of a typical polymer that is similar to native lignin was carefully studied while taking into account the synthesis of several types of lignin models. This provided a strong foundation that made lignin investigations easier. In this regard, we investigated lignin polymerization using several methods.

Lignin is a natural polymer characteristic of wood which constitutes the second biopolymer on earth after cellulose. Lignin is formed by the polymerization of three main monomers which are *p*-coumaryl, coniferyl, and sinapyl alcohols. These monomers are phenols bearing in para position a propenol side chain. They have been used as bio-based building blocks, they bind together through different C–C and C–O linkages after being oxidized by peroxidases in presence of hydrogen peroxide to form a complex tri-dimensional polymer or by radical coupling to form a dimer in presence of riboflavin as a photosensitizer under UV-light (395 nm), using continuous-flow photochemistry in micro-reactors which is an interesting approach to researchers in academia and industry applied for organic synthesis as this technology provides reduced reaction times, higher selectivity, reproducibility, safely use hazardous intermediates in respect to the principles of green chemistry.

A lot of research has been done on the *in vitro* synthesis of lignin model compounds, which have helped us understand some aspects of lignin polymerization and gathered crucial structural information about lignin. Vanillin was chosen as the starting material for the synthesis of the model. Vanillin is a lignin model compound that is created during lignin depolymerization and has recently attracted more interest from scientists across several disciplines, particularly in polymer science. Vanillin dimerization is highly reported in literature, where two forms of

vanillin dimers exists, C-C and C-O coupled dimers. It was investigated whether the immobilized enzymes could oligomerize vanillin. And the results were confirmed by the matrix assisted laser desorption-time of flight (MALDI-TOF) spectrum and nuclear magnetic resonance ( $^1\text{H-NMR}$ ).

The subsequent study of lignin concentrated on the early stages of lignin polymerization, which involve the activity of oxidoreductases. Lignification peroxidases are still elusive as peroxidase are ubiquitous in plant like kinase in mammals. We have shown that the fluorinated analogue of coniferyl alcohol and fluoro-coniferin, its transport form, are inhibitors of lignin biosynthesis [1]. One of classical way for isolating an enzyme for which an inhibitor is known is to add an azide group or a triple bond to the inhibitor, allowing pull-down of the enzyme by conjugating it with biotin via click chemistry. Unfortunately, it has been reported that azides and terminal alkynes inhibit peroxidases [2]. In order to ascertain the difference of reactivity between phenols and terminal alkynes we synthesized monolignols or analogues bearing a propargyl group either on the alcohol of the propenyl chain, on the phenol or on the oxygen ortho to the phenol in coniferyl, and sinapyl alcohols. Labeled version by stable isotopes of these synthesis will also be presented. The reactivity of the synthesized compound with the model peroxidase, Horseradish peroxidase (HRP) will be discussed according to the hole hopping concept [3].

Finally using our microflow reactor, we worked on a new project. The aim of this project was to apply an actinometric protocol with a synthetic water-soluble azobenzene derivative in a photo-microfluidic reactor in order to measure accurately the photon flux of an UV lamp irradiating a blood bag. This work will be a part of a project carries out by the Macopharma pharmaceutical industry in which the research department focus on the treatment of several diseases such as diabetes by using UV irradiation. With the apparition of new aerobic viruses like the Sars Covid 2, it is important to develop the new process of treatment and disinfection. Indeed, the Macopharma research department conduct the development of a new process of UV irradiation against viral infections such as the UVC in order to protect plasma and platelet units from virus infection, bacteria and with UVA for treating diabetes or graft rejection.

# 1. CHAPTER ONE: LITERATURE OVERVIEW

## 1.1.Lignin

One of the most prevalent polymer on the earth is lignin, a biopolymer found in higher plants [4]. It forms with cellulose and hemicellulose the plant lignocellulosic biomass [5]. Lignocellulosic biomass (wood, straw) contains 45% cellulose, 25% hemicellulose and 25% lignin on average (Figure 1-1) [6, 7]. Lignin is an important renewable bioresource that can be used in different industrial approaches. About 5% of chemicals are currently made from renewable resources, the successful conversion of biomass demonstrates that there is a growing interest in biobased products. Nevertheless, it is yearly accumulated in large quantities from pulping and bio-refinery industries and its usage is limited, due to the lack of clear data about the structure of lignin that principally limits its utilization[8, 9]. This polymer has a variety of roles in pharmacology, industry, and human biology [10, 11].

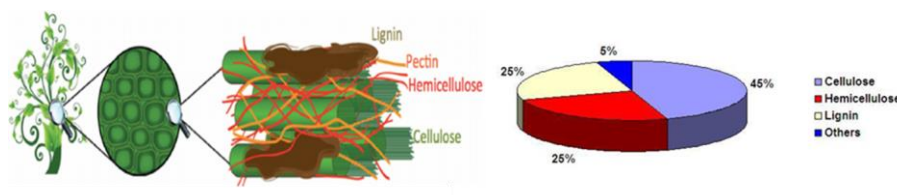


Figure 1-1: Typical lignocellulosic biomass composition

### 1.1.1. Chemical nature and composition

Lignin, a phenolic polymer characterized by a very complex structure [12], is found in the plant secondary cell walls. Mainly, lignin is composed of three monolignols, p-coumaryl alcohol, coniferyl alcohol, and sinapyl alcohol with varying methoxylation levels (Figure 1-2) [13]. When incorporated into the polymer, they are introduced under the form of H unit, G unit and S unit respectively. Lignin has been classified into three types: softwood, hardwood, and grass lignin. Hardwood lignin contains both coniferyl alcohol and sinapyl alcohol, softwood lignin has a lot of coniferyl alcohol, and grass lignin has the three main lignin monomers.



modified lignin, which is lignin that has been reclaimed from industrial byproducts or biomass. The transformation of technical lignin into other value-added compounds or products is the subject of numerous studies.

Kraft lignin (KL) is the main industrial source of technical lignin, but there are a number of other forms of lignin sources as well, including hydrolysis lignin (HL), organosolv lignin (OL), pyrolytic lignin (PL). These technical lignins vary in composition and molecular weight depending on where they come from and how they were extracted [15].

Technical lignin from the industrial by-product can be used as a direct raw material for the synthesis of other chemicals. Technical lignin's aliphatic and aromatic hydroxyl groups are its main active sites; as a result, it can be used directly as polyols for making polyurethane and can replace 30% of the process petroleum-based polyols [16]. However, because the complex structure blocks the reactive site, technical lignin has substantially lower reactivity than lignin fragments. When making polyurethane, the depolymerized lignin fragment can replace up to 50% of the petroleum-based polyols, as opposed to the technical lignin [17]. Depolymerization can thereby increase lignin availability and reveal more reactive sites that are more conducive to subsequent use [18].

### **1.1.3. Lignin and bio-refineries**

Bio-refining is the process of transforming biomass into biobased products (food, chemicals and materials) and bioenergy (biofuels, electricity and heat) [10]. In a sustainability approach, the bio-refineries of the future will need to use the entire plant to produce molecules that were previously made from petroleum while minimizing the environmental footprint [19].

A bio-refinery is described by Moncada et al. [20] as a network of facilities that incorporates equipment and processes for converting biomass into biofuels, energy, and chemicals. This results in a wide range of chemical and energy molecules being represented in new, more effective processes with less negative effects on the environment. The potential for creating and putting into practice renewable energy solutions is represented by the variety of lignocellulosic biomass from agro-industrial waste that is readily available. Lignin have received a lot of attention due to their abundance in biomass, because of their structural diversity and the potential for conversion to useful chemicals. The plant material is subsequently converted into

lower molecular weight organic molecules through chemical digestion or enzymatic hydrolysis. Lignin is currently used as a fuel for direct combustion, as well as in adhesives and binders. The potential for lignin to produce numerous substituted aromatic hydrocarbons is considerable.

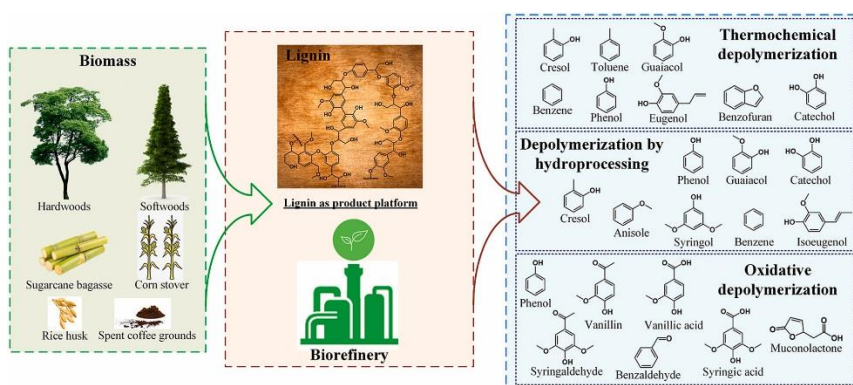


Figure 1-4: The potential use of lignin as a platform in bio-refineries

#### 1.1.4. Lignin biosynthesis-derived linkages

Lignin is produced by a non-reversible process known as “lignification” [21]. This mechanism is highly controlled and is governed by environmental factors. Lignification involves two families of enzymes, laccases and peroxidases, which are playing an important role in lignification.

These enzymes oxidize lignin monomers to form free radicals that are combined to an extending polymer in an endwise mechanism [22]. The random association of radicalized monolignols result a polymer with a structure incorporating various types of linkages that ranges from non-condensed bonds such as  $\beta$ -arylether ( $\beta$ -O-4) to condensed bonds, phenyl coumaran,  $\beta$ -5, resinol,  $\beta$ - $\beta$ , biphenylether, 4-O-5 (Figure 1-5) [23].

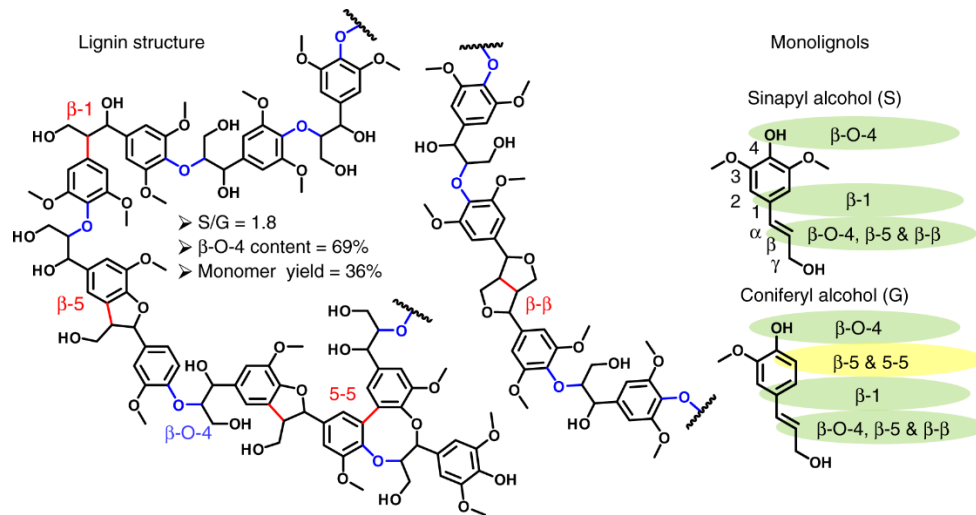


Figure 1-5: Different linkages constitute lignin [24]

Beginning in the primary walls close to the cellulose-depositing cells' corners, lignification progresses to the intercellular layers and primary walls before spreading down the middle lamellae. Lignification of the secondary walls takes place independently once cellulose deposition is complete [25]. Three steps are involved in lignin biosynthesis: biosynthesis, transportation, and polymerization of monolignols [26].

Although lignin deposition is restricted to cell walls, monolignols are biosynthesized in the cell protoplast [27]. Monolignols are produced in the cytoplasm and transferred via a variety of means across the plasma membrane to the cell wall, where lignin polymerization occurs [28].

Figure 1-6 illustrates an example of the link formation during the lignification. When monomers are transported quickly from the cytoplasm to the cell wall, they can couple to form dimers or linkages developing lignin chains. An S monomer must make a  $\beta$ -O-4 ether bond in the case of slow monomer transport if it can only join a developing chain that already has a  $\beta$ - $\beta$  bond [24].

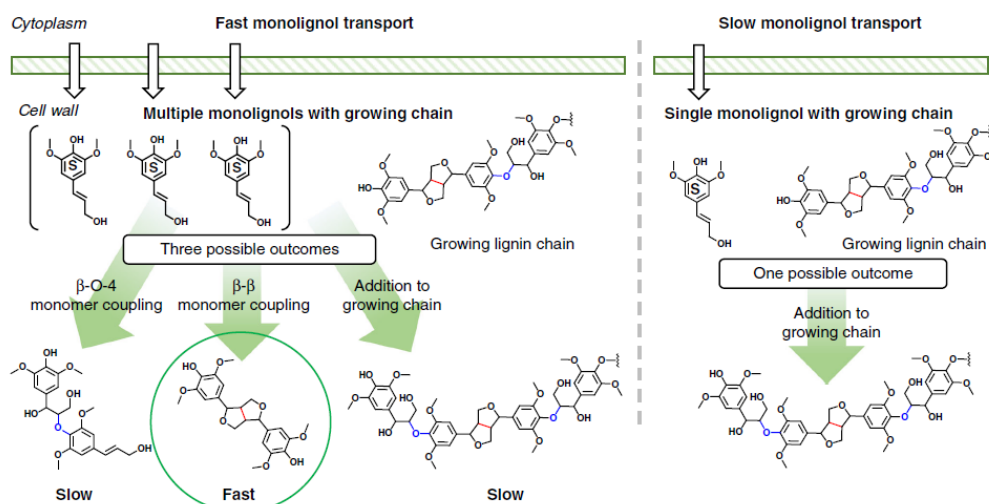


Figure 1-6: Transport of monolignols in plant cells

The final stage of lignification, lignin polymerization, occurs directly in the cell wall as opposed to other cell wall polymers such as hemicelluloses and pectin that are generated distantly and transported to the cell wall [27]. Plant oxidoreductases, primarily peroxidases, are involved in this phase [29]. In fact, there is controversy around laccases role in lignification [30, 31].

### 1.1.5. Oxidoreductases involved in lignin synthesis: Horseradish peroxidase (HRP)

HRP has proved its potency for organic synthesis and polymerization reactions, especially by catalyzing the synthesis of lignin templates [32], and it is capable of oxidizing a variety of organic and inorganic compounds in the presence of hydrogen peroxide [33]. The oxidation of phenolic hydroxyl groups is the first step in the mechanism of lignin polymerization catalyzed by the HRP/H<sub>2</sub>O<sub>2</sub> system. The one pair electron on the phenolic radicals move between the ortho, para, and branching C positions, resulting in the formation of five different types of phenolic radicals. These radicals are coupled to create a polymer with various linkages, such as 5-5',  $\beta$ -5,  $\beta$ -O-4, 4-O-5, and  $\beta$ - $\beta$  among others [34].

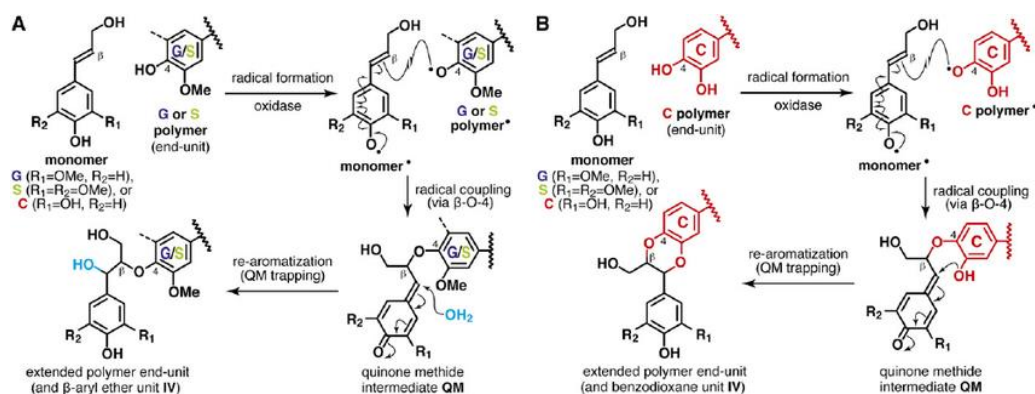


Figure 1-7: Mechanism of lignin polymerization catalyzed by HRP [35]

### 1.1.6. Laccase

A highly well-known group of oxidative enzymes called laccase has been researched since 1883 [36]. In plants, they contribute to the development of the cell wall and lignin (in conjunction with peroxidase), but they also play a role in the depolymerization of lignin with the help of various oxido-reductases [37]. Certain studies has proved that laccase presence along with HRP is necessary for lignin polymerization [30], where it can oxidize lignin by direct oxidation through electron transfer or differently by the transfer of hydrogen atoms leading to its degradation [38].

Additionally, laccase uses the proper substrates to catalyze the creation of polymers with certain structures. The coupling preferentially takes place on the phenol and on the para position when the phenol has two substituents in the ortho position and a free para position, producing either dimers or oligomers with a specific structure. Recently, different researchers reported various studies on the coupling of ortho methoxy para substituted phenol, 2,6-dimethoxyphenol [39], ferulic acid [40, 41], vanillidene derivatives [42] and vanillyl alcohol [43, 44] leads to a dimers catalyzed by laccase (Figure 1-8).

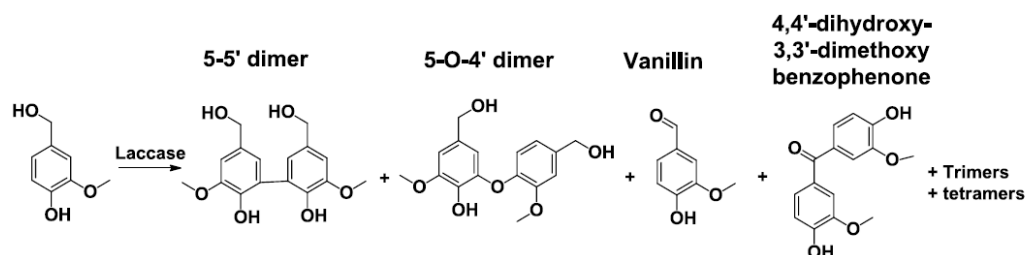


Figure 1-8: Laccase-catalyzed oxidative coupling of vanillyl alcohol

## 1.2. Platform of molecules derived from lignin

A very large organic compounds are produced by lignin. Which's classified in different categories, many useful chemicals can be created from these molecules. The monomers are multipurpose substances with low cost, few byproducts, and excellent purity when produced using standard chemistry.

### Acids/Phenols

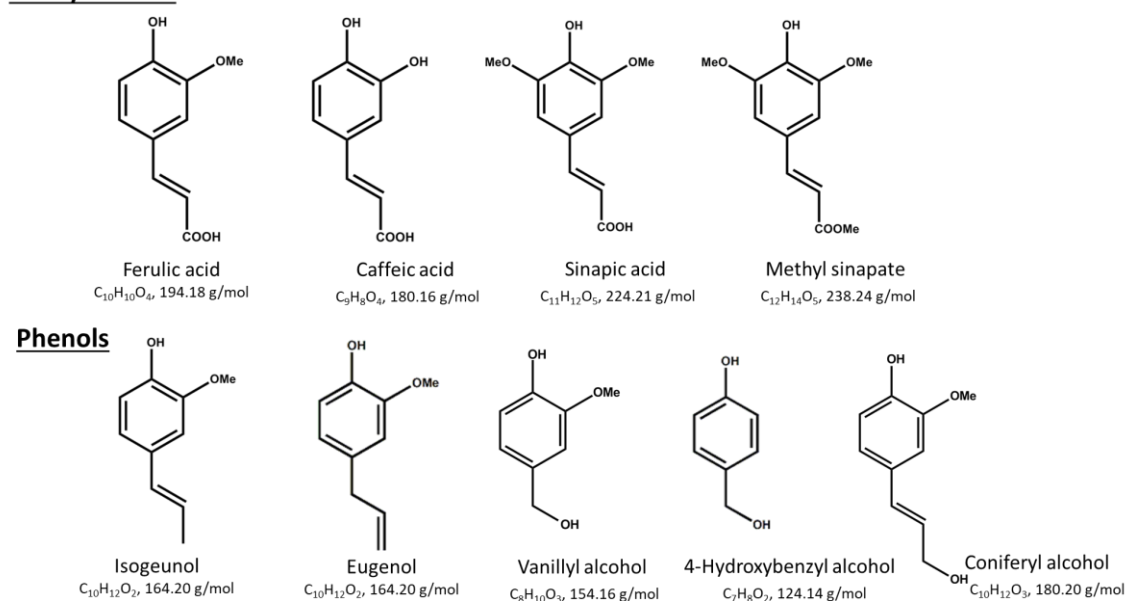


Figure 1-9: Selected phenolic compounds commonly found in bio-oil

Eugenol and isoeugenol are two examples of the guaiacols, a class of phenols often found in bio-oil [45]. Due to their higher concentration in bio-oil than the other phenolic compounds, isoeugenol and eugenol stand out from the other compounds in this group [46]. A monomer involved in the production of lignin is called isoeugenol [47]. Because it is present in bio-oil in better than 7% abundance, it is readily available and practical to utilize [46]. Cloves, nutmeg, and cinnamon are just a few examples of the natural herbs from which the oil component eugenol can be derived. It is frequently used in essential oils and flavorings [48, 49].

Vanilla can be used to extract natural compounds such vanillin and vanillic acid. As a culinary flavoring, vanillin is also utilized in cosmetics and pharmaceuticals. It has been demonstrated that oxidizing vanillin yields a variety of compounds, including divanillin and vanillic acid [50].

Caillol and colleagues have reported the synthesis of a number of bisepoxides from vanillin [51]. Common industrial compounds easily made from vanillin include vanillyl alcohol, vanillic acid and others. These reactions commonly involve  $\text{AgNO}_3$  oxidation and  $\text{NaBH}_4$  reduction.

The sinapic acid and its derivatives can be synthesized from syringaldehyde by the Knoevenagel–Doebner condensation [52, 53]. Since there are two radical species and consequently two potential dimers,  $\beta$ -O-4' and  $\beta$ - $\beta'$ , which can oligomerize further, it is challenging to synthesis  $\beta$ - $\beta'$  dimers of sinapic acid derivatives in good yield and purity [54].

Additionally, the  $\beta$ - $\beta'$  dimerization of sinapic acid is typically followed by an intramolecular rearrangement that results in the synthesis of dilactone and the loss of conjugation (Figure 1-10). By using sinapic acid esters, this type of dilactone can be avoided [55]. One of the recent method to synthesis  $\beta$ - $\beta'$  dimer was to employ copper as the catalyst, pyridine as the ligand, air as the oxidizer, and Cyrene as the solvent [54].

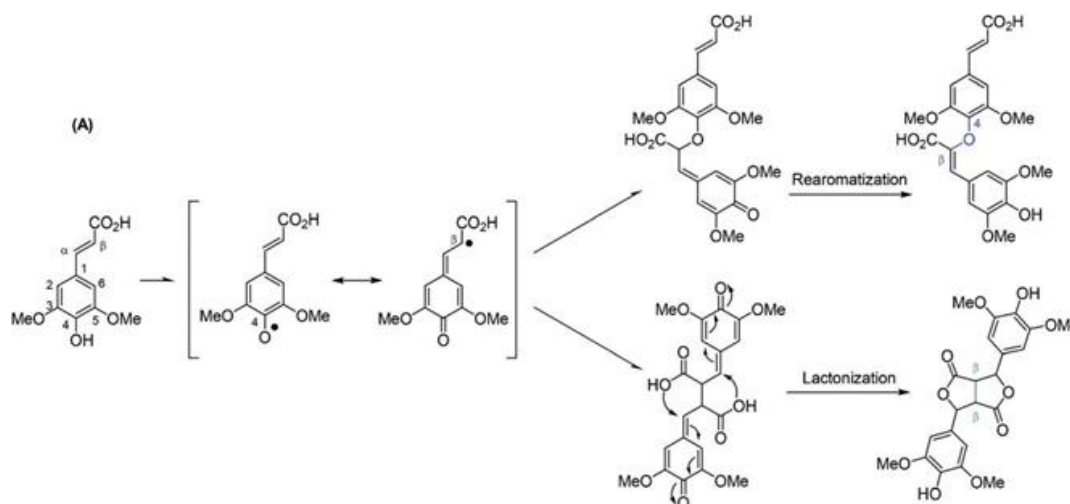


Figure 1-10:  $\beta$ -O-4 and  $\beta$ - $\beta'$  dimers resulting from the oxidative dimerization of sinapic acid [54].

### 1.3.Synthesis of lignin models

Lignin structure has always piqued people's interest [56]. However, lignin's high level of complexity prevents a thorough structural investigation. The substantial advancements made in the study of lignin structure were actually made possible by the understanding of lignin chemistry through the use of in vitro produced lignin models. The synthesis of lignin has been

addressed [57], employing a variety of approaches, including chemical and enzymatic routes, ranging from simple to more complex models.

The manufacture of lignin templates using enzymes derived from plants has been the subject of many investigations. The method proposed by Freudenberg is based on the idea that monolignols can be dehydrogenatively polymerized by peroxidases, and the resulting substance is known as lignin dehydrogenation polymer (DHP) [58].

A variety of isolated enzymes that appeared to have varied affinities to lignin monomers were used to create various forms of DHP. The type of connections generated, the yield, and occasionally the average molecular weight of DHP were significantly influenced by the type and quantity of monomers, as well as the source of the enzymes. Additionally, the type of enzyme utilized affected how the  $\beta$ -O-4 bond formed [59]. Also DHP produced by laccase was discussed [60].

#### **1.4. Chromatography techniques**

Chromatography is a necessary step in any protein purification procedure. It is commonly used to separate molecules based on their partitioning behavior between two phases, stationary (solid, liquid, or a mixture of solid and liquid) and mobile (gas or liquid), which is usually an aqueous buffer. Gel filtration, ion exchange, hydrophobic, affinity, and reverse phase chromatography are all methods for separating proteins based on their properties [61, 62]. All of these types are based on the idea that the initial sample is divided into several fractions, and the purification process is monitored by measuring the protein content in each fraction [63].

#### **1.5. Overview of proximity dependent labeling technologies**

Proximity dependent biotinylation (PDB) techniques are novel methodologies complementary to standard biotinylation methods that have fast made their mark in researching subcellular proteomes and protein interaction networks in vivo since their inception in 2012. Studying subcellular proteomes requires the purification of the protein of interest by affinity purification, followed by identification using mass spectrometry. PDB techniques permit to alleviate the problems that accompanied protein purification, which may cause loss of protein integrity. What is distinguishing about these approaches is that they enable for effective analysis of protein interactions with cellular and organelle integrity being maintained. PDB methods

primarily entail using enzymes that catalyze the transformation of a substrate into a reactive radical capable of covalently attaching to proteins in the form of a tag [64]. Generally, the enzymes are coupled with bait proteins, a targeting signal peptide, or an antibody. The complex formed can be directed to specified cellular components, where they catalyze the covalent transfer of biotin or its derivatives to target proteins near the enzyme. Labelled proteins are then captured by avidin system conjugated to bead matrices [65], digested after elution, or directly digested on beads prior to their analysis by mass spectrometry [66]. In actuality, a number of considerations must be made in order for a protein to be labeled using these methods. The presence of the protein of interest in proximity to the enzyme, and the solvent accessibility of binding sites are two important factors [65]. Four major methods of proximity labeling do exist each having its unique feature, including: proximity-dependent biotin identification (BioID); HRP-based proximity labeling; ascorbate peroxidase - based proximity labeling (APEX) and pupylation-based interaction tagging (PUP-IT) [67].

### **1.5.1. HRP-based proximity labeling**

These techniques are based on the usage of HRP and engineered ascorbate peroxidase (APEX), which has tyrosine as the target amino acid for biotinylation. HRP is a versatile enzyme that can oxidize a wide variety of phenolic substrates including biotin-phenol. When this happens, short-lived biotin phenol radicals are produced, which can then interact with electron-rich amino acids, primarily tyrosine [68]. APEX was created as a replacement for HRP since HRP readily loses activity in intracellular regions due to its decreasing nature, restricting its use to the extracellular environment and endoplasmic membrane lumens [69].

### **1.5.2. Strategies for detecting biotinylated proteins**

Purification strategies based on the covalent labeling of proteins with biotin tags have made significant contributions to the advancement of proteome discoveries. Enrichment of biotinylated proteins with avidin or its analogues conjugated to bead matrices is a common procedure. The captured proteins are then eluted or digested directly on the beads before being identified by MS. The identification and discrimination of target proteins and contaminant

proteins caused by non-specific interactions with the affinity matrix is not guaranteed using this workflow.

To improve biotin complex detection, the Direct Detection of Biotin-containing Tags strategy (DiDBiT) was developed to detect biotinylated proteins with minimal background effects. It can be used for both *in vivo* and *in vitro* analyses. Proteins are first digested, and then biotin-tagged peptides are enriched using an avidin system by increasing the yield of the enriched biotinylated peptides and decreasing the complexity of the sample analyzed by the mass spectrometer, this technique has increased the degree of detection of biotinylated proteins by 200 folds when compared to conventional methods [70].

The second strategy developed for capturing biotinylated peptides is Biotinylation site identification technology (BioSITE), this technique uses a biotin-specific antibody as a capture reagent with lower affinity to streptavidin, allowing for better biotin dissociation. Actually, this strategy aids in overcoming the limitations associated with the high affinity of the biotin-avidin system, which has a significant impact on the elution of biotinylated proteins because they are highly resistant to harsh elution conditions such as salts and detergents. This technique has been successfully applied to proximity dependent labeling methods such as APEX and BioID, as well as biotin-based click chemistry strategies, where it has helped to identify candidate proteins with confidence (Figure 1-11) [71].

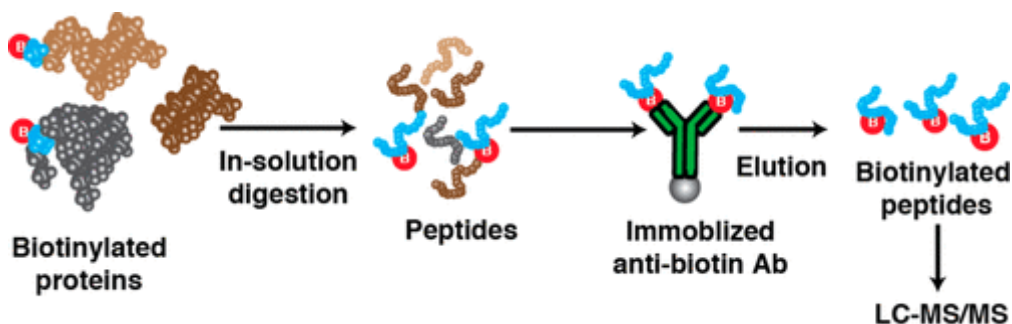


Figure 1-11: Biotinylation site identification strategy [71].

## 1.6. Click chemistry

In 2001, Sharpless first used the phrase "click-chemistry [72]." This reaction allows for the rapid, efficient, and straightforward construction of molecules. It is easy to isolate the end products. Azide-alkyne cycloadditions with copper as the catalyst are one of the most prevalent forms (CuAAC). CuAAC enables the production of 1,2,3-triazole, disubstituted compounds by conjugating the terminal alkyne and azide functional groups (Figure 1-12). Click chemistry has modified the chemistry of biomolecules, in particular the chemistry of bioorthogonal reagents. Small compounds or functional groups known as bioorthogonal reagents are unaffected by biological species. To selectively functionalize probes, they are applied. Using click chemistry, new biological and bioorthogonal probes can be created. Understanding biological processes and discovering new discoveries are two goals of these probes [73].

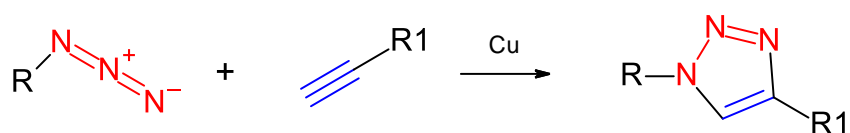


Figure 1-12: CuAAC reaction

## 1.7. Different routes for peroxidase inactivation during the oxidation of phenolic substances

For the substrate-mediated inactivation of peroxidases, various mechanisms have been proposed. These pathways include a peroxidase inhibitor that restricts substrate access by inhibiting the oxidation reaction's polymer [74-77]. Phenoxy radical assault is another method of inactivation [78-80]. Different reactions between phenoxy radicals and HRP are depicted, these include cross-linking between amino acids or between amino acid residues and the polypeptide chain of HRP, as well as interaction with polypeptide chain amino acid residues, most notably tyrosine I and coupling of a phenoxy radical to the HRP heme moiety [80]. The polypeptide chain's amino acids are the final conceivable explanation. The polypeptide chain's amino acids may also undergo modification, such as oxidation, as a final possibility. The reaction conditions and the kind of substrate play a major role in which of these pathways peroxidase inactivates [80].

## **1.8. Phenols probes**

Through a sequence of enzymatic changes, including deamination, hydroxylation, O-methylation, and the conversion of the carboxyl group to an alcohol, monolignols are produced in the cytoplasm of plant cells from phenylalanine. It is unclear how these monolignols are then transferred to the extracellular space before polymerizing [81, 82]. Recent research suggests that the ABC transporters, also known as ATP binding cassette-like transport proteins, are the most plausible transport mechanism [83-86]. The monolignols polymerize once they have crossed the plasma membrane thanks to radical coupling processes that are hypothesized to be started by laccases and peroxidases [84, 87-89].

Copper-catalyzed click chemistry has been an effective method for bioorthogonal metabolic labeling of living cells over the past ten years. This method involves supplying the cells with a metabolite that has been altered by an alkynyl or azido group, which they then incorporate into their structure. A copper-catalyzed click reaction that covalently connects a detection probe, frequently a fluorophore, to the changed metabolite after incorporation allows for the detection of the transformed metabolite. Numerous creatures, including bacteria, animals, and plants, have been labeled using this procedure for nucleic acids and carbohydrates [90-96].

Lignin should be receptive to the integration of a click-compatible monolignol analog due to its chemical method of polymerization, enabling the effective detection of lignification in vitro and in plant tissues.

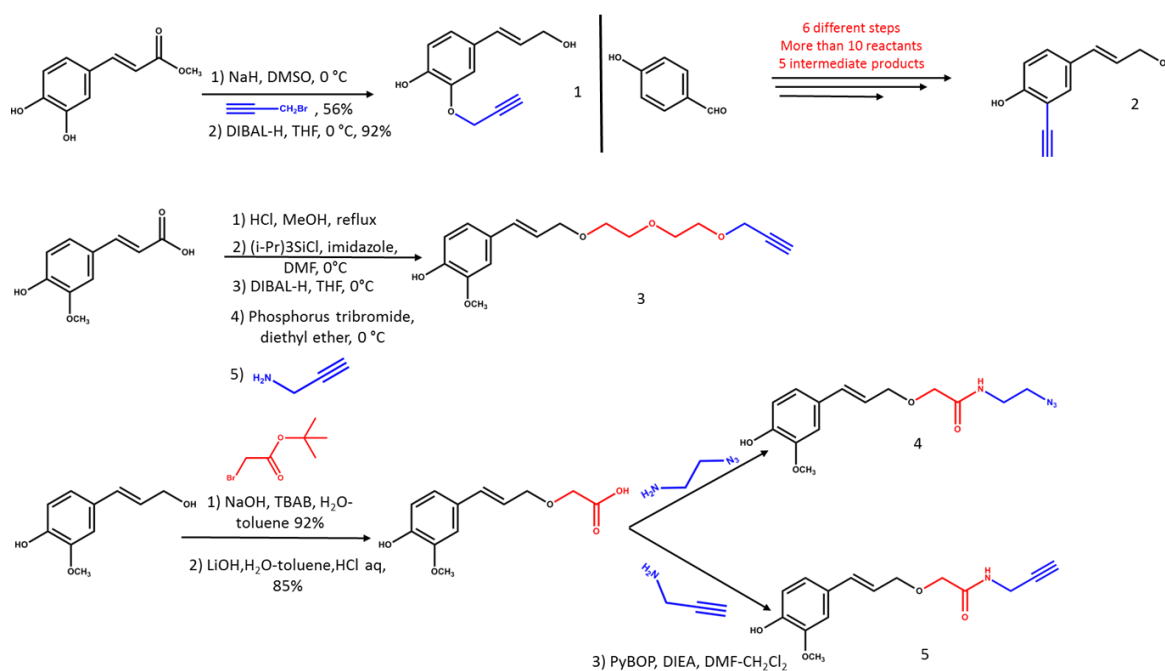


Figure 1-13: Chemical structures of several monolignols probes

Figure 1-13 mostly described the probes that had been produced in the other papers. A terminal alkyne was specifically chosen as the tag of choice, because of its small size and compatibility with reliable click chemistry, which has been used to image glycans in plants and other creatures [97, 98].

They avoided directly modifying aryl/alkenyl carbons in order to attach a terminal alkyne moiety to coniferyl alcohol because doing so could change the phenol's redox potential and potentially have a big effect on lignification [99].

Regioselective alkylation of methyl caffeate served as the precursor for the creation of 3-*O*-propargylcaffeyl alcohol (Figure 1-13/ product 1). By adding too much sodium hydride, the hydroxyl groups of methyl caffeate were deprotonated. The more nucleophilic phenoxide was produced by the less acidic 3-hydroxyl group, and it was then specifically alkylated to yield 56% of the methyl 3-*O*-propargylcaffeate. Diisobutylaluminum hydride was then used to reduce the ester, yielding 92% of the required 3-*O*-propargylcaffeyl alcohol [100].

Pandey et al. developed and synthesized product 2 (*E*)-2-ethynyl-4-(3-hydroxyprop-1-enyl) phenol, or 3-ethynyl p-coumaryl alcohol (3-EPC), using 6 separate procedures, more than 10 reactants, and 5 intermediates [90].

Product 4 and 5 were synthesized by Ralph et al. which are coniferyl alcohol (CA) derivatives infused with azide (CA-Az) and alkyne (CA-Alk) reporter functions [101].

## **1.9. Photochemistry**

A photon of light and an oxidant in the form of oxygen, either from the surrounding air or pure O<sub>2</sub>, are required for photochemical oxidation reactions. Photochemistry focuses on how light affects chemical reactions. A large number of reactions are possible by photochemistry that are not possible through thermochemical or electrochemical pathways. Its involvement led to the shortening of other synthetic routes by swapping out many stages with a one-step photoreaction, making it popular in the disciplines of total synthesis and material science in addition to giving pathways for the synthesis of sophisticated complex [102].

### **1.9.1. Photochemical oxidation for organic synthesis**

Starting from the 20th century, Ciamician and Silber were credited with developing the principles of modern synthetic photochemistry, this group was the first to describe singlet and triplet states, ketone photochemistry, and intramolecular [2+2] cycloaddition [103]. Then, numerous compounds, including cubane [104], caryophyllene alcohol [105], and cedrene [106], have been reported to have been synthesized by photochemistry.

The current worldwide movement toward greener synthetic techniques like a photochemical pathways which focused on the light, especially visible light obtained from a renewable resource. But there are different parameters to taken in consideration in a photochemical reaction which are the glassware, the solvent, the light source and the photoreactor.

The glassware serves as both a container and a filter, thereby removing all of the harmful irradiations that an HPUV (high pressure lamp) emits. For instance, Pyrex has a cut-off of 275 nm while Quartz is transparent starting at 170 nm [107].

Additionally, filtering out all of the radiation that is below 275 nm is accomplished by sandwiching a piece of Pyrex glass between the reaction mixture and the radiation source. The primary UV source utilized by photochemists is the mercury-discharge lamp since it is readily available commercially. Inside a glass vacuum tube with electrical discharges is a mercury

vapor. Mercury atoms will be excited by an electric current, and once they have calmed down, they will release UV rays. Commercially accessible high (365 nm) HP, medium (300 nm) MP, and low pressure (264 nm) LP, mercury lamps offer a variety of irradiations [107]. For the most part, while employing MPUV and HPUV lamps that emit polychromatic radiations, photochemists use filters to obtain the required irradiation wavelength.



Figure 1-14: Lamps used for photochemical syntheses

(a) Low-pressure mercury arc; (b, c) phosphor-coated lamps, emission centered at 305 and 370 nm; (d, e) medium- and high-pressure mercury arcs, respectively (Figure 1-14) [108].

The choice of solvent is also important. The solvent must be able to dissolve a variety of substrates while remaining a weak UV absorber. The solvent should not be subjected to quenching, hydrogen-atom abstraction, or other interactions with the excited state are additional considerations. Because it is affordable, effective at dissolving polar substrates, doesn't absorb above 200 nm, and is simple to remove on a rotary evaporator, acetonitrile has shown to be a highly adaptable solvent [109].

For the reactor, the most dependable apparatus for laboratory scale organic photochemistry has been the immersion-well photoreactor in conjunction with mercury-vapor-discharge lamps (Figure 1-15). This compact batch reactor is an excellent device to carry out preparative photochemistry on scales of milligrams up to a few grams. The lamp is contained in a double-jacketed water-cooled immersion well. This is then placed into a reaction flask containing the chromophoric substrate. This flask is usually standard Pyrex glassware. The solution is normally degassed to remove oxygen in order to diminish the possibility of quenching and other reactions, such as peroxide formation (conveniently achieved with a long needle and nitrogen stream) [108].

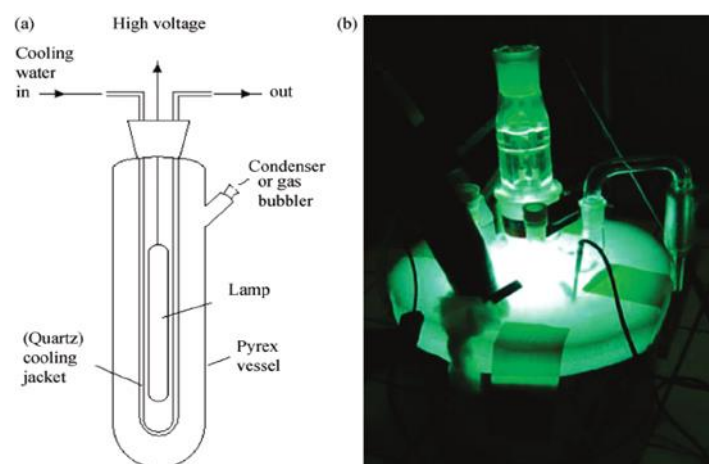


Figure 1-15: (a) Immersion well irradiation apparatus; (b) a refrigerated apparatus for conducting reactions at low temperature.

### 1.9.2. Microreactor technology

Photoreactors cannot use the numerical simulations and expertise that have been acquired for thermochemical reactors. This is because photons are the main actors in these reactions, therefore additional factors need to be taken into account to maximize the reaction's settings. This includes the type of light source used, how far it is from the photoreactor, how evenly the reactor is illuminated, the reactor's geometry, and even the material made up of the reactor.

In addition, scaling up is challenging. This is not an issue at the industrial scale, but in a conventional immersion-well reactor, scaling up in the lab beyond a few grams is frequently exceedingly challenging.

All these limitations can be resolved using the microreactor technology, which is one of the most effective technologies. In response to Ley's work [110, 111] which showed that it was possible to synthesize complex organic compounds using this approach, it began attracting interest among synthetic chemists throughout the past 15 years. Most common batch reactions are now thought to be easily performable in flow reactors [112]. The residence time and the reaction time must be distinguished when using flow microreactors. Every molecule of the reaction mixture remains inside the microreactor during the residence duration. It is in accordance with the exposure period for photochemical reactions. This parameter is affected by the flow rate of the reaction mixture and the volume of the microreactor (which is exposed to radiation)

$$Q = V/t \quad \text{Equation 1}$$

Q (flow rate); V (reactor volume); t (residence time).

In certain conditions, such as when employing tubing as the microreactor, the reactor's volume can be changed. The volume of the reactor is fixed when designed microchips are employed. As a result, by altering the flow rate of the reaction mixture, the change in the irradiation time may be determined: smaller flow rates correspond to longer residence times, and vice versa.

On the other hand, the flow rate and the amount of the reaction mixture that must be purged from the microreactor determine the reaction time. Both the volume injected and the flow rate can be altered to affect this component. If the volume of the reactor is less than the volume of the reaction mixture for a particular flow rate, the reaction time will be longer than the irradiation time. This can be seen as a disadvantage in flow chemistry because that is the case when using micro-scale reactors.

### **1.9.3. Continuous Flow system**

In the 20th century, there were just a few studies that used flow technology for photochemistry. In a spiral glass reactor, vitamin D synthesis was reportedly evaluated in 1959 by Doede & Walker. Coiled Teflon tubing was employed as a gas phase reactor in the 1971 synthesis of methyl chloride [113]. Beginning at the turn of the twenty-first century, the use of microreactor technology in photochemistry began to expand quickly [109].

The nature and implications of the reactions that will be executed in the microreactors must be understood since they can be pre-designed and manufactured, so that the latter may be optimized to the conditions of the former. The flow reactor, an injection system, and a light source should make up the three basic components of a photo-microreactor assembly, regardless of how straightforward or intricate it is. In some circumstances, this assembly can additionally contain mixing, online analytical, or purifying systems.

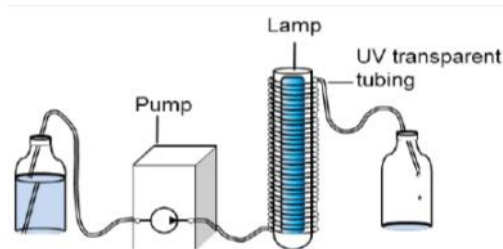


Figure 1-16: Set-up of a photo-microreactor

#### 1.9.4. Materials for the construction of microreactors

Microreactors can be made from a wide variety of materials, but a few factors that should be taken into consideration when choosing the right material.

##### 1.9.4.1. Flow reactor

Two different types of microflow reactors have traditionally been used up until this point. One was the first popular plate type reactor (Figure 1-17 a and b). A microchannel, a cover glass, a few pumps, etc. Plate type reactors are often sturdy because these components are integrated into the unique apparatus. However, there are numerous drawbacks, including high cost, limited versatility in terms of size, scale, and shape, and clogging.

The other is a tubular reactor that uses tubes made of polytetrafluoroethylene (PTFE) or fluorinated ethylene propylene (FEP) (Figure 1-17 c). Due to its numerous advantages, such as their low cost, high degree of flexibility, and simplicity in replacing worn-out tubes, tubular reactors are currently the most popular and are employed extensively. The one drawback of tubular reactors—relatively weak tube robustness—is outweighed by these benefits [107].

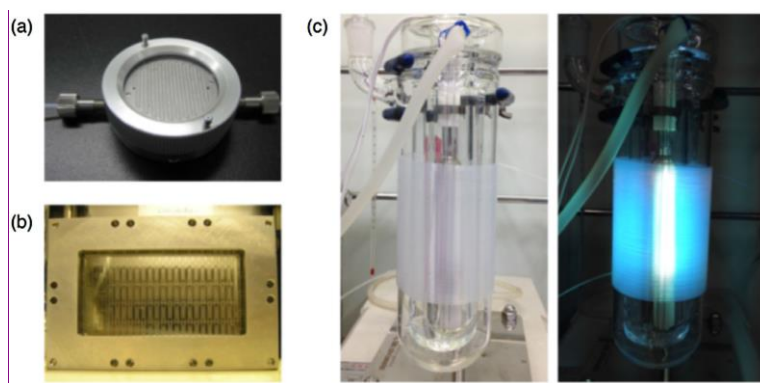


Figure 1-17: Photographs of microchannels in plate-type microflow reactors; (a) KeyChem-Lumino (YMC) and (b) Dwell Device. (c) Photographs of the flow channel in FEP tubing equipped with an Hg lamp [114].

#### 1.9.4.2. Injection system

Injection systems that work with mechanical or non-mechanical pumps regulate the continuous flow. Syringe pumps, peristaltic pumps, and High Performance-Liquid Chromatography (HPLC) pumps are more frequently used examples. The reaction mixture must be kept inside syringes. Flexible tubes that contain the reaction mixture are used in peristaltic pumps. The mixture is forced to exit the tube as a result of the rotor's spinning compressing the tube [115]. In HPLC pumps, the piston drives the liquid at predetermined flow rates through the tube.

The electrohydrodynamic pump is one type of non-mechanical pump that runs on electricity. This type of pump uses its own electrodes to generate an electric field that causes charged molecules to move more quickly and eventually form a flow [116].

Tubing, fittings, connectors, and sleeves are utilized to ensure the connection of the various components in an assembly for a continuous flow system.

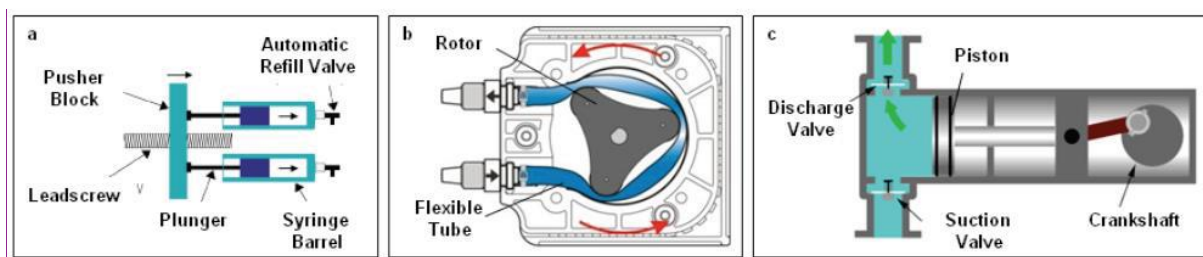


Figure 1-18: Mechanical pumps: (a) syringe pump; (b) peristaltic pump; (c) HPLC pump [117].

### **1.9.4.3. Light source**

Conventional Hg lamps are employed with microfluidic devices. These lights should always be used outside of microreactors because of how much larger they are than the reactors themselves.

Continuous flow photochemistry has recently become quite interested in light emitting diodes (LEDs).

The LEDs are excellent for a variety of reactions because of their ability to produce very narrow emission spectra (20 nm). Compared to other kinds of light sources that are broadband emitters, LEDs are less prone to cause adverse effects. Most of the time, it is also possible to match the LEDs to the chromophore's maximal absorption wavelength, in order to increase the photon flux efficiency and reaction yield. They establish minimal heat energy loss and demand little power input, allowing a fan to cool the system. Additionally, they are inexpensive and compact enough to be mounted on the microreactor [118, 119].

## **1.9.5. Why should photochemistry be used in flow?**

### **1.9.5.1. Photon flux**

The quantity of photons yielded to the reaction mixture during a process per unit of time is known as the photon flux. It might be applied to estimate a reaction's quantum yield. The photon flux can be calculated using chemical actinometry [107] (described in chapter chemical actinometry).

In fact, a number of issues, such as refraction and incompatibility between the dimensions and geometries of the reactor and the light source, may result in a reduction in the number of photons conveyed given by the irradiation system to the reaction.

Loubière and colleagues studied the photon flux received by a batch reactor and a flow reactor since the photon flux has a significant impact on the kinetics of reactions [113].

The photon flux density is calculated by dividing the photon flux value by the reactor's volume. This indicates that the number of photons sent to the microreactor is 150 times greater than that delivered to the batch reactor, with the microreactor having  $301 \text{ Einstein m}^{-3} \text{ min}^{-1}$  compared

to  $1.98 \text{ m}^{-3} \text{ min}^{-1}$  for the batch reactor. This explains why the reaction kinetics in flow reactors have accelerated.

### 1.9.5.2. Efficiency of photonics

A photochemical process can also be defined by its photonic efficiency. It is equivalent to the reaction rate ratio to the photon flux  $Q$ .

$$\xi = \frac{\text{reaction rate}}{Q}$$

This number might range in batch reactors from 0.0086 to 0.0042 [120]. According to a recent study by Noël and colleagues, this value can be increased by up to 0.66 when using microscale irradiation sources like LEDs [121].

### 1.9.5.3. Path length

Beer-Law Lambert's can be used to describe how the photochemical reaction is affected by the short path length.

$$\log \frac{I_0}{I} = \Delta A = \varepsilon c l$$

This demonstrates that for a particular chromophore and a concentration  $c$  ( $\text{mol.L}^{-1}$ ) and molar extinction coefficient  $\varepsilon$  ( $\text{L.mol}^{-1}.\text{cm}^{-1}$ ), respectively, the absorption of light rises with distance  $L$  (cm). If the absorbance is 2, 99% of the light is absorbed by the substrate and just 1% is transmitted after a certain length  $L$  ( $I = 0.01 I_0$ ).

To explain better the situation, we will take the sensitizer 4,4-dimethoxybenzophenone (DMBP) as an example, which has a molar extinction coefficient value of  $135 \text{ M}^{-1}\text{cm}^{-1}$  at 365 nm. By using the aforementioned law with  $c = 0.05 \text{ M}$ , 99% of the light will be absorbed after just 3 mm. The route length of a typical batch reactor, which is in the region of a few centimeters, is far shorter than this number. In other words, no light can penetrate after just 3 mm, therefore only a small percentage of the reaction mixture is lighted.

When the illumination varies within the same reaction mixture, side products result from over-irradiation on the one hand, while productivity declines as a result of under-irradiation on the other. Microreactors with route lengths under 1 mm are used to solve this issue in batch reactors. The reaction mixture is therefore more likely to be completely lighted in continuous flow systems.

### 1.9.6. Models of photochemistry reactions developed in continuous flow

It was stated that a variety of processes, including photocycloaddition, isomerization, cyclization, photocatalysis, and polymerization, had been evaluated utilizing the microreactor technology.

Using a flow-based photochemical reactor (Figure 1-19), Vasudevan described [2+2] intramolecular photocycloaddition reactions of numerous simple alkene-linked coumarins [122]. The photoreactions in the flow system were discovered to be quicker (12 times) and to occur in greater yields (3 times) than those carried out in the batch system. Additionally, it was shown that the yields of cycloadduct production were independent of the starting coumarin concentration in the range of 0.085 to 0.425 M.

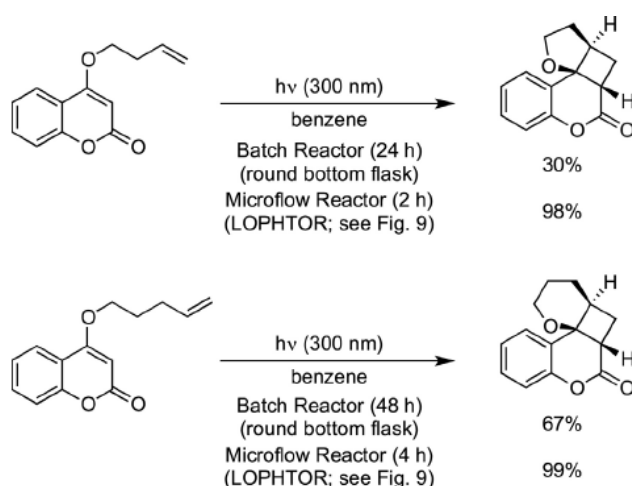


Figure 1-19: [2+2] Intramolecular photocycloaddition reactions of simple alkene-linked coumarins.

Rueping and coworkers reported an instance of continuous-flow photocyclization for the oxidative photocyclization of stilbene derivatives. A high-pressure lamp was used to irradiate the FEP tubing (5 mL), which was used for the reaction. After 83 minutes of radiation, 95% of the (E)-stilbene was converted into phenanthrene by oxidative cyclization [123].

Organic photocatalysis has also recently attracted a lot of attention. Recently, Noel and colleagues reported on the activity of eosin Y in continuous flow. They used this organic catalyst to oxidize thiols to disulfides aerobically in a tube (ID 760  $\mu$ m, 950 l) that was exposed to white LED light (Figure 1-20). Interestingly, complete conversion required 16 hours in batch irradiation while 93-99% yields were attained in just 20 minutes in flow [124, 125].

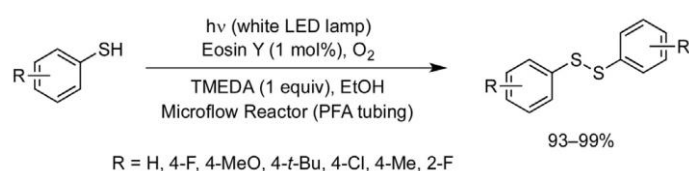


Figure 1-20: Metal-free photocatalytic aerobic oxidation of thiols.

Zeitler reported on similar photoredox reactions brought on by visible light. This work involved the use of a microflow reactor to perform photocatalytic reductive dehalogenation reactions on  $\alpha$ -halocarbonyl compounds in order to generate products in an expedited and high yield way [126].

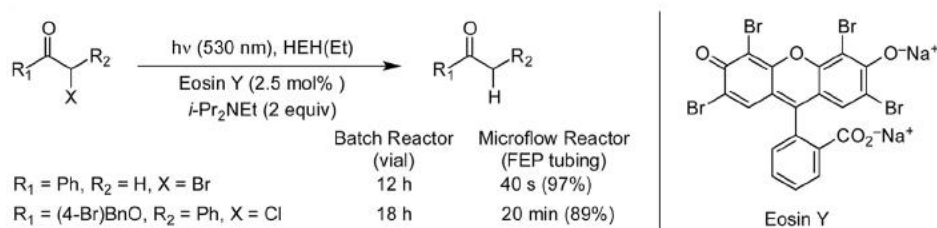


Figure 1-21: Photocatalytic reductive halogenation reactions of halocarbonyl compounds.

### **1.10. Advantages and limitations of microflow reactor**

The beneficial aspects of microflow photochemistry have been emphasized. When compared to batch systems, the majority of photoreactions carried out in microflow reactors do so with superior efficiencies and selectivities. By adopting a different solvent, ultrasonification, or slug flow conditions, the development of secondary products is frequently effectively controlled, and the formation of intractable polymeric or crystalline materials can be prevented.

The additional benefit of microflow photochemistry is its high repeatability and low cost for scaling up reactions. Scaling up in conventional batch systems, particularly to the level of industrial output, necessitates a significant investment in plant and equipment to build and install massive photoreactors. The repeatability linked to small-scale reactions is thus lost. On the other hand, the microflow photochemistry can be easily used to scale up processes by employing more reactors and/or longer irradiation periods. The benefits of reducing equipment costs should outweigh the drawbacks of somewhat long overall flow periods for sample solutions. A remarkable characteristic of the utilization of microflow reactors for photochemical reactions is the ability to apply optimum conditions discovered in investigations of small-scale reactions to large-scale processes. In actuality, a number of large-scale photoreactions carried out in flow reactors have been important steps in the industrial synthesis of natural chemicals.

The microreactor technology has some limitations, much like any other developing technology. To avoid solid precipitation and system blockage, the reagents should be soluble. In comparison to batch technology, which has been used for decades, the difficulty of building such devices must also be considered.

The combination of microreactor technology with photochemistry provides the perfect scenario for green and sustainable synthetic pathways.

### **1.11. Phenoxy radicals: generalities and reactivity**

In the last 15 years, there has been a lot of research into the chemistry of hindered phenols, which are phenols with large ortho substituents. Since several of these phenols produce rather persistent free radicals, and their phenoxy radicals play a key role in the autoxidation inhibition of organic substances. The homolysis of the O-H bond from phenols results in the formation of

phenoxy radicals, which are monovalent oxygen radical species; it has been proven that the unpaired electron delocalizes over the aromatic ring and several side-chain substituents [127]. The delocalization of the electron on the ortho- and para-positions of the benzenic cycle, or intramolecular and intermolecular stabilizations, appears to be the cause of radical stability [128]. Many of the reactions are carried out by phenoxy radicals (both oxygen and carbon radicals) hydrogen abstraction, addition, dimerization, association, oxidation-reduction, disproportionation and isomerization.

### 1.11.1. Ways to generate phenoxy radicals

#### 1.11.1.1. Classical organic chemistry

The most popular techniques for producing high yields of phenoxy radicals from phenols involve the use of inorganic oxidizing agents capable of one-electron reduction, such as  $\text{PbO}_2$ ,  $\text{Ag}_2\text{O}$ ,  $\text{MnO}_2$ ,  $\text{HgO}$ ,  $\text{K}_3\text{Fe}(\text{CN})_6$ , and others.

These reactions typically take place in a heterogeneous system (phenol in an inert solvent solution; oxidizing agent in suspension or aqueous phase), at room temperature, and under nitrogen.

And we can take as an example the generation of guaiacoxy radical with  $\text{K}_3\text{Fe}(\text{CN})_6$ , which produced 41% of dimers [129].

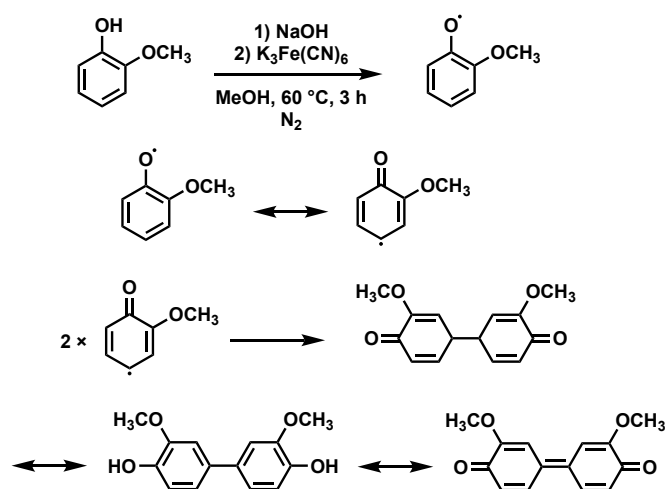


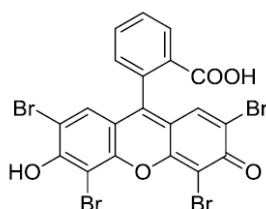
Figure 1-22: Generation of guaiacoxy radical

### 1.11.2. Photochemistry

Phenols have been oxidized to produce dimeric coupling products using a variety of enzymatic methods. Over the last many centuries, numerous synthetically applicable, batch-system-supported photographic chemical reactions have been categorized as using a direct radiation or a photo-sensitized technique (organic oxidizing reagent). A substrate (S) absorbs either a reactant or a photo sensitizer (PS). One of these may undergo a variety of photochemical processes, electron transport, or both to produce its singlet excited state ( $1S^*$ ), which can undergo when an intersystem crosses to produce its triplet state ( $3S^*$ ). Based on the type of molecular change that occurs during a photoreaction, there are numerous classifications that can be used.

The light-absorbing species can participate in a photochemical reaction serve as a photosensitizer that encourages but is not ingested in the procedure. Today's synthetic organic materials, for unknown reasons "Photoredoxcatalysts" is a name that scientists have used to describe what has been referred to as "photosensitizers" and utilized for years. Many chemists mistake "photoredox catalysts" with "photocatalyst". Be aware that, from the viewpoints of "photocatalyst" and "photosensitizer," whereas "photoredox catalysts" are roughly the same as "photosensitizer" such as AIBN, Eosin Y, folic acid, riboflavin. But photocatalyst was initially used for metal-oxide-semiconductors such as  $TiO_2$ .

Eosin Y is the 2',4',5',7'-tetrabromo derivative of fluorescein. The eosin Y is excited to its singlet excited state by exposure to visible light. Rapid intersystem crossing transforms the excited eosin Y into the lowest triplet state. The state of this is 24  $\mu s$  life duration [130, 131] and suitability for photoredox catalysis make it a reasonably long-lived catalyst. Maximum absorption for eosin Y occurs at 539 nm with a molar extinction value of  $60803 M^{-1} cm^{-1}$  [132].



In a preliminary study, the researchers examined the photochemical oxidation of 2, 6-di-*t*-butylphenol (I) using various photo-sensitizers: eosin Y, erythrosin, methylene blue, chlorophyllin, methyl orange, riboflavin tetraacetate, and 2, 5-di-*t*-butyl-*p*-benzoquinone, but it was discovered that erythrosin and eosin Y were most efficient [133].

And specifically, 2, 6-di-*t*-butylbenzoquinone and diphenoquinone are produced when 2, 6-di-*t*-butylphenol is oxidized.

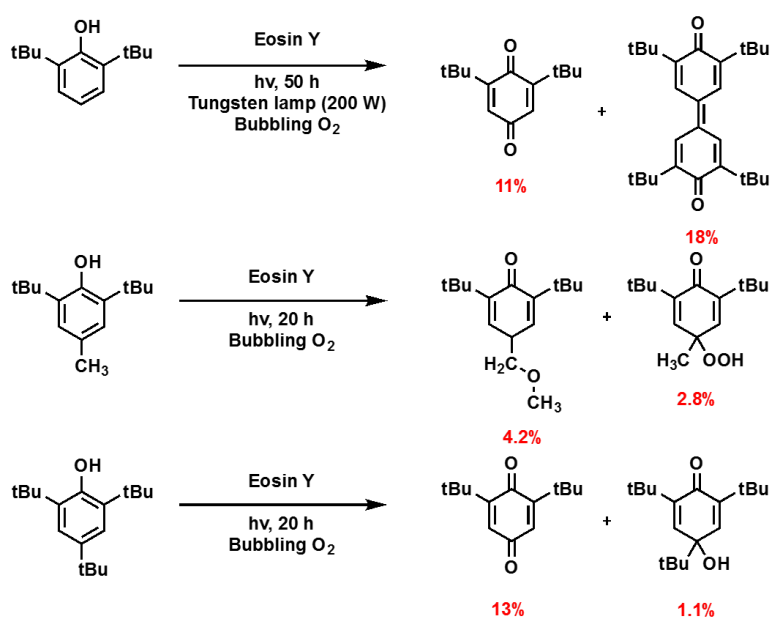


Figure 1-23: Photogeneration of phenoxy radicals with Eosin Y

A *N,N,N,N'*-tetraethylethylenediamine/CuCl mixture was recorded as a catalyst for 4-phenoxyphenol oxidative coupling [134]. As an illustration of coupling of free phenoxy radicals [135], also the polymerization of 4-phenoxyphenol was reported with an equimolar amount of 2,2'-azobisisobutyronitrile (AIBN). The major identifiable products of the AIBN catalyzed polymerization were four dimers, which were identified as O-4 82%, OO-1 12%, OO-2 2%, and OO-3 4% [136].

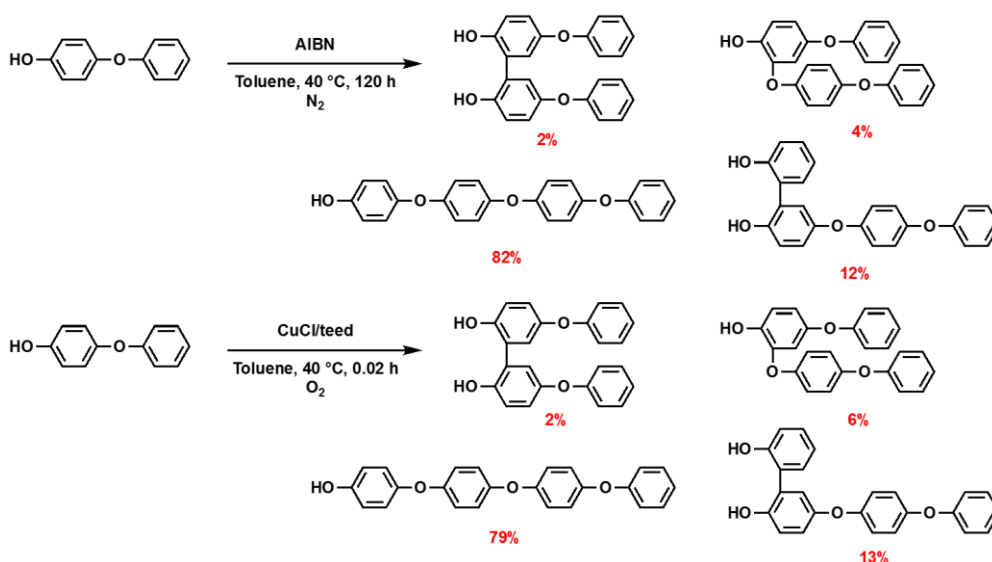
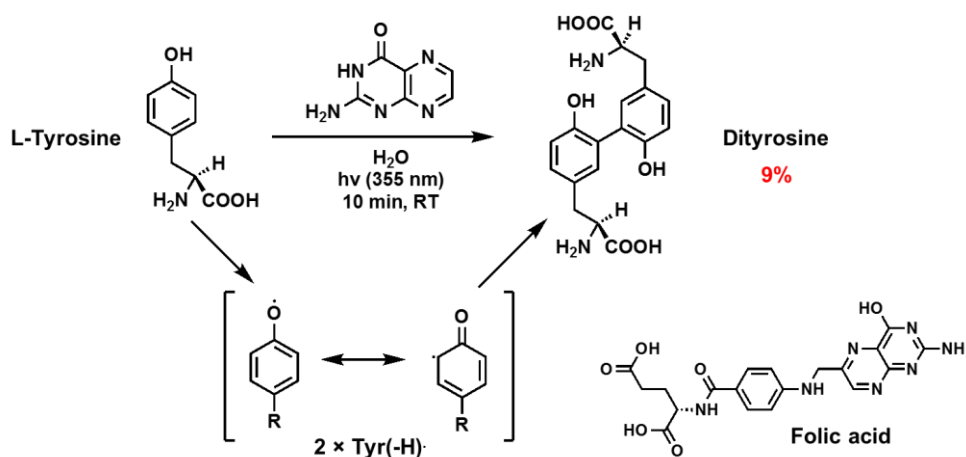


Figure 1-24: Photogeneration of phenoxy radicals with AIBN and Copper Complex

Recently, there has been a noted increase in interest in harnessing light for synthetic organic uses. Boguta and Danciewicz have demonstrated that radiation can facilitate the dimerization of Tyr through the direct absorption of light [137, 138].

After that, Reid and Thomas optimized a straight forward, one-step photocatalyzed synthesis of dityrosine using pterin or folic acid as a photocatalyst. Their process was conducted in aqueous solutions for a brief period of time while exposed to UV-A radiation [139, 140].

Figure 1-25: Generation of *o,o'*-dityrosine with Pterin or folic acid

It's interesting to note that the crosslinking of free Tyr and tyrosyl groups in proteins in a reaction photosensitized by riboflavin (Rb) has been reported to be initiated by a photocatalyzed oxidation reaction [3,21]. The suggested process in this instance was the reduction of the Rb triplet excited state by Tyr, resulting in the Rb radical anion ( $\text{Rb}^{\cdot-}$ ) and the tyrosine radical cation ( $\text{Tyr}^{\cdot+}$ ), which deprotonates to  $\text{Tyr}(-\text{H})^{\cdot}$ . Subsequent dimerization of two  $\text{Tyr}(-\text{H})^{\cdot}$  results in the production of  $\text{Tyr}_2$  [141, 142].

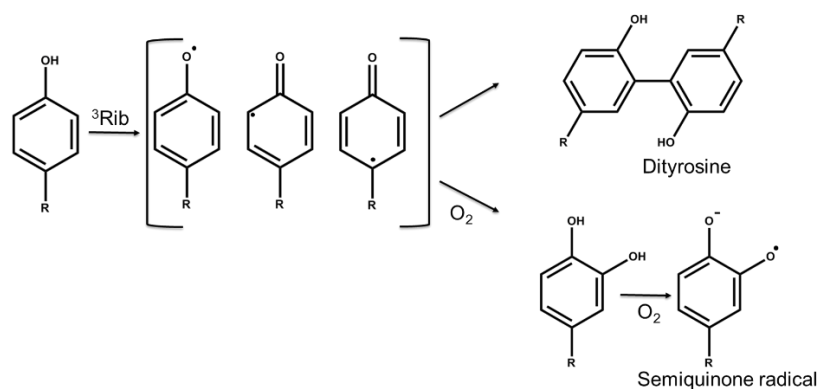


Figure 1-26: generation of dityrosine using riboflavin



## **2. CHAPTER TWO: HIGH RIBOFLAVIN SELECTIVITY FLOW PHOTO-OXIDATION OF PHENOLIC COMPOUNDS DERIVED FROM LIGNIN IN ANAEROBIC ENVIRONMENT**

### **2.1. Introduction**

In light of the global climate warming debate and the depletion of petroleum resources in the near future [5, 143], the chemicals market is exploring alternatives for biomass-based polymer synthesis [21, 144, 145], and more specifically for the substitution of benzene-based aromatic fossil compounds [146]. The Lignin is generic term for a large group of aromatic polymers (aromatic alcohols) found in plant cell walls and is the second most abundant polymer following cellulose on our planet; it is composed of three types of aromatic compounds known as monolignols, p-coumaryl alcohol, coniferyl alcohol and sinapyl alcohol [147, 148]. The complexity of the Lignin structure makes it more resistant to chemical actions, the oxidative degradation of lignin generates aromatic compounds, such as vanillin, syringaldehyde, p-hydroxybenzaldehyde, vanillic acid and syringic acid. Furthermore, ferulic acid, coumaric acid and sinapic acid can be obtained from the corresponding benzaldehydes, i.e. vanillin, p-hydroxybenzaldehyde, and syringaldehyde, respectively. These phenolic compounds have been used as bio-based building blocks, generally, connected through different C–C and C–O linkages specifically by radical coupling [147]. All the aforementioned phenolics can be used for the production of numerous polymers, e.g. epoxy resins, polyurethanes, polyesters and phenolic resins [29, 149-151].

To decrease the imprint of humans on Earth, the demand for bio-based products with low ecological impact is rocketing. Some groups of research have developed a new biobased biphenyl platform, obtained from enzymatic coupling such as divanillin and dieugenol [152], the two enzymes laccase and peroxidase are widely used for the oxidation of functional moieties as biocatalysts [12, 22, 23, 153-157], or for the oxidative coupling phenolic substrates [37, 158]. More enhancements of the processes have been applied to provide a good selectivity and yield in dimer formation using laccase as an enzymatic catalyst [42, 159].

## 2.2. Methods used for the dimerization of phenols

Currently, many research report numerous techniques for phenol dimerization; laccase has been extensively exploited as a biocatalyst for functional group oxidation or phenolic substrate oxidative coupling.

On phenolic substances, laccase does in fact produce radical intermediates that can then undergo self-coupling reactions to produce dimers, oligomers, or polymers. Many factors, including the source of the laccase, the pH, the temperature, the phenol substitution, the co-solvent, etc., affect the selectivity of the coupling and the size of the oligomers. The coupling processes can be made simpler by using a monophenol as a substrate. Nonetheless, if the phenol's ortho position does not contain a substituent, oxidative coupling can take place via a C-C or C-O bond.

The coupling preferentially takes place on the phenol and on the para-position when the phenol has two substituents in the ortho position and a free para position, producing either dimers or oligomers with a specific structure. Indeed, the oxidative polymerization of 2,6-dimethylphenol catalyzed by laccase lead to the formation of dimer [22, 23].

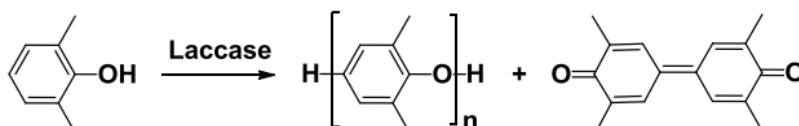


Figure 2-1: Laccase-catalyzed synthesis of poly(2,6-dimethyl-1,4-oxyphenylene) and 3,5,3',5'-tetramethyl-4,4'-diphenylquinone from 2,6-dimethylphenol

The oxidative coupling of ortho methoxy para substituted phenols yield dimers mainly. The result is typically a mixture of several dimers with traces of oligomeric structures. The most effective illustration of this is ferulic acid, the dilactone and the  $\beta$ -5 dimer represent 11% and 38% of the mixture (Figure 2-2) [160].

## High Riboflavin selectivity flow photo oxidation of phenols derived from lignin

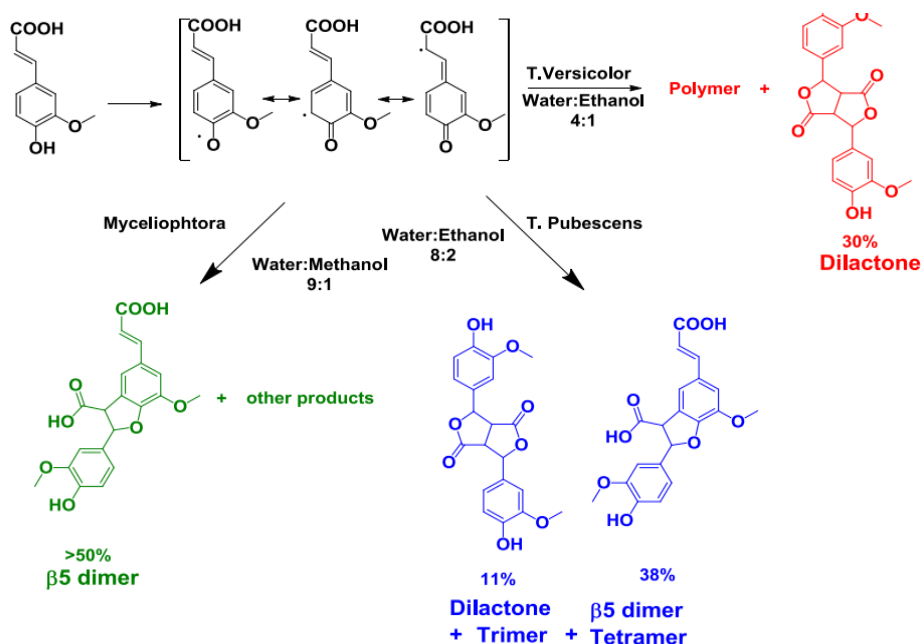


Figure 2-2: Ferulic acid oxidative coupling

Previously, diisogeunol was prepared by adding to a solution of isoeugenol an equal weight of 90% formic acid over a heating for an hour, the crystals formed were separated by suction filtering and were twice crystallized from ethyl alcohol. Yield 92%. Then when isoeugenol in acetone or cyclohexane is exposed to high pressure mercury lamp radiation for 24 hours respectively, two types of dimers are produced: dehydrodiisoeugenol and diisoeugenol. Very low yield [161].

The oxidation of isoeugenol with oxygen-laccase and iron (Ir1) chloride afford a mixture of products which is the  $\beta$ -5-coupled dehydrodi-isoeugenol is the major product of oxidation. By separating an aryl naphthalene derivative as one of the products, evidence for p-p coupling in the oxidation of isoeugenol with iron (III) chloride was obtained [162]. Additionally,  $\beta$ -O-4 coupled dehydro-dimers have been isolated from the dye-sensitized photooxidation of isoeugenol [163].

It is important to note that syringaldehyde, a p-hydroxybenzaldehyde generated from the oxidation of hardwood lignins [164], can also be effectively converted into sinapic acid by the Knoevenagel-Doebner condensation [52]. Moreover, in the case of sinapic acid, the  $\beta$ - $\beta'$  dimerization is usually followed by an intramolecular rearrangement leading to the formation of dilactone and the loss of conjugation (Figure 2-3).

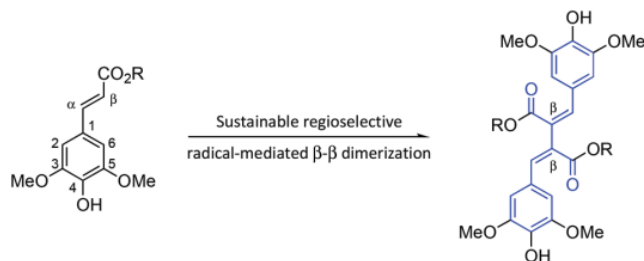


Figure 2-3:  $\beta$ - $\beta'$  dimerization of ethyl sinapate

Several synthesis pathways have been described in the literature for the synthesis of ethyl sinapate  $\beta$ - $\beta'$  dimers, the first method relied on the manganese(II) acetate,  $\text{Mn}(\text{OAc})_2$ -mediated oxidation in the presence of  $\text{NaOH}$  [165], the second pathway involved an electrochemical oxidation with tetraethylammonium hydroxide and tetramethylammonium perchlorate [166], while Benzene and potassium ferrocyanide were used in the third pathway [167].

This chapter will examine the oxidative coupling of various phenols, ranging in structure from simple to complex.

### 2.3. Generality on riboflavin

In the past, researchers have used poly- or monochromatic light sources to examine the photochemical processes brought on by photosensitizers, particularly RF. Light emitting diodes (LED) and light sent across optical fibers by LEDs, however, have recently attracted more attention and utilization. These devices have been employed in the treatment of pathological myopia and in photodynamic therapy (PDT) against skin and breast malignancies, as well as to get rid of bacterial contamination and sterilize water [168, 169].

The Riboflavin, is commonly known as Vitamin B<sub>2</sub>, which has in aqueous media four electronic excitations, one of them in the visible (blue) light range (446 nm) and the three others in the UV range (375, 265, 220 nm) [170-172]. Through this property, the Riboflavin is an efficient photo-sensitizer in a broad range of organic syntheses. Under illumination of UV and visible light, it can both by reduction and oxidation processes pick up and waste a pair of hydrogen atoms, respectively [173, 174]. It may be activated into a singlet state with a short lifetime (5 ns) and subsequently generates an excited triplet state, which is characterized by a longer lifetime (10.2 ns) and a high level of reactivity through inter-system transitions [175].

## 2.4.Mechanism of riboflavin

The UV-visible absorption spectra of riboflavin (RF) in aqueous solutions reveals two bands, one at 375 nm (UVA) and the other at 446 nm (visible area), both with large molar extinction values ( $> 10^4 \text{ M}^{-1} \text{ cm}^{-1}$ ) [176]. These bands are frequently used to activate type 1 or type 2 mechanisms for RF-based photosensitization.

For the type 1 mechanism, the excited triplet state of RF ( $^3\text{RF}_1$ ) and the substrate undergo hydrogen- or electron-transfer processes, resulting in the creation of two ionic (charged) free radicals on RF and the target molecule(s). In contrast to the free radical generated on the substrate, which has been demonstrated to either undergo further oxidation pathways mediated by  $\text{O}_2$  or dimerize to yield crosslinked products through the formation of covalent bonds.

Singlet oxygen, or molecular oxygen in its initial excited state, or  $^1\text{O}_2$ , is created in the type 2 reaction by the transfer of energy from  $^3\text{RF}_1$  to  $\text{O}_2$  [177].  $^1\text{O}_2$  can then react with a variety of biological substrates, such as proteins, unsaturated lipids, cholesterol, and nucleic acids. It is known that a number of variables, including the availability and concentration of  $\text{O}_2$ , have a significant role in determining the likelihood of these two mechanisms (type 1 or type 2) on exposure of RF to UV or visible light [178].

Ferhunde Sahbaz and Güler Somer [179] investigated photodecomposition of ascorbic acid in the presence of riboflavin under anaerobic and aerobic conditions. And for the first time they determined the formation of Hydrogen peroxide in both aerobic and anaerobic conditions.

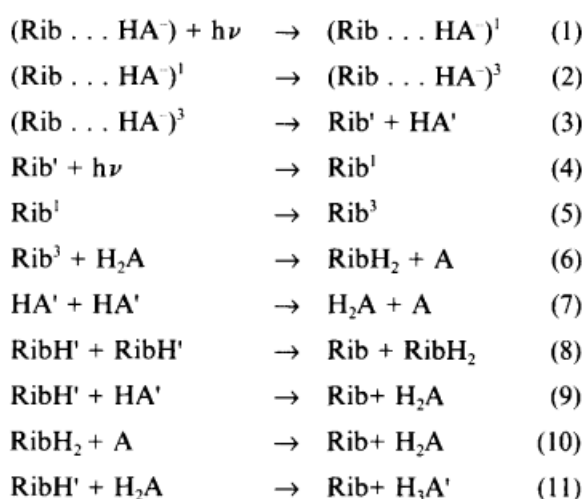


Figure 2-4 Proposed mechanism of riboflavin under aerobic conditions H2A stands for ascorbic acid, HA for the monodehydroascorbic acid and A for dehydroascorbic acid

The reaction mechanism under aerobic conditions can be given as the following:

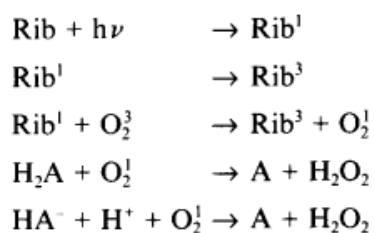


Figure 2-5 Proposed mechanism of riboflavin under anaerobic conditions

Also Strauss and Nickerson [180] proposed that photoexcited riboflavin (Rb) can split water and extract the equivalent of two hydrogen atoms to form dihydroriboflavin (RbH<sub>2</sub>) and hydrogen peroxide. This transfer, they believe, is aided by the presence of an activator (M) methionine or EDTA, which decreases the energy necessary to break the O-H bond.

The water splitting mechanism has been argued against by Holmstrom and Oster [181]. They suggest that the reaction is energetically unfavorable and that the data can be explained by a mechanism involving hydrogen transfer from the ribityl side chain of riboflavin.

In one of the first mechanistic studies on anaerobic photobleaching of riboflavin, Karrer and Meerwein [182] proposed that a primary or secondary alcoholic group at the 2'-position of the side chain coupled to the 9-nitrogen of the isoalloxazine nucleus was most suitable for photoreaction. They discovered that riboflavin is reversibly reduced during anaerobic photolysis, yielding RbH<sub>2</sub>, and that riboflavin is regenerated without loss during oxidation with air. William M. Moore and his colleagues [183] corroborated this result.

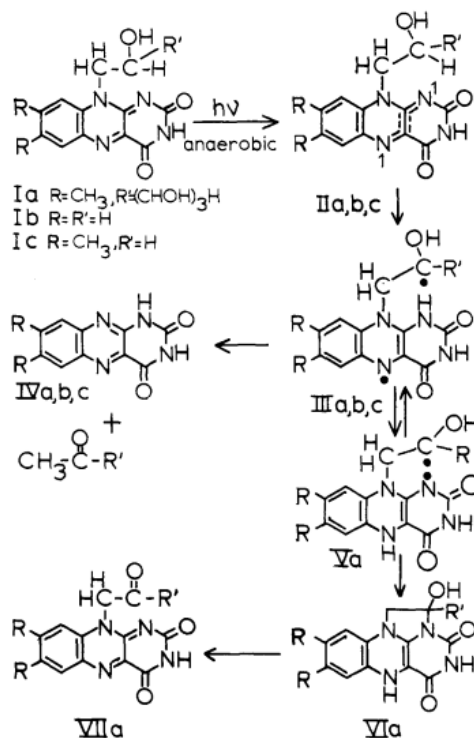


Figure 2-6 Anaerobic photooxidation of riboflavin

And recently Silva and colleagues studied the mechanism type 1 photo-oxidation of Tryptophan (Trp) and riboflavin (RF) which were used in high concentrations, together with a high intensity 365 nm light emitting diode (LED) source, under N<sub>2</sub>, 20%, and 100% O<sub>2</sub> atmospheres. Dimerization of Trp was a significant pathway under the N<sub>2</sub> atmosphere. This was likely due to several back electron transfer reactions between RF<sup>•-</sup> and Trp(H)<sup>•+</sup>. The amount of this reverse electron transfer reaction and the amount of Trp dimerization were both reduced by the presence of O<sub>2</sub>. This difference is related to the fast reaction between Trp<sup>•</sup> and O<sub>2</sub><sup>•-</sup>, which is produced by electron transfer from RF<sup>•-</sup> to O<sub>2</sub> [184].

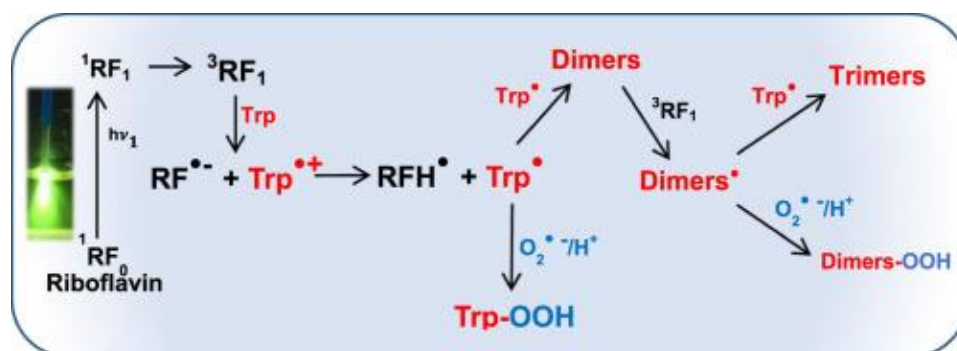


Figure 2-7: The mechanism of photo-oxidation of riboflavin and tryptophan

## 2.5. Flow chemistry

Continuous-flow photochemistry in micro-reactors is an increasingly interesting approach to researchers in academia and industry applied for organic synthesis compared to batch photochemistry as this technology provides reduced reaction times, higher selectivity, reproducibility, safely use hazardous intermediates and gaseous reactants in respect to “the principles of green chemistry” [109, 185-187]. In addition, other benefits, such as a shorter reaction time, high pressurized reaction, improved mass and heat transfer, made the procedures more reproducible and scalable [107] (Figure 2-8). Several investigators have reported the formation of phenoxy radicals in the presence of a photo-sensitizer under an UV-light or a visible light [188-190].

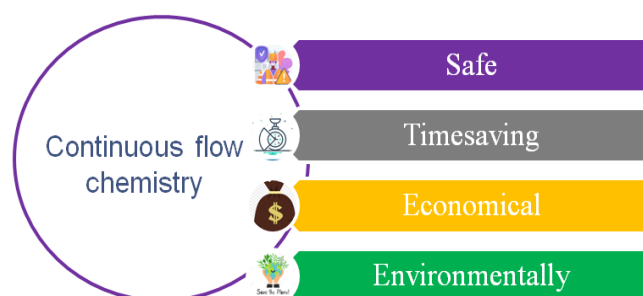


Figure 2-8: Advantages of continuous flow micro-reactor

## 2.6. Objective

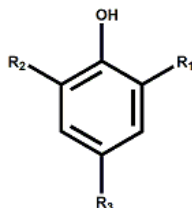
Thus, in our work, we built a “green”, simple and inexpensive micro-reactor continuous-flow system to dimerize several phenolic compounds coupled by C-C, C-O, C-O-4 or  $\beta$ - $\beta$  bond; potentially derived from lignin by oxidative coupling in large quantity, high yield and high purity and constitute interesting building blocks for the synthesis of semi-aromatic and aromatic polymers using riboflavin as “photosensitizer” under UV-light. The highlight in this study is that the dimerization of lignin phenolic derivatives by photo oxidation through a flow system is carried out in an anaerobic environment in contrast to the other metallic or enzymatic catalytic processes [191, 192].

## 2.7. Experimental part

### 2.7.1. Chemicals

Lignin phenolic derivatives and others unsaturated phenolic compounds used in this work are given in the (Figure 2-9) (*vanillyl alcohol (1), vanillin (2), eugenol(3), isogeunol(4) sinapic acid (5), methyl ester of sinapic acid (6) caffeic acid (7), 4-hydroxy-3-methoxy cinamic acid (8) coniferyl alcohol(9) and 4-hydroxybenzyl alcohol (10)*) as well as methanol and the matrix dihydroxybenzoic acid (DHB) for MALDI-TOF mass spectrometry analysis have been purchased from Sigma-Aldrich®, except the vanillin (II) from Alfa Aesar. All phenols used had a purity of ca. 98-99% and were all used as received. The ester derivative of Sinapic acid (6) has been synthesized. The Riboflavin was purchased from TCI (Tokyo Chemical Industry, Tokyo, Japan).

The deuterium solvents used for  $^1\text{H}$  NMR analysis DMSO- $d_6$  (deuterated dimethylsulfoxide) and  $\text{CDCl}_3$  (deuterated chloroform) from Eurisotop. The solvent used for silica gel separation: dichloromethane (DCM), ethyl acetate, petroleum ether, chloroform are of technical grade.



1- vanillyl alcohol:  $\text{R}_1 = \text{H}$ ,  $\text{R}_2 = \text{OCH}_3$ ,  $\text{R}_3 = \text{CH}_2\text{OH}$ ,

2- vanillin:  $\text{R}_1 = \text{H}$ ,  $\text{R}_2 = \text{OCH}_3$ ,  $\text{R}_3 = \text{COH}$ ,

3- eugenol:  $\text{R}_1 = \text{H}$ ,  $\text{R}_2 = \text{OCH}_3$ ,  $\text{R}_3 = -\text{CH}_2-\text{CH}=\text{CH}_2$ ,

4- isogeunol:  $\text{R}_1 = \text{H}$ ,  $\text{R}_2 = \text{OCH}_3$ ,  $\text{R}_3 = -\text{CH}=\text{CH}-\text{CH}_3$ ,

5- sinapic acid:  $\text{R}_1 \text{ R}_2 = \text{OCH}_3$ ,  $\text{R}_3 = -\text{CH}=\text{CH}-\text{COOH}$

6- Methyl Ester of sinapic acid:  $\text{R}_1 \text{ R}_2 = \text{OCH}_3$ ,  $\text{R}_3 = -\text{CH}=\text{CH}-\text{COOCH}_3$ ,

7- caffeic acid:  $\text{R}_1 = \text{H}$ ,  $\text{R}_2 = \text{OH}$ ,  $\text{R}_3 = -\text{CH}=\text{CH}-\text{COOH}$ ,

8- 4-hydroxy-3-methoxy cinamic acid:  $\text{R}_1 = \text{H}$ ,  $\text{R}_2 = \text{OCH}_3$ ,  $\text{R}_3 = -\text{CH}=\text{CH}-\text{COOH}$ ,

9- coniferyl alcohol:  $\text{R}_1 = \text{H}$ ,  $\text{R}_2 = \text{OCH}_3$ ,  $\text{R}_3 = -\text{CH}=\text{CH}-\text{CH}_2\text{OH}$ ,

10- 4-hydroxybenzyl alcohol:  $\text{R}_1 = \text{H}$ ,  $\text{R}_2 = \text{H}$ ,  $\text{R}_4 = \text{CH}_2\text{OH}$ ,

Figure 2-9: Lignin phenolic derivatives and unsaturated phenolic compounds used in this work

### 2.7.2. Microfluidic system

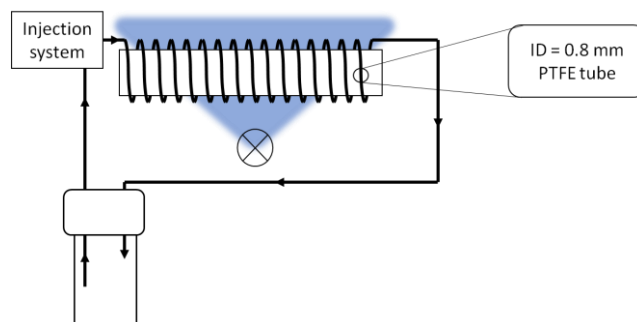


Figure 2-10: Continuous recycle microflow reactor

The continuous recycle microflow reactor was made from fluorinated ethylene propylene (PTFE) tubing (i.d.=0.8 mm, length 12 m, Cluzeau Info Labo (C.I.L.), Sainte-Foy-La-Grande, France) powered by a Corning KP-22 pump as shown in (Figure 2-10). The tube outlet was plugged in small vial (12 mL volume of solution). The volume of the tubular reactor was estimated to be 6 mL that are exposed to the UV-light at wavelength of 395 nm; the flow rate was 0.1 mL/min. The solution of phenols and photosensitizer in methanol was prepared using Schlenk technique under nitrogen. The mixture was transferred into the 12 mL vial under nitrogen atmosphere and pumped by the injection system to recycle through the reactor for 1 h. All reactions were carried out following the same equivalents and procedure.

### 2.7.3. Riboflavin purification

Riboflavin was purified on C18 column equilibrated with ACN. The column was washed several times with acidified water (0.1% FA), before loading the sample. Riboflavin (20 mg) was loaded on the column, washed several times with acidified water and eluted using different gradient including water:ACN (90:10), (80:20), (70:30), (60:40), (50:50), ACN, ACN:MeOH (50:50), followed by 100% MeOH.

#### **2.7.4. Analysis of riboflavin consumption by FT-ICR**

A solution of purified riboflavin (5 mg in 12 mL methanol) was irradiated under UV light 365 nm for different times 30 min, 1,2,4,8 and 24 h. at each time 1 ml was taken and keep it in the fridge for the final analysis. Samples were analyzed by mass spectrometry analysis.

#### **2.7.5. MALDI FT-ICR (Matrix assisted laser desorption ionization-Fourier transform ion cyclotron resonance mass spectrometry)**

A Solari XR FTICR device comprised of a dynamically harmonized cell (BRUKER Daltonics, Bremen, Germany) and a 9.4 T actively shielded superconducting magnet underwent MALDI-FT-ICR analysis. The equipment has an electrospray source and a Smartbeam II, Bruker Nd:YAG3 laser at 355 nm, source for laser desorption ionization. Positive ion MALDI-FT-ICR spectra were obtained with the mass range set at  $m/z$  200-1000 Da. A fixed 15% laser power was used. ACN/water/TFA (70:30:0.1) were used to reconstitute the  $\alpha$ -cyano-4-hydroxycinnamic acid (HCCA) matrix, at a concentration of 10 mg/mL. ACN:water (8:2), were used to dissolve the samples. 1 $\mu$ L of the mixture of samples and matrix was spotted on the target plate in a 50:50 ratio.

#### **2.7.6. Matrix-assisted laser desorption Time of Flight (MALDI-TOF) mass spectrometry**

The MALDI TOF/TOF ABI 4800 ABSciex analyser is the mass spectrometer used for MALDI-TOF analysis. The 4000 Series Explorer program is used to acquire the spectrum, and Date Explorer Software is used to analyze it. The nitrogen YAG laser used for MALDI has a 355nm wavelength and a power setting of 5000. Reflectron TOF detection and positive ionization mode are used in MALDI-TOF mass spectrometry. With an Applied Biosystems Voyager-DETM STR mass spectrometer, matrix-assisted laser desorption time of flight (MALDI-TOF) mass spectra were captured at a voltage of 20 kV. ACN/water/FA (70:30:0.1) and ACN/water/TFA (70:30:0.1) were used to reconstitute the DHB and  $\alpha$ -cyano-4-hydroxycinnamic acid (HCCA) matrices, respectively, at a concentration of 10 mg/mL. ACN:water, DMSO, or methanol were used to dissolve the samples. 1 $\mu$ L of the mixture of samples and matrix was spotted on the

target plate in a 50:50 ratio. Data Explorer Software was used to evaluate the spectra after they had been collected using 4000 Series Explorer program in positive ionization mode.

### **2.7.7. NMR measurements**

Proton and carbon magnetic resonance spectra ( $^1\text{H}$  NMR and  $^{13}\text{C}$  NMR) were recorded on a Bruker AVANCE 300 spectrometer ( $^1\text{H}$  300 MHz and  $^{13}\text{C}$  75 MHz) using tetramethylsilane (TMS) as the internal standard. Chemical shifts,  $\delta$ , are given in ppm and coupling constants in Hz.  $^1\text{H}$  NMR data are reported as follows: chemical shift, multiplicity (s = singlet, d = doublet, t = triplet, tt = triplet of triplets, td = triplet of doublets, dd = doublet of doublets, m = multiplet), coupling constants and integration. Deuterated solvents: chloroform,  $\text{CDCl}_3$ ; acetone,  $\text{CD}_3\text{COCD}_3$ ; and DMSO,  $\text{CD}_3\text{SOCD}_3$  were used. The peak of deuterated chloroforms, acetone and DMSO resonates at 7.24 ppm, 2.05 ppm, 2.50 ppm respectively.

### **2.7.8. Column Chromatography**

The purification of each product after each reaction was performed using column chromatography in silica gel (60-120 mesh) glass column. About 108 mg of crude product were solubilized in 2 ml of solvent, and loaded on to the column of 46×2 cm and eluted with the following linear gradient of solvents: 100% chloroform then 50/50 chloroform/ethyl acetate then 80/20 ethyl acetate/methanol for the products from the starting materials I, III, VIII and IX. 100% DCM up to 80/20 DCM/ethyl acetate then 80/20 ethyl acetate/ methanol. For the products from the starting materials IV, VI, and VII. For caffeic acid, we started with ethyl acetate then 80/20 ethyl acetate /methanol-chloroform followed by chloroform: methanol with increasing polarity. All the collected fractions were subjected to Thin Layer Chromatography (TLC) aluminum backed silica gel using 60 F254 plates (Sigma, South Africa). The Conditions of TLC were the same as those for fractions after silica gel column chromatography. Plates were viewed under UV light at 254 nm. And similar fractions with the  $R_f$  values were pooled and the organic solvent was removed by rotary evaporator. The solvents were used as mobile phases: dichloromethane (DCM), ethyl acetate, chloroform and methanol.

### **2.7.9. General dimerization procedure of lignin phenolic derivatives**

12 mL of methanol solution of 108 mg of lignin phenolic derivative mixed with 2.5 mg of riboflavin under nitrogen atmosphere was stirred at room temperature for 15 min. The mixture then transferred to the reaction channel inlet which connected through a programmable syringe pump to the photoreactor module in which was enclosed on the sides with reflective aluminum foil sheets and at the front with a UV shield to contain the UV light during 24 irradiation time. Upon the continuous photooxidation reaction of phenolic derivatives has been achieved, the methanol was removed from the crude product by rotatory evaporator. Each raw reaction product is purified through a chromatography column as described in paragraph 2.7.8.

### **2.7.10. Synthesis of the methyl ester of sinapic acid**

Sinapic acid (500 mg, 2.23 mmol) was dissolved in methanol (30 mL) containing 1 mL of sulfuric acid, and then the solution was heated at reflux for about 1 h. After cooling at room temperature, the solution was diluted with ethyl acetate (150 mL) and washed with an aqueous solution of NaHCO<sub>3</sub> (5% w/v) until neutral pH. The organic layer was then washed with distilled water and dried over anhydrous Na<sub>2</sub>SO<sub>4</sub>, and the solvent was removed under vacuum. The residues were constituted by the pure methyl ester. (Yield 90%)

## **2.8. Results and discussion**

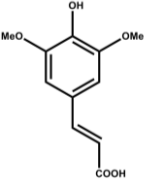
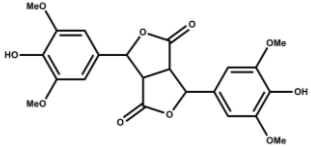
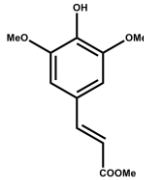
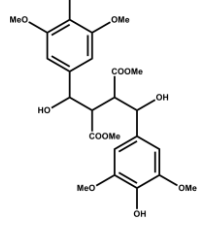
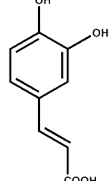
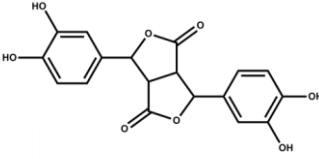
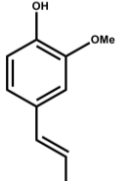
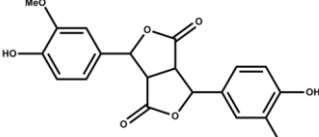
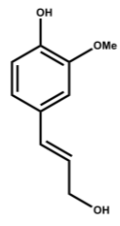
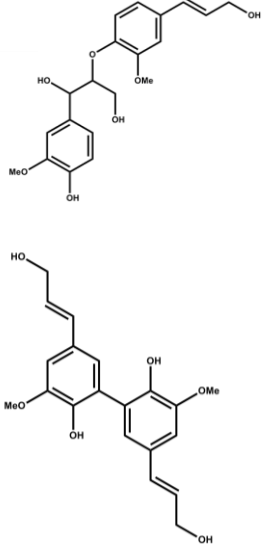
### **2.8.1. Oxidation of phenols mediated by RF photoreactions**

Ten different lignin model compounds were used to study the flow photooxidation reactions of riboflavin with lignin: vanillyl alcohol (1), vanillin (2), eugenol (3), isogeunol(4) sinapic acid (5) and its methyl ester (6), caffeic acid (7), 4-hydroxy-3-methoxy cinamic acid (8), coniferyl alcohol (9) and 4-hydroxybenzyl alcohol (10) Dimerization products from all phenolic derivatives are presented in Table 2-1 with their coupling position and their yield. Firstly, we will describe the photo-oxidation of the vanillyl alcohol (1) in order to optimize the conditions of reactions. Subsequently, we have transposed this study to the other lignin phenolic derivatives from (2) to (10).

Table 2-1: Types of couplings and yields of phenolic derivatives-dimerization products formed by continuous photooxidation

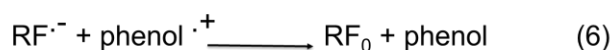
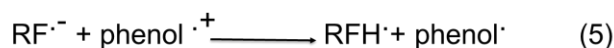
name	structure	product(s)	coupling position	Yields %
vanillyl alcohol (1)			C-C	82
vanillyl alcohol (1)+ vanillin (2)			C-C C-O-4	
4-hydroxybenzyl alcohol (3)			C-C	48
eugenol (4)			C-C	74
isogeunol (5)			$\beta$ -5'	70

*High Riboflavin selectivity flow photo oxidation of phenols derived from lignin*

sinapic acid (6)			$\beta$ - $\beta$	90
methyl ester of sinapic acid (7)			$\beta$ - $\beta$	42
caffeic acid (8)			$\beta$ - $\beta$	76
4-hydroxy-3-methoxy cinnamic acid (9)			$\beta$ - $\beta$	74
coniferyl alcohol (10)			$\beta$ -O-4  C-C	46

### 2.8.2. Proposed mechanism of riboflavin under anaerobic conditions

The exposure of riboflavin  $^1\text{Rib}$  to blue light or UV-A light results in spin-allowed transitions to highly fluorescent short-lived intermediated singlet-excited states  $^1\text{Rib}^*$  (around 5 ns at ambient temperature) equation 1. Intersystem crossing with a high quantum yield  $Q = 0.67$ , generates the triplet-excited state of the flavin  $^3\text{Rib}^*$  very efficiently and has a relatively long-lived (approximately 15  $\mu\text{s}$  at ambient temperature) equation 2 and as a bi-radical a very powerful oxidant with  $E_0 = +1.7\text{ V}$  compared to ground state riboflavin ( $E_0 = -0.3\text{ V}$ ) leading to direct oxidation of most types of biomolecules by  $^3\text{Rib}^*$  [170-172].



$\text{Phenol}^{\cdot+}$  is produced as a result of the electron transfer from phenol to  $^3\text{RF}_1$  in Reaction (3), and it will quickly deprotonate ( $\text{pK}_a$  4.3) [193] to produce neutral phenol ( $\text{phenol}^{\cdot}$ ), as well as anionic  $\text{RF}^{\cdot-}$ , which will quickly protonate to produce  $\text{RFH}^{\cdot+}$  ( $\text{pK}_a$  8.3) in Reaction (5) [194].

When  $\text{O}_2$  is not present, the main pathway for the production of such dimers is electron transfer from phenol to  $^3\text{RF}_1$ . As a result of electron delocalization around the indole ring of  $\text{phenol}^{\cdot}$  and the creation of new stereo-centers, several isomeric C-C and C-O cross-linked species are produced, giving rise to the many peaks recorded from  $\text{phenol}^{\cdot}$ .

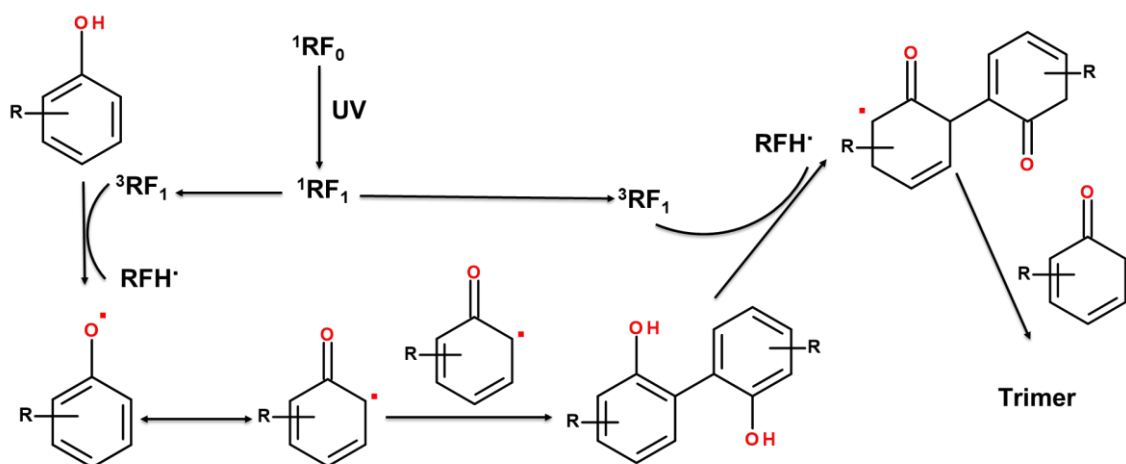


Figure 2-11: Proposed mechanism for dimer and trimer formation from phenol induced by RF photoreactions

In contrary the presence of  $O_2$ , lower steady state levels of phenol $\cdot$  are probably present because of a less effective formation (caused by energy transfer from  $^3RF_1$  to  $O_2$ ) and different removal pathways for phenol $\cdot$  (see above). As the rate of phenol dimerization depends on the phenol $\cdot$  concentration, under relatively low phenol $\cdot$  concentrations, reaction with  $O_2$  clearly becomes competitive.

### 2.8.3. Analysis of purified riboflavin consumption by FT-ICR

It was crucial to ascertain the mechanism of riboflavin before moving on to the photo-oxidation process, so an FT-ICR study was conducted to ascertain the amount of riboflavin consumed during irradiation. When we first evaluate commercial riboflavin without purification; it is surprising that there are extra peaks other than the typical peak of riboflavin  $m/z$  377.14559 (Figure 2-12), this indicates that these peaks correspond to contaminants. For this purpose, we chose to purify commercial riboflavin using a C18 column. Various gradients were utilized, starting with a 90:10 water:ACN mixture and decreasing to 50:50 water:ACN; The pure product was released in the 70:30 water:ACN fraction.

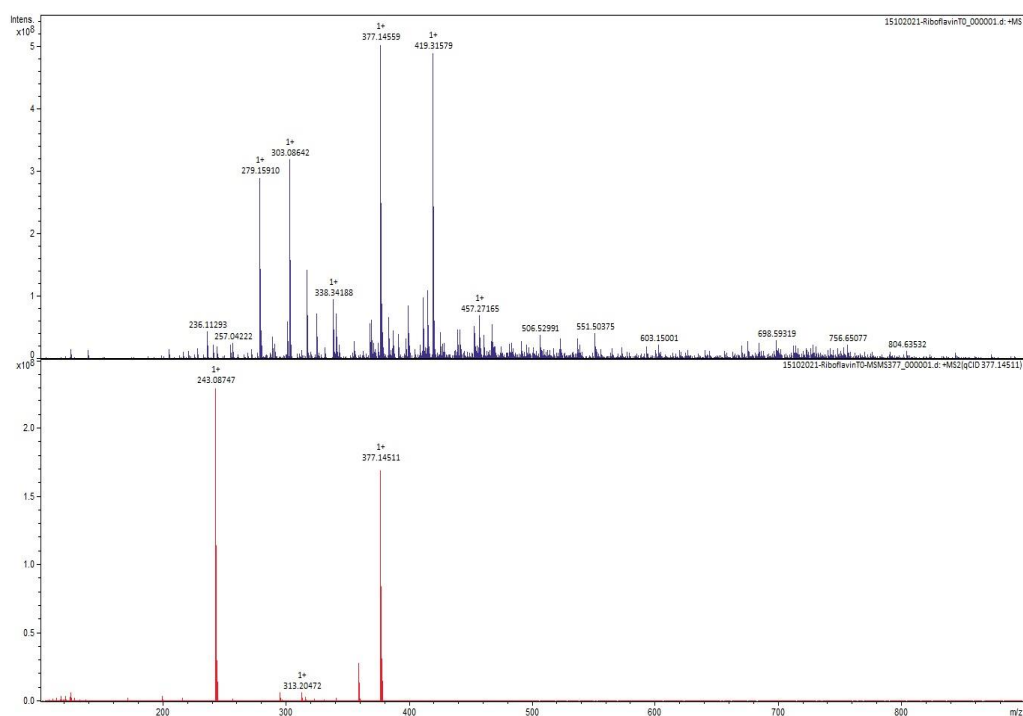


Figure 2-12: MALDI-FT-ICR of non-purified riboflavin

At time 0, there are two characteristic peaks with  $m/z$  377.14557 and 378.15336 (Figure 2-13), which correspond to the initial form and hydrogenated form RFH, respectively, of Riboflavin. After an hour of irradiation, new peaks corresponding to RF-derived products appeared, such as  $m/z$  376.1378, which corresponds to the dehydrogenated form. And over the next 24 hours, we noticed that all of the peaks formed during the irradiation had disappeared from the spectrum and were replaced by the peak  $m/z$  379.0925 that corresponds to the doubly charged form. We also noticed the presence of a new peak with the MS 394.1483, which corresponds to the oxidized form of riboflavin (gain one oxygen).

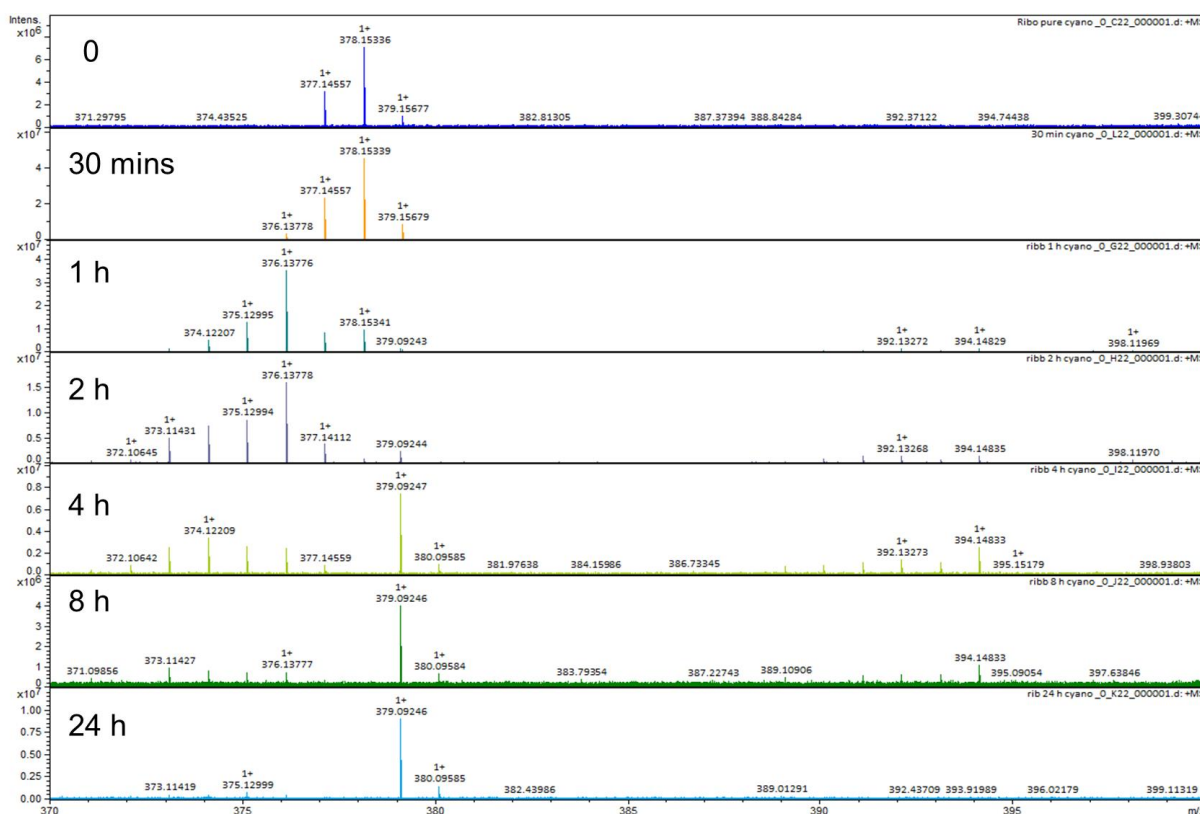


Figure 2-13: Purified riboflavin's FT-ICR spectra after exposure to UV light at various times

#### 2.8.4. Flow photo-oxidation of vanillyl alcohol

As a consequence of the complexity of the chemical structure of lignin, the reactions are most often performed through model compounds. All investigations carried out so far, whether in the case of enzymatic catalysis or by photooxidation with riboflavin converge on the same mechanism. The enzyme catalyzes the oxidation of phenol to a phenoxy radical which can then combine to form dimeric or polymeric products. Thus, the radical  $\text{PhO}^{\bullet}$  recombination occurs in two stages: at the first stage, which is reversible, keto dimer is formed; at the second stage, dienone–phenol rearrangement of the keto dimer with the formation of a dimeric phenol compound. The general mechanism for the recombination of lignin phenolic substrates in both cases is given in (Figure 2-14) [192, 195].

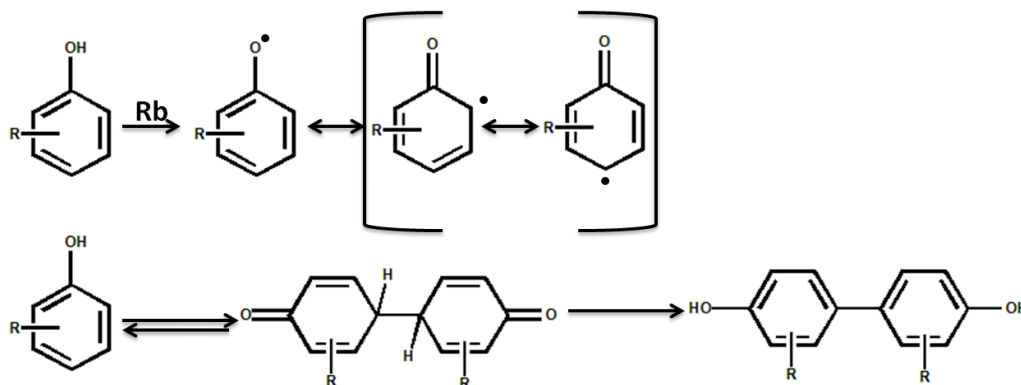


Figure 2-14: The general mechanism for the recombination of lignin phenolic substrates.

From previous studies [43, 196, 197] carried out on vanillyl alcohol (1) by enzymatic oxidation, it is assumed that there are three different products that are initially formed from the two phenoxy radicals of vanillyl alcohol (1): the 5-5' dimer (1a), the 5-O-4' dimer (1b), and vanillin (1c) as shown in (Figure 2-15). The presumed reaction pathways for the formation of each product are explored by Spilä et al [44]. It is commonly mentioned that the coupling of two phenoxy radicals leads to the formation of a quinone, which is rearomatized as the final product as shown in (Figure 2-14).

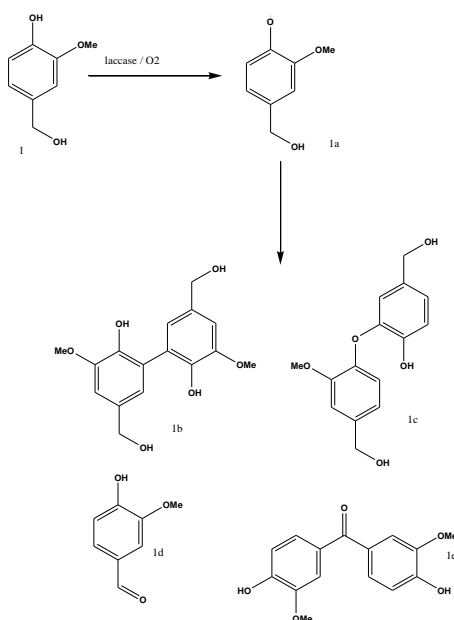
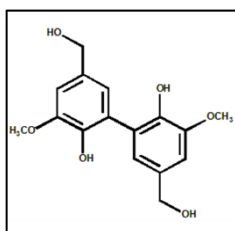


Figure 2-15: The products that were previously reported in the laccase-catalyzed oxidation of vanillyl alcohol [43, 196, 197].

In contrast to the previous studies, in our work only the 5-5' dimer coupling has been obtained at higher yield around 80 % by flow photo-oxidation of vanillyl alcohol (1) using riboflavin as photosensitizer. In our knowledge the high riboflavin selectivity toward the dimer 5-5' coupling have been observed for the first time and no side product have been detected with this flow process. It seems in this work that riboflavin catalyzes the photo-oxidation in anaerobic medium in a fluidic system giving rise exclusively to the dimer (1b) by excluding the formation of the dimer (1c) and the vanillin (1d) in contrast to the enzymatic laccase catalyst in the presence of oxygen [197]. The  $^1\text{H}$  NMR (Figure 2-16) compared to the starting material (1) confirms the formation of such a dimer by the appearance of two doublets at 6.73 and 6.93 ppm respectively, corresponding respectively for  $\text{H}_{1,1'}$ ,  $\text{H}_{2,2'}$ . The high symmetry of doublets in aromatic zone indicates exclusive formation of the dimer (1b), the  $^{13}\text{C}$  NMR (Figure 2-17) and HSQC NMR (Figure 2-18) of such dimer (1b) have been also performed and are in perfect agreement with its  $^1\text{H}$  NMR spectrum (Figure 2-16).



$^{13}\text{C}$  NMR spectra of divanillyl alcohol (DMSO):  $\delta$  ppm 57.5; 56 (s,  $\text{CH}_2$ ), 63; 74.6(s,  $\text{CH}_3$ ), 110;111;121;124.5 (s, CH), 125;125.3;127.5;137.5;140;141;148;148.2 (s, C).

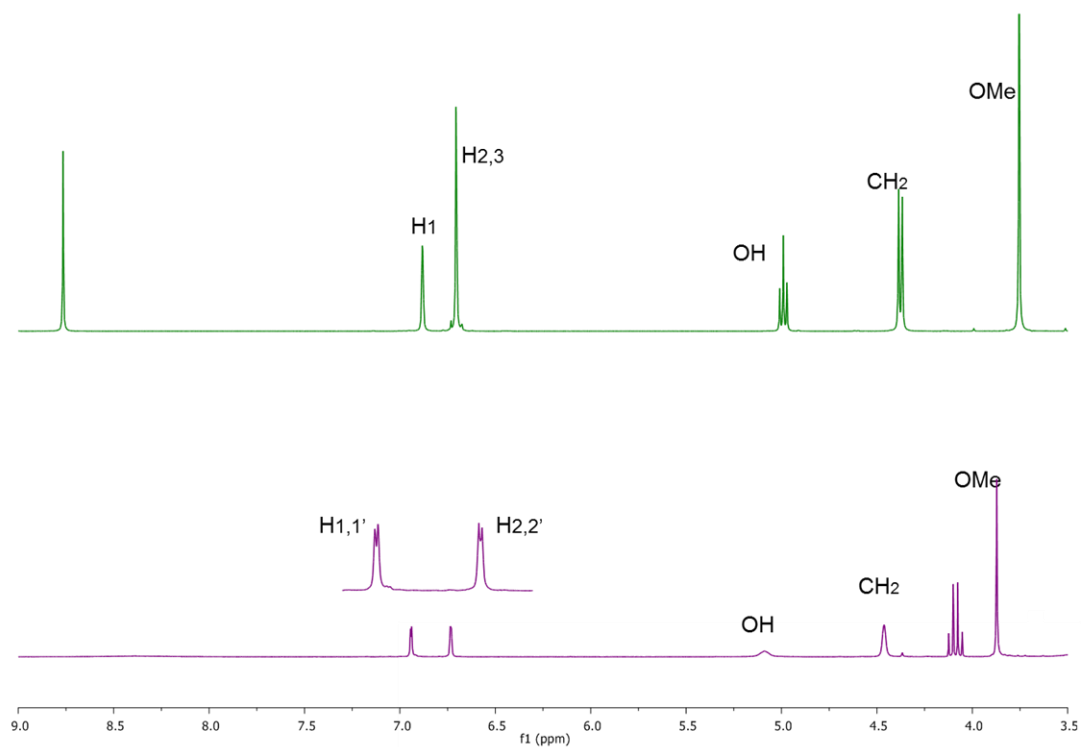


Figure 2-16:  $^1\text{H}$  NMR of vanillyl alcohol (a) and divanillyl alcohol (b)

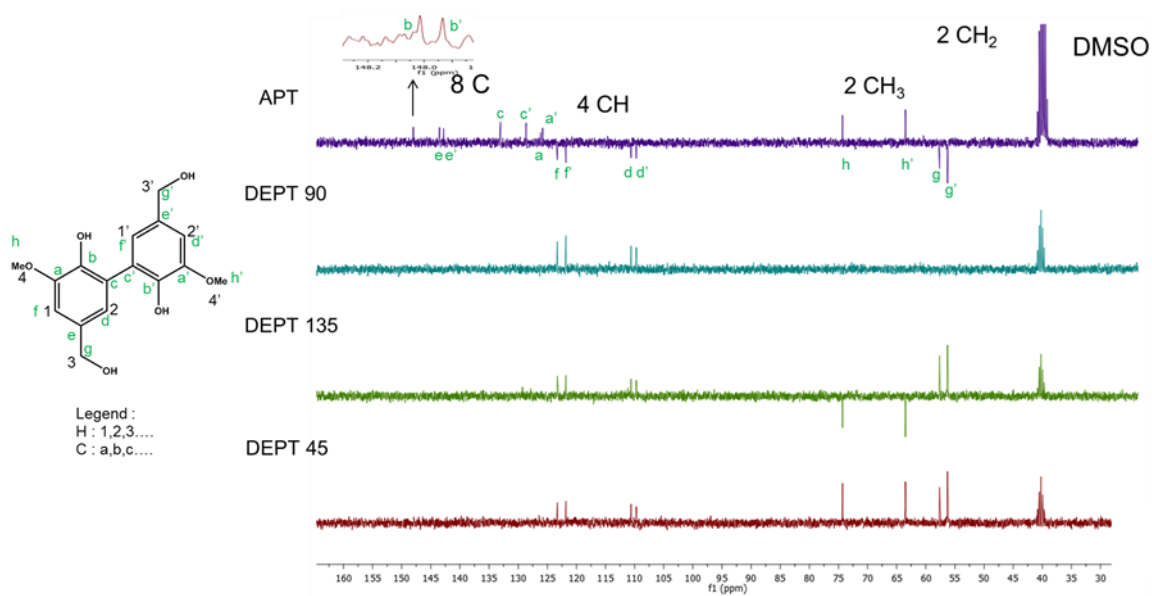


Figure 2-17:  $^{13}\text{C}$  NMR spectra of divanillyl alcohol

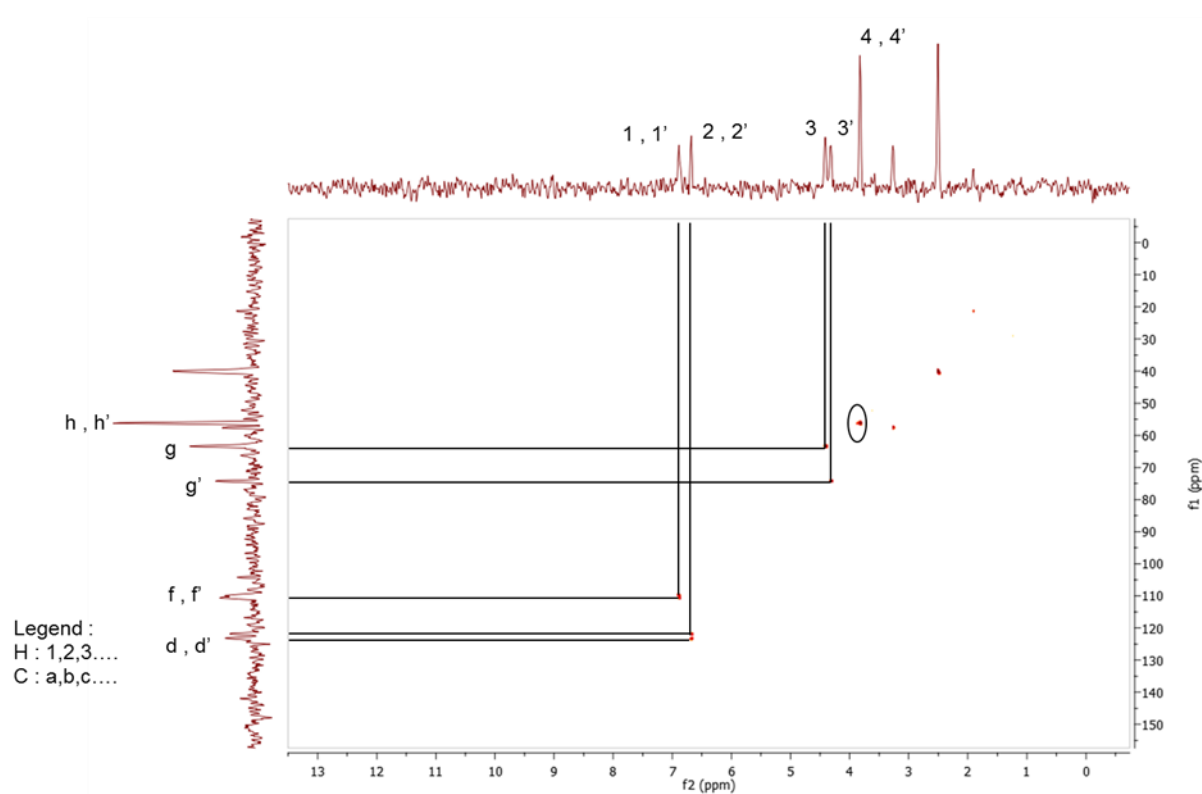


Figure 2-18: HSQC NMR for divanillyl alcohol

The MALDI-TOF mass spectrum revealed peaks correspondent to the C–C coupled divanillyl alcohol carrying  $\text{Na}^+$  or  $\text{K}^+$  that appeared at  $m/z = 329.0423$ , and  $345.00$  respectively (Figure 2-19).

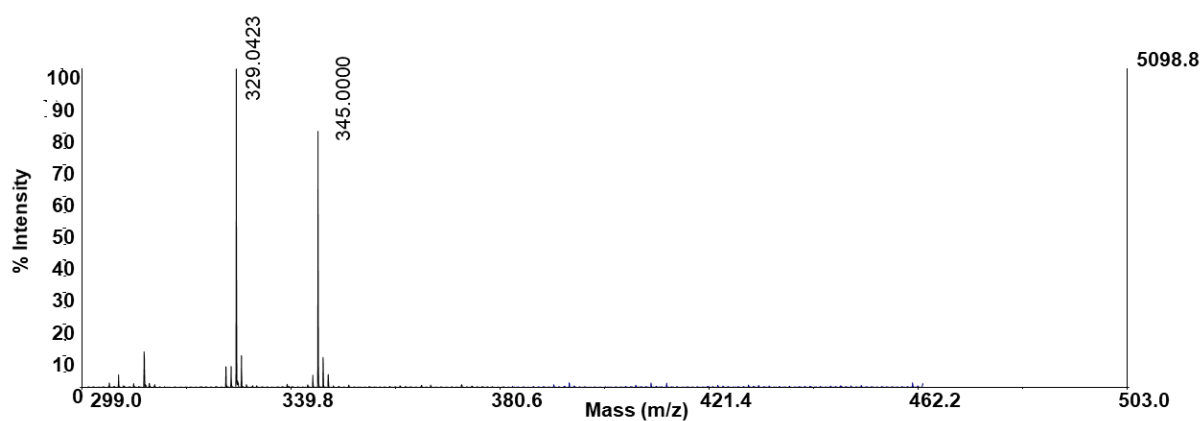


Figure 2-19: MALDI-TOF spectrum of C-C coupled divanillyl alcohol

### **2.8.5. Reaction conditions studied on vanillyl alcohol**

In this work, we explored the influence of different parameters (pH, flow rate and time duration). Thus, some experiments were carried out by varying the pH; at alkaline pH around 9 with addition of triethylamine or aqueous NaOH solution to the reaction mixture, no reaction took place; in acid medium at pH 4 by adding the acetic acid, only 45% yield was obtained, however, the 80% yield was achieved only at neutral pH. The effects of the flow rate on the yield of conversion were performed. The flow rate is an important factor which indicates for how long the reaction mixture is exposed to the UV light. These experiments concluded that the highest rate of conversion with a flow rate of 0.1 mL/min. The reaction time duration was also investigated in this work by programming reaction time intervals of 20 minutes, 1 hour, 2, 4, 12 and 24 hours. This study showed that the yield of the flow photo oxidation reaction of vanillyl alcohol in the presence of riboflavin increases as the reaction time duration also increases, however, beyond 24 hours, the formation of a precipitate may cause problems at the pump.

### **2.8.6. Substrate screening**

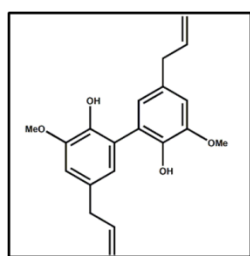
The previously described photo-dimerization using Riboflavin as photo-catalyst was extended to several substrates of lignin phenolic compounds for the selective formation of dimers by a flow photo-oxidation process. The dimerization of ortho-methoxy phenolics with different para-substituents, with the exception of phenolic derivatives (3) and (7), was explored.

The reaction mixture of vanillin (2) and vanillyl alcohol (1) in methanol afforded exclusively mixtures of dehydro-dimers which were separated by silica gel chromatography using chloroform, ethyl acetate and methanol. This reaction afforded two types of dimers, one by 5-5' (C-C) coupling product, and the other by C-O-4 coupling (Table 2-1).

according to Kyosti V. Sarkanen and Adrian F. A. Wallis the reaction of both (*E*)- and (*Z*)-isoeugenol with 1 equiv. of hydrogen peroxide in aqueous acetone containing peroxidase afforded exclusively mixtures of dehydro-dimers which were separated by silica gel chromatography [161, 163].

However, in our work, the photo-dimerization of eugenol (3) and isoeugenol (4) occurred without any side product and with high yield around 74%. The <sup>1</sup>H NMR confirms the formation

of dieugenol coupled by  $\beta$ - $\beta$  linkage (Figure 2-20 b), its show the appearance of two doublets of the aromatic protons with integration 2 in the range of 6.5 to 7 ppm in benefit of a set of several signals in the same chemical shift zone with a 3 proton integration (Figure 2-20 a). In addition, the MALDI-TOF mass spectrum of dieugenol revealed peaks correspondent to the C-C coupled carrying  $H^+$ ,  $Na^+$  or  $K^+$  that appeared at  $m/z = 326.1708$ ,  $349.1515$  and  $365.1118$  respectively (Figure 2-21).



(a) Eugenol: MW =164 g/mol.  $^1H$  NMR (400 MHz,  $CDCl_3$ , (ppm)): 6.86 (d, 1H Ar), 6.82 (dd, 1HAr), 5.93(q, 2H CH- $CH_2$ ), 5.07 (d, 2H cis CH- $CH_2$ ), 5.01 (d, 2H trans CH- $CH_2$ ), 3.77 (s,  $OCH_3$ ), 3.27(d, 2H  $CH_2$ ).

(b) Dieugenol: MW = 326 g/mol.  $^1H$  NMR (400 MHz,  $CDCl_3$ , (ppm)): 6.73 (d, 2H Ar), 6.75 (d, 2HAr), 6.01 (q, 2H CH- $CH_2$ ), 5.13 (d, 2H cis CH- $CH_2$ ), 5.08 (d, 2H trans CH- $CH_2$ ), 3.79 (s,  $OCH_3$ ), 3.37(d, 2H  $CH_2$ ).

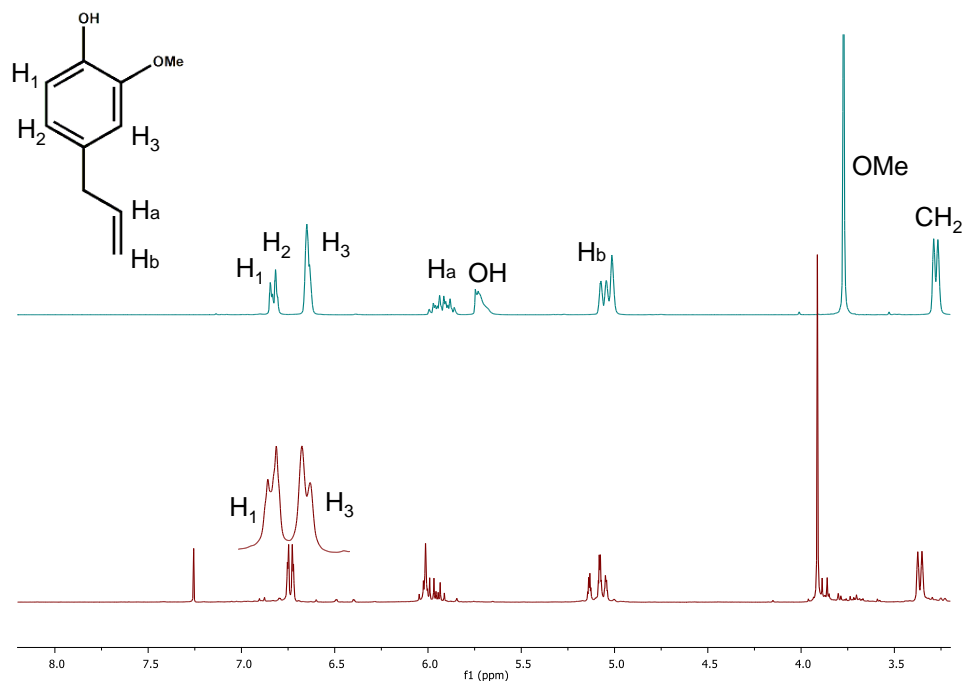


Figure 2-20:  $^1H$  NMR of (a) eugenol and (b)dieugenol

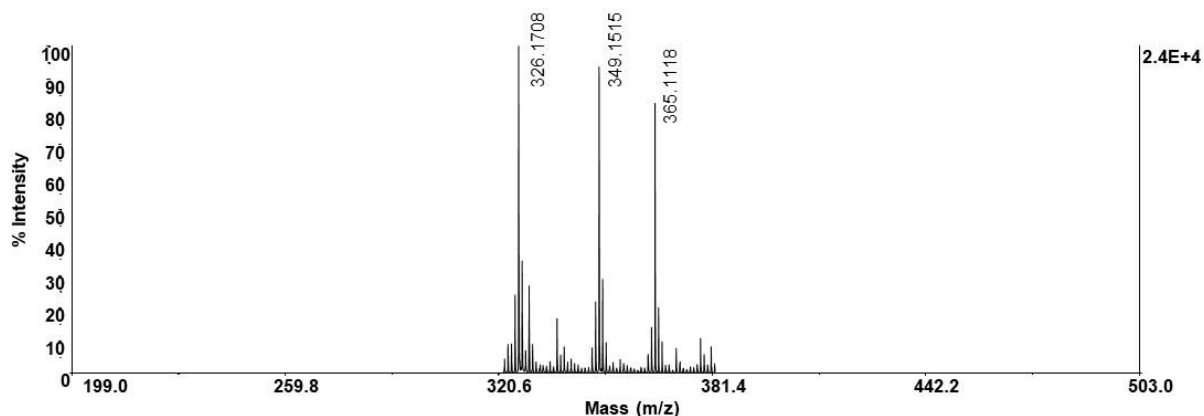
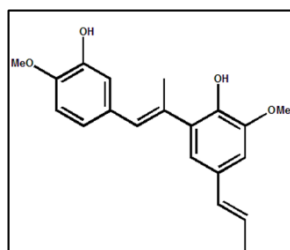


Figure 2-21: MALDI-TOF of dieugenol

But in the other hand the  $^1\text{H}$  NMR of diisogeunol showed the formation of  $\beta$ -5 linkage because of the absence of the peak corresponding to the  $\beta$  position and the MALDI-TOF spectrum confirmed the diisogeunol formation, it shows a revealed peaks correspondent to the  $\beta$ -5 coupled carrying  $\text{Na}^+$  or  $\text{K}^+$  that appeared at  $m/z = 349.1499$  and  $365.1221$  respectively.

The lack of higher molecular weight products suggests that the isoeugenol monomer is being oxidized more quickly than its reaction products, which accounts for the lack of oligomers or side products.



Disogeunol: MW = 326 g/mol.  $^1\text{H}$  NMR (400 MHz,  $\text{CDCl}_3$ , (ppm)): 6.93 (d, 1HAr), 6.88 (dd, 1H Ar), 6.84 (d, 1HAr), 6.38 (d, 1HAr), 6.34 (d, 1HAr), 6.14 (q, 1H CH- $\text{CH}_2$ ), 6.07 (q, 1H CH- $\text{CH}_2$ ), 5.74 (m, 1H CH- $\text{CH}_3$ ), 5.08 (d, 2H  $\text{CH}_2$ ), 3.92 (s,  $\text{OCH}_3$ ), 1.90 (dd,  $\text{CH}_3$ ), 1.95 (dd,  $\text{CH}_3$ ).

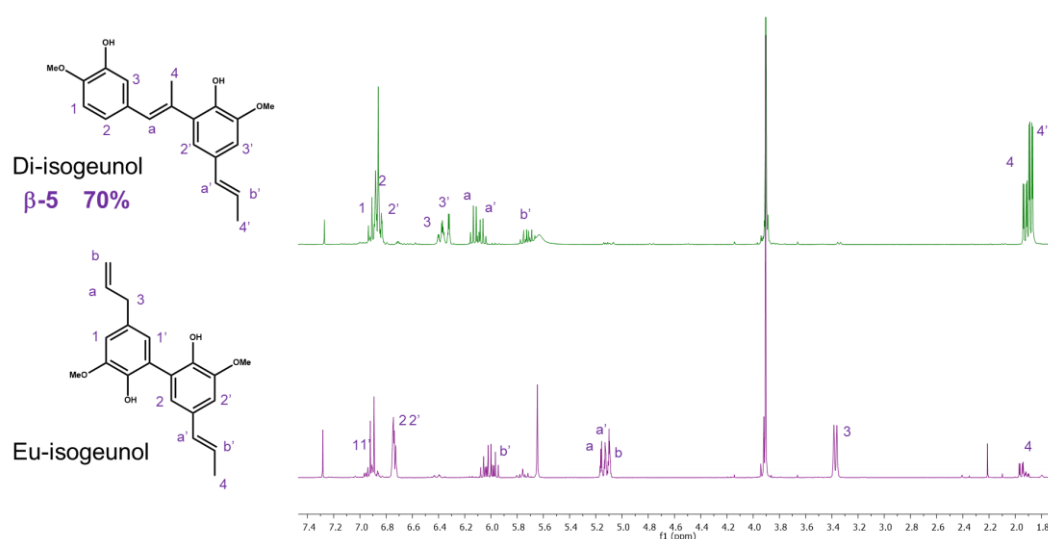


Figure 2-22:  $^1\text{H}$  NMR of diisogeunol

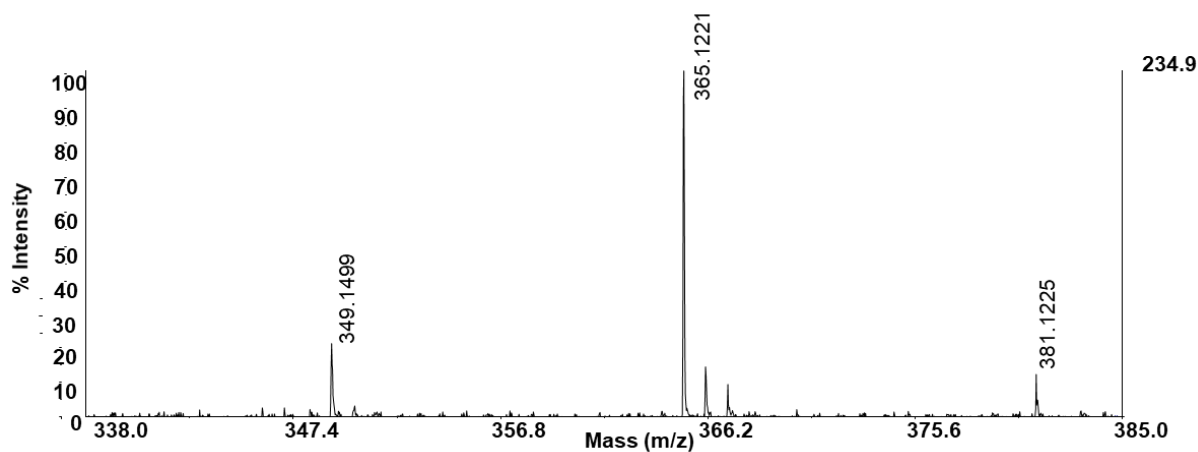


Figure 2-23: MALDI-TOF of di-isoeugenol

In those substrates with a para substituent with a double bond conjugated to the aromatic ring, the lignin model compounds (6) to (9).

The methyl ester of sinapic acid (6) was effectively synthesized from its acid (5), with a high yield of 90%. The NMR spectra displays a new peak about 3.7 ppm, which corresponds to the new methoxy group (Figure 2-24).

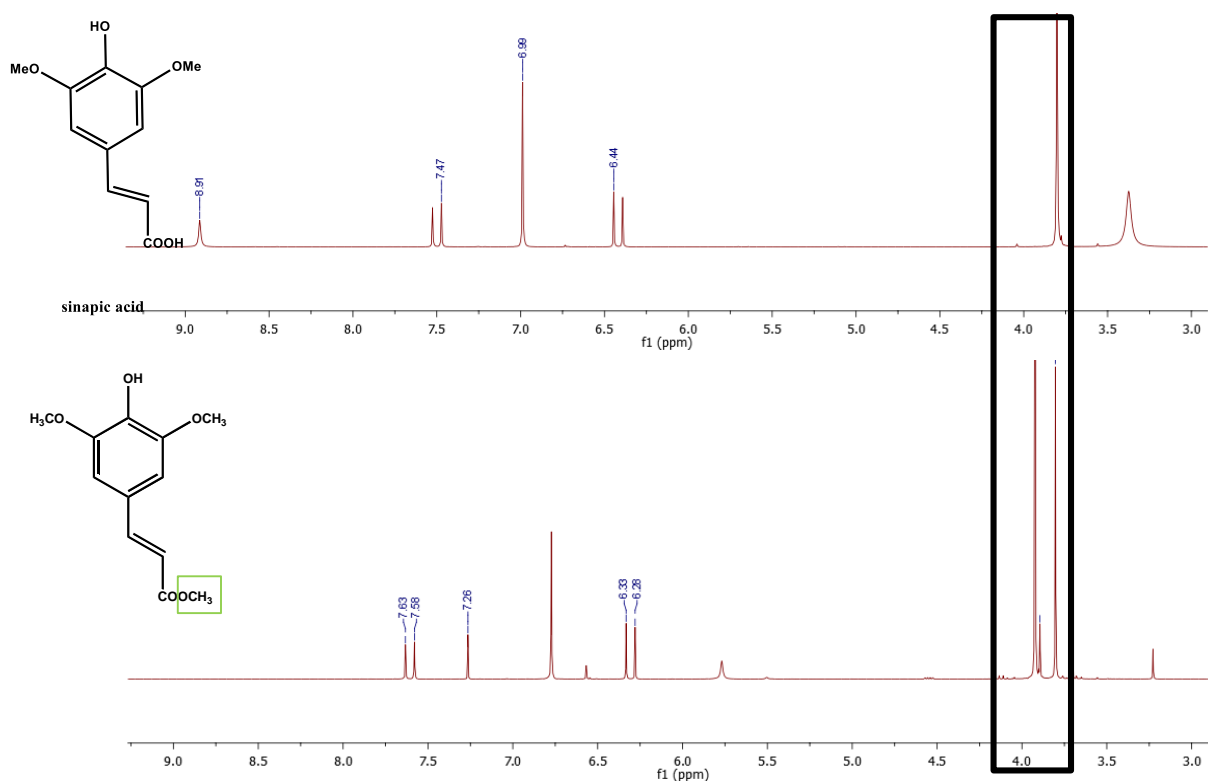


Figure 2-24:  $^1\text{H}$  NMR spectra of methyl ester of sinapic acid (6)

The radical produced by riboflavin flow photo-oxidation under UV light is delocalized over the extended  $\pi$ -system. This conjugation contributes to the formation of further coupling products. As the mechanism shows in (Figure 2-25). The photo-oxidation of the hydroxyl group in phenol acid's para position produces a radical. The lone electron on the subsequent radical can occupy different positions through resonance stabilization. C-C linkage of two phenoxy radicals with unpaired electrons at  $\beta$  positions results in the formation of the  $\beta$ - $\beta$  coupling dimer (Figure 2-26).

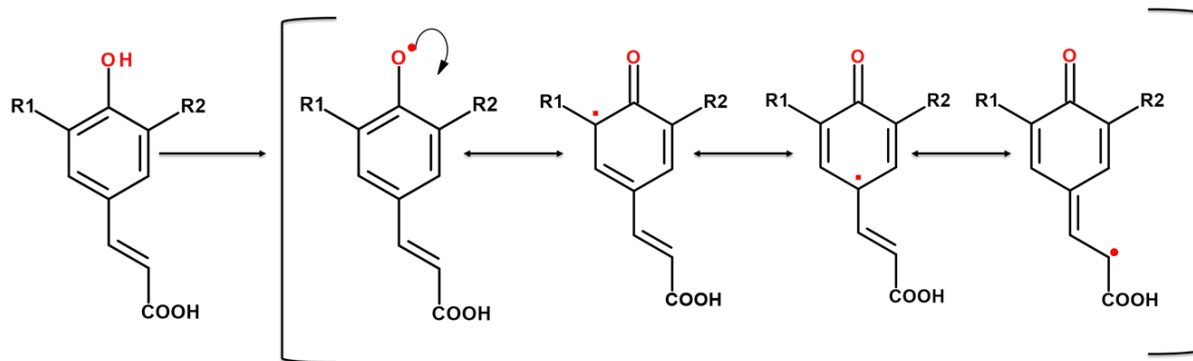


Figure 2-25: mechanism of the mesomeric forms I-V of the phenoxy radical

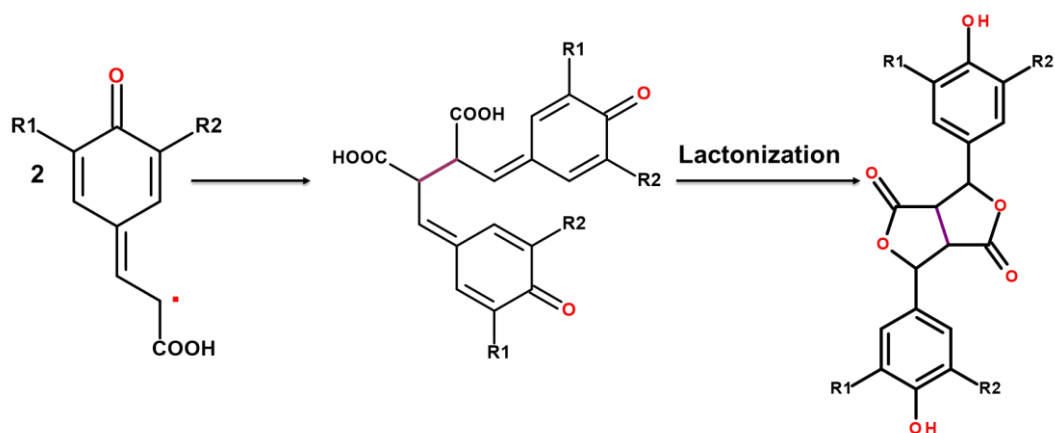
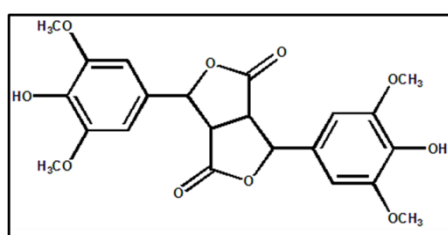


Figure 2-26: Possible combination of phenoxy radicals of 4-hydroxypropanoic acids. The resulting primary bond is shown in the purple color.

However, because there are two radical species and consequently two potential dimers  $\beta$ -O-4' and  $\beta$ - $\beta'$  that can oligomerize further, it is challenging to synthesize  $\beta$ - $\beta'$  resinol dimers of sinapic acid derivatives in good yield and purity through radical-radical coupling. As an example of highly selectively  $\beta$ - $\beta'$  coupling, the  $^1\text{H}$  NMR spectrum of the riboflavin photo-oxidation product of sinapic acid (6) in the photo flow chemistry obtained in a very good yield of about 90%, shows by comparing with the starting material  $^1\text{H}$  NMR spectrum, the disappearing signals of the ethylene protons at  $\delta = 6.44$  and  $7.47$  ppm respectively in benefit of a new signal around  $\delta = 4.7$  ppm which corresponds to a proton from a  $\text{sp}^3$  hybridized carbon ( $\beta$ - $\beta'$  resinol) and around  $\delta = 5.7$  ppm corresponds to the two protons who are next to the  $\beta$ - $\beta'$  linkage (Figure 2-27).



(a) sinapic acid  $^1\text{H}$  NMR ( $\text{CDCl}_3$ ):  $\delta$  3.80 (s, 3H), 6.44 (d, 1H), 6.99 (s, 2H), 7.47 (d, 1H), 8.91 (s, COOH).

(b) Dimer of sinapic acid  $^1\text{H}$  NMR ( $\text{CDCl}_3$ ):  $\delta$  3.78 (s, 3H), 6.70 (s, 4H), 8.91 (s, COOH).

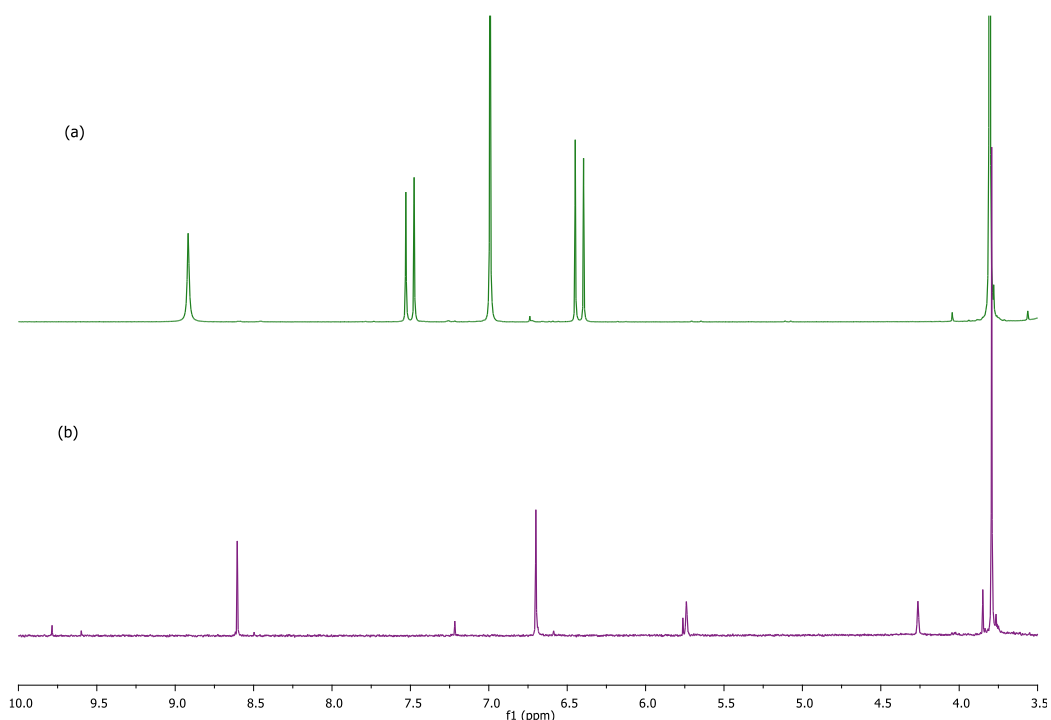


Figure 2-27: <sup>1</sup>H NMR spectra of sinapic acid (5) and of sinapic acid  $\beta$ - $\beta$  coupling dimer

We chose to purify the commercial riboflavin before rerunning all the photo-oxidation studies with it because the preliminary NMR spectra of the sinapic acid dimer revealed some contaminants. The (Figure 2-28) shows the purer dimer.

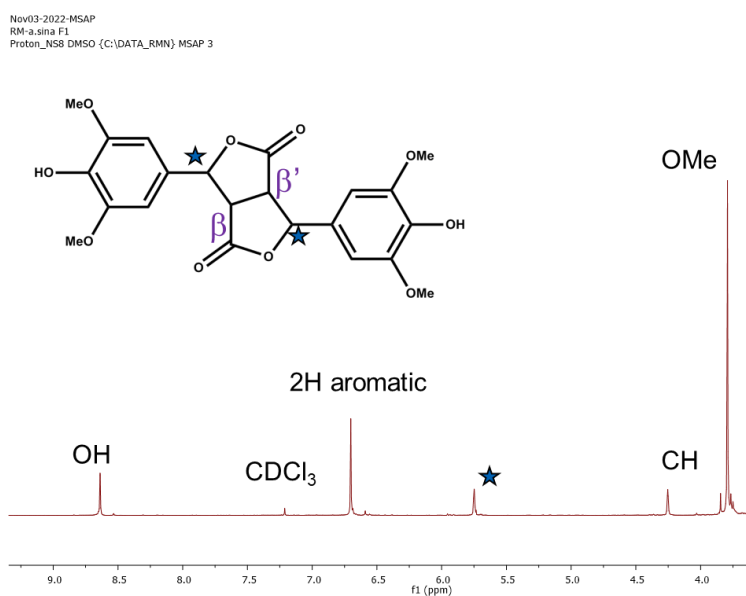


Figure 2-28: <sup>1</sup>H NMR spectra of sinapic acid (5) and of purified sinapic acid  $\beta$ - $\beta$  coupling dimer

We validated the structure of the dimer created using Allais F. and his colleagues' research [54] who focus on the dimerization of sinapate esters in the environmentally friendly solvent Cyrene toward sustainable antioxidant and anti-UV components. When our NMR spectra were compared to those of the dimers created by these groups, it was discovered that none of their dimers underwent cyclization or lactonization after stopping at the dimerization step.

We then performed a MALDI-TOF analysis in order to further establish the structure of our dimers, and as can be seen in the (Figure 2-29) there is two MS  $m/z$  469.0353 and 485.0024, these values match, respectively, to the dimer of sinapic acid with  $\text{Na}^+$  and  $\text{K}^+$  and have the formula  $\text{C}_{22}\text{H}_{22}\text{O}_{10}$ .

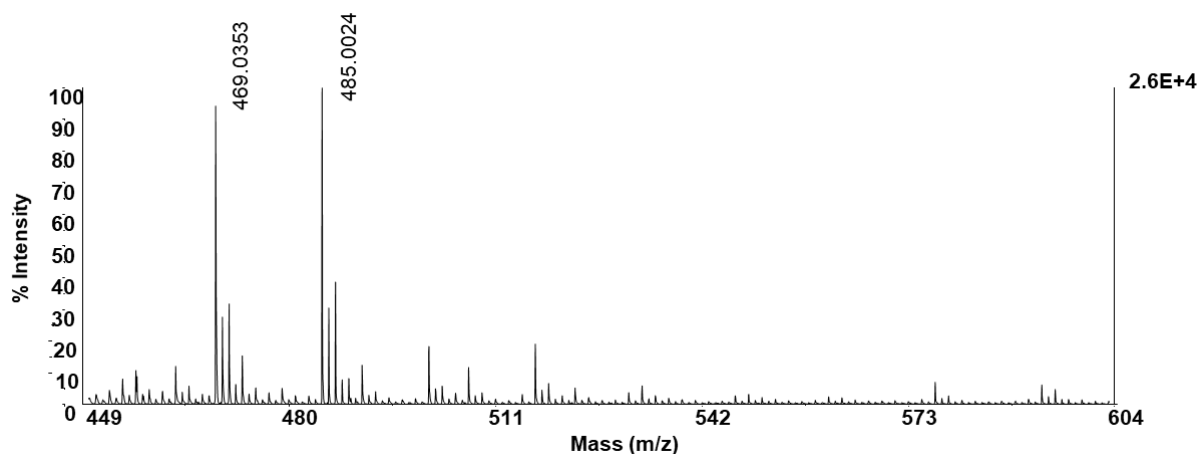


Figure 2-29: MALDI-TOF of  $\beta$ - $\beta'$  dimer resulting from the oxidative dimerization of sinapic acid (5)

The coupling of such two radicals results in  $\beta$ - $\beta'$  creation of a novel bond bridging the two monomers. In this context, a sustainable and highly selective biomimetic  $\beta$ - $\beta'$  dimerization of phenol acid has been successfully synthesized for the four lignin phenolic derivatives (6), (7) and (8).

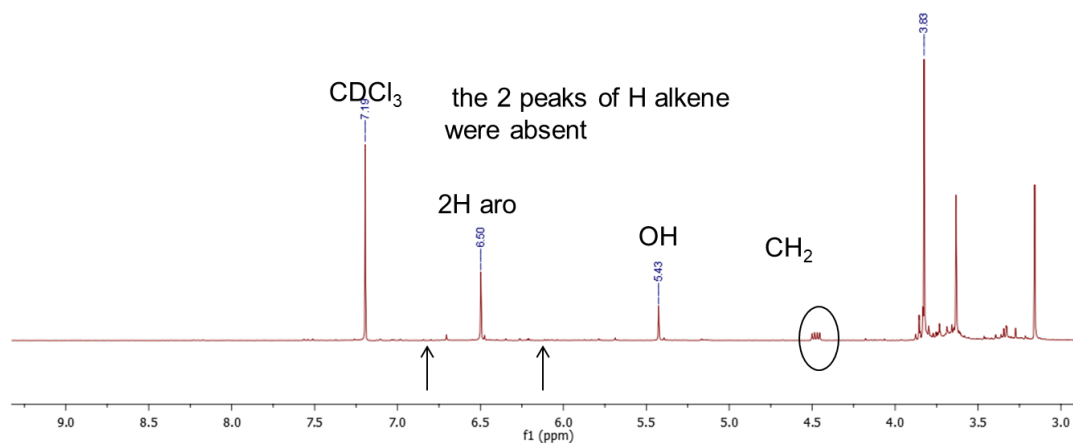


Figure 2-30:  $^1\text{H}$  NMR of methyl ester dimer of sinapic acid

Methyl ester of sinapic acid  $^1\text{H}$  NMR ( $\text{CDCl}_3$ ):  $\delta$  3.80 (s, 3H), 3.92 (s, 3H), 6.28 (d, 1H), 6.77 (s, 2H), 5.77 (s, 1H), 7.58 (d, 1H).

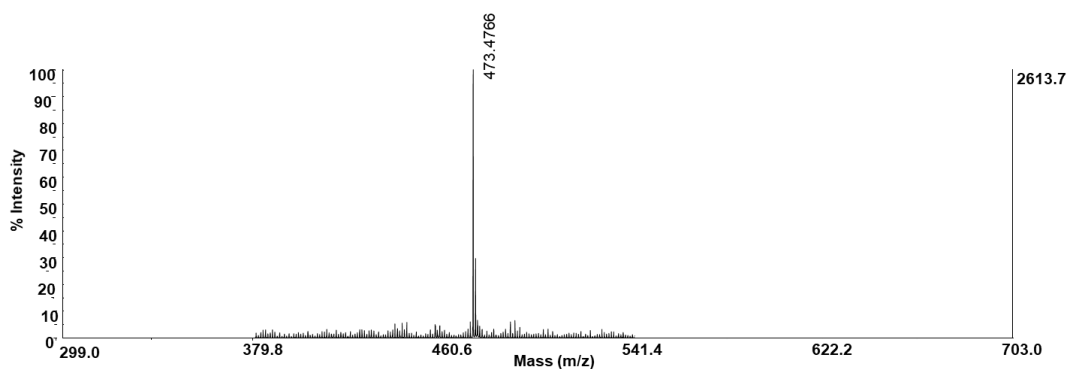
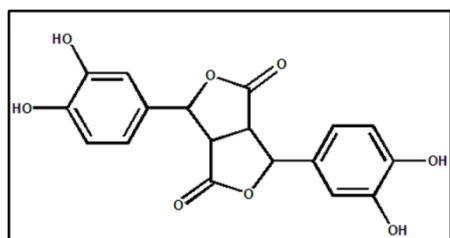


Figure 2-31: MALDI-TOF spectrum of the dimer of methyl ester of sinapic acid (6)



(a) caffeic acid: MW = 180 g/mol.  $^1\text{H}$  NMR (400 MHz, DMSO, (ppm)): 7.01 (d, 1H Ar), 6.98 (dd, 1H Ar), 6.54 (d, 1H Ar), 6.21 (d, 1H CH=CH), 7.45 (d, 1H CH=CH).

(b) caffeic acid coupled by  $\beta$ - $\beta$  bond: MW = 394 g/mol.  $^1\text{H}$  NMR (400 MHz, DMSO, (ppm)): 6.75 (d, 1H Ar), 6.65 (dd, 1H Ar), 6.84 (d, 1H Ar), 4.02 (dd, 2H  $\text{CH}_2$ ), 5.53 (s, OH), 9.03 (s, COOH)

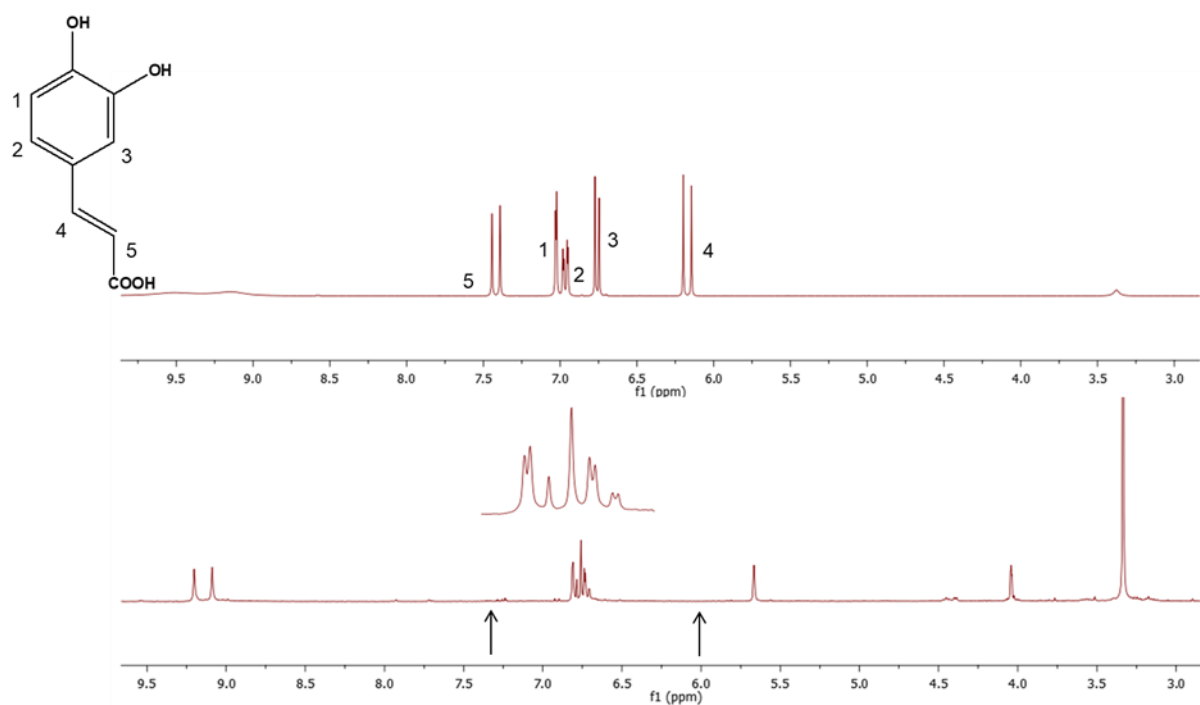


Figure 2-32:  $^1\text{H}$  NMR spectra of caffeic acid (7)

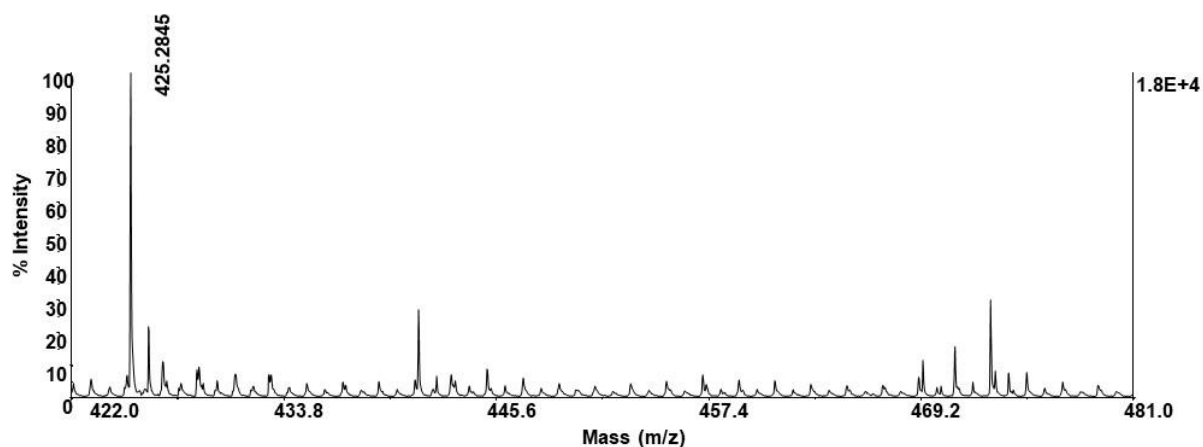
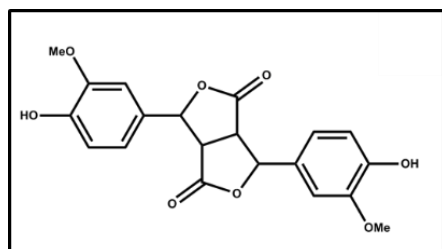


Figure 2-33: MALDI-TOF spectrum of caffeic acid (7)



(a) 4-hydroxy-3-methoxycinnamic acid: MW = 194 g/mol.  $^1\text{H}$  NMR (400 MHz, DMSO, (ppm)): 7.01 (dd, 1H Ar), 7.25 (d, 1H Ar), 6.74 (d, 1H Ar), 6.3 (d, 1H CH=CH), 7.5 (d, 1H CH=CH), 3.78(s, OCH<sub>3</sub>), 12.1(s, COOH).

(b) ferulic acid coupled by  $\beta$ - $\beta$  bond: MW = 422 g/mol.  $^1\text{H}$  NMR (400 MHz, DMSO, (ppm)): 7(d, 1H Ar), 6.65 (d, 1H Ar), 6.84 (dd, 1H Ar), 5.73 (s, OH), 3.78(s, OCH<sub>3</sub>), 4.21(s, CH<sub>2</sub>).

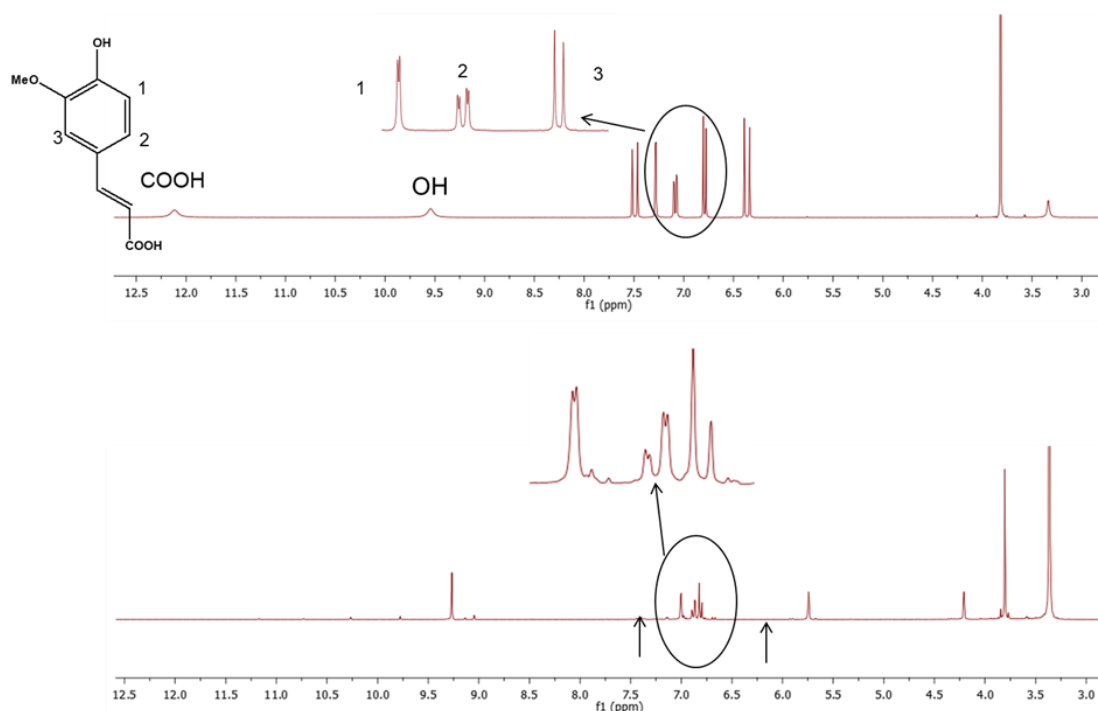


Figure 2-34:  $^1\text{H}$  NMR spectra of ferulic acid (8)

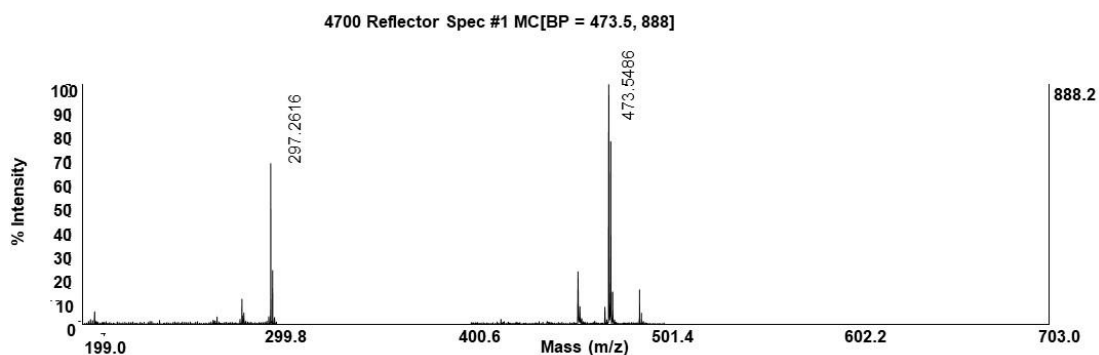
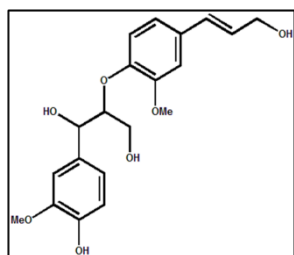


Figure 2-35: MALDI-TOF of ferulic acid dimer (8)

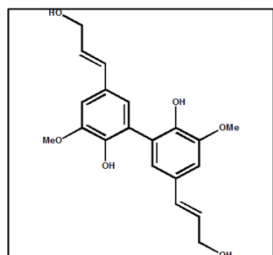
With the exception of the coniferyl alcohol (9) which afford two types of dimers, coupled by two types of linkages (5-5') (Figure 2-38) and  $\beta$ -O-4 coupling (Figure 2-37), with almost of 50% yield of the last dimer product ( $\beta$ -O-4) which is the most abundant linkage in natural lignin.

*High Riboflavin selectivity flow photo oxidation of phenols derived from lignin*



(a) coniferyl alcohol: MW = 180 g/mol.  $^1\text{H NMR}$  (400 MHz, DMSO, (ppm)): 7 (d, 1H Ar), 6.78 (dd, 1H Ar), 6.72 (d, 1H Ar), 6.21 (dt, 1H CH=CH-CH<sub>2</sub>), 6.45 (d, 1H CH=CH), 4.07 (dd, 2H CH<sub>2</sub>), 4.75 (t, OH), 9 (s, OH).

(b) coniferyl alcohol coupled by C-O bond: MW = 375 g/mol.  $^1\text{H NMR}$  (400 MHz, DMSO, (ppm)): 7.45 (d, 1H Ar), 7.40 (dd, 1H Ar), 6.96 (d, 1H Ar), 6.90 (d, 1H Ar), 6.73 (dd, 1H Ar), 6.80 (d, 1H Ar), 6.21 (dt, 1H CH=CH-CH<sub>2</sub>), 6.45 (d, 1H CH=CH), 4.02 (dd, 2H CH<sub>2</sub>), 4.53 (t, OH), 9.75 (s, OH).



(c) coniferyl alcohol coupled by C-C bond: MW = 358 g/mol.  $^1\text{H NMR}$  (400 MHz, DMSO, (ppm)): 6.95 (d, 2H Ar), 6.78 (d, 2H Ar), 6.25 (dt, 2H CH=CH-CH<sub>2</sub>), 6.48 (d, 2H CH=CH), 4.03 (dd, 2H CH<sub>2</sub>), 5 (t, OH), 9.02 (s, OH).

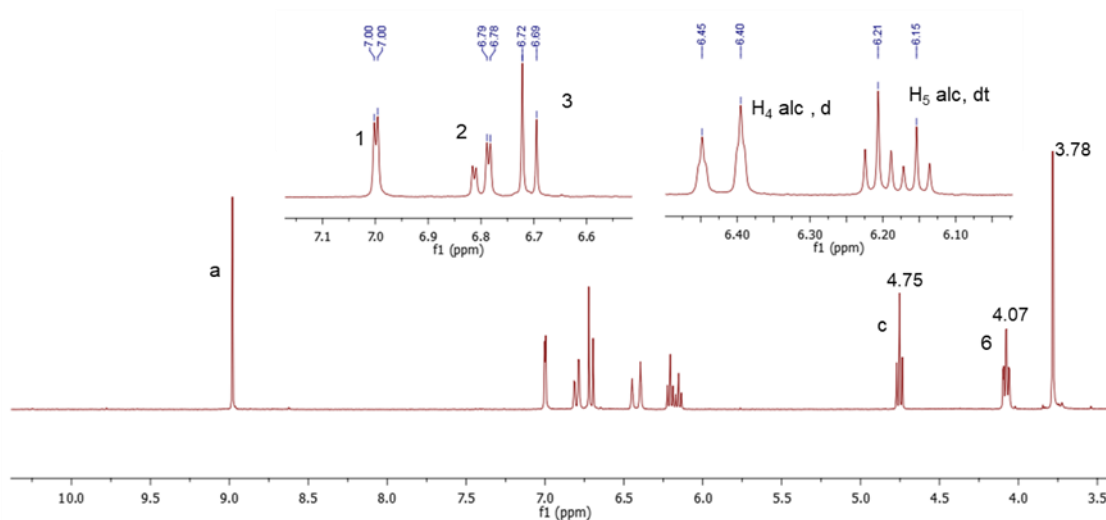


Figure 2-36:  $^1\text{H NMR}$  spectrum of coniferyl alcohol

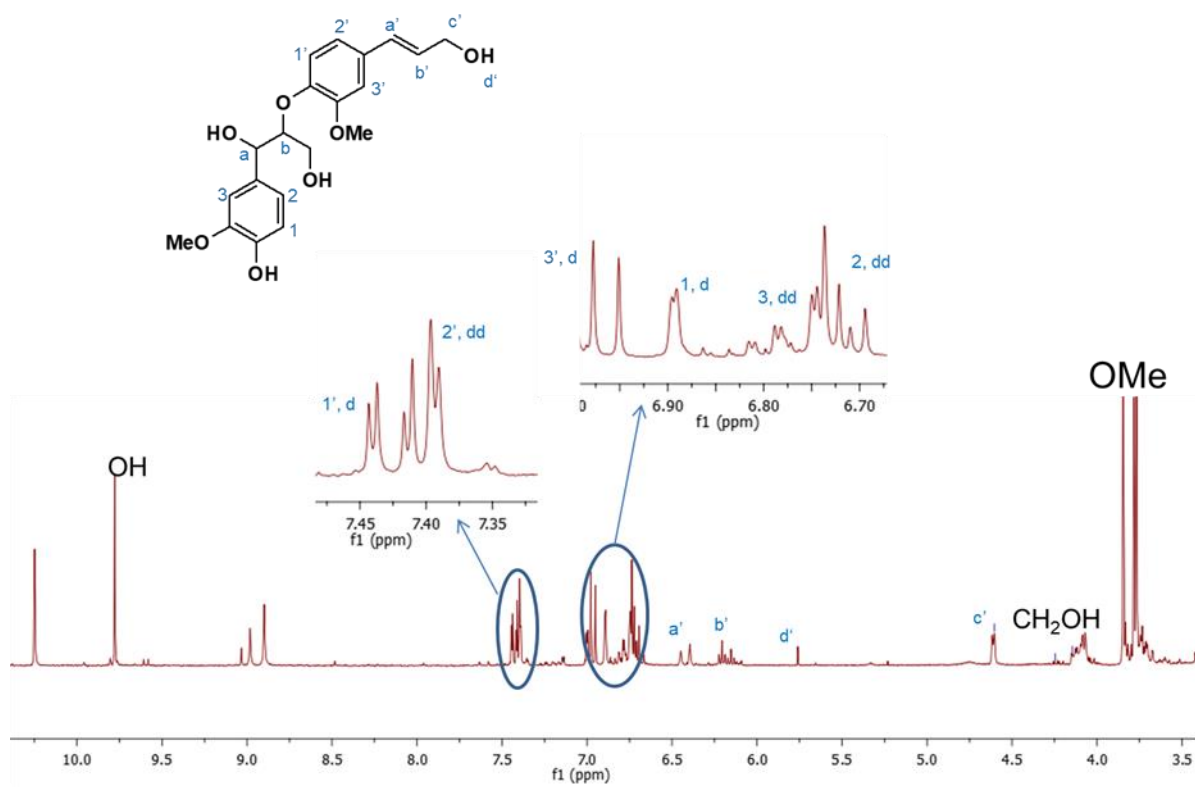


Figure 2-37:  $^1\text{H}$  NMR spectrum of di-coniferyl alcohol coupled by C-O linkage

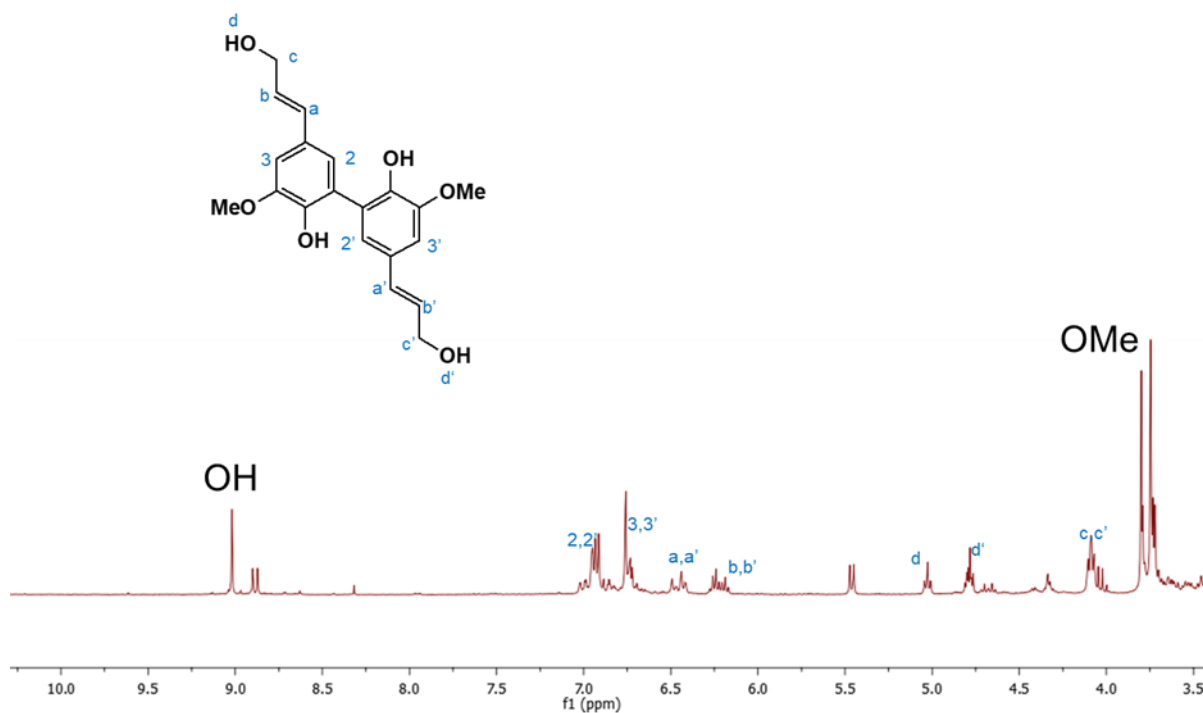
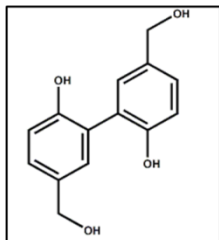
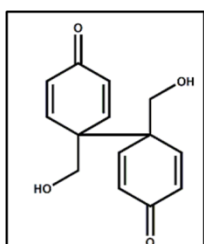


Figure 2-38:  $^1\text{H}$  NMR spectrum of di-coniferyl alcohol coupled by C-C linkage



(a) 4-hydroxybenzyl alcohol: MW = 124 g/mol.  $^1\text{H}$  NMR (400 MHz, DMSO, (ppm)): 7.12 (d, 2H Ar), 6.71 (d, 2HAr), 4.35 (s, 2H CH<sub>2</sub>), 9.24(s, OH), 4.93 (s, OH).

(b) 4-hydroxybenzyl alcohol 2,2' dimer: MW = 246 g/mol.  $^1\text{H}$  NMR (400 MHz, DMSO, (ppm)): 7.77 (d, 2H Ar), 6.71 (d, 2HAr), 7.15 (dd, 2HAr), 4.26 (s, 2H CH<sub>2</sub>), 9.79(s, 2H OH).



(c) 4-hydroxybenzyl alcohol 4,4' dimer: MW = 248 g/mol.  $^1\text{H}$  NMR (400 MHz, DMSO, (ppm)): 7.14 (d, 4H Ar), 6.74 (d, 4HAr), 4.34 (s, 4H CH<sub>2</sub>), 9.35(s, 2H OH).

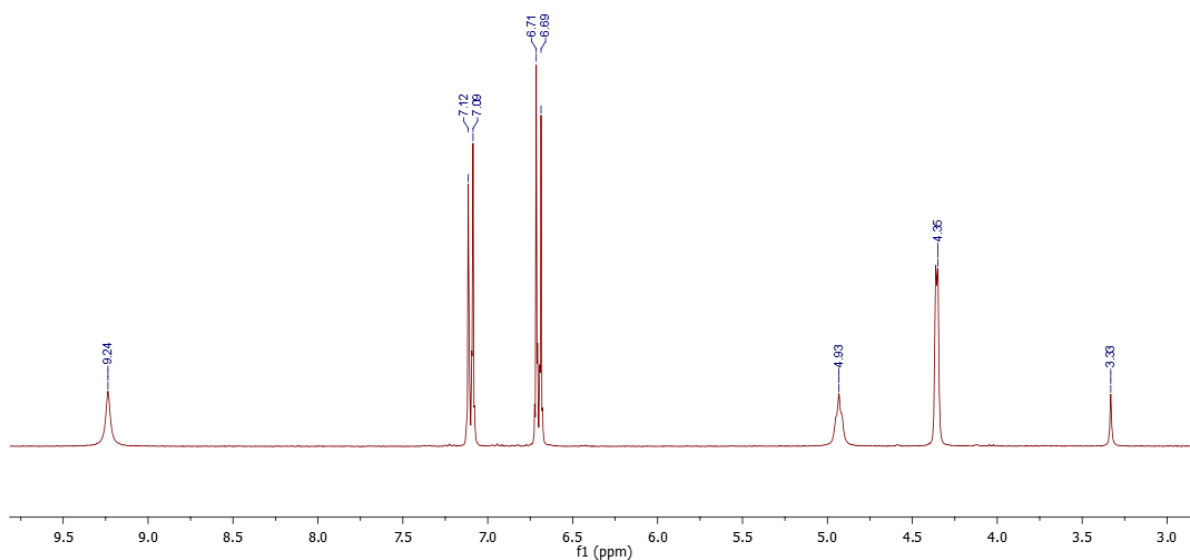


Figure 2-39:  $^1\text{H}$  NMR of 4-hydroxybenzyl alcohol

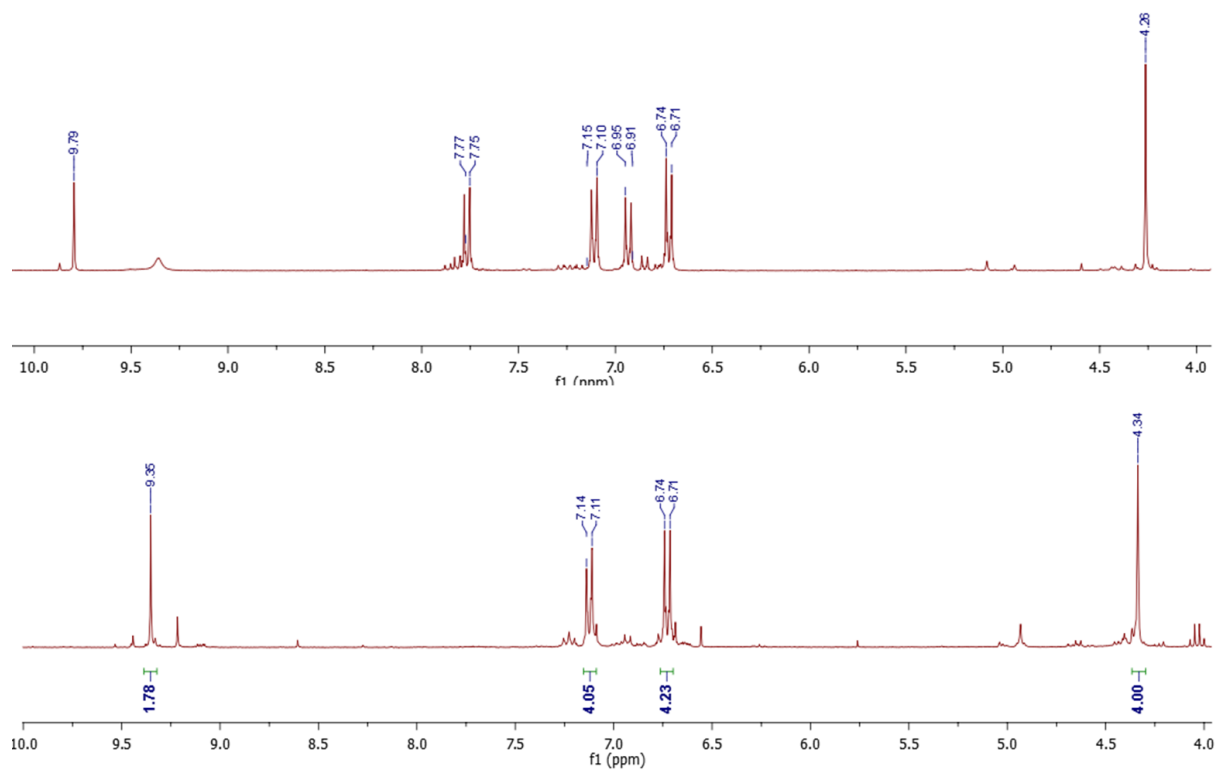


Figure 2-40:  $^1\text{H}$  NMR of 4-hydroxybenzyl alcohol dimer coupled by C-C linkage

## **2.9. Conclusion**

A green and easy continuous flow photooxidation way to synthesize the 5-5' dimer coupling derivative obtained at higher yield around 80 % by flow photo-oxidation of vanillyl alcohol (1) using riboflavin as photosensitizer. In our knowledge the high riboflavin selectivity toward the dimer 5-5' and  $\beta$ - $\beta$  coupling have been observed for the first time and no side product have been detected with this flow process. This process presents several advantages: (i) the 5-5' dimer formation occurs in flow system at room temperature without using any oxidant, (ii) the product purification is easy (iii) Furthermore, this dimerization procedure was extended to several lignin model which affords mainly the (5-5') biphenylic derivatives products. Some parameters such as pH, flow rate and time duration have been carried out to study the selectivity and yield of riboflavin catalyzed the coupling reactions, the highest yield have been achieved only at neutral pH with a flow rate of 0.1 mL/ min during 1 hours. Such a platform of symmetrical and functional aromatic dimers is of high interest for the design of novel rigid (semi) aromatic bio-based polymers.



### **3. CHAPTER THREE: C-O COUPLED-POLYVANILLIN BY DEHYDROGENATIVE POLYMERIZATION OF VANILLIN USING IMMOBILIZED HORSERADISH PEROXIDASE**

#### **3.1. New possibility for lignin models based on vanillin**

Vanillin, a naturally occurring phenolic aldehyde with promising applications in a variety of sectors, has emerged as a major force in polymer chemistry. Natural vanillin from vanilla pods costs more than synthetic vanilla, which costs between 12-40 dollars per kilogram [198, 199]. The fraction of synthetic vanilla derived from renewable resources is rising [200]. In particular, synthetic vanilla is made in large quantities from lignin rich in  $\beta$ -O-4 links [201]. vanilla produced by biotechnology from renewable resources is deemed as natural and can be utilized in food, composites, medicine delivery, antibacterial coatings and water treatment [202]. It costs roughly 800 dollars per kilogram [198]. Vanillin is an excellent precursor for producing a bio-sourced aromatic polymer because of its phenol and aldehyde functionality and its attractive price [202]. In recent years, multiple reports have been published on the synthesis of aromatic polymers based on vanillin employing diverse chemistries. Instead of using vanillin itself, two of its symmetrical dimers have been incorporated into polymer network:

1. C-C divanillin obtained by dehydrogenative oxidation of vanillin [203-205];
2. hydrovanillin formed by electrochemical reduction of the aldehyde function [206, 207].

In the first step, vanillin is dimerized into C-C divanillin by dehydrogenative oxidation using HRP [208]. The C-O divanillin, which is naturally found in lignin [209] and can be generated by dehydrogenative oxidation [210], is an appealing strategy for the preparation of vanillin based polymers that lead to further reaction. This phenyl oxide polymer family is very robust and has a wide range of industrial applications [211]. There is a lot of interest in researching lignin synthesis, thus it is necessary to look for new, straightforward methods with fewer steps in the reactions. Models of lignin are useful tools for imagining new lignin structural features and for estimating its reactivity. They also reduce the complexity of lignin, which helps us comprehend the processes that underlie its synthesis. Vanillin, guaiacol, ferulic acid, among many other aromatic compounds, are released during lignin depolymerization. The creation of lignin-based polymers heavily utilizes the ingredients vanillin and ferulic acid. A highly strong

phenolic aldehyde that is widely accessible in large quantities and has a high potential for polymer synthesis is vanillin [51, 212].

### **3.1.1. Vanillin and its extraction**

The primary flavoring of vanilla, vanillin, was traditionally made from vanilla pods [213]. Later, other extraction techniques for vanillin were created. The most notable commercial process, which produces 85% of the world's vanillin supply, is the manufacture of vanillin from the petrochemical guaiacol. Lignin is a different source of vanillin, contributing 15% to its production [214-216]. Natural phenolic aldehydes like vanillin have amazing potentials in the food, fragrance, and pharmaceutical industries, and polymer chemistry has tapped into this line of research [217].

### **3.1.2. Vanillin as a model for lignin**

A lignin monomeric molecule called vanillin [218] shares several functional groups with the major monomers of lignin [219]. At an industrial scale, it is made from lignin [200]. Vanillin yield was found to be significantly influenced by the type of lignin linkages present, with lignin rich in  $\beta$ -O-4 links producing the highest output [201]. The production of biobased materials using environmentally friendly and sustainable methods, such as the synthesis of lignin models [220-222], as well as other polymers like vinyl [223] and cyanate ester resin [224] in addition to epoxy resins [51]. Thus, using vanillin-based products as instruments to imagine some novel uses for lignin, vanillin production via lignin valorization routes imposes a new research mindset.

### **3.1.3. Divanillin**

Dehydrodivanillin, commonly known as divanillin, is a crucial antioxidant and taste ingredient in medicinal, food, and cosmetic industries. According to earlier reports, it is also utilized in polymer synthesis and microlithography [225]. It has been produced using a variety of techniques over time, including enzymatic and chemical ones.

### **3.1.3.1. Synthesis of divanillin via chemical methods**

Different chemical processes are frequently used to create divanillin. By oxidative phenol coupling with iron (II) chloride ( $\text{FeCl}_3$ ) or iron (II) sulfate ( $\text{FeSO}_4$ ), it has been created. In 1885, the first  $\text{FeCl}_3$ -based divanillin synthesis was described, and several others followed [226-228]. The ortho position of the phenol group was oxidized using stoichiometric amounts of  $\text{FeCl}_3$ . As a result, divanillin precipitated, was washed, and was filtered out of the mixture. A 57% yield was attained.

In 1918, the first potassium/sodium persulfate-based divanillin synthesis was described [50, 204, 228, 229]. Recent improvements to this synthetic method led to an increased yield of 95%, which is 20% more than in the earlier work, vanillin was oxidized using an iron (II) sulfate heptahydrate and sodium peroxodisulfate in hot water to produce divanillin.

To be more precise, water was combined with vanillin and  $\text{FeSO}_4$  and agitated for 10 minutes at 50 °C before  $\text{Na}_2\text{S}_2\text{O}_8$  was added. The brown precipitate was filtered out and dissolved in NaOH after a 5 day reaction period (2 M). Following the addition of HCl (2 M), the precipitate was separated by filtering. Both of these techniques use non-renewable metal catalysts and need lengthy reaction times to produce high yields. An enzymatic pathway was created in order to avoid the use of hazardous substances (sodium persulfate) and inorganic salts.

### **3.1.3.2. Synthesis of divanillin via enzymatic coupling**

Enzymatic polymerization has grown in popularity and made significant contributions to the advancement of lignin research in light of the growing demand for sustainable and secure green synthesis. Such procedures entail the oxidation of phenolic substances using peroxidases, primarily HRP, and fungal laccases.

Following the oxidation of vanillin in aqueous solution with peroxidase in the presence of hydrogen peroxide, divanillin was discovered for the first time in 1972 [230]. While oxidizing vanillin with peroxidase in dairy products, some studies reported the presence of divanillin. The structural diversity of o-methoxyphenols' oxidation products that were catalyzed by peroxidase was examined by Dordick and colleagues in 2004 [231].

### *Polyvanillin by coupling of vanillin on immobilized horseradish peroxidase*

The enzyme soybean peroxidase, which is readily available and very active, was utilized. The substrate was dissolved in 0.5 L of aqueous buffer containing 1.0 g/mL of enzyme, 12 mM vanillin, and 1% (v/v) DMF. H<sub>2</sub>O<sub>2</sub> was slowly introduced to start the reaction. Oligomers are created as a result of this process. The number of units in the resultant oligomers was controlled by the amount of DMF.

For the synthesis of oligomers with 2 to 5 units, 1% of DMF was sufficient. An overall yield of 80% was attained after 12 hours. Furthermore, the reaction is pH-dependent. In fact, the synthesis of dimers, numerous trimers, and minor fractions of tetramers, pentamers, and quinone were all promoted by somewhat acidic circumstances. To get a good selectivity in dimer production, the circumstances still needed to be improved.

For instance, Vosburg and colleagues (2010) found that employing 1000 units of enzyme, decreasing the pH to 4 using acetic acid, and adding 3% hydrogen peroxide to 1 g of product results in a yield of 80% dimers after 5 min [203].

### **3.2. Polymerization triggered by peroxidase**

Enzymes known as peroxidases have been used frequently in radical aromatic polymerization. Two radical species (oxidized substrates) are formed during the catalytic cycle of peroxidases, specifically at the point where compound (II) returns to the resting state after being abstracted of two hydrogen from the reducing substrate. These radical species are what trigger the polymerization process. When performing peroxidase-catalyzed synthesis, a crucial aspect needs to be considered. To prevent the enzyme from being inhibited, the right H<sub>2</sub>O<sub>2</sub> concentration must be chosen [232, 233].

## *Polyvanillin by coupling of vanillin on immobilized horseradish peroxidase*

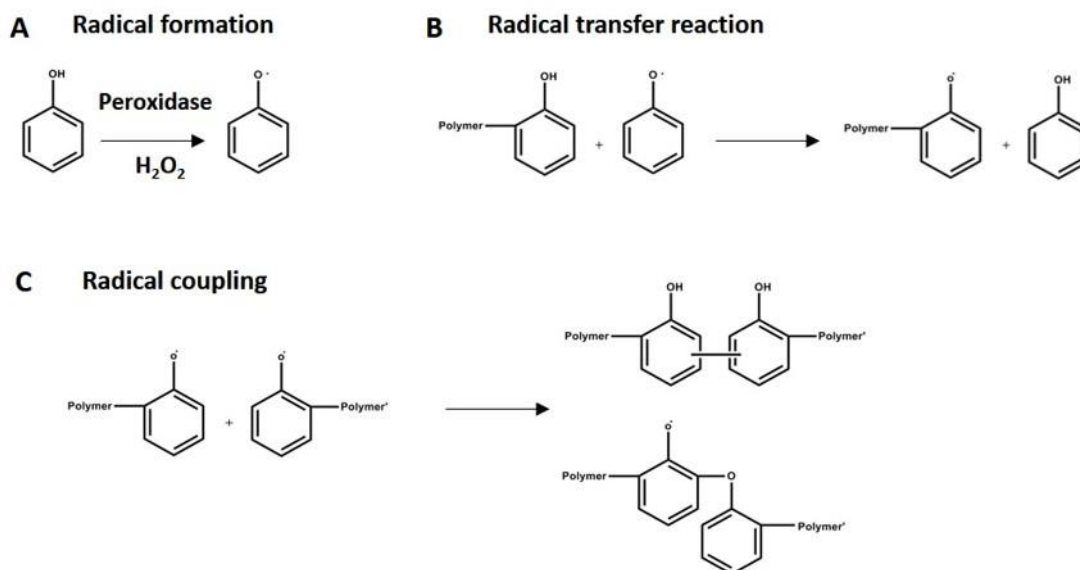


Figure 3-1: Mechanism of phenol polymerization by peroxidase. A. Phenoxy radicals first form. B. a radical combination. C. polymerization and radical transfer [234].

For understanding lignin structure and synthesis mechanism, new lignin models must be created. The goal of this research is to present a straightforward and trustworthy method for polymerizing vanillin, a good option for the production of renewable polymers [235, 236]. By revisiting the traditional pathways that result in vanillin dimerization and using novel enzymatic techniques, this method enables the collection of structural data on the manner of bond formation in peroxidase-catalyzed processes as well as the analysis of vanillin oxidation.

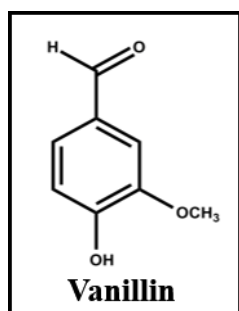
### **3.4. Experimental part**

#### **3.4.1. Chemicals**

Vanillin, vanillyl alcohol, sodium acetate, ferrous sulfate, hydrochloric acid, magnesium sulfate, potassium carbonate, chloroform, ethyl acetate, methanol, tetrahydrofuran, acetone, acetic acid, HRP type (I), P8125; HRP type (II), P8250, dichloromethane, petroleum ether, sodium bicarbonate, dimethylsulfoxide, sodium hydroxide, 2-iodoacetamide, hydrogen peroxide, anhydrous magnesium sulfate, acidic anhydride, tetrakis(acetonitrile)copper(I) triflate were purchased from Sigma Aldrich. Sodium persulfate was purchased from Alfa Aesar.

### 3.4.2. C-C vanillin dimerization by chemical way

To a solution containing vanillin (70 mmol) in water (700 mL), FeSO<sub>4</sub> (1.4 mmol) was added under stirring. After heating at 50 °C for 10 min, Na<sub>2</sub>S<sub>2</sub>O<sub>8</sub> (37.5 mmol) was added. After stirring the reaction mixture at 50°C for 5 days, brown precipitates were formed, filtered off, and dissolved in NaOH (2 M) solution. Upon the addition of HCl (2 M) solution, the precipitates formed were isolated by filtration.

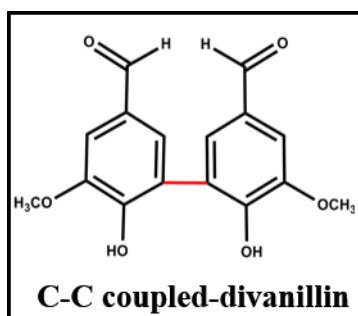


<sup>1</sup>H-NMR (300 MHz, (CD<sub>3</sub>)<sub>2</sub>CO) δ 3.94 (s, 3H, OMe), 8.63 (s, 1H, OH), 7.03 (dd, *J* = 7.5, 0.8 Hz, 2H, Ar-H), 7.46 (s, 1H, Ar-H), 7.49 (dd, *J* = 1.9 Hz, 1H, Ar-OH), 9.8 (s, 1 H, HCO).

<sup>13</sup>C-NMR (300 MHz, (CD<sub>3</sub>)<sub>2</sub>CO) δ 55.45, 110.07, 115.08, 126.13, 129.87, 148.08, 152.66, 190.25, 205.50.

### 3.4.3. C-C vanillin dimerization using HRP type I/II

1 g vanillin (6.6 mmol) was dissolved in 100 mL of deionized water by heating the mixture to 50° C. Acetic acid (0.022 mmol) was added to decrease the pH to 4. To this mixture 9 mg of horseradish peroxidase Type I or II (1000 U) was added followed by hydrogen peroxide (3% in water, 6.6 mmol). After 15 min of stirring at room temperature, a brown precipitate was formed and collected by filtration on Buchner and dried overnight in the oven. Yield 90%.



<sup>1</sup>H-NMR (300 MHz, CD<sub>3</sub>SOCD<sub>3</sub>) δ 9.82 (s, 2H, HCO), 7.44 (dd, *j* = 3.6, 1.8 Hz, 4H, Ar-H), 3.94 (s, 6H, OMe).

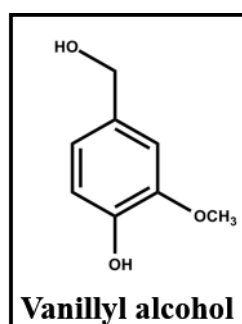
<sup>13</sup>C-NMR (300 MHz, CD<sub>3</sub>SOCD<sub>3</sub>) δ 56.48, 109.09, 125.03, 128.40, 128.99, 148.62, 150.90, 191.72.

#### 3.4.4. C-C vanillin dimerization using laccases

Vanillin was oxidized by two fungal laccases: laccase from *Trametes versicolor* (12.4 mg, 20 U) and from *Myceliophthora thermophila* expressed in *Aspergillus sp.* under the same conditions reported by Savonnet et al. [210]. Vanillin (1.5 g, 10 mmol) was solubilized in acetone (20 mL) before sodium acetate buffer (NaOAc) buffer (180 mL, 0.1 M) was added to set pH to 5.0. The reaction was initiated by the addition of laccase. After stirring the reaction mixture for 24 h at room temperature, greenish precipitates were formed. The precipitates were recovered by filtration and dried in the oven overnight.

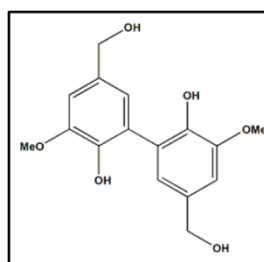
#### 3.4.5. Divanillin reduction to divanillyl alcohol

Divanillin (0.075 g, 0.25 mmol) was dissolved in 2.5 mL DMSO. Sodium borohydride (0.023 g, 0.60 mmol) was then added slowly under agitation at room temperature. After 30 min, the reaction was stopped by the addition of 1 ml saturated NaCl. Finally, the reaction was neutralized using HCl (3M), and divanillyl alcohol was extracted with excess of dichloromethane/water. Dichloromethane was dried over MgSO<sub>4</sub> before being removed by evaporation (Yield 80%). Divanillyl alcohol MW = 306 g/mol. <sup>1</sup>H NMR (DMSO-d<sub>6</sub>) δ 4.45(s, CH<sub>2</sub>), 5.02 (s, OH), 6.73 (2H, d, J, H-Ar), 6.93 (2H, d, J, H-Ar).



<sup>1</sup>H-NMR (300 MHz, (CD<sub>3</sub>)<sub>2</sub>CO) δ 3.83 (s, 3H, OCH<sub>3</sub>), (s, 1H, OH), 4.54 (2H, d, J = 5.8, CH<sub>2</sub>), 6.8 (2H, t, J = 1, Ar-H), 6.98 (s, 1H, Ar-H), 7.43 (1H, s, Ar-OH).

<sup>13</sup>C-NMR (300 MHz, (CD<sub>3</sub>)<sub>2</sub>CO) δ 55.31, 63.94, 110.57, 114.56, 119.47, 133.90, 145.59, 147.31, 205.62.



<sup>1</sup>H NMR (DMSO), δ 3.82 (3H, s, OMe), 5.02 (1H, t, OH), 4.42 (2H, d, J 4.42, CH<sub>2</sub>), 6.67 (2H, H<sub>22</sub>'), 6.89 (2H, H<sub>11</sub>'), 8.75 (1H, Ar-OH).

### **3.4.6. Vanillin or vanillyl alcohol derivatization using different bases**

#### **3.4.6.1. DBU (1,8-Diazabicyclo(5.4.0)undec-7-ene)**

1 equivalent of vanillin (0.5 mmol) dissolved in 1.7 mL DMF then 1 equivalents of DBU (75 microliter) was added, and 1.2 equivalents of 2-iodoacetamide (0.6 mmol) were slowly added, and the reaction mixture was further stirred at room temperature under nitrogen for 24 h in the dark. To remove the excess of DBU a washing with sulphuric acid solution (1M) was did .Then the product was extracted with ethylacetate and washed with water then dried over MgSO<sub>4</sub> the solvent was removed under rotary evaporator. Yield: 64%. And when 3 equivalents of DBU were used in place of 1 the yield was 34%.

#### **3.4.6.2. NaOH**

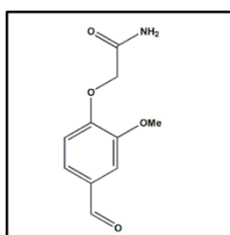
1 equivalent of vanillin or vanillyl alcohol (0.5 mmol) dissolved in 1.7 mL DMF (dimethylformamide) then 1 or 3 equivalents NaOH (20 mg/60 mg) respectively was added, after 1h of agitation; 1.2 or 3.8 equivalents of 2-iodoacetamide (0.6 mmol/1.8 mmol) were slowly added, and the reaction mixture was further stirred at room temperature for 20 h in the dark. The product was extracted with ethylacetate and washed with water then dried over MgSO<sub>4</sub> the solvent was removed under rotary evaporator. Yield: 100%.

#### **3.4.6.3. Phosphazene Phosphazene base P1-t-Bu-tris (tetramethylene)**

1 equivalent of vanillin or vanillyl alcohol (0.5 mmol) dissolved in 1.7 mL DMF, then 1 or 3 equivalents of phosphazene (0.16 mL/0.46 mL) respectively was added, after 1h of agitation; 1.2 or 3.8 equivalents of 2-iodoacetamide (0.6 mmol/1.8 mmol) were slowly added, and the reaction mixture was further stirred at room temperature for 20 h in the dark. The excess of the base was removed by washing with acidic solution (HCl 0.1M) .The product was extracted with ethyl acetate and washed with water then dried over MgSO<sub>4</sub> the solvent was removed under rotary evaporator. Yield: 100%.

#### 3.4.6.4. $K_2CO_3$ as a base

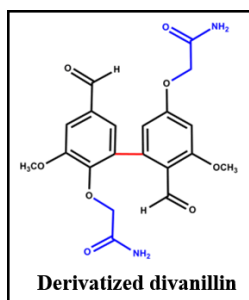
1 equivalent of vanillin or vanillyl alcohol (0.5 mmol) dissolved in 1.7 mL DMF then 1 or 3 equivalents NaOH (20 mg/60 mg) respectively was added, after 1h of agitation; 1.2 or 3.8 equivalents of 2-iodoacetamide (0.6 mmol/1.8 mmol) were slowly added, and the reaction mixture was further stirred at room temperature for 20 h in the dark. The product was extracted with ethylacetate and washed with water then dried over  $MgSO_4$  the solvent was removed under rotary evaporator. Yield: 100%.



$^1H$  NMR ( $CDCl_3$ ),  $\delta$  3.95 (3H, s, OMe), 9.88 (1H, s, COOH), 6.31 (1H, s, NH<sub>2</sub>), 6.99 (1H, d), 7.48 (1 H, d), 7.41 (1 H, dd), 4.55 (2H, s, CH<sub>2</sub>).

#### 3.4.7. Functionalization of 5-5' dehydrodivanillin

1 equivalent of divanillin (0.5 mmol) dissolved in 6 ml DMSO then 3 equivalents of potassium carbonate ( $K_2CO_3$ ) (0.43 mmol) was added, and 3.6 equivalents of 2-iodoacetamide (1.8 mmol) were slowly added, and the reaction mixture was further stirred at room temperature for 24 h in the dark. The product was extracted with excess of dichloromethane/water then dried over  $MgSO_4$  the solvent was removed under rotary evaporator. Yield: 60%.



$^1H$ -NMR (300 MHz,  $CDCl_3$ ), 3.92 (s, 6H, OMe), 4.25 (s, 4 H, CH<sub>2</sub>), 5.89 (s, 2H, NH<sub>2</sub>), 6.56 (s, 2H, NH<sub>2</sub>), 7.42 (dd,  $j = 33.2, 1.9$  Hz, 4H, Ar-H),  $\delta$  9.87 (s, 2H, HCO)

#### **3.4.8. Purification of derivatized polyvanillin**

The obtained product was purified on silica gel chromatography using mixture of solvent ethylacetate/methanol 80:20, followed by C18 column using water/acetonitrile 70:30 to the MALDI analysis.

#### **3.4.9. Polyvanillin synthesis on HRP immobeads®150P**

The oxidation of vanillin using the immobilized enzymes was carried out following the protocol of another PhD student in our laboratory. The mixture consisted of 0.2 g of HRP wet beads were added to a solution containing vanillin (0.15 g, 1 mmol), acetic acid (0.012 mmol) and H<sub>2</sub>O<sub>2</sub> (30% in water, 1.45 mmol) in 33.3 mL water. The reaction mixture was shaken for 2 h, and the obtained product remained attached to the beads, where the color of the beads turned into beige color after 1 to 2 min upon the addition of vanillin and this color became brown at the end of the reaction. The product was then recovered by soaking the beads in dichloromethane overnight. The obtained product was precipitated by the addition of water on ice to remove the excess of vanillin. The organic phase was then recovered, dried over MgSO<sub>4</sub> and evaporated. Yield 46%.

#### **3.4.10. Derivatization of polyvanillin using iodoacetamide in basic medium (amidation reaction)**

1 equivalent of purified polyvanillin (0.5 mmol) dissolved in 6 ml DMSO then 3 equivalents of potassium carbonate (K<sub>2</sub>CO<sub>3</sub>) (0.43 mmol) was added, and 2.4 equivalents of 2-iodoacetamide (1.2 mmol) were slowly added, and the reaction mixture was further stirred at room temperature for 5 h in the dark to prevent the formation of polyacetamide. The product was extracted with excess of dichloromethane/water then dried over anhydrous MgSO<sub>4</sub> the solvent was removed under rotary evaporator. Yield: 20%.

The obtained product was purified on C18 column using water/acetonitrile 70:30 to the MALDI analysis.

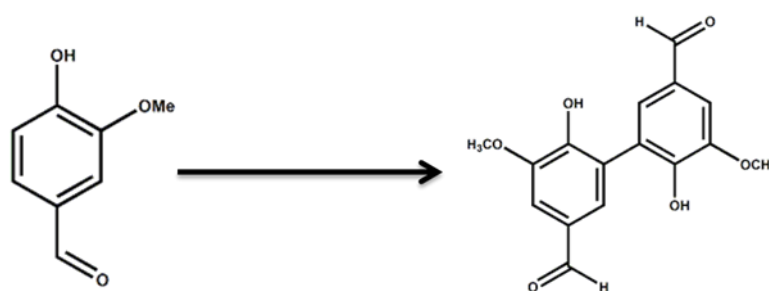
### 3.4.11. Derivatization of polyvanillin using acetic anhydride (acylation reaction)

In 25 mL round-bottom flask, polyvanillin (0.02 g, mmol, 1 equivalent) dissolved in 6 mL dichloromethane and acetic anhydride (0.38 mL, 4.0 mmol, 8 equivalents) were added under nitrogen. Tetrakis (acetonitrile) copper (I) triflate catalyst (0.038 g, 20  $\mu$ mol %) was then added to the reaction mixture which was stirred at room temperature for 3 hours. After that, saturated aqueous  $\text{NaHCO}_3$  (4 mL) was added and stirred for 45 min to neutralize the excess of acetic anhydride.

## 3.5. Results and discussion

### 3.5.1. Different routes for vanillin oxidation

It is obvious from prior research that vanillin is a superb option for the synthesis of renewable polymers. The primary goal of this work was to present a straightforward and trustworthy method for vanillin polymerization for the first time. Vanillin oxidation was thoroughly examined by revisiting the traditional pathways that results in vanillin dimerization in order to gather structural data regarding the method of links formation in peroxidase-catalyzed processes.



First, vanillin was subjected to an early documented conventional chemical oxidation reaction that implied the use of sodium persulfate and ferric oxide as catalysts, producing 5-5' dehydrodivanillin with a 96% yield [204]. The method suggested by Nishimura et al., which entails the dimerization of vanillin using HRP (type I) in slightly acidic aqueous medium, remains the most preferred method in light of the growing demand for green processes. It enables high conversion (85%) of the 5-5' divanillin to be obtained in 5-15 minutes rather than 5 days and does not involve the use of any toxic reagents [203].

## *Polyvanillin by coupling of vanillin on immobilized horseradish peroxidase*

In this investigation, two kinds of horseradish peroxidases (HRP type I and type II) that differ by the amount of isoforms they contain were employed. Vanillin was converted into the 5-5' dimer with a yield of 90–95% when HRP (type I) oxidized it. Nevertheless, 5-5' divanillin with a 90% conversion was also produced using HRP type II under the same reaction circumstances. When HRP is added, 5-5' divanillin-corresponding brown precipitates are immediately generated and are quickly recovered by filtration. The aromatic hydrogens of divanillin were identified in the multiplet at 7.44 ppm that the  $^1\text{H}$  NMR study revealed (Figure 3-4).

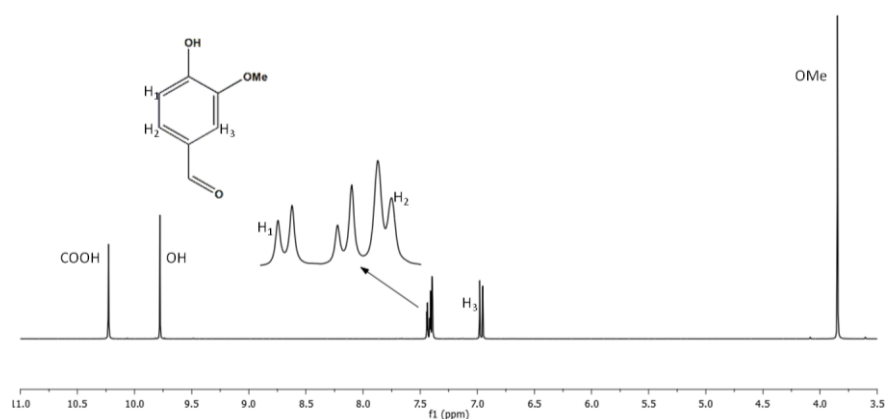


Figure 3-2:  $^1\text{H}$  NMR of vanillin in DMSO

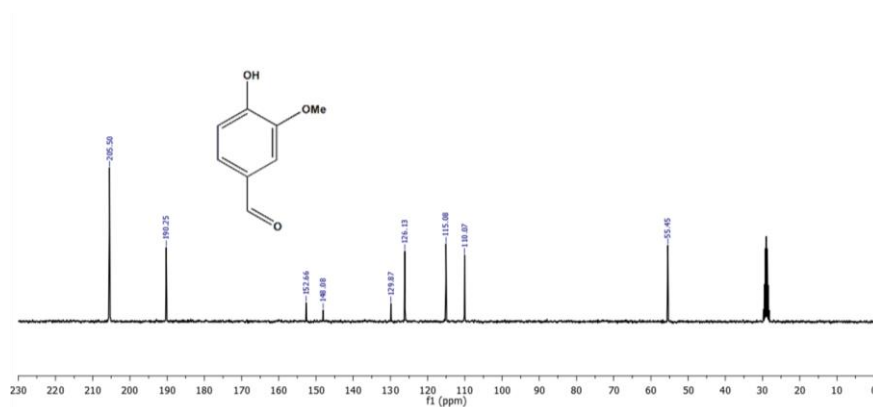


Figure 3-3:  $^{13}\text{C}$  NMR of vanillin

## Polyvanillin by coupling of vanillin on immobilized horseradish peroxidase

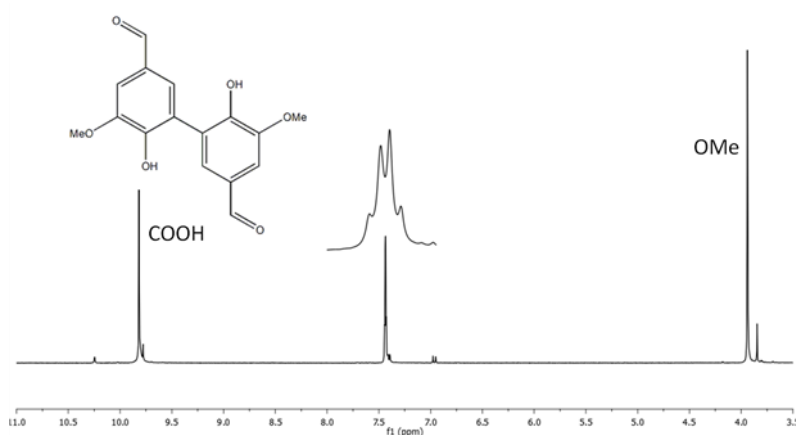


Figure 3-4:  $^1\text{H}$  NMR of divanillin

Aside from peroxidases, laccases are also known to oxidize vanillin, with the majority of the dimers produced in this process giving trimers and higher molecular weight oligomers in trace amounts [152, 231]. Oligomeric materials were found in the investigation of Krings et al., who employed laccase from *Funalia trogii* for the oxidation of vanillin [152]. Following the methodology of Savonnet et al. [210], the oxidation of vanillin utilizing two types of fungal laccases (laccase from *Trametes versicolor* and laccase from *Myceliophthora thermophila*) was studied in this work.

Vanillin was first dissolved in acetone, and then an acetate buffer was added to raise the pH to 5.0. The reaction result precipitates under these circumstances, while the reactant remains soluble. The color of the solution changed to yellow with the addition of laccases, indicating the potential generation of radicals or quinone. Vanillin mostly has electron-withdrawing para substituents, which promote quinone production [159]. According to  $^1\text{H}$ -NMR results, both enzymes could produce 5-5' dehydrodivanillin without enriching the medium with oxygen.

As the kind of links depends on the position of the stabilization of the radical on the aromatic cycle, which preferably happens at position five of vanillin, the 5-5' divanillin was mostly generated regardless of the type of enzyme utilized.

### 3.5.2. Amidation of vanillin/ divanillin using iodoacetamide

The functionalization step of 5-5' divanillin that was carried out aiming at masking the phenolic hydroxyl groups which came up with several benefits including:

## *Polyvanillin by coupling of vanillin on immobilized horseradish peroxidase*

- 1) Optimization of the solubility of divanillin;
- 2) Counting of the free hydroxyl groups present in the molecule,
- 3) Higher resolution of MALDI-TOF spectra,
- 4) Development of a separation procedure.

Thus, we decided to work firstly on vanillin to optimize the reaction conditions, Preliminary alkylation reactions were performed in the presence of NaOH as the base and we got a highly yield, which was then replaced by different types of bases to prevent the toxicity of NaOH on the MALDI-TOF machine like DBU, phosphazene, and  $K_2CO_3$  because they are a milder reagent for MS.

Using 1 equivalent of DBU as a base, we got 64% of conversion and when we increased the equivalent to 3 we got a lower conversion 32%. So it's replaced by phosphazene which gave a 100% of conversion but we had a big problem with this type of base, it's very hard to remove the excess of this base even after several washing using acidic water so we skipped to another type which is  $K_2CO_3$  which gave the best result (Figure 3-5). So, the next step was to work on divanillin.

Table 3-1: Summary of the conditions for the derivatization reaction of vanillin and vanillyl alcohol.

Vanillin	Vanillyl alcohol	NaOH	DBU	Phosphazene	Conversion (%)
0.5 mmol	–	0.5 mmol	–	–	100
–	0.5 mmol	1.5 mmol (3 eq.)	–	–	100
0.5 mmol	–	–	0.5 mmol	–	64
0.5 mmol	–	–	1.5 mmol (3 eq.)	–	34
–	0.5 mmol	–	1.5 mmol (3 eq.)	–	0
0.5 mmol	–	–	–	0.5 mmol	100

## Polyvanillin by coupling of vanillin on immobilized horseradish peroxidase

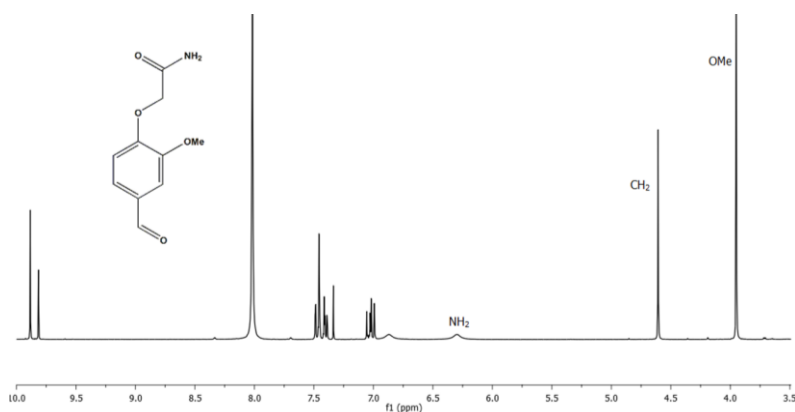


Figure 3-5:  $^1\text{H}$  NMR of derivatized vanillin

Table 3-2: Summary of the conditions for the derivatization reaction of 5,5' dehydrodivanillin and polyvanillin.

Divanillin	Polyvanillin	Phosphazene	NaOH	$\text{K}_2\text{CO}_3$	Conversion (%)	Difficulties observed
1 eq.	–	3 eq.	–	–	100	Difficulty in removing the excess of phosphazene
1 eq.	–	–	3 eq.	–	50	-
1 eq.	–	–	–	3 eq.	60	-
–	1 eq.	–	–	10 eq.	20	Polyacetamide formation
–	1 eq.	–	–	1 eq.	0	-
–	1 eq.	–	–	2 eq.	20	Small quantity of derivatized polyvanillin is obtained following normal and reverse phase (C18) silica gel column

Although the nature and the symmetrical arrangement of divanillin make it an interesting molecule for biobased polymeric materials, however it poses two main limitations including solubility difficulties and fragility under basic conditions which causes the transformation of divanillin into divanillyl alcohol. Initially, the reduction of divanillin was performed following the protocol of Savonnet et al. who used NaOH as the solvent [237]. Unexpectedly, divanillin was not completely soluble under these conditions, which hindered the progress of the reaction. So that, we solubilized divanillin in DMSO, since all other trials to dissolve it in common organic solvents and alcohols (MeOH, EtOH,  $\text{CHCl}_3$ , DCM, DMF (soluble but at very high

## *Polyvanillin by coupling of vanillin on immobilized horseradish peroxidase*

quantity of solvent) were not successful. This led to the formation of divanillyl alcohol with 80% yield and high purity.

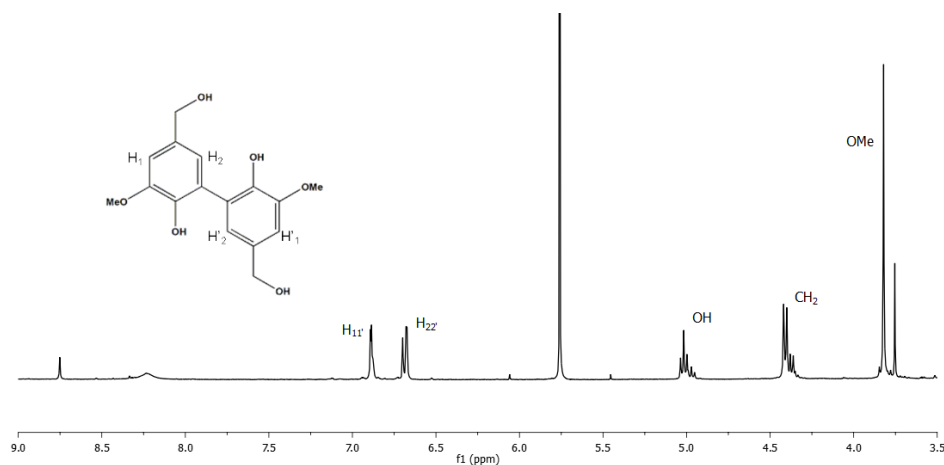


Figure 3-6: <sup>1</sup>H NMR of divanillyl alcohol

In these regards, the functionalization step became a necessity to improve the solubility and detectability of C-C divanillin by mass spectrometry, we were directed toward derivatization is among the most commonly used methods for chemical analysis to improve the properties of chemical compounds [238, 239]. Preliminary alkylation reactions were performed using NaOH as the base, which was then replaced by K<sub>2</sub>CO<sub>3</sub> because it is a milder reagent for MS. In the C-C coupled dimer, the two phenolic hydroxyl groups of vanillin are present. Accordingly, upon derivatization of the 5-5' divanillin, a mass increase of 2×57.02 Da is shown (Figure 3-8). Also the MALDI-TOF and FT-ICR spectra revealed that the presence of a trimer of vanillin, which appeared as the sodium adduct at *m/z* 589 Da possessing two amide groups [H(C<sub>8</sub>H<sub>6</sub>O<sub>3</sub>)<sub>3</sub>H + 2 C<sub>2</sub>H<sub>4</sub>NO + Na]<sup>+</sup>. Similar study was carried out by et al. where the type of linkages was clarified by silylation [152].



## *Polyvanillin by coupling of vanillin on immobilized horseradish peroxidase*

oxidation is influenced by the type of solvent utilized. For instance, the quick precipitation that results from the oxidation of phenolic compounds in fully aqueous solvents prevents the generation of products with higher degrees of polymerization [241].

As peroxidases can maintain their catalytic activity in such systems at well-defined concentrations, it is possible to conduct oxidation reactions involving them in a mixture of organic and aqueous solvent [242]. Researchers frequently use similar systems to change the state of their enzyme-catalyzed reactions from oligomerization to polymerization [232]. For this form of polymerization, the phosphate buffer: methanol system is the best system. In order to oligomerize/polymerize vanillin, oxidation of vanillin was conducted in a solution containing 40% methanol and 60% sodium phosphate buffer at pH 6.5.

### **3.5.3. Vanillin oxidation using immobilized oxidoreductases**

In this study, HRP was immobilized on immobeads®150P epoxy carrier to improve the findings of vanillin oxidation. Considering the simplicity of synthesis, product recovery, and degree of polymerization achieved, immobilized HRP was chosen as the best catalyst for vanillin polymerization. With a yield of 46%, the polymer obtained was recovered in dichloromethane while still being attached to the beads. A preliminary understanding of the structure of polyvanillin was obtained from the structural assignments of the ions produced by MALDI-TOF analysis, which revealed oligomeric series showing signals for sodium or potassium adducts and another indicating a loss of carbonyl group  $[H (C_8H_6O_3)_n H + Na]^+$ ,  $[H (C_8H_6O_3)_n H + k]^+$ , and  $[H (C_8H_6O_3)_n H - CO + K]^+$ . The primary distribution, which begins at  $m/z$  421.11 and continues with a difference of 150 Da, ends at  $m/z = 1963.12$  Da, was composed of the peaks corresponding to the  $K^+$  adducts. The second ion series begins at  $m/z$  763.06 and finishes at  $m/z$  1525.07 Da, and the third abundant series begins at  $m/z$  475.09 and ends at  $m/z$  1813.03 all with a mass increase of 150 units (Figure 3-10).

## Polyvanillin by coupling of vanillin on immobilized horseradish peroxidase

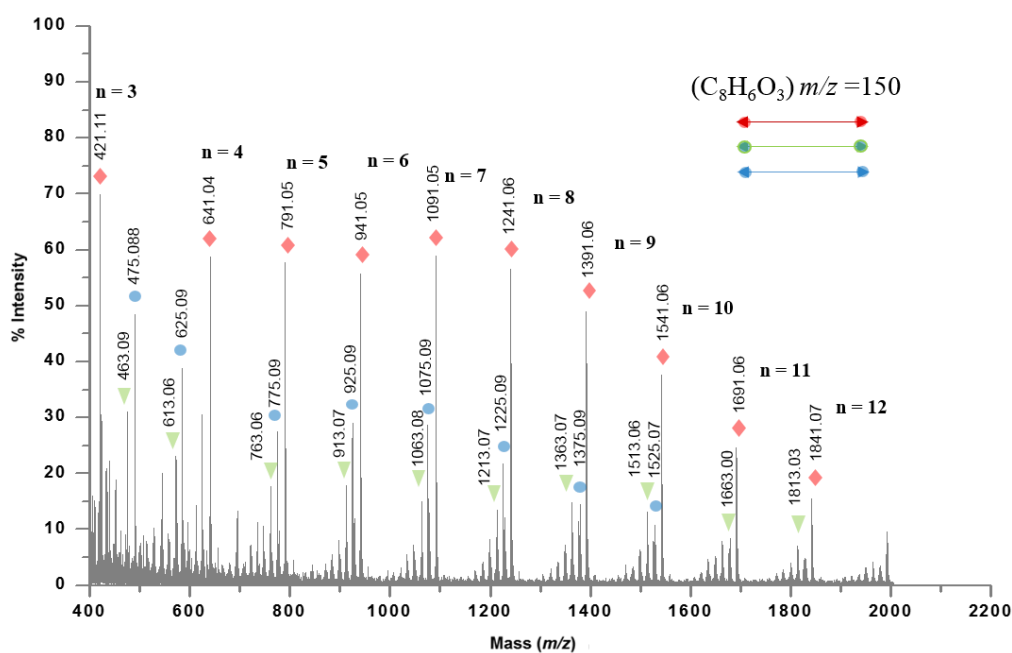


Figure 3-10: oligomers produced by immobilized HRP following vanillin oxidation.

The addition of water helped the oligomeric products that were already dissolved in dichloromethane (DCM) to precipitate even more on ice. This process increased the purity of polyvanillin. See (Figure 3-11).

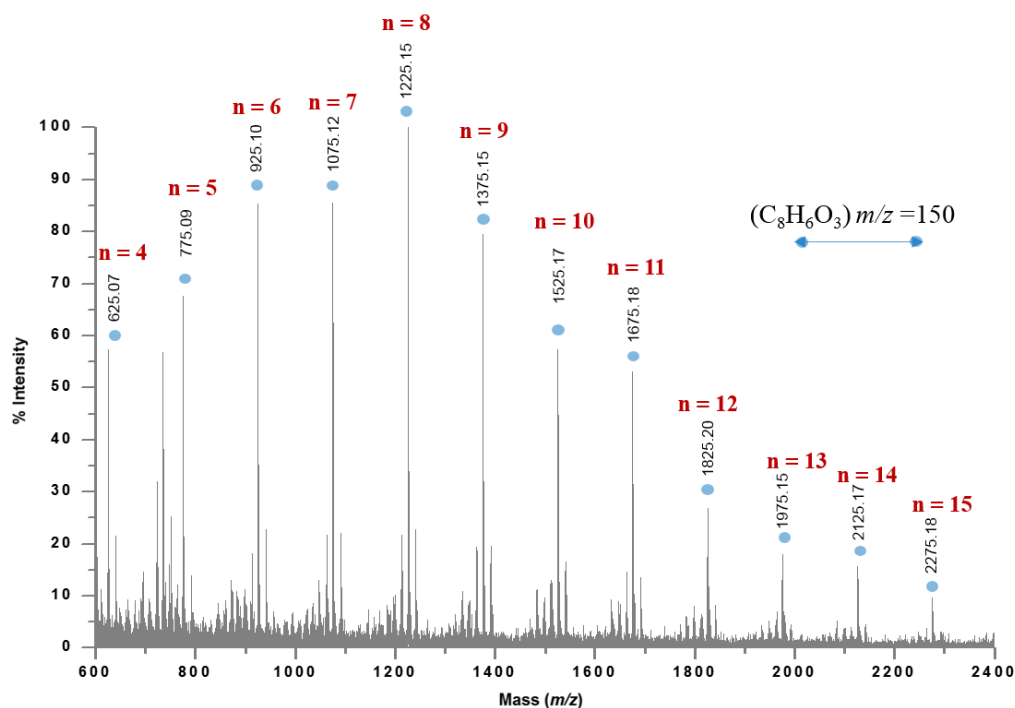


Figure 3-11: Oligomer produced following DCM/water treatment.

In order to elucidate the structure of polyvanillin by confirming whether a C-C or a C-O-4 linkage was established, two different functionalization processes were performed. Notably, the solubility of the obtained product in polar organic solvents such as acetone and dichloromethane, was an indication of the presence of high level of C-O linkages, and this was not the case of the 5-5' dimer, where its solubility was limited to DMSO.

Based on literature, polyvanillin formation was limited to electrochemical polymerization leading to the reduction of the formyl group which results in a Schiff base formation from vanillin [243]. Vanillin Schiff bases were used to prepare epoxies [237]. Other studies also reported the synthesis of biobased polymers from vanillin, but none of these attempts resulted in the formation of homopolymer of vanillin presenting on the most significant couplings in lignin.

Structural characterization using MALDI-TOF and FT-ICR showed that the derivatization processes helped significantly reduce impurities and made hydroxyl functional groups identifiable. Following derivatization of polyvanillin with iodoacetamide, spectrum shows the presence of three different series;  $[H (C_8H_6O_3)_n H + (C_2H_3NO) + Na]^+$  is the formula for this

## Polyvanillin by coupling of vanillin on immobilized horseradish peroxidase

series. The first one showing a mass increment of 57.02 Da which corresponds to the addition of one amide unit, means that all the hydroxyl groups were implied in C-O couplings leaving only one free terminal hydroxyl function for a side-chain C-C bond.. The formula for the second ion series, which has C-O couplings, is  $[H(C_8H_6O_3)_n H + (C_2H_3NO)_2 + Na]^+$ . The formula  $[H(C_8H_6O_3)_n H + (C_2H_3NO)_3 - 2CO + Na]^+$  correspond for the third ion series, which indicates the existence of two terminal C-C bonds, was also used to define a family of polyvanillins (Figure 3-12).

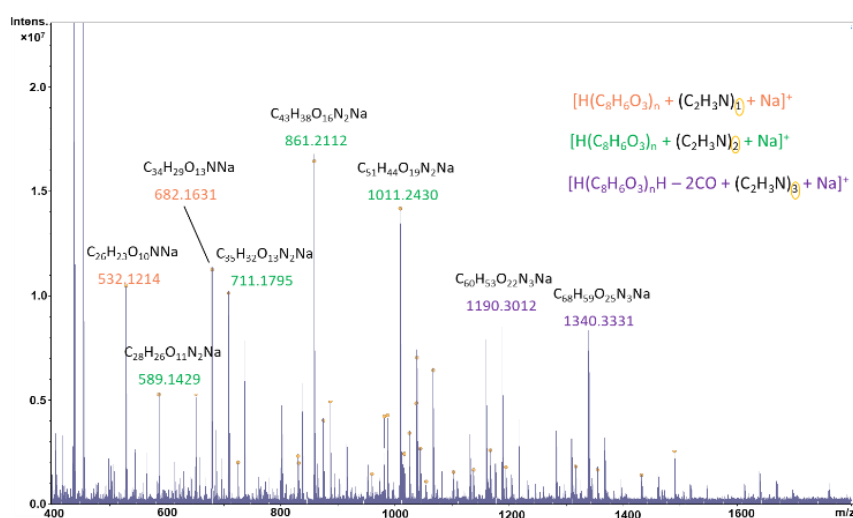


Figure 3-12: polyvanillin derivatized using iodoacetamide.

The table below displays the MS data for the identified products; the  $m/z$  values that were not visible on the spectrum were manually verified.

Table 3-3: a summary of the three series of polyvanillin in basic medium

series	Formula	Molecular formula	$m/z$ calculated	$m/z$ measured	Error (ppm)

*Polyvanillin by coupling of vanillin on immobilized horseradish peroxidase*

+0	$[\text{H}(\text{C}_8\text{H}_6\text{O}_3)_3\text{H}+(\text{C}_2\text{H}_3\text{ON})+\text{Na}^+]$	$\text{C}_{26}\text{H}_{23}\text{O}_{10}\text{NNa}$	532.1222	532.1214	0.11
1	$[\text{H}(\text{C}_8\text{H}_6\text{O}_3)_5\text{H}+(\text{C}_2\text{H}_3\text{ON})+\text{Na}^+]$	$\text{C}_{42}\text{H}_{35}\text{O}_{16}\text{NNa}$	832.1862	832.1848	-0.32
	$[\text{H}(\text{C}_8\text{H}_6\text{O}_3)_8\text{H}+(\text{C}_2\text{H}_3\text{ON})+\text{Na}^+]$	$\text{C}_{66}\text{H}_{53}\text{O}_{25}\text{NNa}$	1432.3121	1432.3119	0.88
2	$[\text{H}(\text{C}_8\text{H}_6\text{O}_3)_3\text{H}+(\text{C}_2\text{H}_3\text{ON})_2+\text{Na}^+]$	$\text{C}_{28}\text{H}_{26}\text{O}_{11}\text{N}_2\text{Na}$	589.1434	589.1429	-0.11
	$[\text{H}(\text{C}_8\text{H}_6\text{O}_3)_8\text{H}+(\text{C}_2\text{H}_3\text{ON})_2+\text{Na}^+]$	$\text{C}_{68}\text{H}_{56}\text{O}_{26}\text{N}_2\text{Na}$	1339.3019	1339.3035	0.016
	$[\text{H}(\text{C}_8\text{H}_6\text{O}_3)_{10}\text{H}+(\text{C}_2\text{H}_3\text{ON})_2+\text{Na}^+]$	$\text{C}_{84}\text{H}_{68}\text{O}_{32}\text{N}_2\text{Na}$	1639.3652	1639.3674	-0.022
3	$[\text{H}(\text{C}_8\text{H}_6\text{O}_3)_4\text{H}+(\text{C}_2\text{H}_3\text{ON})_3-(\text{CO})+\text{Na}^+]$	$\text{C}_{37}\text{H}_{35}\text{O}_{14}\text{N}_3\text{Na}$	768.2017	768.2022	-0.05
	$[\text{H}(\text{C}_8\text{H}_6\text{O}_3)_5\text{H}+(\text{C}_2\text{H}_3\text{ON})_3-(\text{CO})+\text{Na}^+]$	$\text{C}_{45}\text{H}_{41}\text{O}_{17}\text{N}_3\text{Na}$	918.2333	918.2328	0.06
	$[\text{H}(\text{C}_8\text{H}_6\text{O}_3)_7\text{H}+(\text{C}_2\text{H}_3\text{ON})_3-(\text{CO})+\text{Na}^+]$	$\text{C}_{61}\text{H}_{53}\text{O}_{23}\text{N}_3\text{Na}$	1218.2967	1218.2960	0.17

Furthermore, tetrakiscope (II) triflate was used to functionalize polyvanillin in an acidic media. Functionalization in an acidic medium made the product extraction simpler than with iodoacetamide since it required fewer washing steps and produced a better yield. The MALDI-TOF peaks' mass discrepancies were validated by the MALDI-FT-ICR spectra and correspond to the addition of one acetyl group (42 units), and has the following formula  $[\text{H}(\text{C}_8\text{H}_6\text{O}_3)_n\text{H}+(\text{C}_2\text{H}_2\text{O})+\text{Na}]^+$ . Therefore, 4-O-5 bonds were ascribed to all of the polyvanillin's interunit connections. These findings are consistent with the work of Nanayakkara et al., who demonstrated that HRP adsorbed on silica nanorods could generate phenol radicals that could then be polymerized via C-O linkages to form linear polymers.

The importance of this bond resides in many aspects, 1) it is among the ether units ( $\beta$ -O-4,  $\alpha$ -O-4, and 4-O-5) that are highly abundant in lignin, constituting around 80% of the bond formation. Further, it is characterized by high resistance to depolymerization [239].

The alternative series, which has the formula  $[\text{H}(\text{C}_8\text{H}_6\text{O}_3)_n\text{H}+(\text{C}_2\text{H}_2\text{O})_2+\text{O}+\text{K}]^+$ , also has a C-C bond and C-O couplings with a gain of oxygen. There was also a series that did not exhibit derivatization but rather oxidation,  $[\text{H}(\text{C}_8\text{H}_6\text{O}_3)_n\text{H}+\text{O}+\text{H}]^+$ . Another one is represented by the formula  $[\text{H}(\text{C}_8\text{H}_6\text{O}_3)_n\text{H}+(\text{C}_2\text{H}_2\text{O})+(2\text{O})+\text{K}]^+$ , which displays a gain of 42.01 units and two oxygen atoms, in Figure 3-13. These results lead us to the conclusion that vanillin was oxidized with immobilized HRP to produce a variety of polyvanillin families with a predominance of C-O interunit linkages.

## Polyvanillin by coupling of vanillin on immobilized horseradish peroxidase

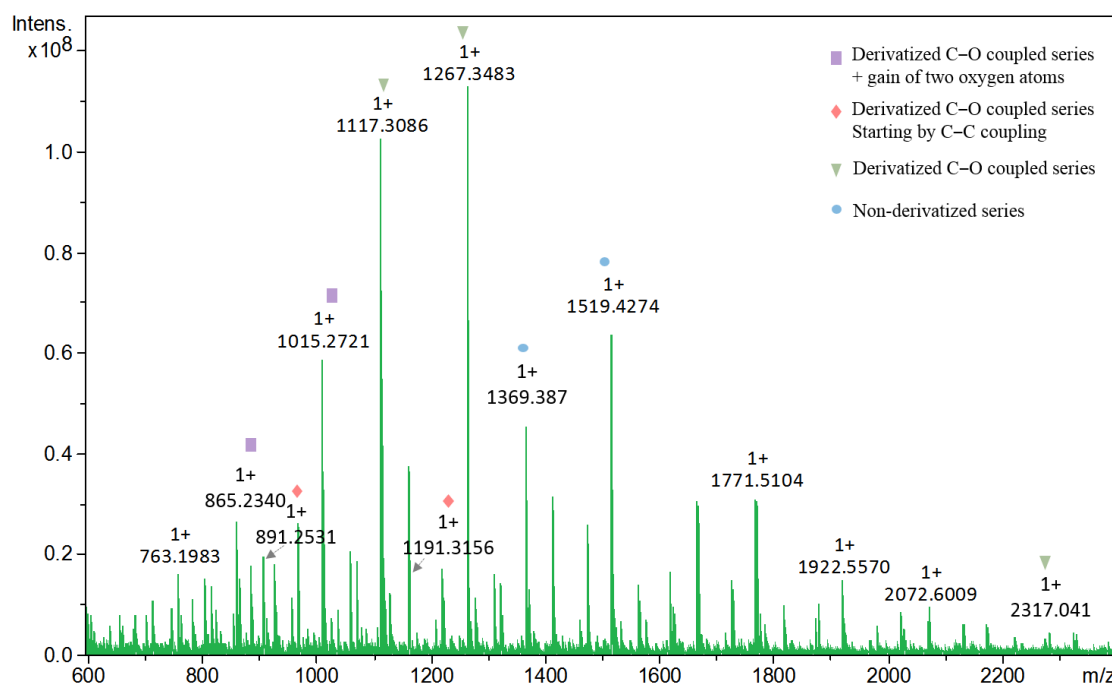


Figure 3-13: polyvanillin derivatized in acidic medium.

Table 3-4: a summary of the three series of polyvanillin in acidic medium

series	Formula	Molecular formula	$m/z$ measured
1	$[\text{H} (\text{C}_8\text{H}_6\text{O}_3)_7 \text{H} + (\text{C}_2\text{H}_2\text{O}) + \text{Na}^+]$	$\text{C}_{58}\text{H}_{46}\text{O}_{22}\text{Na}$	1117.3086
	$[\text{H} (\text{C}_8\text{H}_6\text{O}_3)_8 \text{H} + (\text{C}_2\text{H}_2\text{O}) + \text{Na}^+]$	$\text{C}_{66}\text{H}_{52}\text{O}_{25}\text{Na}$	1267.3483
	$[\text{H} (\text{C}_8\text{H}_6\text{O}_3)_{15} \text{H} + (\text{C}_2\text{H}_2\text{O}) + \text{Na}^+]$	$\text{C}_{122}\text{H}_{94}\text{O}_{46}\text{Na}$	2317.041
2	$[\text{H} (\text{C}_8\text{H}_6\text{O}_3)_5 \text{H} + (\text{C}_2\text{H}_2\text{O})_2 + (2 \times \text{O}) + \text{Na}^+]$	$\text{C}_{44}\text{H}_{36}\text{O}_{19}\text{Na}$	891.2531
	$[\text{H} (\text{C}_8\text{H}_6\text{O}_3)_7 \text{H} + (\text{C}_2\text{H}_2\text{O})_2 + (2 \times \text{O}) + \text{Na}^+]$	$\text{C}_{60}\text{H}_{48}\text{O}_{25}\text{Na}$	1191.3156
	$[\text{H} (\text{C}_8\text{H}_6\text{O}_3)_{17} \text{H} + (\text{C}_2\text{H}_2\text{O})_2 + (2 \times \text{O}) + \text{Na}^+]$	$\text{C}_{140}\text{H}_{108}\text{O}_{55}\text{Na}$	2691.1114
3	$[\text{H} (\text{C}_8\text{H}_6\text{O}_3)_5 \text{H} + (\text{C}_2\text{H}_2\text{O}) + (2 \times \text{O}) + \text{K}^+]$	$\text{C}_{42}\text{H}_{34}\text{O}_{18}\text{K}$	865.2340
	$[\text{H} (\text{C}_8\text{H}_6\text{O}_3)_6 \text{H} + (\text{C}_2\text{H}_2\text{O}) + (2 \times \text{O}) + \text{K}^+]$	$\text{C}_{50}\text{H}_{40}\text{O}_{21}\text{K}$	1015.2721
	$[\text{H} (\text{C}_8\text{H}_6\text{O}_3)_{12} \text{H} + (\text{C}_2\text{H}_2\text{O}) + (2 \times \text{O}) + \text{K}^+]$	$\text{C}_{98}\text{H}_{76}\text{O}_{39}\text{K}$	1915.4950

It is important to note that the polyvanillin created in this study has a number of noteworthy characteristics, the most significant of which is the presence of the C-O bond, a relevant bond in natural lignin distinguished by its strong resistance to depolymerization and opening up a new avenue for research in this field.

## *Polyvanillin by coupling of vanillin on immobilized horseradish peroxidase*

According to published research, the only approach that could successfully polymerize vanillin was one that combined the production of the 5-5' dimer through a dehydrogenative oxidation reaction catalyzed by HRP with an electrochemical reaction that reduced the aldehyde groups [208]. Vanillin was also the subject of other research that discussed the synthesis of biobased polymers, but none of these endeavors produced homopolymers of vanillin that exhibit the strongest couplings in lignin [206, 244].

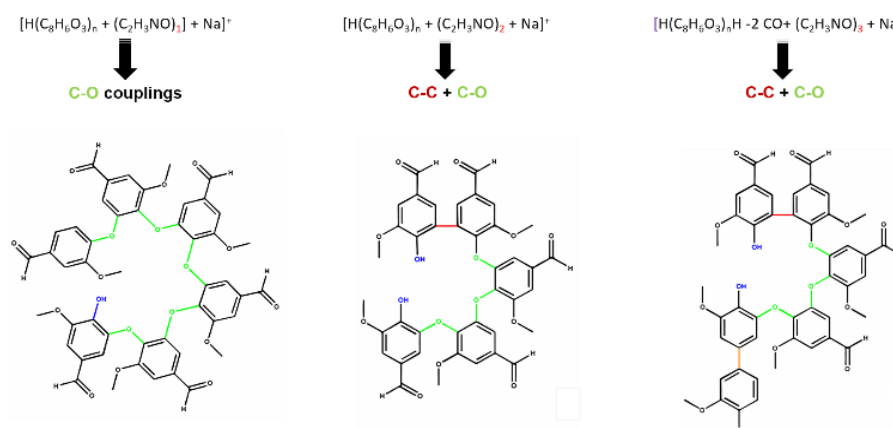


Figure 3-14: Polyvanillin's suggested structures

### 3.6. Conclusion

Divanillin was the subject of all initial tests, which made it possible to upgrade tactics more easily because of its accessibility and ease of use. Additionally, this dimer served as a model chemical for the creation of a well-structured approach that made it possible for improved polyvanillin characterization.

Immobilization of enzymes has a lot of benefits. In this work, the simple separation of the reaction product and the production of an oligomer with higher purity and degree of polymerization were found to be the key benefits of utilizing mounted HRP versus free enzyme. The study of polyvanillin can be utilized as a model to investigate both the production and depolymerization of lignin. Instead of working directly on isolated lignin, it will be more practical to investigate C-O bond susceptibility to degradation using a straightforward and

## *Polyvanillin by coupling of vanillin on immobilized horseradish peroxidase*

accessible template. This makes room for quick and inexpensive system upgrades. In various ways, this study will aid lignin research:

- 1) It provides a sound framework for understanding the processes that give rise to the C-C and C-O linkages, which make up the majority of lignin.
- 2) It serves as a matrix for research into the ether bond cleavage that has been the subject of numerous investigations [C-O cleavage of diphenyl ether followed by C-C coupling reactions over hydrophobized Pd/HY catalysts].

## **4. CHAPTER FOUR: SYNTHESIS OF SUICIDE INHIBITORS OF LIGNIFICATION**

### **4.1. Introduction**

Lignin is biosynthesized by polycondensation of phenol-alcohols. The mechanism involves the oxidation coupling of these phenols, via the formation of radicals, which then couple upon oxidation by peroxidases. The identification of peroxidases involved in lignin synthesis offers a viable route for modulating lignin composition in plants by providing access to their genetic modification.

Heme-peroxidases of the class III plant family, primarily HRP, catalyze the one-electron oxidation of phenolic compounds in a way that suggests the presence of H<sub>2</sub>O<sub>2</sub> [245]. The native enzyme is transformed into compounds I and II throughout this mechanism, and phenoxy radicals are produced before the enzyme returns to its normal state. Both H<sub>2</sub>O<sub>2</sub> and phenolic substrates can influence the activity of peroxidases during this phase, which can result in the enzyme's deactivation [246-248]. Many inactivation mechanisms have been postulated, and HRP has been at the focus of investigations on the mechanism-based inactivation of peroxidases.

The investigation of the mechanism of HRP inactivation provides insights into the mechanisms involving additional heme-containing enzymes [249]. Also, it supports the creation of novel strategies that enable the manufacturing of peroxidases with enhanced catalytic capabilities. In this regard, a technique was created to investigate the process of lignification peroxidases' deactivation during the oxidation of specific lignin monomers.

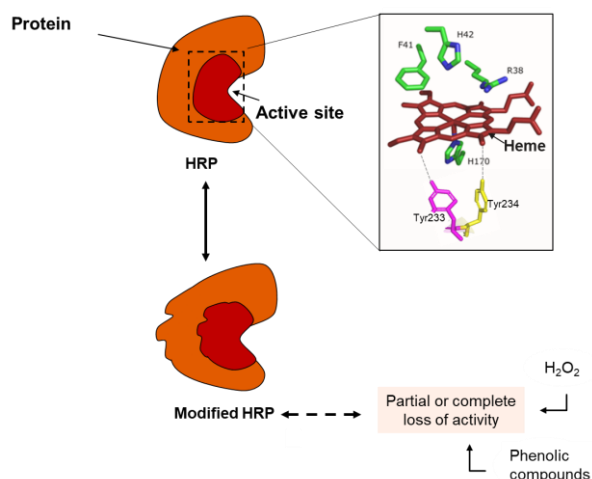


Figure 4-1: Process of lignification peroxidases' deactivation during the oxidation of specific lignin monomers.

Nicolas Daubresse et al. demonstrated that fluoroferulic acid is able to inhibit the activity of peroxidases, by substituting a hydrogen atom with a fluorine atom, which is comparable to hydrogen but more reactive when added on a reactive position, such as the  $\beta$ -vinyl position. In addition, it has been indicated that the fluorinated analog of coniferyl alcohol is considered to be a specific inhibitor of lignin biosynthesis [250].

## 4.2. Horseradish peroxidase (HRP): a versatile enzyme

Peroxidases belong to oxidoreductase family that use hydrogen peroxide as the electron receptor. The catalytic cycle of peroxidases, also known as the Poulos-Kraut mechanism, was first illustrated in 1980 by Poulos et al [251, 252].

The catalytic cycle of HRP starts by the interaction of the enzyme in the resting state with hydrogen peroxide, leading to a two-electron oxidation of heme iron to a high oxidation state intermediate compound I, which consists of a Fe (IV) oxoferryl center and a porphyrin-based cation radical. Next, compound I is transformed into compound II (the Fe (IV) oxoferryl state) following a one-electron reduction of the porphyrin radical cation by the substrate. Finally, compound II undergoes a second one electron reduction and it goes back to the resting state [253-255] (Figure 4-2).

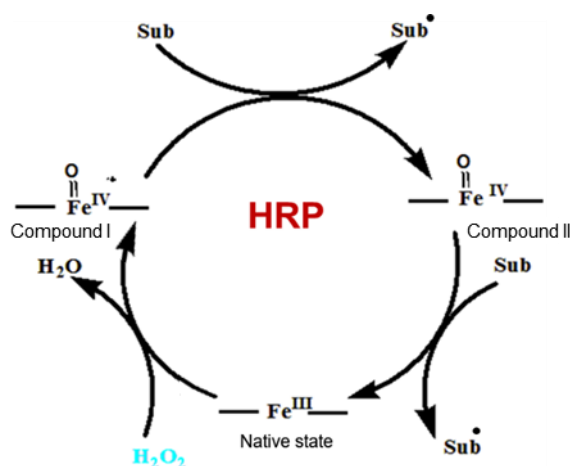


Figure 4-2: Peroxidase catalytic cycle [254].

Peroxidase's mechanism of action has been extensively researched and is explained in three subsequent reactions [256]:

- (1)  $\text{Fe(III) [P]} + \text{H}_2\text{O}_2 \rightarrow \text{Fe(IV)O [P}^{\bullet+}] + \text{H}_2\text{O}$
- (2)  $\text{Fe(IV)O [P}^{\bullet+}] + \text{RH}_2 \rightarrow \text{Fe(IV)O} + \text{RH}^{\bullet} + \text{H}^+$
- (3)  $\text{Fe(IV)O} + \text{RH}_2 \rightarrow \text{Fe(III)} + \text{RH}^{\bullet} + \text{OH}^-$

[P<sup>•+</sup>]: is porphyrin radical of heme

RH<sub>2</sub>: is the organic substrate

### **4.3. Several routes by which peroxidase is inactivated during the oxidation of phenolic substances**

The catalytic cycle of peroxidases involves a number of side reactions that result in the deactivation or inhibition of peroxidases [74, 257]. High amounts of H<sub>2</sub>O<sub>2</sub> results in the conversion of compound II into a catalytically inactive form, compound III, [258]. Although HRP has a pseudo catalase activity that serves as a key defense against H<sub>2</sub>O<sub>2</sub> inactivation, P-670, an irreversibly inactive form, the verdohemoprotein can also form [259]. The HRP catalytic cycle with the possible inhibitory pathways is shown in Figure 4-3.

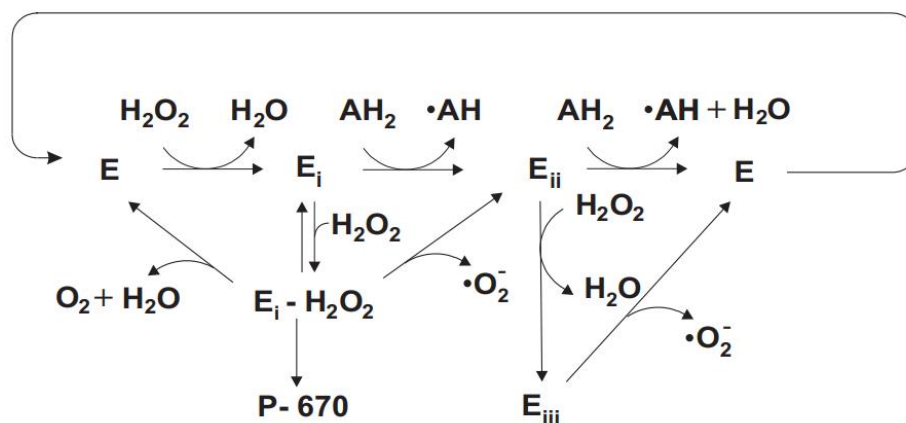


Figure 4-3: Peroxidase's full catalytic cycle displaying the two side reactions. Compounds I, II, and III each have a ground state identified by the letters E<sub>i</sub>, E<sub>ii</sub>, and E<sub>iii</sub>, respectively. AH<sub>2</sub> and A.P-670, also known as verdohaemoprotein, is the inactive form of peroxidase [260].

The inactivation can turn into suicide in the presence of a donor substrate [246]. There are different pathways for the inactivation of peroxidases by the substrate, including the inhibition of peroxidase by the polymer of the oxidation reaction that limits the access to the substrate [74-76]. Phenoxy radicals can react with HRP following different pathways illustrated in Figure 4-3. These pathways include cross-linking between amino acids (v) or between amino acid residues and the polypeptide chain of HRP (iv), as well as interaction with polypeptide chain amino acid residues, most notably tyrosine I (i) and coupling of a phenoxy radical to the HRP heme moiety (ii). The polypeptide chain's amino acids may also undergo modification, such as oxidation (iii). The reaction conditions and the type of the substrate play a major role in determining which of these routes will contribute to peroxidase inactivation (Figure 4-4).

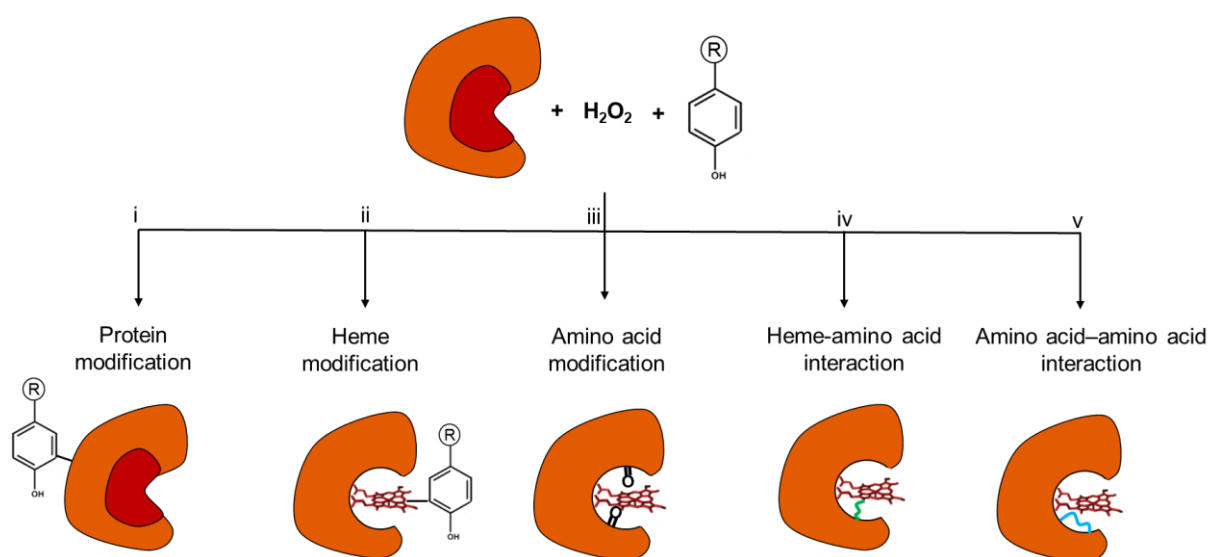


Figure 4-4: The several mechanisms by which phenoxy radicals inactivate peroxidases.

#### **4.4. Click chemistry**

Click chemistry enables with assembly of molecules excellent yields and quick, versatile, and efficient, [72]. There exist several types of click chemistry reactions, such as cycloaddition reactions (1,3-dipolar cycloaddition and Diels-Alder reactions), nucleophilic ring-opening reactions, carbonyl chemistry, including aromatic heterocycles, in addition to carbon-carbon multiple bonds. Click chemistry is used in a wide range of domains including radiochemistry, bioconjugation, material science, and drug discovery [261]. In addition to the immobilization of enzymes at specific sites [262].

#### **4.5. Azide-alkyne cycloaddition process catalyzed by copper (I) (CuAAC)**

The CuAAC catalyzed by copper (I), is the most prevalent common click reaction. It involves the cycloaddition of an azide and an alkyne to produce 1,4-substituted triazole [263, 264]. For copper to rest copper in an oxidizing state during CuAAC reactions, an excess reducing agent such as sodium ascorbate is required [265, 266]. It is one of the most often utilized biorthogonal click reactions and is used in a variety of fields, including the synthesis of probes with various functional groups and architectural configurations [73] and the production of drugs [267].

Click chemistry has been used in conjunction with proteomic methods to selectively label and enrich proteins prior to their identification and quantification. The overall workflow is comparable to traditional shotgun proteomic methods in that proteins in cells, tissues, or lysates are labeled with a click moiety (either an azide or an alkyne tag), followed by a click reaction integrating a complementary protein-enrichment tag linked to a clickable functional group, like biotin. Labeled proteins are subsequently isolated using an affinity matrix, put through proteolysis, and finally put through MS analysis.

#### **4.6. CuAAC reaction mechanism**

Kolb and co-workers [72] proposed the CuAAC reaction mechanism. The azide partner is coordinated to copper (I) at the alkylated nitrogen during the production of the copper (I) acetylide in the first step, which results in the development of a complex of all three components

(1). The first C-N bond is created, and this complex then becomes a metallacycle (2). The copper core is moved from oxidation state +1 to oxidation state +3 in this stage. As a result, a ring contraction happens when copper (III) is reduced to copper (I), creating cuprous triazolide (3). If no alternative proton source is available, the cuprous triazolide takes a proton from an alkyne molecule to produce a full triazole (4) (Figure 4-5).

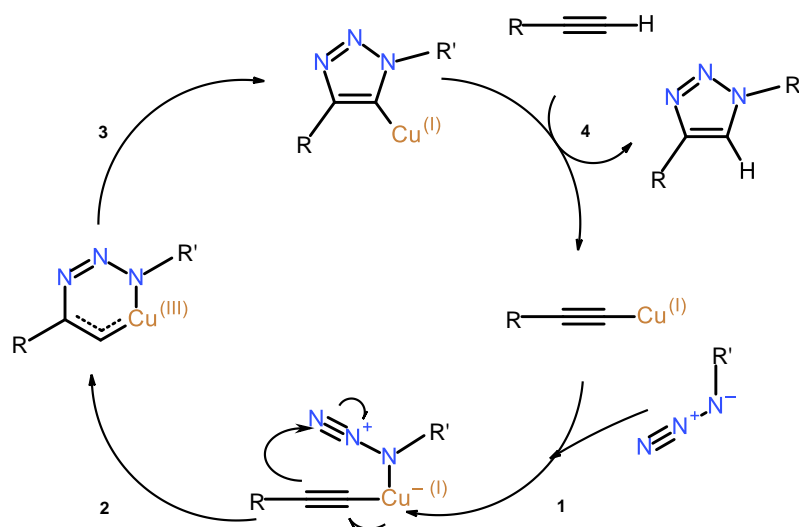


Figure 4-5: The CuAAC reaction's postulated mechanism by Kolb et al. [72].

#### **4.7. Adding reactive handles (such as azide or alkyne) to biological compounds**

Biomolecules can be functionalized in a variety of ways using alkyne or azide handles. There are two typical techniques for doing this: using an N-hydroxysuccinimide (NHS) for the formation of an amide bond between amine and carboxylic acid, or using a substituted maleimide,[73]. Unnatural amino acids (UAAs) or non-canonical amino acids coupled to azide or alkyne functionalities have been produced and used, especially for the functionalization of proteins [268].

#### **4.8. Inhibitor of lignification**

In order to determine the reactivity order of the hydroxyl or the alkyne group, mono- and bi-alkyne groups were introduced into the modified lignin monomers. These inhibitors could be convenient both for the inhibition or the pull down of lignification peroxidases. So the final goal is to synthesize coniferyl alcohol derivatives and their analogues. At first, we focused on

the ferulic acid to know if our peroxidase prey recognizes the modified alcohol before proceeding to a more complex synthesis.

Thus, nine biotin-phenol analogues were designed as specialized lignification peroxidases identifiers/inhibitors comprising mono- and bi-alkyne functionalized substrates. These monomers differed by their size, levels of steric hindrance, substitution, and redox potentials. To link biotin and coniferyl alcohol derivative, we planned to use a click-chemistry reaction.

#### **4.9.Objective**

The goal of this study is to better understand the mechanisms of interaction between lignification peroxidases in the presence of their phenolic substrates. In this work we focused on the inactivation of HRP, a model enzyme highly used in lignification studies. Using specialized substrates made from lignin monomers. These substrates include clickable handles that can be used in click-chemistry-based purification systems. The mechanism of HRP inactivation by its aromatic substrates was explained using kinetic and mass spectrometry investigations. The specialized substrates are similar to the commercial biotin-tyramide used to identify proteins interacting with a particular protein using an approach called proximity-dependent biotinylation. In our study, different hydroxycinnamic acids have been functionalized with a triple carbon bond linker.

The general strategy consist of:

- Synthesis of hydroxycinnamic acid derivatives
- Incubation of the enzyme extract with the lignin monomers derivative
- Trapping peroxidases-lignin monomer derivatives to biotin azide using click-chemistry reaction
- Isolation and identification of lignification peroxidases.

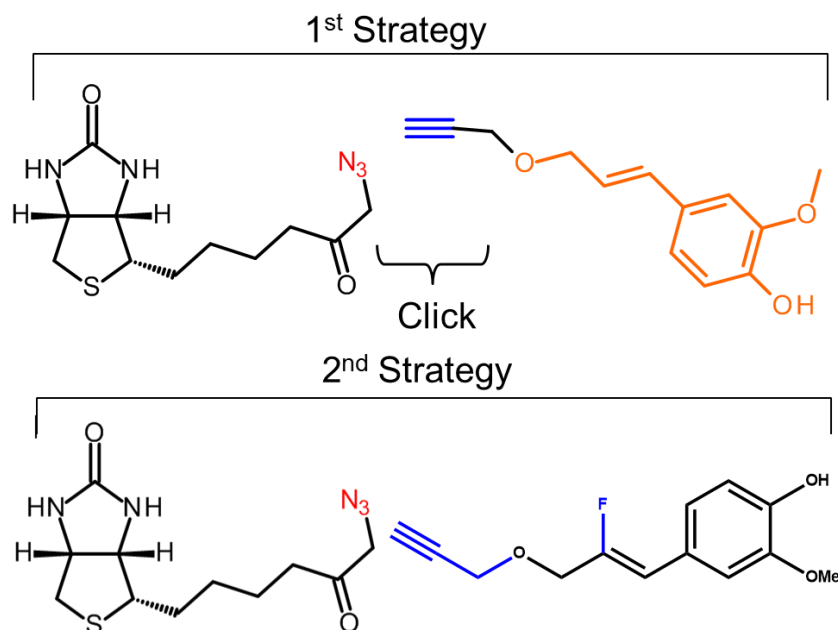


Figure 4-6: Functionalization of coniferyl alcohol for pull-down of lignification peroxidase by a bait and prey strategy

## 4.10. Experimental part

### 4.10.1. Chemicals

HRP type II (P8250), biotin phenol, phosphate buffered saline, biotin-PEG3 azide, potassium acetate, sodium ascorbate, acetonitrile, toluene, methanol and copper sulfate pentahydrate, sodium ascorbate, 2-butanone, formic acid,  $\alpha$ -Cyano-4-hydroxycinnamic acid, DMSO, Tween-20, hemin chloride, Paratoluene sulfonic acid (PTSA), 2-propyl-1-ol, ferulic, coumaric, sinapic and 3,4-dimethoxycinnamic acids were from Sigma Aldrich, C18 SPE column was from thermofisher scientific.

### 4.10.2. Fisher esterification of phenols

485 mg of ferulic acid (2.5 mmol) and 70 mg PTSA (0.4 mmol) were dissolved in 280 mL of toluene and 13.6 ml of 2-propyl-1-ol (235 mmol), the mixture was stirred for 24 h at 100 °C. After cooling down, the desired product was extracted in 60 mL of ethyl acetate, neutralized with 5% NaHCO<sub>3</sub>, and washed 3 times with water. The organic phase was dried over anhydrous

MgSO<sub>4</sub>, filtered, and evaporated. The product was then purified on chromatography column using chloroform. The same procedure was used for coumaric, sinapic and 3,4-dimethoxycinnamic acids however the desired product was obtained after chromatographic separation using solvent gradient of CHCl<sub>3</sub>: MeOH.9:1.

#### **4.10.3. Functionalization of ferulic ester with propargyl bromide**

500 mg Ferulic acid (2.23 mmol) was dissolved in 30 mL methanol containing 1 mL of sulfuric acid, and then the solution was heated at reflux for 1 h. After cooling at room temperature, the solution was diluted with 150 mL ethyl acetate and washed with an aqueous solution of NaHCO<sub>3</sub> (5% w/v) until pH is neutral. The organic layer was then washed with distilled water and dried over anhydrous MgSO<sub>4</sub>, and the solvent was removed under vacuum. The residues were constituted by the pure methyl ester. Yield 90%.

66 mg of NaH (1.1 mmol) was washed with 6 mL n-pentane (5 times), and then dissolved in 3 mL of acetonitrile in glacial bath, 104 mg of ferulic ester (0.5 mmol) dissolved in 1 mL acetonitrile was added slowly followed by the addition of 0.039 mL of propargyl bromide solution (0.45 mmol). The mixture was stirred overnight at room temperature. The reaction was then stopped with 1 mL of formic acid solution (1%). The desired product was obtained after extraction using dichloromethane followed by washing with water 3 times; and was used directly for the next step without further purification. Yield: 44%.

#### **4.10.4. Bifunctionalization of ferulic acid**

485 mg of ferulic acid (2.5 mmol) and 70 mg PTSA (0.4 mmol) were dissolved in 280 mL of toluene and 13.6 mL of 2-propyl-1-ol (235 mmol), the mixture was stirred for 24 h at 100 °C. After cooling; 60 mL of ethyl acetate was added followed by washing with 5% NaHCO<sub>3</sub> and water 3 times. The organic phase was dried over anhydrous MgSO<sub>4</sub>, filtered, and evaporated. The product was purified on chromatography column using chloroform.

92 mg of NaH (1.54 mmol) was washed with 6 mL n-pentane (5 times) then it was dissolved in 6 mL of acetonitrile in glacial bath, 234 mg of ferulic ester (0.7 mmol) dissolved in 1 mL

acetonitrile was added slowly; after that a 54  $\mu\text{L}$  of propargyl bromide solution (0.63 mmol) was added to the mixture solution and it was stirred overnight at room temperature. The reaction was stopped with 2 mL of formic acid solution (1%) the desired product was obtained after extraction using dichloromethane followed by washing with water 3 times; and was used directly for the next step without further purification. Yield: 36%.

#### **4.10.5. Deuterated propargylated ferulic acid**

##### *4.10.5.1. Deuterated vanillin synthesis*

500 mg of 3,4-Dihydroxybenzaldehyde (3.6 mmol) was dissolved in 3.7 mL of NaOH solution (2 M in ethanol) then 510 mg of Iodomethane  $\text{d}_3$  (3.5 mmol), diluted in ethanol (20 ml) was added slowly during 15 minutes; the reaction mixture was stirred at room temperature for 48 hours. To prevent the emulsion, the solution was evaporated on a rotary evaporator under vacuum, the result product was dissolved in a large excess of water (37 ml) and extracted with dichloromethane (3 x 10 mL). The aqueous phase was taken and acidified with acetic acid solution 5% and extracted with  $\text{CH}_2\text{Cl}_2$  (4 x 20 mL). The pure vanillin  $\text{d}_3$  was obtained after several washing with water of the organic phase, dried over  $\text{MgSO}_4$  and evaporated. Yield 39%.

##### *4.10.5.2. Deuterated ferulic acid synthesis by knoevenagel reaction*

160 mg of deuterated vanillin (1 mmol) with 178 mg malonic acid (2 mmol) were dissolved in 0.51 mL pyridine (7.4 mmol). Then, the piperidine (35  $\mu\text{L}$ , 0.4 mmol) was added. The mixture was heated at 70°C for 2.5 h. After cooling, pyridine was removed by evaporation; the result product was diluted in saturated  $\text{NaHCO}_3$  solution; then concentrated HCl solution was added it on an ice bath until pH 3 was reached. Then, the solution was kept in the fridge for 2 days, in order to obtain stimulate precipitation. Precipitates were washed with distilled water and dried in the oven overnight Yield 50%.

*4.10.5.3. Fisher esterification*

60 mg of deuterated ferulic acid (0.3 mmol) and 8.7 mg PTSA (0.04 mmol) were dissolved in 35 ml of toluene and 1.68 ml of 2-propyl-1-ol (mmol), the mixture was stirred for 24 h at 100 °C. After cooling; 20 ml of ethyl acetate was added followed by washing with 5% NaHCO<sub>3</sub> and water 3 times. The organic phase was dried over anhydrous MgSO<sub>4</sub>, filtered, and evaporated. The product was purified on chromatography column using chloroform: ethyl acetate.

**4.10.6. Coniferyl alcohol analogue**

*4.10.6.1. Selective protection of coniferyl alcohol*

180 mg of coniferyl alcohol (1 mmol) was dissolved in 15 mL dichloromethane at 0 °C. Then 188 mg of MOMBr (1.5 mmol) and 258 mg DIPEA (2 mmol) were respectively added slowly into the solution and the reaction was stirred at room temperature overnight. The reaction was quenched with 15 mL distilled water. The organic phase was washed with hydrochloric acid solution (0.5 M), followed by washing with sodium hydroxide solution (1M) until neutralization and dried over anhydrous MgSO<sub>4</sub>.

After evaporation on rotary evaporator, the resultant product was purified on chromatography column packed with the silica pre-soaked in 1% triethylamine overnight. The solvent gradient used was Dichloromethane: Methanol 80:20) yield: 79%.

*4.10.6.2. Functionalisation of protected coniferyl alcohol*

80 mg of NaH (1.32 mmol) was washed with 6 mL n-pentane (5 times) then it was dissolved in 3 mL of acetonitrile in an ice bath, 143 mg of protected coniferyl alcohol (0.6 mmol) dissolved in 1 mL acetonitrile was added slowly; after that a 0.047 mL of propargyl bromide solution (0.54 mmol) was added to the mixture solution and it was stirred overnight at room temperature.

The reaction was stopped with 1 mL of formic acid solution (1%) and the desired product was obtained after extraction with CH<sub>2</sub>Cl<sub>2</sub>, followed by washing with water 3 times; and was used directly for the next step without further purification. Yield: 39%.

4.10.6.3. *Deprotection of propargyleted coniferyl alcohol*

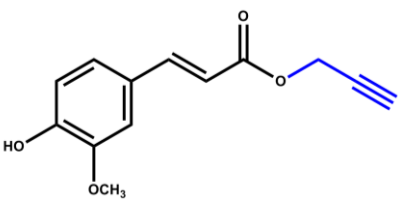
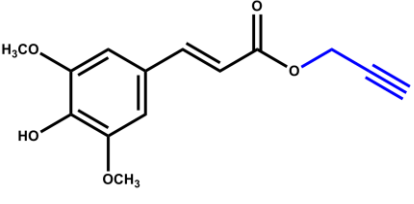
A 50 mg of the protected coniferyl alcohol, was dissolved in 7 mL methanol and 8 mL of hydrochloric acid solution 0.1M. The reaction mixture was heated at 60 °C under nitrogen during 36 h. The organic phase was extracted with ethylacetate (20 mL) and washed with water (3 times) then dried over MgSO<sub>4</sub>. The resultant product was purified on C18 column using acidic water: acetonitrile 70:30 (yield 70%).

**4.10.7. Purification on column chromatography**

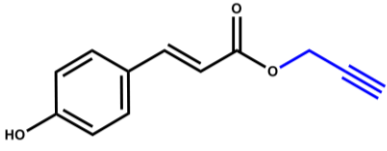
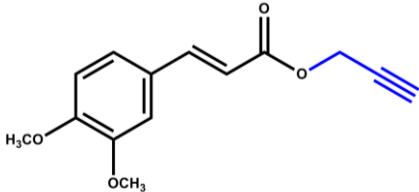
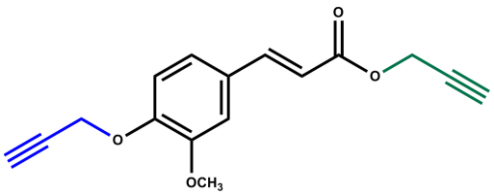
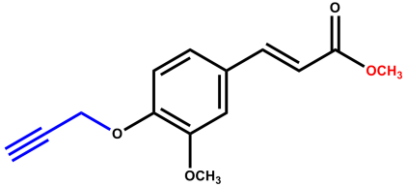
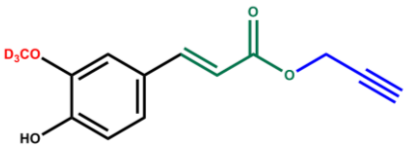
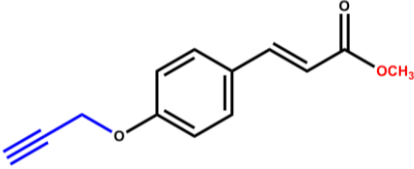
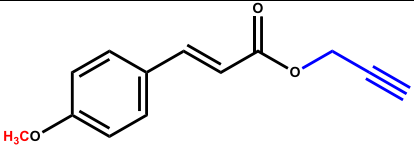
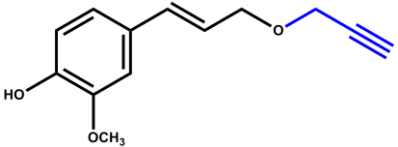
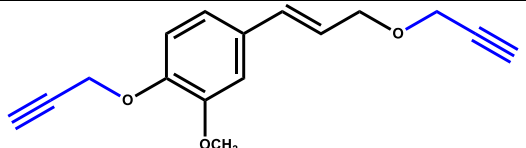
Following each reaction, each product was purified using column chromatography in a glass column made of silica gel (60–120 mesh). Approximately 50 mg of the crude product were dissolved in 2 ml of solvent, put onto the 46×2 cm column, and eluted using the linear gradient of solvents as follows: all the end products mentioned in the Table 4-1 were extract starting with 100% chloroform, 50/50 chloroform/ethyl acetate, and finally 80/20 ethyl acetate/methanol. Thin Layer Chromatography was used to analyze all of the obtained fractions.

**4.10.8. Summary of all inhibitors synthesized**

Table 4-1: Summary of all modified lignin monomers synthesized in this work

Modified lignin monomers	Name	Symbol
	Propargyl ferulate	PF
	Propargyl sinapate	PS

*Synthesis of suicide inhibitors of lignification*

	Propargyl coumarate	PC
	Propargyl cinnamate	PCI
	Bi-propargyl ferulate	BPF
	Propargyl methyl ferulate	PMF
	Deuterated propargyl ferulate	DPF
	Propargyl methyl coumarate	PMC
	Methyl propargyl coumarate	MPC
	Propargylated coniferyl alcohol	PCA
	Bi-propargylated coniferyl alcohol	BPCA

#### **4.10.9. Self-labeling of HRP with alkyne-lignin monomer probes**

Alkyne probes (100 µg) dissolved in 6% DMSO in PBS solution were added to a solution containing HRP (100 µg) in PBS, and then H<sub>2</sub>O<sub>2</sub> was added (100x). During 45 minutes, the reaction was rotated end to end during incubation. The samples were centrifuged at 14 000 rpm for 30 minutes in centrifugal filter apparatuses that had been treated overnight in Tween-20 solution (5%). The reaction was then halted, and the sample rinsed several times with PBS. After being cleaned, the materials were kept at -20°C until they were put through protein digestion.

#### **4.10.10. CuAAC reaction of biotin-PEG3-azide with alkyne handles**

Equivalent amounts of biotin-PEG3-azide, sodium ascorbate, and copper sulfate pentahydrate were added to a solution containing alkyne handles in PBS (100 µg). The mixture was agitated for two hours while rotating from end to end in the dark, and then centrifuged and washed several times with PBS to remove the excess of the reagents. After washing, the samples were stored at -20°C until subjected to protein digestion.

#### **4.10.11. Kinetic study of HRP inactivation**

To generate a final concentration of HRP of 586 nM and 58.6 nM, respectively, HRP was added to a typical reaction mixture including equivalent amounts of H<sub>2</sub>O<sub>2</sub> and phenolic substrate (0.1 mM in 0.6 or 1.2 mL DMSO) in a final volume of 4 or 40 mL PBS, pH 7.4. A similar experiment was also carried out in a smaller reaction volume (0.45 mL), with the reaction mixture consisting of H<sub>2</sub>O<sub>2</sub> (0.1 M) in PBS and phenolic compounds (0.1 M) solubilized in DMSO (0.05 or 0.1 mL). A HRP addition started the reaction (0.1 mM). Using the same reactional conditions, but without lignin derivatives, control studies using HRP alone or HRP with H<sub>2</sub>O<sub>2</sub> were employed. In the immediate aftermath of HRP insertion, Aliquots were taken immediately after

the addition of HRP, diluted, and then transferred to cuvettes containing 2 mL of ABTS assay. For 20 minutes, absorbance values were taken every 5 minutes to gauge the HRP's residual activity. All of the solutions were freshly made and stored in dark areas until use. Using a Perkin Elmer UV-vis instrument, assays were observed at 420 nm.

#### **4.10.12. Acetone precipitation of HRP**

HRP was precipitated with cold acetone (4× the sample volume) at -20°C for 4 hours. Proteins were then recuperated after centrifugation at 10 000 rpm for 20 minutes.

#### **4.10.13. HRP subjected to protein digestion**

After the kinetic study, HRP was precipitated from the samples by acetone precipitation and then digested by the eFASP (Enhanced Filter-Aided Sample Preparation) method was performed according to Erde et al. with some modifications [269]. Ultra-filtration units (filters) were incubated overnight in 5% (v/v) Tween-20 in water. After incubation, the filter units were rinsed thoroughly by three immersions in water for 20 minutes under agitation. Protein samples (25-100 µg) were suspended in lysis buffer containing 4% SDS (sodium dodecyl sulfate), 0.2% and 50 mM DTT (dithiothreitol) and 100 mM NH<sub>4</sub>HCO<sub>3</sub> buffer, pH 8.8 and was left under vortex overnight at 4°C. 200 µL exchange buffer were added to lysates dispensed to passivated filters to eliminate SDS (0.1 M Tris-HCL 8 M urea, 0.2% DCA, 100 mM ABC(ammonium bicarbonate) buffer (pH 8.8) and spun at 14 000 rpm for 20 minutes), this step was repeated thrice. Then, the samples were treated with an alkylation buffer containing 8 M urea and 50 mM iodoacetamide in 100 mM ABC buffer, pH 8.8, and kept under agitation in the dark. After 1 hour, samples were centrifuged at 14 000 rpm for 30 minutes. Three buffer exchange were performed, followed by the addition of 200 µL digestion buffer (0.2% DCA (Deoxycholic acid), 50 mM ABC buffer, pH 8.8) to each filter unit that was centrifuged at 14 000 rpm for 20 minutes in order to remove urea. This step was repeated thrice. Next, 100 µL digestion buffer were added to the filter units, followed by the addition of trypsin (1:50 w/w). Digestion proceeded overnight at 37 °C. The filters were transferred to new collection tubes, and two wash and centrifugation steps, each with 100 µL of 50 mM NH<sub>4</sub>HCO<sub>3</sub> buffer were done. Peptides'

## *Synthesis of suicide inhibitors of lignification*

recovery was performed by ethyl acetate extraction; first 200  $\mu\text{L}$  ethyl acetate was added to the peptides solubilized in 50 mM ABC buffer, and the medium was acidified by the addition of 0.1% TFA. Then big quantity of ethyl acetate (800  $\mu\text{L}$ ) was added and the samples were centrifuged at 14 000 rpm for 10 minutes, and the upper organic phase was discarded. This step was repeated thrice. Samples were put at 60°C for the evaporation of ethyl acetate, and then evaporated in the speed vac. After complete evaporation, peptides were dissolved in 0.1% acidified water, and protein content was determined using Denovix spectrophotometer and later subjected to LC-MS/MS analysis.

## 4.11. Results and Discussion

### 4.11.1. Synthesis of the coniferyl alcohol derivative

The aim of this first strategy is to synthesize derivative phenols analogues. But at first, the synthesis of our target is too complicated. In fact, there are two hydroxyl groups in competition and the phenol is more competitive than the alcohol. Before starting a more complex synthesis, we decided to work on ferulic acid. The acid group being more reactive, the esterification is easier to implement than an etherification. The general synthetic procedure is shown in (Figure 4-7). The alkyne handles were inserted into these phenolic acids following acyl nucleophilic substitution via Fisher esterification using propargylic alcohol as the triple bond donor. Principally, for the synthesis of singly-alkyne functionalized probes, lignin monomers were treated with 2-propyl-1-ol, in the presence of the acid catalyst (PTSA) that was used to activate the hydroxyl group of the carboxylic acid [270], to ensure that the phenolic hydroxyl group will remain free for the oxidation by HRP.

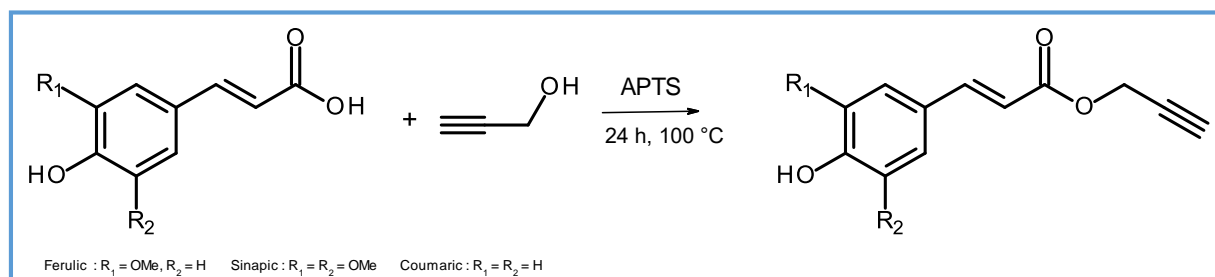


Figure 4-7: synthesis of propargylated phenols

### 4.11.2. Ferulic acid derivative

First, the reaction mixture was stirred at 40 °C for 6 h according to the article that corresponded to the reaction. The first test showed that the reaction was working but the yield was very low 5%. So, the reaction was repeated with larger quantities to improve the analysis. However, the yield problem was still present. To overcome this problem, the reaction time was increased to 24 h and the solution was stirred at reflux which gave a yield of 26%. After that it was considered to follow the reaction by kinetic monitoring to optimize the reaction time by increasing of the temperature to 100 °C.

**Ferulic acid:**  $^1\text{H NMR}$  (300 MHz,  $\text{DMSO-d}_6$ ): COOH  $\delta = 12.12$  ppm (s, 1H), OH 9.54 (s, 1H), H4 7.49 (d, 1H), H1 7.29 (d, 1H), H2 7.09 (dd, 1H) H3 6.80 (d, 1H) H5 6.37 (d, 1H) OMe 3.83 (s, 3H)

**Esterified Ferulic acid:**  $^1\text{H NMR}$  (300 MHz,  $\text{CDCl}_3$ ): H4 7.49 (d, 1H), H1 6.93 (d, 1H), H2 6.90 (dd, 1H), H3 6.77 (d, 1H), H5 6.14 (d, 1H),  $\text{CH}_2$  4.68 (d, 2H), OMe 3.74 (s, 3H) H 2.44 (t, 1H)

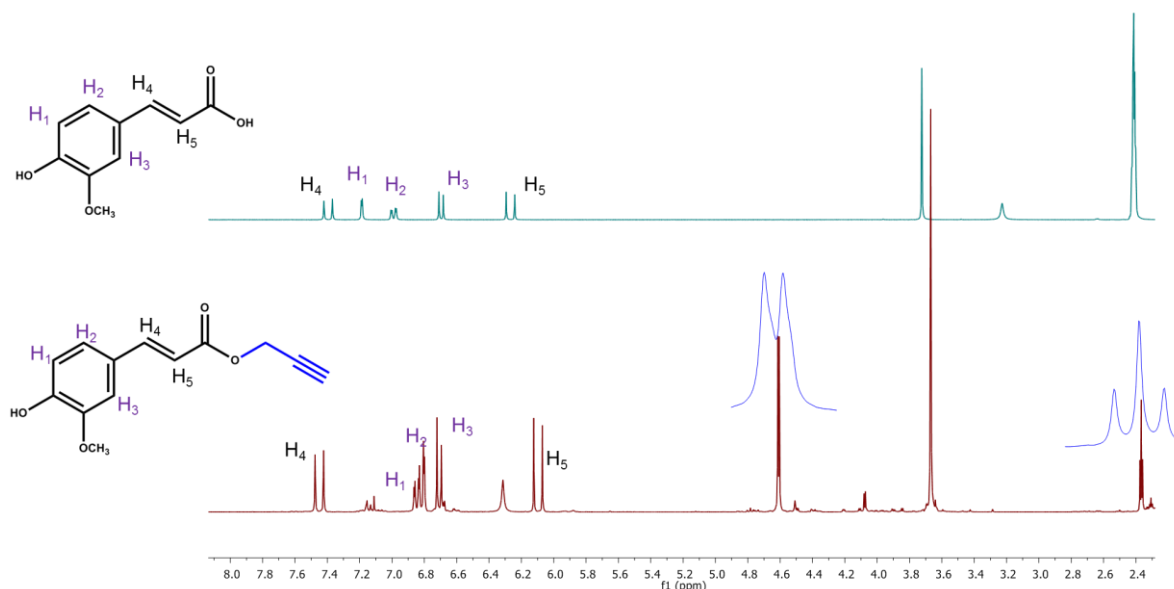


Figure 4-8:  $^1\text{H NMR}$  of ferulic acid and propargylated ferulic acid

#### 4.11.3. Extension to other lignin acids

After optimizing the esterification of ferulic acid, the same was done for other analogues of lignin monomers p-coumaric, p-sinapic and cinammic acids. However, an additional purification step was did on the coumaric acid as the product was not pure enough. Purification on C18 column was added followed. And we got with all the phenols good results.

For the propargyl sinapate, we obtained a yield of 22%, even the percentage of the final product is low but for the biological manipulations, only incredibly little volumes are required. The spectra of the sinapic acid and the synthesized product are in Figure 4-9, the chemical shifts are attributed below.

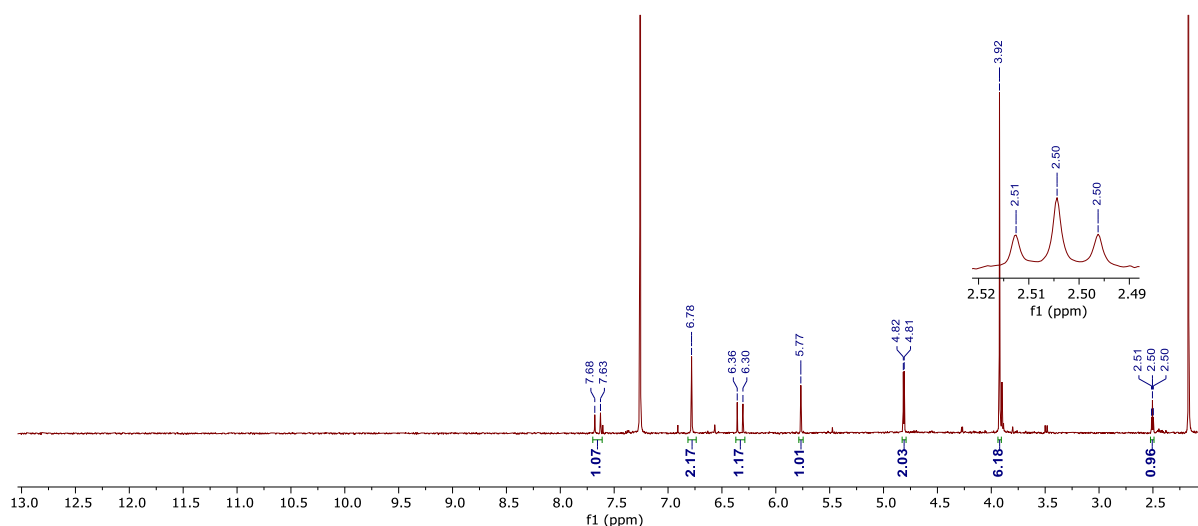


Figure 4-9:  $^1\text{H}$  NMR of propargyl sinapate

**Sinapic acid:**  $^1\text{H}$  NMR (300 MHz, DMSO): Hf  $\delta$  = 12.10ppm (s,1H), OH 8.88 (s,1H), Hd 7.49 (d,1H), Ha 6.98 (s, 2H), He 6.40 (d,1H), OMe 3.83 (s, 6H)

**Propargyl sinapate:**  $^1\text{H}$  NMR (300 MHz,  $\text{CDCl}_3$ ): Hd  $\delta$  = 7.65 (d,1H), Ha 6.78 (s,2H), He 6.33 (d, 1H), OH 5.77 (s,1H), Hf 4.82 (d, 2H), OMe 3.92 (s,6H), Hg 2.50 (t,1H)

For coumaric acid, the same procedure was used, but an additional purification step was added because the result was not sufficiently pure. Following the addition of a purification on a C18 column, a mass spectrometry analysis was used to identify the fractions that contained the product. The peaks at 4.7 ppm and 2.4 ppm always indicate that the required product was obtained. The reaction has a 24% yield (Figure 4-10).

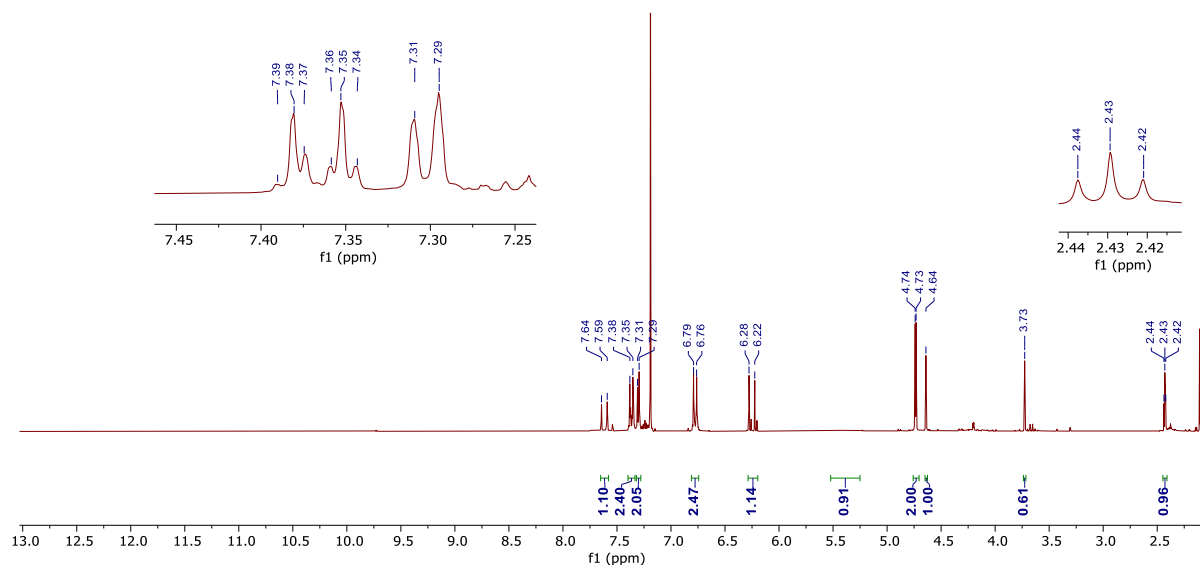


Figure 4-10: <sup>1</sup>H NMR of propargyl coumarate

**Coumaric acid:** <sup>1</sup>H NMR (300 MHz, DMSO): Hf  $\delta$  = 12.11 ppm (s,1H), OH 9.96 (s,1H), Hd 7.54 (d,1H), Ha 7.5 (s, 2H), Hb 6.80 (d,2H), He 6.29 (d, 1H)

**Coumaric acid esterified:** <sup>1</sup>H NMR (300 MHz, CDCl<sub>3</sub>): Hd  $\delta$  = 7.62 (d,1H), Ha 7.37 (d,2H), Hb 6.78 (d, 2H), He 6.25 (d, 1H), OH 5.39 (s,1H), Hf 4.74 (d, 2H), Hg 2.42 (t,1H)

#### 4.11.4. Coniferyl alcohol etherification

Following the confirmation of HRP recognition of esterified ferulic acid, the etherified coniferyl alcohol was synthesized. The synthesis was accomplished in two methods. A synthesis that includes a protection step and a synthesis that does not include a protection step.

First, the results of the synthesis without the protection step demonstrate that there are two propargylated functions on both alkyl and phenolic OH, therefore we went the other way, using the MOM group to protect the alkyl and phenolic OH [271]. After the propargylation procedure, the MOM was deprotected under several conditions, including at room temperature with dichloromethane and trifluoroacetic acid, followed by a washing step with NH<sub>3</sub>, however the result was destroyed under these conditions, so milder conditions were used (0.1M HCl in methanol for 36 h at reflux) [272].

**Coniferyl alcohol:**  $^1\text{H NMR}$  (300 MHz, DMSO): OH  $\delta$  = 8.96 ppm (s,1H), H<sub>1</sub> 7 (d,1H), H<sub>2</sub> 6.79 (dd,1H), H<sub>3</sub> 6.70 (d, 1H), H<sub>4</sub> 6.42 (d,1H) H<sub>5</sub> 6.17 (dt,1H), OH 4.74 (t,1H), H<sub>6</sub> 4.07 (td,2H), OMe 3.78 (s,3H)

**Protected coniferyl alcohol:**  $^1\text{H NMR}$  (300 MHz, CDCl<sub>3</sub>): H<sub>1</sub>  $\delta$  = 7.07 ppm (d,1H), H<sub>2</sub> 6.88 (d,1H), H<sub>3</sub> 6.96 (dd, 1H), H<sub>4</sub> 6.578 (d,1H), H<sub>5</sub> 6.16 (dt,1H), H<sub>6</sub> 4.21 (dd,2H) OMe 3.88 (s,3H) OMe (MOM) 3.47 (s,1H), H 4.67 (s, 2H)

**Protected coniferyl alcohol etherified:**  $^1\text{H NMR}$  (300 MHz, CDCl<sub>3</sub>) H<sub>1</sub>  $\delta$  = 7.07 ppm (d,1H), H<sub>2</sub> 6.90 (d, 1H), H<sub>3</sub> 6.96 (dd, 1H), H<sub>4</sub> 6.56 (d, 1H), H<sub>5</sub> 6.21 (dt, 1H), H<sub>6</sub> 4.22 (dd,2H), OMe 3.89 (s,1H), OMe (MOM) 3.5 (s, 1H,) H 4.68 (s, 2H), H 2.54 (t, 1H)

**Coniferyl alcohol di-etherified:**  $^1\text{H NMR}$  (300 MHz,CDCl<sub>3</sub>) H<sub>1</sub>  $\delta$  = 6.99 ppm (d,1H), H<sub>2</sub> 6.90 (d, 1H), H<sub>3</sub> 6.96 (dd, 1H), H<sub>4</sub> 6.56 (d, 1H), H<sub>5</sub> 6.14 (dt, 1H), H<sub>6</sub> 4.22 (dd,2H), OMe 3.89 (s,1H), CH<sub>2</sub> 4.76 (s, 2H), CH<sub>2</sub> 4.24 (s, 2H), H 2.51 (t, 1H), H' 2.49 (t, 1H)

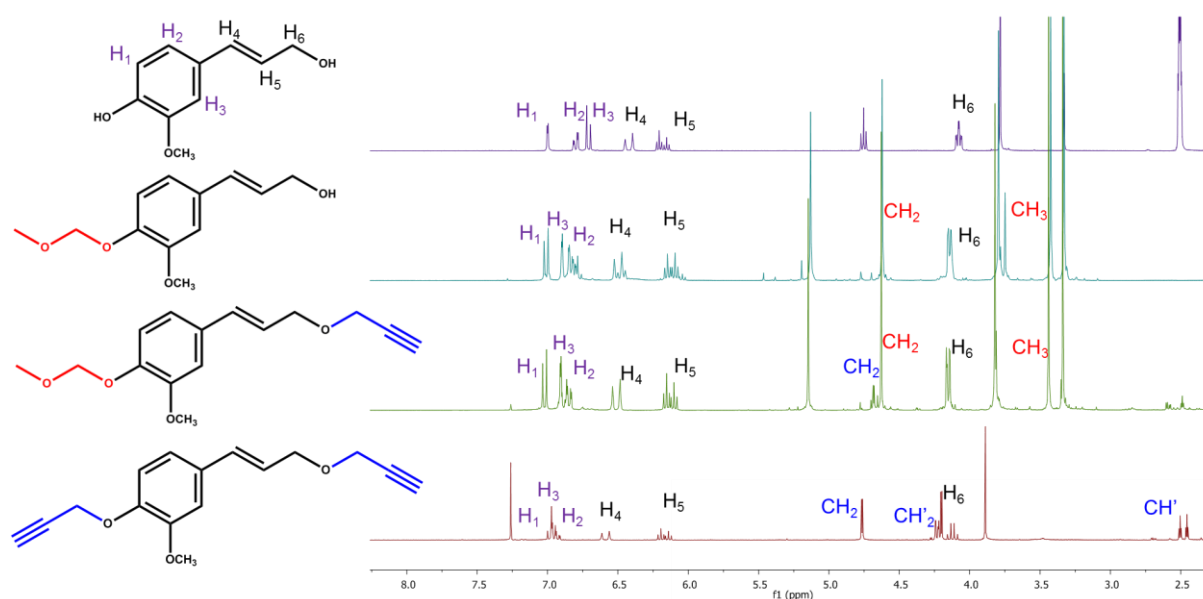


Figure 4-11: Protected coniferyl alcohol and protected coniferyl alcohol etherified

#### 4.11.5. Bifunctional phenols

To make singly-alkyne functionalized probes, lignin monomers were treated with 2-propyl-1-ol in the presence of the acid catalyst (PTSA) that was used to activate the carboxylic acid's hydroxyl group, ensuring that the phenolic hydroxyl group remained free for HRP oxidation. However, it's possible that the HRP coupling occurs on the triple bond donor rather than the free hydroxyl group, so we chose to protect the two OH groups with a triple bond to observe if the HRP reacts on the triple bond or on the monomer through a C-C linkage.

## Synthesis of suicide inhibitors of lignification

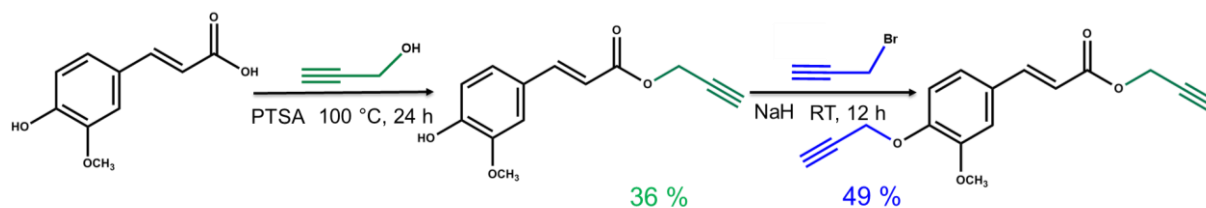


Figure 4-12: Bifunctionalization of ferulic ester with triple bond

The panel of alkyne-bearing probes was extended and two more probes with varied substitution groups were created to explore the reactivity of both the phenolic hydroxyl and the alkyne group toward HRP. To make the bi-alkylated ferulic tag, the phenolic hydroxyl group of PFA was either masked with a methoxy group (PMF) or a second alkyne function was added (BPF).

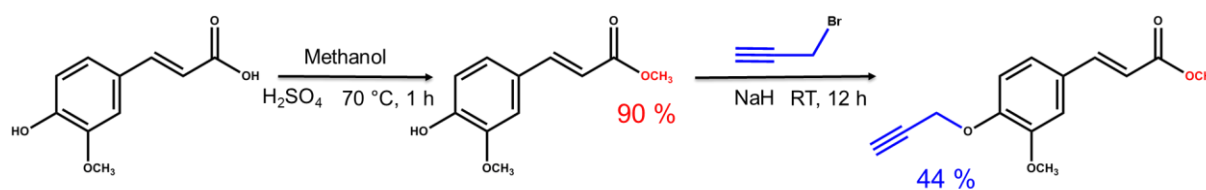


Figure 4-13: Synthesis of PMF

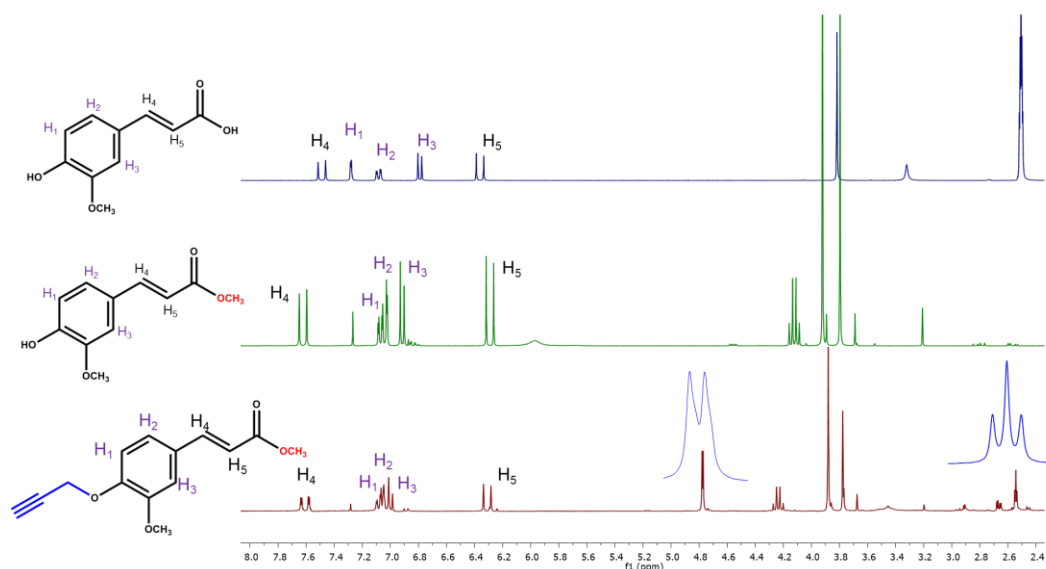


Figure 4-14: <sup>1</sup>H NMR of PMF

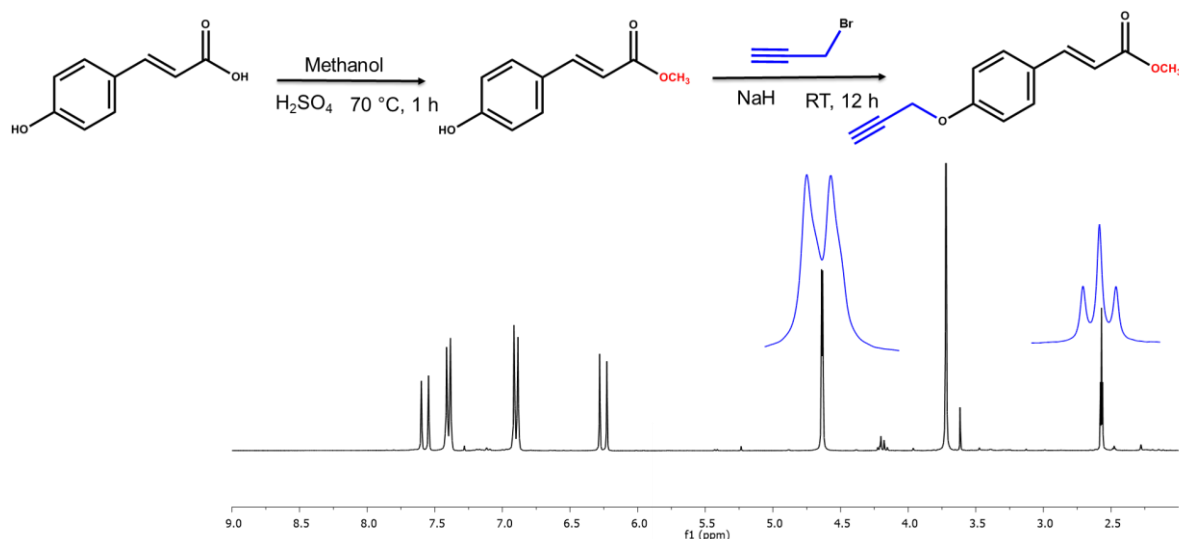


Figure 4-15: Synthesis mechanism and  $^1\text{H}$  NMR of PMC

#### 4.11.6. HRP self-labelling is being developed using lignin monomer tags

The interaction between HRP and the lignin monomer derivatives was investigated in this study. The mono- and bi-alkyne functionalized substrates possess different reactivity toward HRP [273]. Three main monolignols, *p*-coumaric, sinapic, and ferulic acids were first used. Figure 4-16 illustrates the structure of the three primary lignin monomer derivatives: propargyl coumarate (PC), propargyl ferulate (PF), and propargyl sinapate (PS).

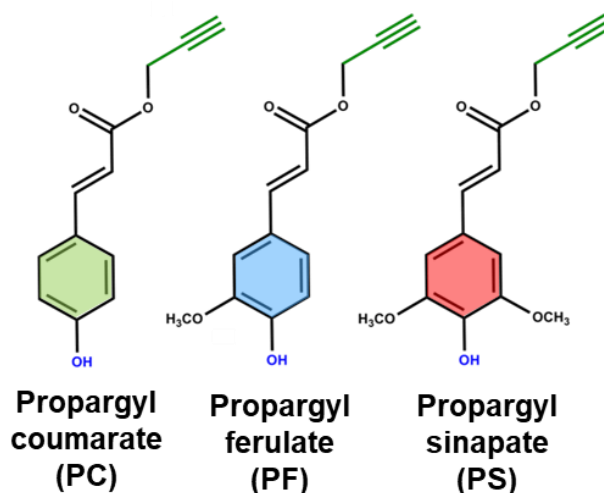
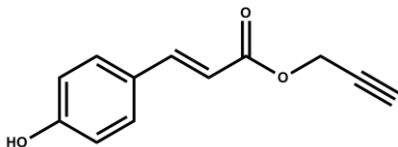
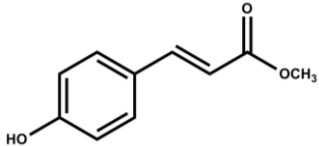
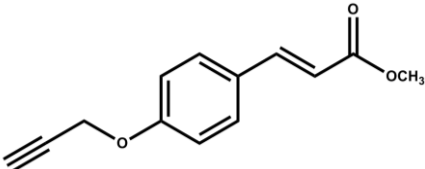
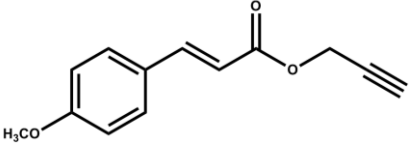


Figure 4-16: Novel clickable lignin monomers

The reaction was started by adding H<sub>2</sub>O<sub>2</sub> to HRP (100 g), which was then incubated with the modified monomers (100 g) (100x equivalent to HRP). Using centrifugal units, the preparations were rinsed three to four times with PBS after being incubated for 45 minutes (Amicon 10 kDa). Proteomic analysis was then used to assess the labeling of HRP with the mono-alkylated probes, and the results showed that PC was the most reactive probe among the others. The MS/MS spectrum, which displays the reporter ion corresponding to the immonium ion of tyrosine conjugated to PC, Figure 4-19, verified the labeling of HRP with PC. None of the other employed probes (PF and PS) could change HRP in any way. It was unexpected that there was no labeling with ferulic acid derivatives. Hence, the panel of probes employed in this work was broadened in order to better understand the process by which HRP interacts with these substrates. In addition to numerous other lignin monomer derivatives with various structures and levels of substitution, these included ferulic acid derivatives with the hydroxyl group covered by a methoxy function, such as propargyl methyl ferulate (PMF) or with a second alkyne function introduced to yield bi-alkylated ferulic acid derivatives known as bi-propargyl ferulate (BPF). These substances are detailed in Table 4-2. Tyr 233, is thought to be the HRP-labeling site as demonstrated by the reaction with biotin phenol and PC substrates.

Table 4-2: List of the phenolic compounds used in the HRP labeling experiment. The modifications and the signature ions used in mass spectrometry are also provided.

Monomer	Modification on tyrosine		Reporter ions	
	Formula	Neutral adduct	Formula	Monoisotopic mass
 Propargyl coumarate (PC)	C <sub>12</sub> H <sub>8</sub> O <sub>3</sub>	200.0473	C <sub>20</sub> H <sub>15</sub> O <sub>4</sub>	319.0965
			C <sub>20</sub> H <sub>18</sub> NO <sub>4</sub>	336.1230
			C <sub>21</sub> H <sub>18</sub> NO <sub>5</sub>	364.1180
	C <sub>10</sub> H <sub>8</sub> O <sub>3</sub>	176.0473	C <sub>18</sub> H <sub>15</sub> O <sub>4</sub>	295.0965
			C <sub>18</sub> H <sub>18</sub> NO <sub>4</sub>	312.1230

 Methyl <i>trans-p</i> -coumarate ( <b>MC</b> )			C <sub>19</sub> H <sub>18</sub> NO <sub>5</sub>	340.1179
 Propargyl methyl coumarate ( <b>PMC</b> )	C <sub>13</sub> H <sub>10</sub> O <sub>3</sub>	214.0624	C <sub>21</sub> H <sub>17</sub> O <sub>4</sub>	333.1121
			C <sub>21</sub> H <sub>20</sub> NO <sub>4</sub>	350.1387
			C <sub>22</sub> H <sub>20</sub> O <sub>4</sub>	348.1356
 Methyl propargyl coumarate ( <b>MPC</b> )	C <sub>13</sub> H <sub>10</sub> O <sub>3</sub>	214.063	C <sub>21</sub> H <sub>17</sub> O <sub>4</sub>	333.1121
			C <sub>21</sub> H <sub>20</sub> NO <sub>4</sub>	350.1387
			C <sub>22</sub> H <sub>20</sub> O <sub>4</sub>	348.1356

#### 4.11.7. A "click" technique is used to bind acetylene-containing monomers to biotin with an azide terminus

The viability of our method was examined using two acetylene-containing monomers (PC and PF). Due to this, equimolar amounts of copper sulfate, sodium ascorbate, and biotin azide were combined with PC and PF. MALDI-TOF mass spectrometry was used to study the development of the cycloaddition reaction between the modified monomers and biotin-azide. According to the MALDI-TOF spectra, the click reaction performed most effectively when working under equimolar circumstances. Peaks for [M+H]<sup>+</sup>, [M+Na]<sup>+</sup>, and [M+K]<sup>+</sup> were observed in the MALDI-TOF spectra acquired using a PC at *m/z* 647.25 Da, 669.23 Da, and 685.20 Da, respectively. Moreover, at *m/z* 663.24 Da, the oxidized form [(M+O) +H]<sup>+</sup> was discovered (Figure 4-17).

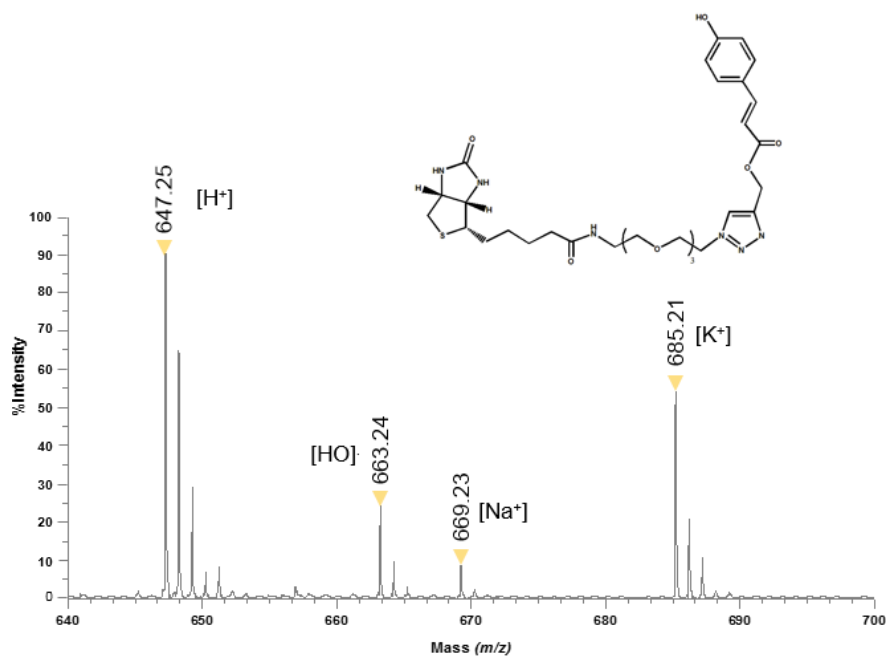


Figure 4-17: MALDI-TOF spectrum of PC linked to biotin-azide by click reaction.

Click-reaction between biotin azide and PF resulted in different signals observed at  $m/z$  677.19 Da, 699.17 Da and 715.15 Da correspondent to the  $[M+H]^+$ ,  $[M+Na]^+$  and  $[M+K]^+$  adducts respectively. Besides, an adduct  $[(M+O) + H]^+$  corresponding to the oxidized form of the click product was detected at  $m/z$  693.14 Da, Figure 4-18.

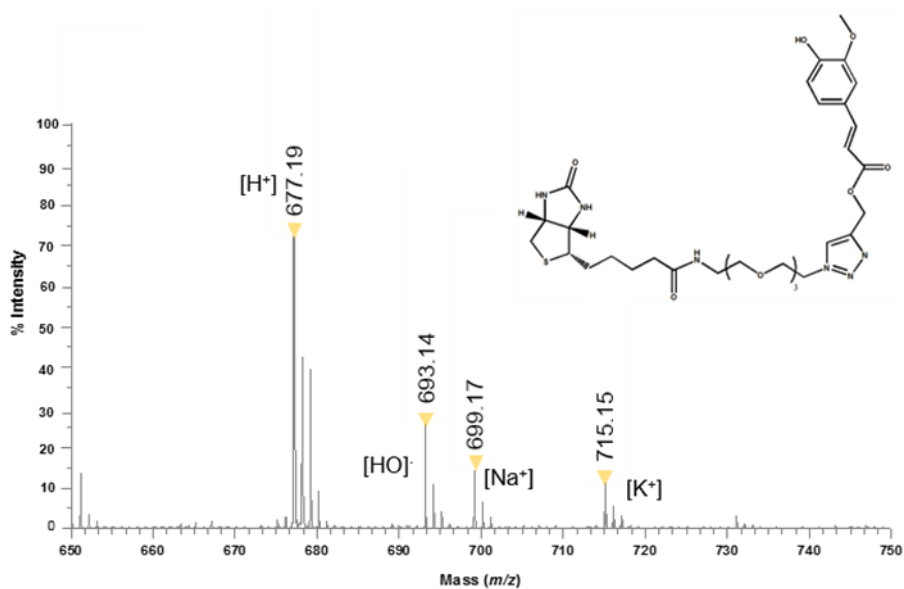


Figure 4-18: MALDI-TOF spectrum of PF linked to biotin-azide by click reaction.

Unnatural amino acids with triple bonds that are added into proteins during synthesis are typically used to introduce an alkyne functionality into a protein [274-276]. The copper-catalyzed azide-alkyne cycloaddition procedure is subsequently used to attach these proteins to affinity probes [277-279]. This work used a different approach to insert alkyne-containing compounds into HRP. Simple hydroxycinnamic acid derivatives, such as propargyl coumarate, propargyl ferulate, and propargyl sinapate, were used in the earliest experiments.

A similar technique to that utilized for HRP's self-labeling was applied to assess these probes' reactivity to HRP.

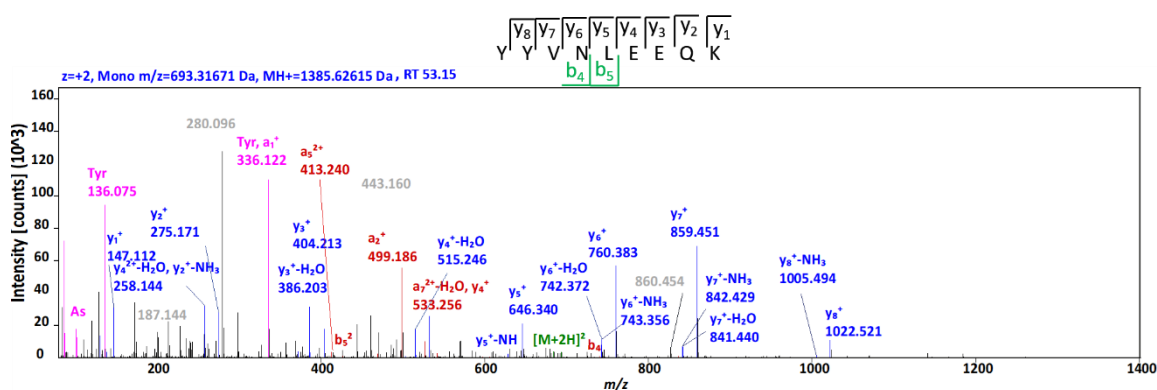


Figure 4-19: MS/MS spectrum revealing the labeling of KZWW6 isoform of HRP with PC. Peaks in magenta ( $m/z$  366.12 Da) corresponds to immonium ion of the labeled tyrosine.

#### 4.11.8. Peroxidase inactivation mechanism during phenol oxidation

After the success of labelling of HRP with PC, the inactivation of HRP during the interaction with lignin monomer derivatives was addressed taking into consideration that specifically HRP are susceptible to progressive loss of activity in the presence of its indispensable substrate,  $H_2O_2$ , where they undergo a mechanism-based inactivation [280].

Although the prosthetic heme moiety's architectural conformation protects peroxidases against attack by reactive species, it is not a defense against radicals produced during the catalytic cycle. These species are capable of exerting diverse effects on the heme group or the protein moiety of the enzyme or can cause the heme group to produce irreversible modifications of the protein situated within the active region [281].

For this purpose, different types of propargyld and non-propargyld lignin monomers were used, conditions were optimized, and HRP inactivation was studied.

#### **4.11.9. HRP is rendered inactive by the oxidation of its aromatic substrates**

Using kinetic analysis, the impact of phenolic substrates on HRP activity was discovered. Comparative analyses were conducted on control samples made of either HRP alone or HRP treated with H<sub>2</sub>O<sub>2</sub>, as well as samples of HRP treated with the phenolic substrate and H<sub>2</sub>O<sub>2</sub>. Kinetic investigations were carried out utilizing the ABTS to measure the HRP residual activity.

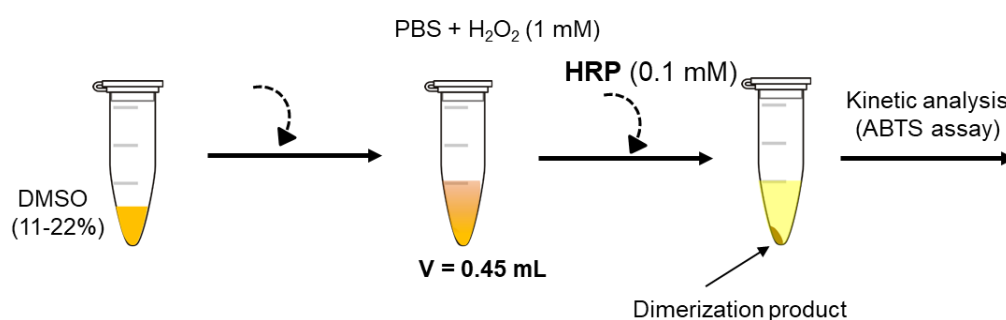
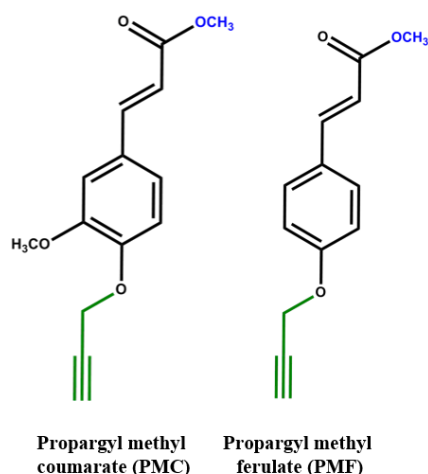


Figure 4-20: Inhibition of HRP under optimized proximity conditions

In the presence of aromatic substrates called suicide substrates/inhibitors or mechanism-based inhibitors, peroxidases are inactivated through suicide. The catalytic and inactivation phases are followed by the enzyme's response with this kind of substrate [282]. Four distinct lignin monomer derivatives, PC, PF, PMC (propargyl methyl coumarate), and PMF, were used in the main studies to explore HRP inactivation (propargyl methyl ferulate). These two compounds' structures are depicted.

## Synthesis of suicide inhibitors of lignification



Within the first five minutes of treatment with propargyl coumarate (PC) at a ratio of  $1:17 \times 10^3$ , HRP activity was reduced by almost 97%. Consequently, under these circumstances, the largest percentage of HRP activity reduction was seen.

To further understand the mechanism of HRP inhibition, the effects of three other substrates (PF, PMF, and PMC) on HRP activity were also examined under the exact identical circumstances (HRP: phenolic compound  $1:17 \times 10^3$ ).  $H_2O_2$  was always supplied to the phenolic substrate in equimolar amounts.

In order to mask the free hydroxyl groups, propargyl groups were added to the aromatic ring of coumaric acid and ferulic acid to create PMC and PMF, as shown in Figure 4-22. Almost minimal HRP activity reduction was noticed in the presence of PF (8% within 20 minutes). Within 5 minutes of the reaction when HRP was treated with PMC, practically all of the HRP activity was lost.

Ferulic acid derivatives (PF and PMF) diminished the impact of  $H_2O_2$ . These results are consistent with Kim et al. research's which showed that ferulic acid therapy had no effect on the peroxidase. The amount of methoxy side groups on the aromatic ring was correlated with the absence of inhibition; more residual enzyme activity was seen as their number rose. In addition, protection of the enzyme against  $H_2O_2$  was also noted in the presence of ferulic acid [248]. However, the PC and PMC coumaric acid probes had a suicidal impact on HRP. Figure 4-21 displays the percentage of HRP's residual activity after being exposed to monolignol derivatives and  $H_2O_2$ .

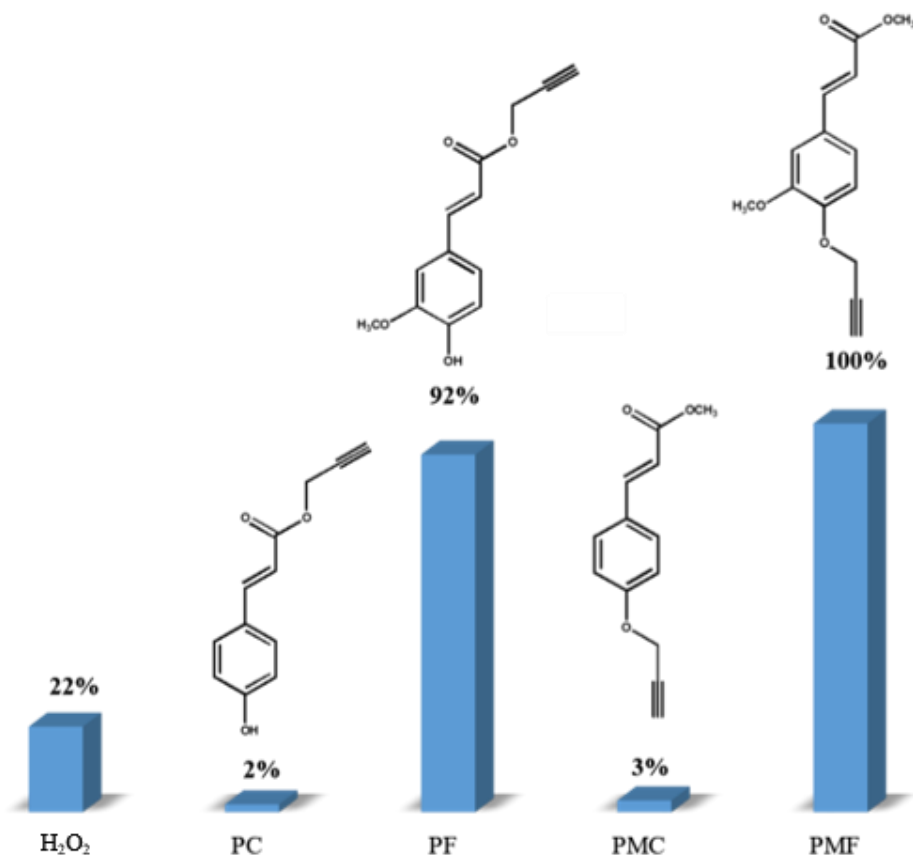


Figure 4-21: % Residual activity after treatment with PC, PF, PMC, PF, and H<sub>2</sub>O<sub>2</sub> at a ratio of 1:17×10<sup>3</sup> for HRP to substrate.

The proximity of HRP to its substrate is essential for HRP labeling to take place. Yet, the proximity influence is ignored under these diluted situations. In order to test HRP inactivation under proximity conditions, coumaric acid derivatives were used since they were the only substrates possessing inhibitory activity against HRP, Figure 4-22.

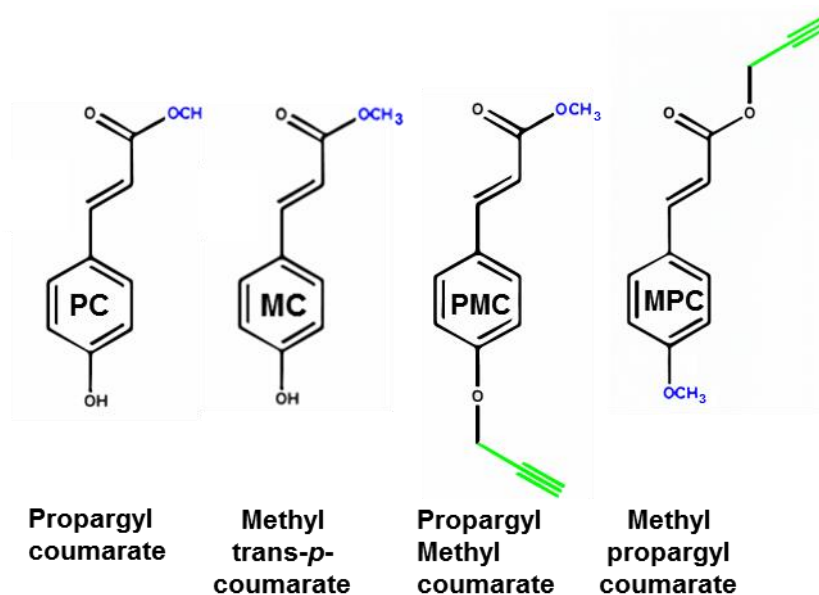


Figure 4-22: Modified lignin monomers

To guarantee proximity between HRP and its substrates, the total reaction volume was decreased to 0.45 mL. An equimolar mixture (0.1 M) of H<sub>2</sub>O<sub>2</sub>, the phenolic substrates were dissolved in 11% DMSO for PC and 22% DMSO for the second coumaric acid derivative. HRP (1 mM) was then added to the mixture. The only coumaric acid probes employed were PC and PMC since they are thought to be the most reactive to HRP.

As it was noted that HRP denaturation occurs at concentrations higher than 20% [283], the amount of DMSO was controlled at around 20% (% v/v), but serious effects on HRP structure appear at concentrations greater than 70% [284]. According to a different investigation, HRP was stable in the presence of 3.5 and 20% DMSO [285]. It is significant to note that DMSO had no impact on HRP activity in this investigation. Since there was no sign of activity reduction when HRP was treated without H<sub>2</sub>O<sub>2</sub> with phenolic substrate that had been dissolved in DMSO.

Nearly all activity was lost under these circumstances (HRP to substrate ratio: 1:1000) with PC (93%), whereas PMC (87%). Under the same circumstances, HRP was also used to react with two new substrates, methyl trans-*p*-coumarate (MC) and methyl propargyl coumarate (MPC).

Treatment of HRP with MC and MPC caused activity reduction of 83% and 97%, respectively. Within the first five minutes of the reaction, a significant decline in HRP activity is shown when all of the coumaric acid probes are employed. Using probes containing the propargyl group, higher inhibition percentages were seen Figure 4-23.

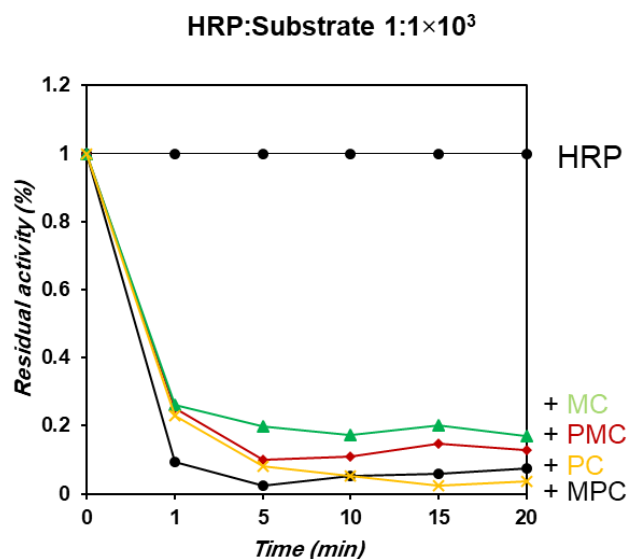


Figure 4-23: Residual activity of HRP (0.1 mM) after being exposed to coumaric acid derivatives PC/MC/PMC/MPC (0.1 M) in 0.45 mL PBS, pH 7.4 in the presence of H<sub>2</sub>O<sub>2</sub> (0.1 M).

With each of these coumarate substrates, a decline in HRP's residual activity was seen. Indeed, HRP reactivity is significantly linked with the architecture of the contact between HRP and its substrate [286].

Coumaric acid derivatives failed to protect the enzyme from H<sub>2</sub>O<sub>2</sub> inactivation, despite the fact that phenols can help in some cases. This suggests that phenoxyl radical coupling played a significant role in the loss of HRP activity. The loss of activity was not attributed to the inactivation of the enzyme by the reaction product.

The absence of PC and MC polymers indicates that the inactivation of HRP was not inactivated by polymeric products that can obstruct its active site. When phenoxyl radical attack is presumed to be the cause of the enzyme inactivation, two potential paths should be considered. One involves the radical-radical interaction of phenoxyl radicals to generate dimers. The other involves covalent bonding to generate a complex between the enzyme and the oxidized phenolic molecule. The likelihood of a major decline in the enzyme's activity increases when the second pathway dominates the first one. 21 phenylalanine and 5 tyrosine residues may be found in HRP. These two aromatic amino acids can combine with phenolic compounds to produce complexes through covalent bonding [248].

The kinetic investigation was conducted to provide quantitative data on the activity loss of HRP, however it was challenging to determine what changes in the structure of the enzyme are occurring. Consequently, additional evaluations are required.

#### 4.11.1. HRP polypeptide chain modification

After the kinetic study, HRP was recovered from the reaction mixture of the samples assayed at less diluted reaction conditions (0.45 mL), HRP was precipitated from the reaction mixture using cold acetone. After precipitation, HRP was subjected to trypsin digestion. LC-MS/MS analysis revealed that only with PC and MC substrates modification of amino acid tyrosine TYR233/234 of the polypeptide chain of HRP took place, Figure 4-24.

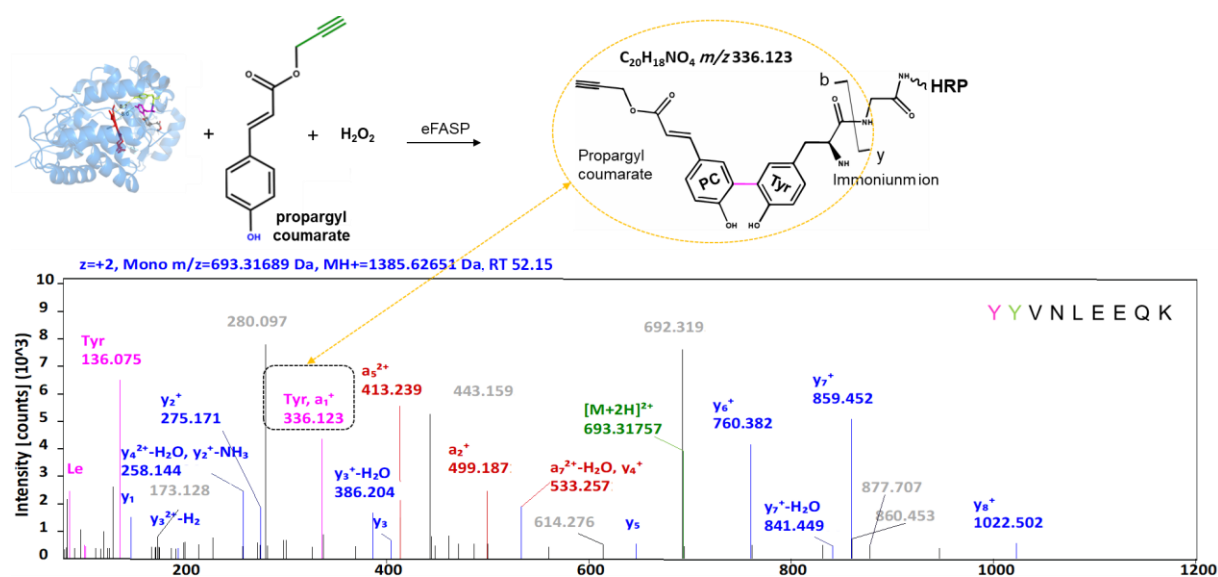


Figure 4-24: MS/MS spectrum showing PC tagging of the HRP KZWW6 isoform. Magenta-colored peaks ( $m/z$  366.12 Da) represent immonium ions from the tagged tyrosine.

#### **4.12. Conclusion**

In this study, the major goal was to develop a strategy that involved lignin monomer derivatives that can be used as identifiers/inhibitors of lignification peroxidases. This was approached by examining how HRP behaved in the presence of phenolic substances, particularly lignin monomers. All of the tags created are intended to label plant peroxidases, allowing them to be identified, but they can also operate as inhibitors by covalently reacting with lignification peroxidases. This is a particularly promising feature for studies aimed at lignification inhibition. This technique could be used as a potential tool for molecular targeting and other applications.

A unique strategy incorporating the two methods of proximity dependent biotinylation and click chemistry was developed.

HRP was treated with unique lignin-derived substrates that have a clickable moiety intended to isolate target proteins when clicked to biotin. These substrates were divided according to their structure into three categories, (i) possessing a free hydroxyl group's non-propargylated, (ii) propargylated having a free hydroxyl group, (iii) propargylated but having no free hydroxyl group. These probes were made specifically to provide HRP identifiers and inhibitors with enhanced features that allow for the identification of the enzyme's target location.

When H<sub>2</sub>O<sub>2</sub> and phenolic substrates are present, HRP is known to be inhibited. H<sub>2</sub>O<sub>2</sub> did not have a suicidal effect on HRP activity, but it did increase as the reaction volume shrank. As this inhibitory action increased in the presence of aromatic compounds, it is likely that additional mechanisms contribute to the inactivation of HRP during phenolic compound oxidation.

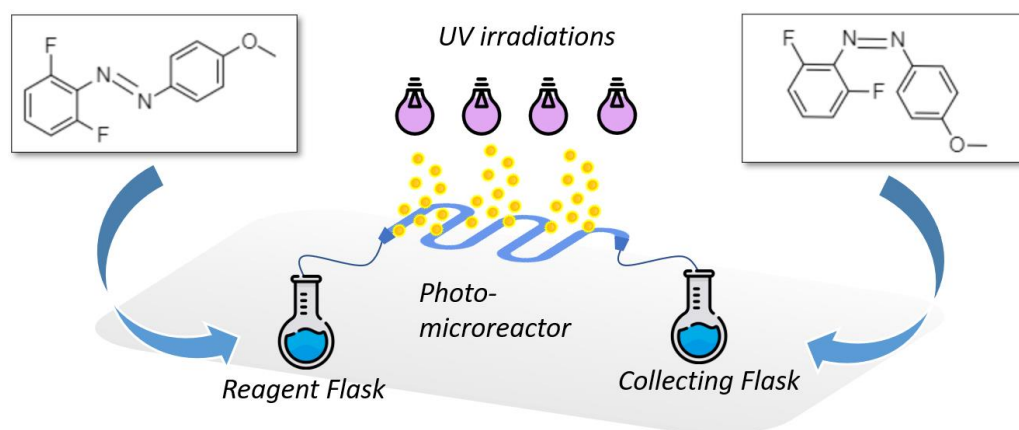
Propargyl coumarate and methyl trans-*p*-coumarate were two lignin-derived probes that could bind HRP, however they did so with varying degrees of efficiency, specificity, and potency. A kinetic analysis revealed that the residual activity is reduced when propargylated substances are present.

## **5. CHAPTER FIVE: CHEMICAL ACTINOMETRY**

### **5.1. Introduction**

UV irradiation is an efficient method for destroying the virus lipidic membrane but is also permit to access to other biological materials. Therefore, there is a strong demand to measure radiation intensities as accurately as possible in biological fluids. The external measurement of the irradiating light source, only gives approximate values as the material of which disposable devices are constituted, have very different transmission in function of the wavelength of the light source. Recently, our laboratory has developed an actinometry protocol in microreactors by flow chemistry based on the isomerization pathway to convert *E*-azobenzene by light to the *Z* isomer. It is known that the *Z*-azobenzene isomer is stable enough to allow determining the *E, Z* ratio by NMR. Unfortunately, the commercial azobenzene is practically insoluble in water. Thus, the aim of this project was to apply this actinometric protocol with a synthetic water-soluble azobenzene derivative in a photo-microfluidic reactor in order to measure accurately the photon flux of an UV lamp irradiating a blood bag. In addition, in this work, we optimize the actinomteric protocol in order to have the highest *Z/E* ratio at the photo-stationary state.

This work will be a part of a project carries out by the Macopharma pharmaceutical industry in which the research department focus on the treatment of several diseases such as diabetes by using UV irradiation. With the apparition of new aerobic viruses like the Sars Covid 2, it is important to develop the new process of treatment and disinfection. Indeed, the Macopharma research department conduct the development of a new process of UV irradiation against viral infections such as the UVC in order to protect plasma and platelet units from virus infection, bacteria and with UVA for treating diabetes or graft rejection.



## 5.2. Determining the exact amount of light necessary to inactivate a blood component

Due to the high rate of skin cancer development over the past few decades, UV has acquired a negative reputation in our society. In fact, UV exposure is the cause of more than 90% of skin cancers, with the exception of melanoma [287]. On the other hand, exposure to UV rays has a number of advantages. The most well-known is that they are the origin of the D hormone, calcitriol, which is produced in human bodies. Additionally, UV radiation has been used successfully since the 1940s to treat diseases like diabetes and pneumonia. And more recently, it has been demonstrated that treating blood with UV is an effective way to cure viral illnesses like Ebola or SARS-CoV-2 [288]. In fact, certain viruses can be rendered inactive by UV light irradiation by creating radical molecules like hydroxyl.

These UV treatments must now improve their accuracy in order to treat both old and new diseases more effectively and safely. One recent instance is the UV sterilization treatment given to the SARS Covid-2. Because the goal is to eliminate the viruses with UV in the transfusion blood without denaturing important molecules like proteins or peptides by a UV irradiation with a too high intensity, an appropriate irradiation is necessary [289].

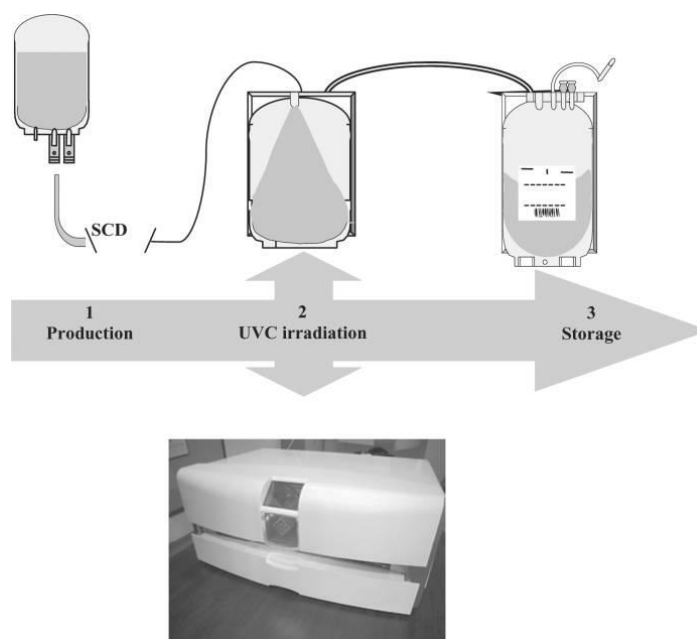


Figure 5-1: Machine for UV blood irradiation from Macopharma [289]

In the fields of biotherapy and blood transfusion research and innovation, Macopharma is a major participant. They create UV irradiation as a method to get rid of bacteria and viruses in plasma and platelet single-use bags. The photopheresis procedure was created by Macopharma and involves exposing harvested cells to UVA radiation in order to treat diabetes or transplant rejection. They created their own equipment to irradiate blood bags, as shown in Figure 5-1.

Macopharma found the actinometric protocol developed by the MSAP laboratory in the literature, and it got in touch with them to work on a method of regulating UV light intensity so that this protocol could be used to routinely control UV treatment of blood bags.

### 5.3. Chemical actinometers

Chemical actinometers are substances that undergo chemical transformations such reduction, isomerization, and decomposition when exposed to radiation of a particular wavelength. The actinometers are preferred to be used for standard measurements of light energy even if they appear to behave similarly to other photosensitive compounds. The IUPAC [290] provided a list of characteristics that effective chemical actinometers possess in 2004.

- The actinometer is readily accessible in stores and is simple to use.

- The photochemical process should be as straightforward as possible and easily observable using spectroscopic methods.
- The actinometer has undergone extensive research, and the literature provides quantum yield values for the used wavelengths.

#### **5.4. Overview of chemical actinometers examples**

A lot of chemical actinometers are extensively described in literature. Uranyl oxalate actinometer  $\text{UO}_2^{2+}$  is used as a photosensitizer for the decomposition of the oxalate into  $\text{CO}$ ,  $\text{CO}_2$  and  $\text{H}_2\text{O}$  [291, 292]. This actinometer was subsequently swapped out with a ferrioxalate actinometer since titration of the residual oxalate ions will result in the loss of the reactant.

Then Ferrioxalate actinometer  $\text{Fe}(\text{C}_2\text{O}_4)_3^{3-}$  is used in the UV and the Visible range. The ferrioxalate will break down after exposure to radiation, producing free ferrous ions, the reaction is monitored by measuring the amount of the liberated  $\text{Fe}^{2+}$  ions following their complexation with phenanthroline. Keep in mind that only the ferrous ions that have undergone irradiation's breakdown can complex with phenanthroline [293, 294].

One of the SCN groups of  $\text{Cr}(\text{NH}_3)_2(\text{SCN}_4)^-$  or Reinecke's salt is photo-substituted by water when it is irradiated at a wavelength between 317 and 730 nm. The released  $\text{SCN}^-$  is complexed with ferric nitrate to produce a red-blood complex with a maximum wavelength of 450 nm [295, 296], which is used to monitor the reaction. Due to the potential for hydrogen cyanide to be released, this actinometer's use is restricted.

The other category of actinometers, referred to as photochromic actinometers, includes substances like Fulgide Aberchrome 540 and Azobenzene that can change reversibly between two forms when exposed to light [297]. The benefit of these actinometers is that the photochemical change is reversible, making it simple to recreate the starting material.

Based on all the actinometers described in literature, our group has chosen to use the azobenzene as an excellent option for the chemical actinometry of our microfluidic system since our photoreactions in the UV region are usually done at  $\lambda = 365$  nm and the azobenzene absorbs at this wavelength.

## 5.5. Azobenzene

A diazene derivative with two phenyl groups is azobenzene, chemical formula  $C_{12}H_{10}N_2$ . It is regarded as a straightforward photo-switchable molecule that has Trans (*E*) and Cis (*Z*), two distinct structural isomers (Figure 5-2).

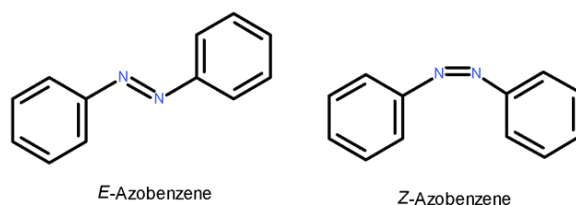


Figure 5-2: The structure of *E* and *Z* azobenzene

As the (*Z*) isomer is less stable than the (*E*) isomer [298], was first identified by Hartely in 1937 as a solution to a problem with the repeatability of the UV/Vis spectrum of the (*E*) form after being exposed to light. This publication was the first that documented the azobenzene's cis-trans photoisomerization [299].

## 5.6. MSAP laboratory state-of-the-art: Nassim El Achi's PhD thesis

Nassim El Achi worked on an actinometric procedure for photo-microfluidic systems during her thesis [300]. The objective was to measure a UV lamp's photon-flux by shining UV light through an azobenzene solution. This approach was developed to estimate the amount of photons released more precisely than just taking a physical measurement at the microreactor's exterior. A wide range of applications and azobenzene's solubility in organic solvent led to its selection as a chemical actinometer.

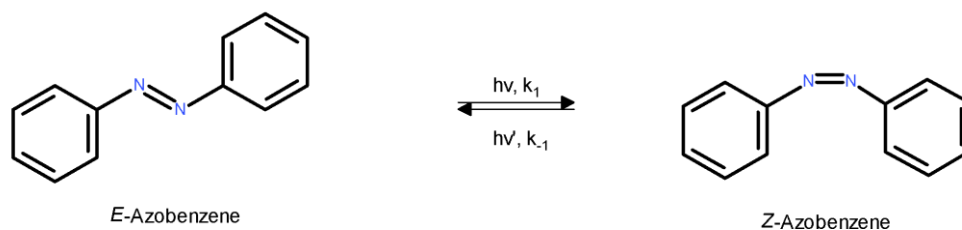


Figure 5-3: Azobenzene isomerization reaction

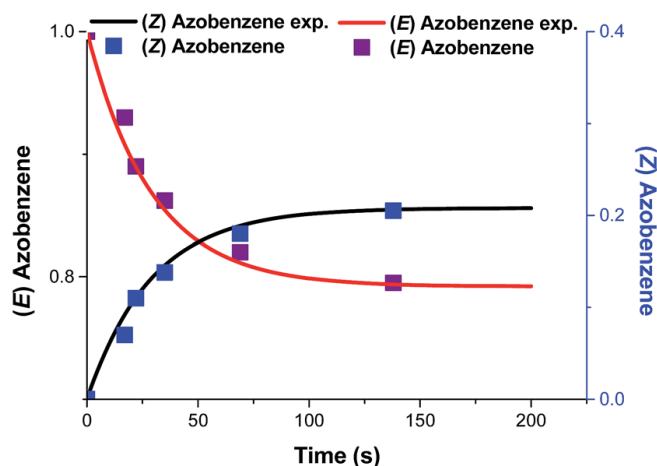
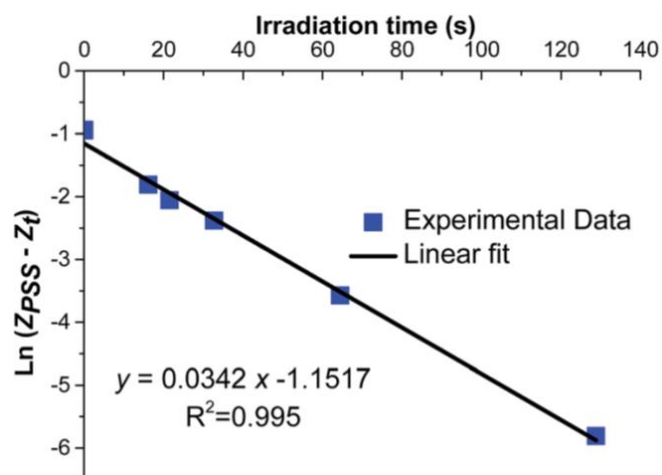


Figure 5-4: Evolution of the *E* and *Z* isomers during the radiation period [300]

In fact, irradiation on a broad range between 180 nm and 540 nm can be used to carry out the reaction of isomerization of the azobenzene [301], *E*-azobenzene is isomerized into *Z*-azobenzene on the one hand, but *Z*-azobenzene is isomerized into *E*-azobenzene on the other. Consequently, azobenzene reaches a Photo Stationary State (PSS) (Figure 5-4), and if it isn't spontaneously exposed to UV or visible light, it slowly undergoes thermal isomerization to restore its most stable shape.

For the purpose of calculating photon flux, the PSS parameter is crucial. According to El Achi's research, which is based on a work by Zimmerman et al., we were able to generate Equation 2, a straightforward first order kinetic equation, by performing a kinetic monitoring of the irradiation of the azobenzene using Equation 1 and the Beer Lambert and Fresnel laws [302]. This equation can be expressed as Equation 3, where  $k$  is a coefficient combining all the coefficients except the  $I_{\text{photon}}$ , given the quantum yield and the extinction coefficient for the *E* isomer. She derived a linear relationship by graphing  $\ln(Z_{\text{PSS}} - Z_t)$  vs time as seen in Figure 5-5.

Figure 5-5: Graph of  $\ln(Z_{PSS}-Z_t)$  vs time (s)

And using the linear coefficient, she was able to isolate the parameter  $I_{Photon}$  since all the other parameters were known. This coefficient relates the amount of light that the solution absorbs per unit surface area. We must multiply this  $I_{Photon}$  by the energy of 1 mole of photons (327500 J) in order to obtain the photon flux (equation 4):

$$\frac{d[\text{photoisomer}]}{dt} = \phi \frac{\Delta I}{V} \quad (1)$$

$$\frac{d[Z_{PSS}-Z]}{dt} = \frac{I_{Photon} \ln 10 \phi_E \epsilon E}{Z_{PSS}} [Z_{PSS} - Z] \quad (2)$$

$$\frac{dZ}{dt} = I_{Photon} \times k \times \left[1 - \frac{Z}{Z_{PSS}}\right] \quad (3)$$

$$Q = I_{Photon} \times 327500 \quad (4)$$

## 5.7. The target of azobenzene

We must carefully select the azobenzene to be manufactured in order to meet the Macopharma's requirements, which are to employ the actinometric technique of Nassim El Achi in a biological fluid. The azobenzene must first be water soluble. It will be able to form strong interactions with water molecules, such as hydrogen bonds, due to the presence of polar groups, which will make the molecule stable in water. Additionally, the inclusion of electron-donor groups would increase the formation of hydrogen bonds between the azobenzene rings and water by bolstering the pi network of the azobenzene ring [294].

The quantity of *Z* isomer present at PSS is the second factor to be considered. In fact, a high  $Z_{PSS}$  indicates a significant difference between the *E* and *Z* isomer signals in the NMR spectra. When using the actinometric procedure, we will measure the integration of very low signal intensity if, for instance, the  $Z_{PSS}$  is around 1%, which raises the uncertainty. So, with a correct  $Z_{PSS}$ , we will be able to perform precise measurements.

The ratio of the two molar extinction coefficient isomers is the final crucial factor in selecting an azobenzene. A high ratio is associated with a slower thermal isomerization that results in a longer *Z*-life time, according to a study by Ahmed Z et al. [295]. Using NMR spectra, we can compute the proportion of *Z* isomer to get the highest ratio and longest *Z* lifetime achievable.

A list of derivative azobenzenes along with their *Z* lifetimes are shown in Table 5-1. Several compounds with extended *Z* lifetimes (41.8 h for compound 1 monofluorinated and 430 h for compound 3 difluorinated) (Figure 5-6) and high  $Z_{PSS}$  (93% and 94%, respectively) are reported in this article [303]. The disadvantage was the multistep synthesis needed to obtain fluorophenols. Due to its favorable qualities, we consulted our bibliography on related azobenzene.

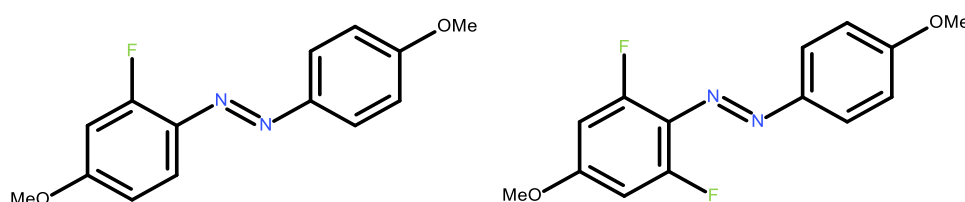


Figure 5-6: Molecule of interest 1 and 3

Table 5-1: Spectral and photochemical characteristics of several azobenzene types

Compd	$\lambda_{\max}$ (nm)	$\epsilon$ ( $M^{-1} \text{ cm}^{-1}$ )	$\tau$ ( $s \text{ h}^{-1}$ )	<i>cis</i> -% at PSS <sup>c</sup>
<b>1</b>	357/432	29110/3608	$41.8 \pm 1.3 \text{ h}^a$	93
<b>2</b>	359/432	25810/3185	$60.2 \pm 0.5 \text{ h}^a$	93
<b>3</b>	350/432	24652/2286	$430 \pm 150 \text{ h}^{ab}$	94
<b>4</b>	340/462	12693/12749	$15.2 \pm 0.1 \text{ s}$	73
<b>5</b>	341/402	14924/10075	$9.1 \pm 0.3 \text{ h}$	75
<b>6</b>	344/479	13777/15042	$258 \pm 30 \text{ s}$	71
<b>7</b>	488/514	3701/3456	$1.21 \pm 0.01 \text{ s}$	62
<b>9</b>	335/411/454	16739/8006/7792	$72 \pm 8 \text{ h}^a$	80



Laminar flow,  $Re < 2100$ Turbulent flow,  $Re > 4200$ 

Figure 5-8: difference irradiation according to the nature of the flow

To determine the type of flow used we have to calculate the Reynolds number ( $Re$ ) based on the equation 6. The diameter of the tubing and the velocity both affect the Reynolds number. The Reynolds number increases as the flow rate increases. Additionally, the Reynolds number decreases as the diameter increases. In a cylindrical channel, if Reynold's number is less than 2100, the flow will be laminar (Figure 5-8), in which the fluid flows in parallel layers without interruption [305, 306]. In contrast, when  $Re$  is between 2040 and up to 4000, the flow regime will be turbulent flow. In the two equations 3 and 5, the constant  $k$  in equation 3 corresponds to the approximation that the flow is turbulent, on the other side in equation 5 a new parameter was integrate called  $k'$  represents the non-approximate case which's the laminar flow.

$$\frac{dZ}{dt} = I_{\text{photon}} \times (k - k' \times I_{\text{photon}}) \times \left[ 1 - \frac{Z}{Z_{\text{PSS}}} \right] \quad (5)$$

$$Re = \frac{Q \times 4}{v \times D \times \pi} \quad (6)$$

$Re$  (Reynolds number);  $V$  (average velocity);  $d$  (hydraulic diameter of the channel);  $\mu$  (viscosity).

## 5.10. Materials and methods

### 5.10.1. Materials

The compounds used in this work are: azobenzene, difluoroaniline, Phenol azobenzene and dimethyl sulphate as well as the matrix dihydroxybenzoic acid (DHB) for MALDI-TOF mass spectrometry analysis have been purchased from Sigma-Aldrich®. All products used had a purity of ca. 98-99% and were all used as received.

The deuterium solvents used for  $^1\text{H}$  NMR analysis  $\text{C}_2\text{NCD}_3$  (deuterated acetonitrile) and  $\text{CDCl}_3$  (deuterated chloroform) from Eurisotop. The solvent used for silica gel separation: dichloromethane (DCM), ethyl acetate, petroleum ether, chloroform are of technical grade.

### 5.10.2. Photo microfluidic reaction of (*E*)-Azobenzene

The microflow reactor was made from fluorinated ethylene propylene (PTFE) tubing (i.d.=0.8 mm, length 6 m, Cluzeau Info Labo (C.I.L.), Sainte-Foy-La-Grande, France) powered by a Corning KP-22 pump as shown in Figure 5-9. The volume of the tubular reactor was estimated to be 3 mL that are exposed to the UV-light at wavelength of 365 nm or 395 nm. We used acetonitrile and water as a solvent.

$$V = l \times R^2 \times \pi$$

l: length of the tube R: Radius of the tube

$$V = 6 \times \left(\frac{8}{2}\right)^2 \times \pi = 3 \text{ cm}^3$$

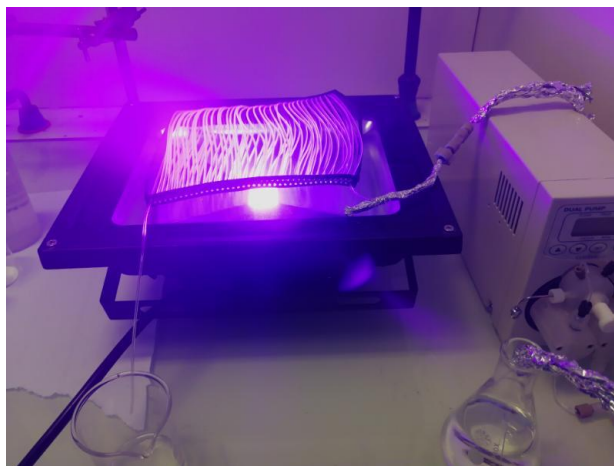


Figure 5-9: Set-up for photo microfluidic reaction

### 5.10.3. NMR measurements

Proton and Fluor magnetic resonance spectra ( $^1\text{H}$  NMR and  $^{19}\text{F}$  NMR) were recorded on a Bruker AVANCE 300 spectrometer using tetramethylsilane (TMS) as the internal standard. Chemical shifts,  $\delta$ , are given in ppm and coupling constants in Hz.  $^1\text{H}$  NMR data are reported as follows: chemical shift, multiplicity (s = singlet, d = doublet, t = triplet, tt = triplet of triplets, td = triplet of doublets, dd = doublet of doublets, m = multiplet), coupling constants and integration.

### 5.10.4. Synthesis of derivated fluorinated azobenzene

We tried different way to synthesize the water soluble azobenzene that will be described further.

#### 5.10.4.1. Oxidative coupling pathway

Based on the work of De Souza et al [307]. Who have produced a number of couplings of derivative azobenzene, the target product was obtained with a good yield using aqueous conditions and without metal catalyst.

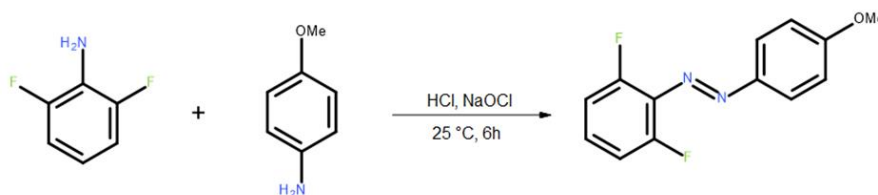


Figure 5-10: Synthesis of (*E*)-1-(2,6-difluorophenyl)-2-(4-methoxyphenyl) diazene

(*E*)-1-(2,6-difluorophenyl)-2-(4-methoxyphenyl) diazene: Hydrochloric acid was mixed with 4-methoxyaniline (0.5 mmol) and difluoroaniline (1.5 mmol) (1 mL, 2.5 M). Sodium hypochlorite solution (8 mL, 5% w/w) was added dropwise to the reaction mixture. At 1150 rpm, the reaction medium was agitated for 5 hours. 50 mL of EtOAc were used to quench the reaction mixture. The organic layer was concentrated by evaporation after being dried with anhydrous  $\text{MgSO}_4$ . A proportion 95:5 of Hexane/EtOAc was used in a column chromatography to purify the crude product.

#### 5.10.4.2. Electrophilic substitution and methylation pathway

This strategy is the second way to synthesis the derivative azobenzene and it is divided in two steps.

The first step is the electrophilic substitution which based on the works of Lishan Li and al [308].

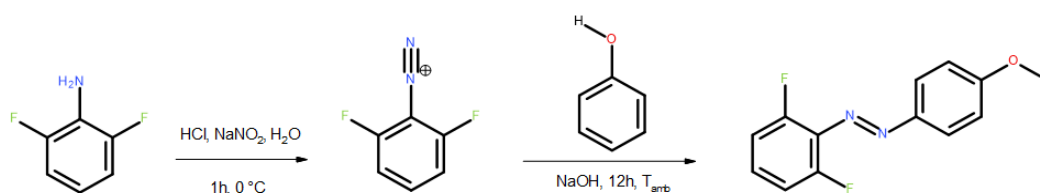


Figure 5-11: Synthesis of (*E*)-4-((2,6-difluorophenyl) diazenyl) phenol

Phenol azobenzene: difluoroaniline (0.05 mol) was added in 15 mL of hydrochloridric acid (12 M) and 30 mL of water. The reaction mixture was stirred for 30 mins at room temperature and cooled to 0°C. Then, sodium nitrite was dissolved into 100 mL of water and added slowly to the reaction mixture. The reaction medium was agitated for 30 mins and then it was added slowly to a solution of phenol (0.05 mol) dissolved in sodium hydroxide (5 g, 125 mL) at 0° C. During the adding of the salt diazonium solution, the pH was maintained between 9 and 10 with sodium carbonate solution (50 g in 400 mL of water). The reaction mixture was stirred vigorously during 1 h at 0°C, then at room temperature during 12 h. After that hydrochloric acid solution (1 M) was added in order to attempt a pH between 5 and 7. The reaction mixture was left to decant and the precipitate is purified by column chromatography.

The second step is the methylation; two ways of synthesis were used, firstly using dimethyl sulphate like methyl-donor.

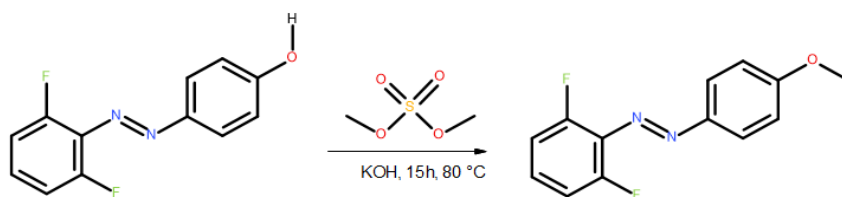


Figure 5-12: Synthesis of (*E*)-1-(2,6-difluorophenyl)-2-(4-methoxyphenyl) diazene

Water-soluble azobenzene: Phenol azobenzene (500 mg) was dissolved into 10 mL of DMF. Potassium hydroxide (254 mg) was added slowly. Then, dimethyl sulphate (620  $\mu$ L) was added slowly and the reaction mixture was stirred for 15 h at 80°C. The organic layer is dried with  $MgSO_4$  and concentrated in vacuum. The crude product is purified by C18 column chromatography (gradient  $H_2O/ACN$ ). The  $^1H$  NMR spectrum analysis shows that the target product was not obtained; therefore, another pathway reaction was carried out in order to produce the methylated azobenzene.

In this case, the second trial which gave the good results was described below:

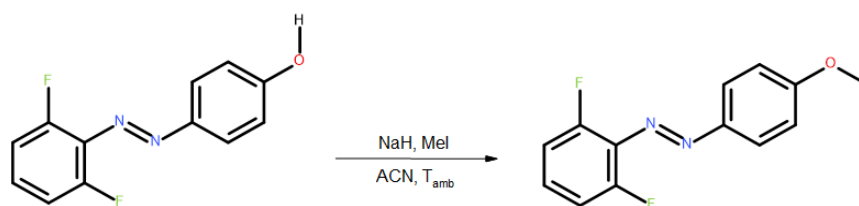


Figure 5-13: synthesis of (*E*)-1-(2,6-difluorophenyl)-2-(4-methoxyphenyl) diazene

Water-soluble azobenzene: Sodium hydride (2.385 mmol) was added into 15 mL of anhydrous pentane. The reaction mixture is stirred 3 min and was left to decant to remove pentane (repeated five times). Then, the sodium hydride is dissolved into 7 mL of ACN. Phenol azobenzene (2.385 mmol) was dissolved in 2.5 mL of ACN and added dropwise to the reaction mixture, at 0°C. Iodomethane was solubilised into 2.5 mL of ACN and added in the reaction media. The reaction mixture is stirred overnight at room temperature. The reaction was quenched with 2.4 mL of acidic water (0.1% formic acid), and 2.4 mL of DCM was added. The organic layer is dried by MgSO<sub>4</sub> and the solvent was evaporated. The crude product is firstly purified by C18 column chromatography (gradient H<sub>2</sub>O/ACN) then purified by column chromatography (silica gel, Chloroform).

### 5.10.5. Experimental Actinometric Measurements

The main goal of our work is to establish a set technique for azobenzene and WSA based chemical actinometric research in microfluidic systems. A number of variables were evaluated:

- The ratio of moderately concentrated solutions
- The type of solvents.
- The type of UV LED used: (365 nm, irradiance up to 250 mW.cm<sup>-2</sup>) Omnicure® AC475 model from Lumen Dynamics (Mississauga, Canada) (HP LEDs B). The power of this UV LED can be changed, power used: 90 mW.cm<sup>-2</sup> or using a UV light 395 nm.

The variable conditions performed are summarized in Table 5-2. The prepared solution of azobenzene or WSA was injected at various flow rates into the microfluidic system that was illuminated by the UV LEDs and kept at a constant temperature with a concentration of 6.4 ×10<sup>-4</sup> mol/L.

Table 5-2: Summary of the experiments done for the chemical actinometric assessment

Entry	reactant	solvent	Wavelength nm
1	AZO	10:90 Ethanol/water	395
2	AZO	10:90 Ethanol/water	365
3	WSA	Acetonitrile	395
4	WSA	Acetonitrile	365
5	WSA	10:90 Ethanol/water	395
6	WSA	10:90 Ethanol/water	365

Every irradiation solution's *Z* and *E* component composition was determined by first employing a rotary evaporator to evaporate the solvent, then dissolving the residue in 500  $\mu\text{L}$  of  $\text{CDCl}_3$  or  $\text{CD}_3\text{CN}$  before injecting it into the NMR spectrometer. Utilizing the  $^1\text{H}$  spectrum, the degree of conversion was determined by integrating the peaks for the *Z* and *E* isomers. The peaks that correspond to the various isomers could be easily differentiated, proving that NMR is a superb and efficient method of analysis.

A sample was exposed to radiation for a prolonged period of time in order to assess the composition at the PSS. The literature was consulted to find the quantum yield values for each solvent and cited in the table below [297].

Table 5-3: Physical constants used for calculations

Substance	Refractive index n	$\epsilon_E$ (L.mol <sup>-1</sup> cm <sup>-1</sup> )	$\Phi_E$	$\Phi_Z$
air	1	--	--	--
Foturan glass ®	1.515	--	--	--
methanol	1.3284	312	0.15	0.35
acetonitrile	1.3441	277	0.15	--
isooctane	1.3914	95	0.12	0.48

## 5.11. Results and discussions

### 5.11.1. Actinometric protocol for the azobenzene

In this work, we decided to work at the beginning under the same conditions of Nassim el Achi works but with little changes. In fact, she used a thermostat in addition to a particular micro-reactor for UV- irradiation and she got a  $Z_{PSS}$  of 20.8%. It was predicted that the  $Z_{PSS}$  would change slightly because we employed a different setup. Azobenzene solutions ( $6.4 \times 10^{-4}$  mol/L in acetonitrile) were produced and injected into the microreactor while being exposed to UV light 395 nm for 2 h. The values of each Z proportion obtained are calculated based on the NMR spectra shown in Table 5-4 using this formula.

$$\%Z = \frac{I_Z}{I_E + I_Z}$$

Table 5-4: Results for the conversion (Z) – Azobenzene

Type of pump	Q (min/mL)	$Z_{PSS}$ (2 replicates)
Syringe pump	0.05	18.75
HPLC pump	0.05	18.40
HPLC pump (recycling)	10	19.10

The next phase involved doing a number of photo-experiments with various irradiation periods ranging from 18 s to 277 s (Table 5-5). And based on these results we can plot  $\ln (Z_{PSS}-Z)$  with time to determine the photon flux (Figure 5-14). In order to determine the photo flux, we supposed that we reached, in our conditions, a  $Z_{PSS}$  of 22.5%.

Table 5-5: Irradiation of *E* – Azobenzene for different durations

Flow rate (mL/min)	Irradiation time (s)	% Z- azo	Ln ( $Z_{PSS}-Z_t$ )
10.0	18	5.8	-1.79
7.5	24	10.6	-2.13
5.0	36	14.9	-2.58
2.50	72	16.9	-2.89
1.25	144	20.9	-4.12
0.65	277	22.4	-6.81

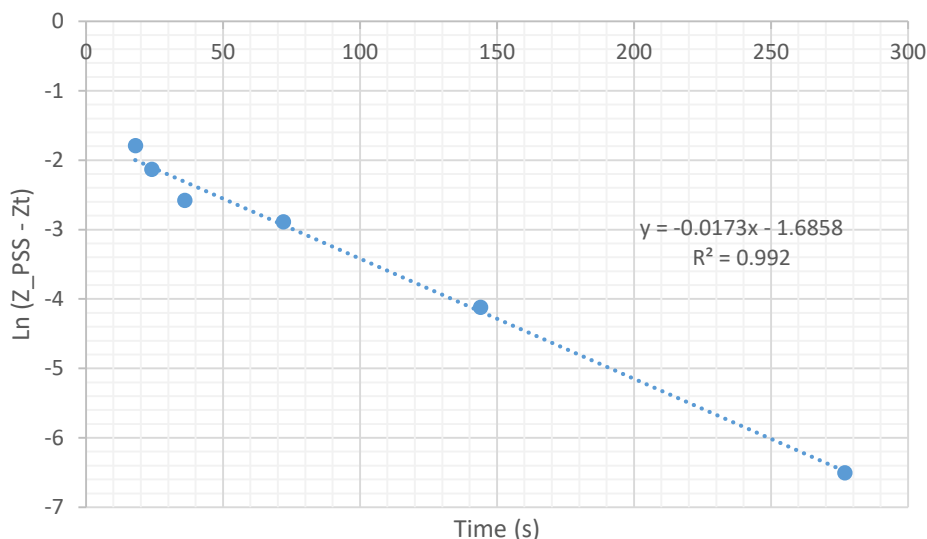


Figure 5-14: Graph of  $\ln(Z_{PSS} - Z_t)$  vs time (s) following the irradiation

### 5.11.2. Calculation of Photon Flux emitted by the UV LEDs

A linear relationship is seen in the corresponding graph, and the correlation coefficient is high (0.99) and the slope ( $0.0173 \text{ s}^{-1}$ ) is the constant  $w$ , will be used to calculate the irradiance of the light ( $I_{\text{photon}}$ ) inside the microreactor.

$$\frac{d[Z]}{dt} = \frac{I_{\text{photon}} \ln 10 \phi_E \varepsilon_E}{Z_{PSS}} [Z_{PSS} - Z]$$

Where  $W = \frac{I_{\text{photon}} \ln 10 \phi_E \varepsilon_E}{Z_{PSS}}$

Consider  $y = Z_{PSS} - Z$ ,

Integrating Equation, will finally give equation  $\ln y = -wt + \text{constant}$

So, plotting the graph of  $\ln y$  vs. time will exhibit a linear relationship whose slope will be used to determine the value of  $I_0$ . With

$$Z_{PSS} = 0.225,$$

$$\varepsilon_E \text{ of acetonitrile} = 277 \text{ (L.mol}^{-1}.\text{cm}^{-1}\text{)}$$

$$\phi_E = 0.15$$

$$I_{\text{photon}} = 4.07 \times 10^{-3} \text{ ein.s}^{-1}.\text{m}^{-2}.$$

$$E_{\text{photon}} = N_A \times hc / \lambda = 6 \times 10^{23} \times 6.63 \times 10^{-34} \times 3 \times 10^8 / 395 \times 10^{-9} = 326959 \text{ J}$$

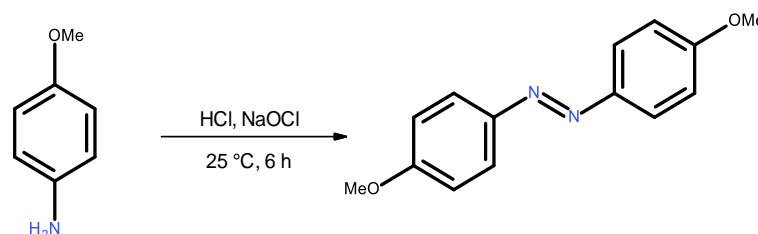
$$Q_{\text{inside exp}} = I_{\text{photon}} \times E$$

$$Q_{\text{inside exp}} = 1331 \text{ W} \cdot \text{m}^{-2}$$

Now that the calculations have been verified and the outcomes of the Nassim approach and our method have been compared, the values are fairly similar even when using a different microfluidic system and a different type of UV lamp. We can move on to the next step, which entails using same process but this time using water-soluble azobenzene to match the requirements of Macopharma bags.

### 5.11.3. Water soluble azobenzene

For the first trial to synthesis the WSA using the oxidative coupling, after the reaction a dark black liquid was produced and after a purification on chromatography column using hexane/ETOAc; 95:5, the  $^{19}\text{F}$  NMR spectrum showed there is no signal correspond to the target product, meaning that the self-coupling of p-anisidine was obtained instead of the cross coupling.



Thus, we shifted to the second way. The crude product obtained after the first step (electrophilic substitution) was purified by a chromatography column (100% Chloroform) and 1.893 g of product was obtained, which corresponds to a yield of 16%. The azobenzene phenol:  $^1\text{H}$  NMR (300 MHz,  $\text{CD}_3\text{CN}$ , ppm): Hc  $\delta = 7.84$  (d, 2H), Ha 7.43 (m, 1H), Hb 7.16 (t, 2H), Hd 7.01 (d, 2H).

After that, we must to do the methylation, the dimethyl sulfate methylation has been documented in multiple articles with good yields, but in our experiment, it didn't work. Contrarily, the second reaction using iodomethane worked effectively and 243 mg of WSA has been obtained, which corresponds to a yield of 41%. NMR analysis confirmed the synthesis of

WSA:  $^1\text{H}$  NMR (300 MHz,  $\text{CD}_3\text{CN}$ , ppm) (Figure 5-15): Hc  $\delta = 7.90$  (d, 2H), Ha 7.45 (m, 1H), Hb 7.15 (t, 2H).  $^{19}\text{F}$  NMR (282 MHz,  $\text{CD}_3\text{CN}$ ):  $\delta = -124.08$  (Figure 5-16).

*E*-WSA was predominantly synthesized but the signals of the *Z*-WSA was also observed. The methyl signals make it possible to calculate how much of each produced isomer there is.

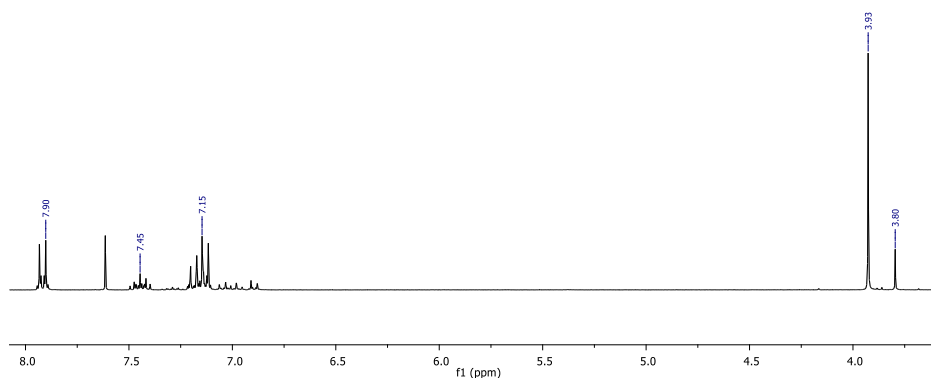


Figure 5-15:  $^1\text{H}$  NMR of water soluble azobenzene

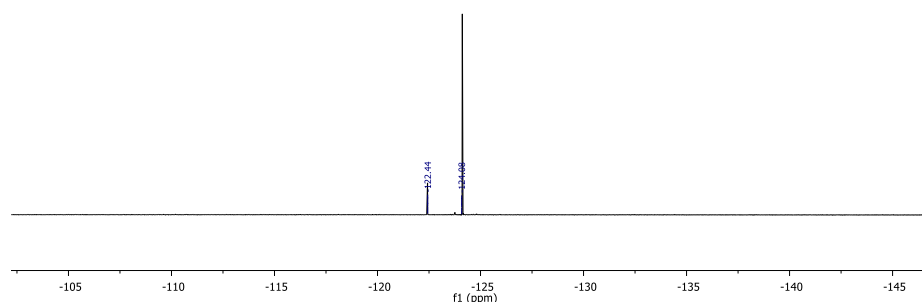


Figure 5-16:  $^{19}\text{F}$  NMR of water soluble azobenzene

#### 5.11.4. Actinometric protocol for the water soluble azobenzene

Several solutions of WSA ( $6.4 \times 10^{-4}$  mol/L in acetonitrile) was prepared and injected into the microreactor, the WSA solution was irradiated during 1h and 2h with an UV lamp of 395 nm, in order to discover the behavior of the WSA under UV light.

As it's shown in Table 5-6, for 1h of irradiation, a conversion of 42.8% was attempted, which is more than any irradiation of the classic azobenzene. Afterwards, this same experiment has been repeated but in 10:90 ethanol/water to improve the solubility of the product. All percentages are calculated using this formula.

$$\%Z = \frac{I_Z - OCH_3}{I_{E-OCH_3} + I_{Z-OCH_3}}$$

Table 5-6: Results for the conversion (Z)-WSA

Entry	solvent	irradiation time	flow rate	% Photostationary state
1	acetonitrile	1 h	1 ml/min	42.9
2	acetonitrile	2 h	0.05 ml/min	44.2
3	water	1 h	1 ml/min	42.7

In order to study the thermal isomerization of the WSA, we exposed all of the NMR tubes from each experiment—WSA 1, 2, and 3—to UV radiation before exposing them to visible light for 36 hours. Table 5-7 shows that each compound has increased its proportion of (Z)-WSA, which was unexpected because we expected to acquire a smaller proportion of (Z)-WSA with thermal isomerization than following irradiation. Brown et al. claim that the Z isomer is more soluble than the E isomer, especially in aqueous solution and that this difference could tip the Z-E equilibrium in favor of the Z isomer [9].

Table 5-7: Evolution (Z)-WSA after rest time

Number of experiments	Conversion after irradiation	Time of rest	Proportion of (Z)-WSA
WSA 1	42.9	12 h	42.9
WSA 2	44.2	12 h	44.2
WSA 3	42.7	12 h	42.7

After having these results, the goal was to test this actinometric protocol in a bag with parameters comparable to the blood bags of MacoPharma, while respecting the actinometric protocol. So we did some experiments in plastic bag with a thickness of 2 mm with azobenzene and WSA in water ( $6.4 \times 10^{-4}$  mol/L) under UV light at 365 and 395 nm. To collect our product from water after the irradiation, we did an extraction using chloroform or DCM because we should not do evaporation for the product to remain stable. As shown in Table 5-8, we achieved the best conversion of (Z) which's 66% with WSA under UV light 365 nm. The outcomes for azobenzene are comparable to those in flow that we previously attained.  $Z_{PSS}$  is always higher at 365 nm than at 395 nm.

Table 5-8: Results for the conversion (Z) in the plastic bag

Entry	Irradiation time	Solvent	$\lambda$ nm	%Photostationary state
azobenzene	1 h	10:90 ethanol/water	395	17.5
azobenzene	1 h	10:90 ethanol/water	365	25.7
WSA	1 h	10:90 ethanol/water	395	31
WSA	1 h	10:90 ethanol/water	365	66

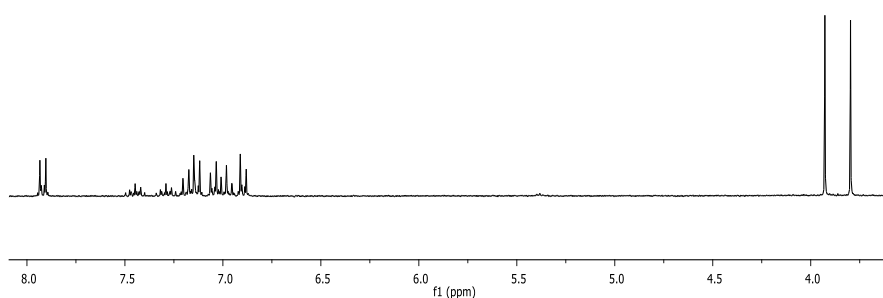


Figure 5-17:  $^1\text{H}$  NMR of WSA under  $\lambda=365$  nm

Finally, we repeated the same experiments but in blood bag of MacoPharma, we irradiated the azobenzene and WSA using different concentration ( $6.4 \times 10^{-4}$  mol/L and  $6.4 \times 10^{-5}$ ) in their tow machines UVA and UVC.

Table 5-9: Results for the conversion (*Z*) in the blood bag

Entry	Type of machine	Solvent	Concentration	%Photostationary state
azobenzene	UVC	10:90 ethanol/water	$6.4 \times 10^{-5}$	60
azobenzene	UVA	10:90 ethanol/water	$6.4 \times 10^{-5}$	64
WSA	UVC	10:90 ethanol/water	$6.4 \times 10^{-4}$	42
WSA	UVA	10:90 ethanol/water	$6.4 \times 10^{-4}$	59
WSA	UVC	10:90 ethanol/water	$6.4 \times 10^{-5}$	46
WSA	UVA	10:90 ethanol/water	$6.4 \times 10^{-5}$	50

These results show that both with UVA and C the photostationary state is reached with the normal irradiation time of the Macopharma illumination devices, we obtained as we have expected the high values of *Z/E* ratio in short time around 30 s and 5 min respectively. For UVC (280 nm) a conversion of 60% is expected but surprisingly for the azobenzene the 64% conversion in UVA (365 nm) is too high in comparison to the previous values obtained under the same conditions of light and concentration, this high value is due to the polychromatic nature of the UV source.

To solve this problem, we chose to change the machine's radiant energy for UVA while conducting a kinetic investigation on the isomerization of WSA at various durations, ranging from 32 seconds to 300 seconds. However, this is not the case for UVC because we were unable to alter either the duration of the exposure or the radiant energy using this device, therefore we attempted to alter the thickness by varying the volume of the solutions in the blood bags.

Table 5-10: Results for the conversion (Z) in the blood bag ( second trial )

Entry	Irradiation time (s)	Radiant energy (J)	Type of device	% Photostationary state
1	32	0.1	UVA	59.0
2	60	0.2	UVA	53.0
3	106	0.4	UVA	52.9
4	149	0.6	UVA	52.7
5	193	0.8	UVA	51.9
6	300	1.0	UVA	50.0
WSA 235 ml	30	–	UVC	37.8
WSA 600 ml	30	–	UVC	37.0
WSA 900 ml	30	–	UVC	39.0

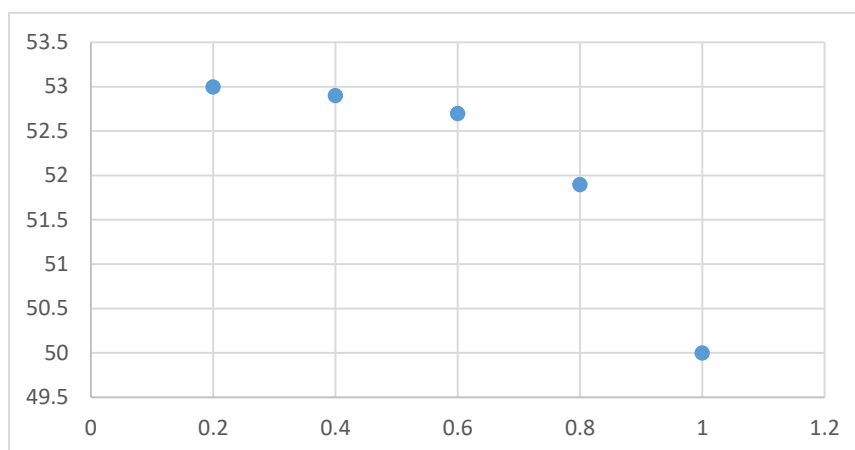


Figure 5-18: Graph of  $Z_{PSS}$  vs radiant energy (J) following the irradiation of  $6.4 \times 10^{-5}$  M WSA in ethanol/water

As can be seen from the results in the table above, for UVA we didn't get a straight line as in the case of azobenzene and WSA with our lamps even after lowering the concentration of the solutions in order to decrease the intensity of light on the product. As a result, we had to either use a filter to purify the light and resolve the lamp's polychromaticity issue or conduct additional research that would allow us to work more on the concentration instead of the light of lamps, because in our situation we cannot work with lower concentration. For UVC we didn't see a significant difference in the values because the settings were so constrained.

#### 5.11.5. Pyridine actinometer

Two other actinometers were developed by Dulin and Mill [309] based on the photonucleophilic substitution of excited state nitrobenzene derivatives by pyridine. The quantum yields can be adjusted by varying the pyridine concentration, opening up a wide range of experimental time scales. Environmental photochemists have used the actinometers p-nitroanisole/pyridine (PNA-pyr) and p-nitroacetophenone/pyridine (PNAP-pyr) widely. PNA-pyr is used more frequently than PNAP-pyr. The basis for PNA-pyr is substitution of pyridine for the methoxy group in excited state PNA.

## 5.11.5.1. Pyridine Dependence of PNA-pyr Quantum Yield

Laszakovits et al. [310] investigate the relationship between the pyridine concentration dependence of the PNA-pyr quantum yield and compare the photon irradiance values calculated by PNA-pyr at various wavelengths, and they propose a updated equation for concentration dependence of pyridine in order to ameliorate the quantum yield established by Dulin and Mill.

They performed different experiments using a wide range of pyridine concentrations 10, 12.5, or 15 mM with 10  $\mu$ M PNA. All of the experiments for these articles were conducted in a quartz test tubes (1 cm) or between 1 and 3 mL in a 1 cm quartz cuvettes. PNA's irradiation periods were adequate to accomplish at least 15% elimination, which was measured by HPLC.

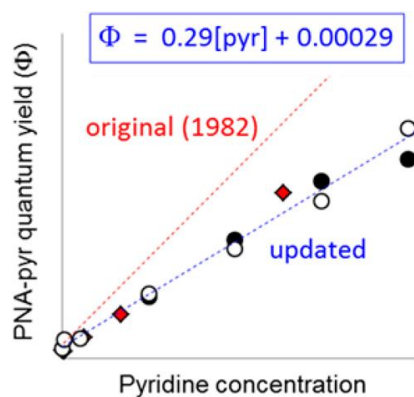


Figure 5-19: Pyridine concentration dependence of PNA-Pyr photolysis quantum yield

Pyridine concentration-dependent PNA-pyr photolysis quantum yield, was calculated using the formula mentioned. Dulin and Mill's  $\Phi = 0.44[\text{pyr}] + 0.00028$  is shown as a red dashed line. The white circle represents rate constants that were established using recrystallized PNA in this study (Laszakovits works).  $\Phi = 0.29[\text{pyr}] + 0.00029$ , where  $[\text{pyr}]$  is the molar concentration of pyridine, is the line that best fits the data (black dashed line) Figure 5-19.

However, in our research, we must use our microflow system to implement the identical actinometer methodology as these two studies. Our ultimate goal is to calculate the quantum yield using the more straightforward method (using NMR spectra), so in order to try this, we decided to replace PNA with FNB (floronitrobenzene). Because with the ring contains a fluorine atom, we can estimate the conversion of the reaction using  $^{19}\text{F}$  NMR.

## 5.11.5.2. Photochemical reaction of pyridine and 1-fluoro-4-nitrobenzene

We performed the reaction between pyridine and FNB in a plastic bag containing 500 ml of aqueous pyridine solution (5 mM) and various concentrations of FNB (30, 60 or 90  $\mu\text{M}$ ). These bags were irradiated at UV light 365 nm over several times including 24 and 72 hours.

Table 5-11: summary of experiments performed for PNA-pyr actinometer

Pyridine [mM]	P-FNB [ $\mu\text{M}$ ]	Irradiation time (h)
10	30	24
10	60	24
5	60	24
5	90	24
5	90	72
5	200	72

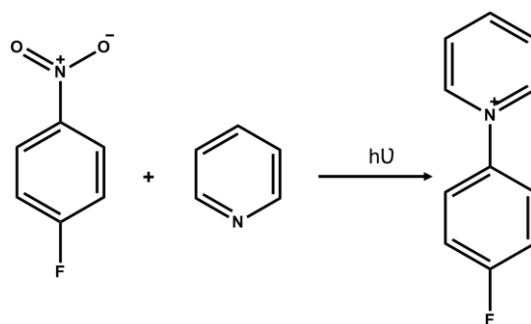


Figure 5-20: Reaction between pyridine and FNB

Nitroarenes are particularly intriguing electrophiles, because they can interact with nucleophiles in a variety of ways. The aromatic ring is electron deficient due to the nitro group, primarily in the conjugated ortho- and para locations. Additionally, the nitro group itself is an electron-

deficient fragment. Active single-electron-accepting compounds include nitroarenes. These characteristics allow for a number of starting reactions between nucleophiles and nitroarenes, such as direct addition to the ring to produce nitrocyclohexadienyl adducts, proton abstraction from the ring to produce nitroaryl carbanions, attack on the nitro group, and single-electron transfer (Figure 5-21).

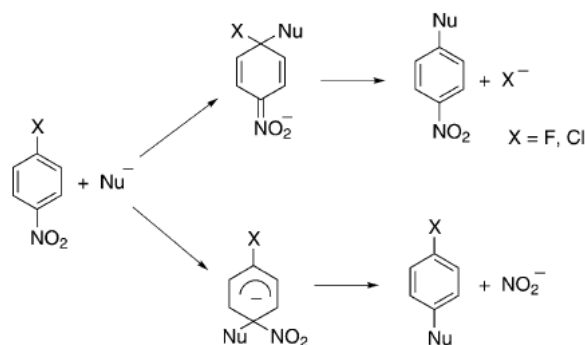


Figure 5-21: Proposed mechanism for nucleophilic substitution of halogen atoms and nitro group in nitroarenes [311]

#### 5.11.5.3. Kinetic study of pyridine chemical actinometers

A kinetic experiments was started to track the chemical alterations that the reagents underwent during irradiation. For pyridine, the concentration was fixed at 5 mM, while for 1-fluoro-4-nitrobenzene, it was 90  $\mu$ M, and we added to the solution an internal standard methyl-4-fluorobenzoate (5 mg), the bags were then exposed to radiation for 5, 10, 15, 20, 25, and 30 minutes, respectively.

Table 5-12: Results for the irradiation solutions for different durations

irradiation time (min)	% of FNB	% of standard
5	0.49	0.38
10	0.34	0.23
15	0.16	0.12

20	0.04	0.03
25	0.03	0.02
30	0.02	0.01

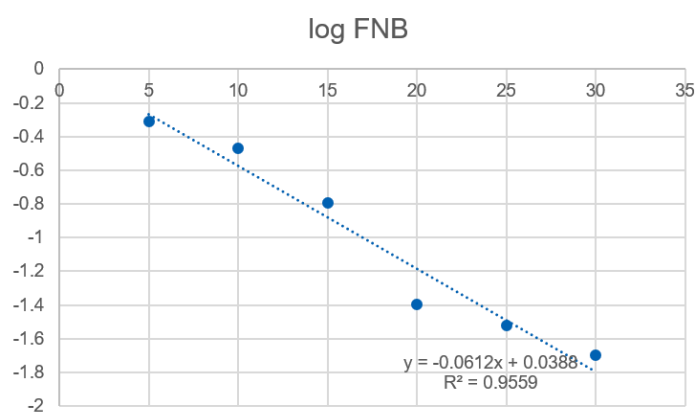


Figure 5-22: Graph of log FNB vs time (s) following the irradiation

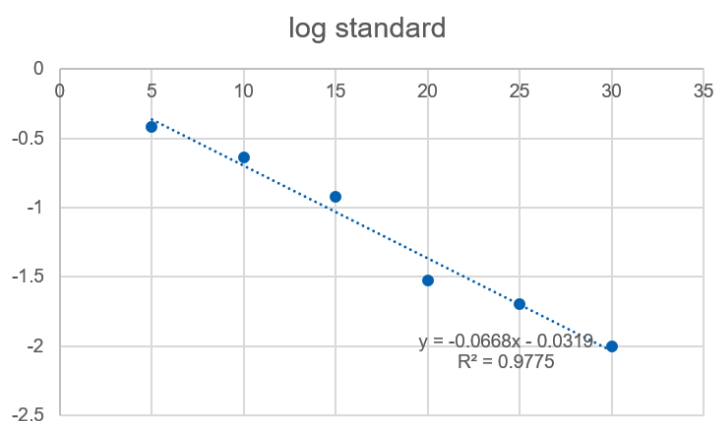


Figure 5-23: Graph of log standard vs time (s) following the irradiation

Surprisingly, we discovered during the kinetic study that the internal standard was react as a reactant due to its fluorinated structure. As a result, we drew the graph for the 2 reactants, which shows straight lines with slopes of -0.0612 and -0.0668, respectively. We can therefore conclude that methyl-4-fluorobenzoate/pyr and 1-fluoro-4-nitrobenzene/pyr have shown to be promising chemical actinometers.

The following step is to improve this type of actinometer by utilizing a non-fluorinated standard like TMB (trimethoxybenzene), and then to try the same actinometric process using 2,6-lutidine and picoline due to their structures with methyl groups to slow down their reactivity. After that, we may use this method with the Macopharma machines.

## **5.12. Conclusion**

In this work, the main focus was to synthesis a water soluble azobenzene with the aim of using this one in an actinometric protocol already established in our laboratory in an attempt to develop a way to fight viruses and diseases with UV therapy which is the aim of Macopharma industry.

To fulfill this purpose, a pure water soluble azobenzene was synthesized in two steps. Finally, the WSA was subjected to several experiments in order to identify its properties. Thermal stability, cis lifetime and  $Z_{PSS}$  are parameters which have been analyzed during this internship, in order to determine if the WSA could correspond to the actinometric protocol. However, we succeed to isomerize the WSA in water and obtained a high amount of Z isomer, which could be a potential result for a  $Z_{PSS}$ . After having made some first studies in the lab, the substance has been employed in the UVC and UVA machines of Macopharma.

This method was established in order to determine the number of photons emitted during the irradiation by following by NMR the apparition of Z-Azobenzene and its reaching of the Photo Stationary State (PSS) the photon flux can be determined. But unfortunately, this procedure did not work when used with Macopharma machines for two reasons; first the photostationary state is reached with the normal irradiation time of the Macopharma illumination devices which demonstrate the very sensitive effect of both UVA and UVC, second the problem of polychromaticity of the lamp UVA which has reached the photostationary state in short time around 30 s. Thus, we must find a method to modulate the reactivity. Following a recent paper comparing the quantum yield of two widely used actinometers: p-nitroanisole/pyridine and p-nitroacetophenone/pyridine, we present in this report the photochemical reaction between 1-Fluoro-4-nitrobenzene and Pyridine in a Polyethylene bag that will be reproduced later on in a microreactor

## **6. GENERAL CONCLUSION**

This report examines lignin from both a chemical and biological standpoint.

**Chapter 1** The structure, composition, biosynthesis, and uses of lignin were all discussed. It also detailed the efforts undertaken for the in vitro creation of lignin models, including chemical and enzymatic mechanisms. Also, the various methodologies for phenoxy radical production are presented.

**Chapter 2** Describes a green and simple continuous flow photooxidation method for obtaining the 5-5' dimer coupling derivative with a higher yield of roughly 80% by flow photo-oxidation of vanillyl alcohol (1) with riboflavin as photosensitizer. The strong riboflavin selectivity toward the dimers 5-5' and  $\beta$ - $\beta'$  coupling was reported for the first time in our knowledge, and no side products were discovered with this flow procedure. This method has various advantages: (i) The 5-5' dimer synthesis happens in the flow system at room temperature without the need of any oxidant, (ii) product purification is simple (iii) Additionally, this dimerization process was applied to several lignin models, yielding primarily (5-5') biphenylic derivatives.

**Chapter 3** Covered the synthesis of a lignin model by examining various pathways for the oxidation of vanillin, a simple lignin model chemical. It also concentrated on enzyme-catalyzed oxidation processes for vanillin polymerization. Vanillin oxidation via enzymatic and chemical pathways resulted in the creation of C-C linked divanillin. Interestingly, in addition to divanillin, HRP-catalyzed vanillin oxidation produced other oligomeric compounds. Following various purification processes, mass spectrometry examination of these oligomers showed several oligomeric families. Vanillin oxidation with HRP mounted on hydrophobic support produced purer polyvanillin. A derivatization phase showed the sort of linkages that make up polyvanillin, which was discovered to be primarily linked by C-O bonds, with the existence of a C-C bond.

**Chapter 4** Examines the behavior of HRP toward a panel of lignin modified substrates to propose a unique way for researching lignification peroxidases based on proximity labeling and click-chemistry techniques. First, the ability of HRP to perform in vitro proximity labeling of

proteins was assessed. HRP has endogenous tagging on its own tyrosine residues, which was discovered. Following that, specially engineered lignification tags were tested for their reactivity to HRP, allowing researchers to investigate the mechanism of peroxidase inhibition using various methodologies. A kinetic study revealed a complete decrease of HRP activity following treatment with these tags. The use of mass spectrometry enabled the discovery of structural alterations to the polypeptide chain of HRP caused by the oxidation of two coumaric acid tags, which were manifested by a coupling between lignin monomer tags and HRP-tyrosine residues.

**Chapter 5** provides a revolutionary method for developing an actinometric protocol in order to find a strategy to combat viruses and diseases utilizing UV therapy, which is the goal of the Macopharma enterprise. A water-soluble azobenzene was synthesized for this purpose, and it may be used in Macopharma's UVC and UVA machines. Because UVA and UVC have such a sensitive effect, a new actinometric procedure was developed to control their reactivity. In this chapter, we present the photochemical interaction between 1-Fluoro-4-nitrobenzene and Pyridine in a Polyethylene bag, which will be replicated subsequently in a microreactor.

## 7. LIST OF REFERENCES

1. Daubresse, N., et al., *Rational design, synthesis and biological evaluation of the firstinhibitor of lignin polymerization*. Chemical Communications, 1997(16): p. 1489-1490.
2. Dexter, A.F. and L.P. Hager, *Transient heme N-alkylation of chloroperoxidase by terminal alkenes and alkynes*. Journal of the American Chemical Society, 1995. **117**(2): p. 817-818.
3. Gray, H.B. and J.R. Winkler, *Functional and protective hole hopping in metalloenzymes*. Chemical Science, 2021. **12**(42): p. 13988-14003.
4. Watkins, D., et al., *Extraction and characterization of lignin from different biomass resources*. Journal of Materials Research and Technology, 2015. **4**(1): p. 26-32.
5. Sheldon, R.A., *Green and sustainable manufacture of chemicals from biomass: state of the art*. Green Chemistry, 2014. **16**(3): p. 950-963.
6. Nishimura, H., et al., *Direct evidence for a ether linkage between lignin and carbohydrates in wood cell walls*. Scientific reports, 2018. **8**(1): p. 1-11.
7. Boerjan, W., J. Ralph, and M. Baucher, *Lignin biosynthesis*. 2003.
8. Aminzadeh, S., L. Zhang, and G. Henriksson, *A possible explanation for the structural inhomogeneity of lignin in LCC networks*. Wood Science and Technology, 2017. **51**(6): p. 1365-1376.
9. Welker, C.M., et al., *Engineering plant biomass lignin content and composition for biofuels and bioproducts*. Energies, 2015. **8**(8): p. 7654-7676.
10. Vinardell, M.P. and M. Mitjans, *Lignins and their derivatives with beneficial effects on human health*. International journal of molecular sciences, 2017. **18**(6): p. 1219.
11. Figueiredo, P., et al., *Properties and chemical modifications of lignin: Towards lignin-based nanomaterials for biomedical applications*. Progress in Materials Science, 2018. **93**: p. 233-269.
12. Mogharabi, M. and M.A. Faramarzi, *Laccase and laccase-mediated systems in the synthesis of organic compounds*. Advanced Synthesis & Catalysis, 2014. **356**(5): p. 897-927.
13. Cesarino, I., et al., *An overview of lignin metabolism and its effect on biomass recalcitrance*. Brazilian Journal of Botany, 2012. **35**: p. 303-311.
14. Akbarzadeh, E., M.M. Ibrahim, and A.A. Rahim, *Corrosion inhibition of mild steel in near neutral solution by kraft and soda lignins extracted from oil palm empty fruit bunch*. Int. J. Electrochem. Sci, 2011. **6**(11): p. 5396-5416.
15. Chio, C., M. Sain, and W. Qin, *Lignin utilization: a review of lignin depolymerization from various aspects*. Renewable and Sustainable Energy Reviews, 2019. **107**: p. 232-249.
16. Cateto, C., M. Barreiro, and A. Rodrigues, *Monitoring of lignin-based polyurethane synthesis by FTIR-ATR*. industrial crops and products, 2008. **27**(2): p. 168-174.
17. Mahmood, N., et al., *Depolymerization of lignins and their applications for the preparation of polyols and rigid polyurethane foams: A review*. Renewable and Sustainable Energy Reviews, 2016. **60**: p. 317-329.
18. Arshanitsa, A., et al., *Exploring the application potential of incompletely soluble organosolv lignin as a macromonomer for polyurethane synthesis*. Industrial Crops and Products, 2016. **92**: p. 1-12.
19. Naseem, A., et al., *Lignin-derivatives based polymers, blends and composites: A review*. International Journal of Biological Macromolecules, 2016. **93**: p. 296-313.
20. Vickers, N.J., *Animal communication: when i'm calling you, will you answer too?* Current biology, 2017. **27**(14): p. R713-R715.
21. Xu, C., et al., *Lignin depolymerisation strategies: towards valuable chemicals and fuels*. Chemical Society Reviews, 2014. **43**(22): p. 7485-7500.
22. Kobayashi, S. and H. Higashimura, *Oxidative polymerization of phenols revisited*. Progress in Polymer Science, 2003. **28**(6): p. 1015-1048.
23. Kobayashi, S. and A. Makino, *Enzymatic polymer synthesis: an opportunity for green polymer chemistry*. Chemical reviews, 2009. **109**(11): p. 5288-5353.
24. Anderson, E.M., et al., *Differences in S/G ratio in natural poplar variants do not predict catalytic depolymerization monomer yields*. Nature communications, 2019. **10**(1): p. 1-10.

25. Higuchi, T., *Lignin biochemistry: biosynthesis and biodegradation*. Wood Science and Technology, 1990. **24**(1): p. 23-63.
26. Takabe, K., et al., *Immunolocalization of enzymes involved in lignification*, in *Progress in biotechnology*. 2001, Elsevier. p. 177-186.
27. Barros, J., et al., *The cell biology of lignification in higher plants*. Annals of botany, 2015. **115**(7): p. 1053-1074.
28. Labeeuw, L., et al., *Ancient origin of the biosynthesis of lignin precursors*. Biology Direct, 2015. **10**(1): p. 1-21.
29. Tobimatsu, Y. and M. Schuetz, *Lignin polymerization: how do plants manage the chemistry so well?* Current Opinion in Biotechnology, 2019. **56**: p. 75-81.
30. Zhao, Q., et al., *Laccase is necessary and nonredundant with peroxidase for lignin polymerization during vascular development in Arabidopsis*. The Plant Cell, 2013. **25**(10): p. 3976-3987.
31. O'Malley, D.M., et al., *The role of laccase in lignification*. The Plant Journal, 1993. **4**(5): p. 751-757.
32. Lim, C.H. and Y.J. Yoo, *Synthesis of ortho-directed polyaniline using horseradish peroxidase*. Process Biochemistry, 2000. **36**(3): p. 233-241.
33. Yadav, M., N. Rai, and H.S. Yadav, *The role of peroxidase in the enzymatic oxidation of phenolic compounds to quinones from Luffa aegyptiaca (gourd) fruit juice*. Green Chemistry Letters and Reviews, 2017. **10**(3): p. 154-161.
34. Yang, D., et al., *Model compounds study for the mechanism of horseradish peroxidase-catalyzed lignin modification*. Applied Biochemistry and Biotechnology, 2020. **191**(3): p. 981-995.
35. Tobimatsu, Y., et al., *Coexistence but independent biosynthesis of catechyl and guaiacyl/syringyl lignin polymers in seed coats*. The Plant Cell, 2013. **25**(7): p. 2587-2600.
36. Yoshida, H., *LXIII.—chemistry of lacquer (Urushi). Part I. communication from the chemical society of Tokio*. Journal of the Chemical Society, Transactions, 1883. **43**: p. 472-486.
37. Mot, A. and R. Silaghi-Dumitrescu, *Laccases: complex architectures for one-electron oxidations*. Biochemistry (Moscow), 2012. **77**(12): p. 1395-1407.
38. Mattinen, M.-L., et al., *Polymerization of different lignins by laccase*. BioResources, 2008. **3**(2): p. 549-565.
39. Ikeda, R., et al., *Enzymatic oxidative polymerization of 2, 6-dimethylphenol*. Macromolecules, 1996. **29**(27): p. 8702-8705.
40. Mikolasch, A. and F. Schauer, *Fungal laccases as tools for the synthesis of new hybrid molecules and biomaterials*. Applied Microbiology and Biotechnology, 2009. **82**(4): p. 605-624.
41. Aljawish, A., et al., *Laccase-catalysed oxidation of ferulic acid and ethyl ferulate in aqueous medium: A green procedure for the synthesis of new compounds*. Food chemistry, 2014. **145**: p. 1046-1054.
42. Constantin, M.-A., J. Conrad, and U. Beifuss, *Laccase-catalyzed oxidative phenolic coupling of vanillidene derivatives*. Green Chemistry, 2012. **14**(9): p. 2375-2379.
43. Lahtinen, M., et al., *On the reactions of two fungal laccases differing in their redox potential with lignin model compounds: products and their rate of formation*. Journal of agricultural and food chemistry, 2009. **57**(18): p. 8357-8365.
44. Lahtinen, M., et al., *On the factors affecting product distribution in laccase-catalyzed oxidation of a lignin model compound vanillyl alcohol: experimental and computational evaluation*. Organic & biomolecular chemistry, 2013. **11**(33): p. 5454-5464.
45. Dorfner, R., et al., *Real-time monitoring of 4-vinylguaiacol, guaiacol, and phenol during coffee roasting by resonant laser ionization time-of-flight mass spectrometry*. Journal of Agricultural and Food Chemistry, 2003. **51**(19): p. 5768-5773.
46. Fernando, S., et al., *Biorefineries: current status, challenges, and future direction*. Energy & Fuels, 2006. **20**(4): p. 1727-1737.
47. Eskins, K., et al., *Dimers of isoeugenol by dye-sensitized photooxidation*. Tetrahedron Letters, 1972. **13**(9): p. 861-864.
48. Elgendy, E. and S. Khayyat, *Oxidation reactions of some natural volatile aromatic compounds: anethole and eugenol*. Russian Journal of Organic Chemistry, 2008. **44**(6): p. 823-829.

49. Jadhav, B.K., et al., *Formulation and evaluation of mucoadhesive tablets containing eugenol for the treatment of periodontal diseases*. Drug Development and Industrial Pharmacy, 2004. **30**(2): p. 195-203.
50. Anklam, E., S. Gaglione, and A. Müller, *Oxidation behaviour of vanillin in dairy products*. Food chemistry, 1997. **60**(1): p. 43-51.
51. Fache, M., et al., *Vanillin, a promising biobased building-block for monomer synthesis*. Green Chemistry, 2014. **16**(4): p. 1987-1998.
52. Janvier, M., et al., *Syringaresinol: a renewable and safer alternative to bisphenol A for epoxy-amine resins*. ChemSusChem, 2017. **10**(4): p. 738-746.
53. Mouterde, L.M. and F. Allais, *Microwave-assisted Knoevenagel-Doebner reaction: an efficient method for naturally occurring phenolic acids synthesis*. Frontiers in chemistry, 2018. **6**: p. 426.
54. Mention, M.M., et al., *Biomimetic regioselective and high-yielding Cu (I)-catalyzed dimerization of sinapate esters in green solvent Cyrene<sup>TM</sup>: Towards sustainable antioxidant and anti-UV ingredients*. Green Chemistry, 2020. **22**(6): p. 2077-2085.
55. Koschorreck, K., et al., *Cloning and characterization of a new laccase from Bacillus licheniformis catalyzing dimerization of phenolic acids*. Applied Microbiology and Biotechnology, 2008. **79**(2): p. 217-224.
56. Nakatsubo, F., K. Sato, and T. Higuchi, *Synthesis of guaiacylglycerol- $\beta$ -guaiacyl ether*. 1975.
57. Forsythe, W.G., et al., *An efficient and flexible synthesis of model lignin oligomers*. Green chemistry, 2013. **15**(11): p. 3031-3038.
58. Freudenberg, K., *Structure and formation of lignin*. Industrial & Engineering Chemistry, 1957. **49**(9): p. 1384-1384.
59. Moon, S.-J., et al., *In vitro analysis of the monolignol coupling mechanism using dehydrogenative polymerization in the presence of peroxidases and controlled feeding ratios of coniferyl and sinapyl alcohol*. Phytochemistry, 2012. **82**: p. 15-21.
60. Xie, Y., et al., *Preparation of oligomeric dehydrogenation polymer and characterization of its antibacterial properties*. Bioresources, 2019. **14**(2): p. 2842-2860.
61. Janson, J.-C., *Protein purification: principles, high resolution methods, and applications*. 2012: John Wiley & Sons.
62. Ahmed, H., *Principles and reactions of protein extraction, purification, and characterization*. 2017: CRC press.
63. Issaq, H.J., et al., *Methods for fractionation, separation and profiling of proteins and peptides*. Electrophoresis, 2002. **23**(17): p. 3048-3061.
64. Chen, C.L. and N. Perrimon, *Proximity-dependent labeling methods for proteomic profiling in living cells*. Wiley Interdisciplinary Reviews: Developmental Biology, 2017. **6**(4): p. e272.
65. Samavarchi-Tehrani, P., R. Samson, and A.-C. Gingras, *Proximity dependent biotinylation: key enzymes and adaptation to proteomics approaches*. Molecular & Cellular Proteomics, 2020. **19**(5): p. 757-773.
66. Schiapparelli, L.M., et al., *Direct detection of biotinylated proteins by mass spectrometry*. Journal of proteome research, 2014. **13**(9): p. 3966-3978.
67. Bosch, J.A., C.L. Chen, and N. Perrimon, *Proximity-dependent labeling methods for proteomic profiling in living cells: An update*. Wiley Interdisciplinary Reviews: Developmental Biology, 2021. **10**(1): p. e392.
68. Li, X.-W., et al., *New insights into the DT40 B cell receptor cluster using a proteomic proximity labeling assay*. Journal of Biological Chemistry, 2014. **289**(21): p. 14434-14447.
69. Hopkins, C., et al., *Chimeric molecules employing horseradish peroxidase as reporter enzyme for protein localization in the electron microscope*. Methods in enzymology, 2000. **327**: p. 35-45.
70. Schiapparelli, L.M., et al., *Proteomic screen reveals diverse protein transport between connected neurons in the visual system*. Cell reports, 2022. **38**(4): p. 110287.
71. Kim, D.I., et al., *BioSITE: a method for direct detection and quantitation of site-specific biotinylation*. Journal of proteome research, 2018. **17**(2): p. 759-769.
72. Kolb, H.C., M. Finn, and K.B. Sharpless, *Click chemistry: diverse chemical function from a few good reactions*. Angewandte Chemie International Edition, 2001. **40**(11): p. 2004-2021.

73. Pickens, C.J., et al., *Practical considerations, challenges, and limitations of bioconjugation via azide–alkyne cycloaddition*. *Bioconjugate chemistry*, 2017. **29**(3): p. 686-701.
74. Nicell, J., et al., *Enzyme catalyzed polymerization and precipitation of aromatic compounds from aqueous solution*. *Canadian Journal of Civil Engineering*, 1993. **20**(5): p. 725-735.
75. Nakamoto, S. and N. Machida, *Phenol removal from aqueous solutions by peroxidase-catalyzed reaction using additives*. *Water Research*, 1992. **26**(1): p. 49-54.
76. Tatsumi, K., H. Ichikawa, and S. Wada, *Dephenolization from aqueous solution by treatment with peroxidase and a coagulant*. *Water Science and Technology*, 1994. **30**(9): p. 79.
77. Villalobos, D. and I. Buchanan, *Removal of aqueous phenol by *Arthromyces ramosus* peroxidase*. *Journal of Environmental Engineering and Science*, 2002. **1**(1): p. 65-73.
78. Mao, L., et al., *Horseradish peroxidase inactivation: heme destruction and influence of polyethylene glycol*. *Scientific Reports*, 2013. **3**(1): p. 1-7.
79. Huang, L., C. Colas, and P.R. Ortiz de Montellano, *Oxidation of carboxylic acids by horseradish peroxidase results in prosthetic heme modification and inactivation*. *Journal of the American Chemical Society*, 2004. **126**(40): p. 12865-12873.
80. Kim, S.J., et al., *Peroxidase inactivation by covalent modification with phenoxyl radical during phenol oxidation*. *Journal of the Korean Society for Applied Biological Chemistry*, 2014. **57**(6): p. 743-747.
81. Liu, C.-J., *Deciphering the enigma of lignification: precursor transport, oxidation, and the topochemistry of lignin assembly*. *Molecular Plant*, 2012. **5**(2): p. 304-317.
82. Wang, Y., et al., *Plant cell wall lignification and monolignol metabolism*. *Frontiers in plant science*, 2013. **4**: p. 220.
83. Kaneda, M., K. Rensing, and L. Samuels, *Secondary cell wall deposition in developing secondary xylem of poplar*. *Journal of Integrative Plant Biology*, 2010. **52**(2): p. 234-243.
84. Schuetz, M., et al., *Laccases direct lignification in the discrete secondary cell wall domains of protoxylem*. *Plant physiology*, 2014. **166**(2): p. 798-807.
85. Alejandro, S., et al., *AtABCG29 is a monolignol transporter involved in lignin biosynthesis*. *Current Biology*, 2012. **22**(13): p. 1207-1212.
86. Miao, Y.-C. and C.-J. Liu, *ATP-binding cassette-like transporters are involved in the transport of lignin precursors across plasma and vacuolar membranes*. *Proceedings of the National Academy of Sciences*, 2010. **107**(52): p. 22728-22733.
87. Ralph, J., et al., *Lignins: natural polymers from oxidative coupling of 4-hydroxyphenyl-propanoids*. *Phytochemistry reviews*, 2004. **3**(1): p. 29-60.
88. Vanholme, R., et al., *Lignin biosynthesis and structure*. *Plant physiology*, 2010. **153**(3): p. 895-905.
89. Weng, J.K. and C. Chapple, *The origin and evolution of lignin biosynthesis*. *New Phytologist*, 2010. **187**(2): p. 273-285.
90. Pandey, J.L., et al., *A versatile click-compatible monolignol probe to study lignin deposition in plant cell walls*. *PLoS One*, 2015. **10**(4): p. e0121334.
91. Anderson, C.T., I.S. Wallace, and C.R. Somerville, *Metabolic click-labeling with a fucose analog reveals pectin delivery, architecture, and dynamics in *Arabidopsis* cell walls*. *Proceedings of the National Academy of Sciences*, 2012. **109**(4): p. 1329-1334.
92. Seo, T.S., et al., *Photocleavable fluorescent nucleotides for DNA sequencing on a chip constructed by site-specific coupling chemistry*. *Proceedings of the National Academy of Sciences*, 2004. **101**(15): p. 5488-5493.
93. Prescher, J.A. and C.R. Bertozzi, *Chemistry in living systems*. *Nature chemical biology*, 2005. **1**(1): p. 13-21.
94. Link, A.J., M.K. Vink, and D.A. Tirrell, *Presentation and detection of azide functionality in bacterial cell surface proteins*. *Journal of the American Chemical Society*, 2004. **126**(34): p. 10598-10602.
95. Siegrist, M., et al., *Biol. 2013, 8, 500–505; b) P. Shieh, MS Siegrist, AJ Cullen, CR Bertozzi*. *Proc. Natl. Acad. Sci. USA*, 2014. **111**: p. 5456-5461.
96. Flors, C., *Super-resolution fluorescence imaging of directly labelled DNA: from microscopy standards to living cells*. *Journal of Microscopy*, 2013. **251**(1): p. 1-4.

97. Rouhanifard, S.H., et al., *Chemical probing of glycans in cells and organisms*. Chemical Society Reviews, 2013. **42**(10): p. 4284-4296.
98. Sletten, E.M. and C.R. Bertozzi, *Bioorthogonal chemistry: fishing for selectivity in a sea of functionality*. Angewandte Chemie International Edition, 2009. **48**(38): p. 6974-6998.
99. Syrjänen, K. and G. Brunow, *Oxidative cross coupling of p-hydroxycinnamic alcohols with dimeric arylglycerol  $\beta$ -aryl ether lignin model compounds. The effect of oxidation potentials*. Journal of the Chemical Society, Perkin Transactions 1, 1998(20): p. 3425-3430.
100. Bukowski, N., et al., *Development of a clickable designer monolignol for interrogation of lignification in plant cell walls*. Bioconjugate Chemistry, 2014. **25**(12): p. 2189-2196.
101. Van de Wouwer, D., *A click chemistry strategy for visualization of plant cell wall lignification*. Chemical Communications, 2014. **50**(82): p. 12262-12265.
102. Laurino, P., *Photochemical transformations in continuous flow devices*. 2011, ETH Zurich.
103. Ciamician, G. and P. Silber, *Chemische Lichtwirkungen*. Berichte der deutschen chemischen Gesellschaft, 1901. **34**(2): p. 2040-2046.
104. Eaton, P.E. and T.W. Cole, *The cubane system*. Journal of the American chemical society, 1964. **86**(5): p. 962-964.
105. Corey, E. and S. Nozoe, *The total synthesis of  $\alpha$ -caryophyllene alcohol*. Journal of the American Chemical Society, 1965. **87**(24): p. 5733-5735.
106. Wender, P. and J. Howbert, *Synthetic studies on arene-olefin cycloadditions: total synthesis of (+)- $\alpha$ -cedrene*. Journal of the American Chemical Society, 1981. **103**(3): p. 688-690.
107. Cambie, D., et al., *Applications of continuous-flow photochemistry in organic synthesis, material science, and water treatment*. Chemical reviews, 2016. **116**(17): p. 10276-10341.
108. Albin, A. and L. Germani, *Photochemical methods*. 2010, Wiley Online Library. p. 1-24.
109. Knowles, J.P., L.D. Elliott, and K.I. Booker-Milburn, *Flow photochemistry: Old light through new windows*. Beilstein journal of organic chemistry, 2012. **8**(1): p. 2025-2052.
110. Baxendale, I.R., et al., *A flow process for the multi-step synthesis of the alkaloid natural product oxomaritidine: a new paradigm for molecular assembly*. Chemical communications, 2006(24): p. 2566-2568.
111. Baxendale, I.R., et al., *Multistep synthesis using modular flow reactors: Bestmann–Ohira reagent for the formation of alkynes and triazoles*. Angewandte Chemie, 2009. **121**(22): p. 4077-4081.
112. Mason, B.P., et al., *Greener approaches to organic synthesis using microreactor technology*. Chemical reviews, 2007. **107**(6): p. 2300-2318.
113. Aillet, T., et al., *Photochemical synthesis of a “cage” compound in a microreactor: Rigorous comparison with a batch photoreactor*. Chemical Engineering and Processing: Process Intensification, 2013. **64**: p. 38-47.
114. Mizuno, K., et al., *Utilization of microflow reactors to carry out synthetically useful organic photochemical reactions*. Journal of Photochemistry and Photobiology C: Photochemistry Reviews, 2016. **29**: p. 107-147.
115. Strike, D., et al., *Glucose measurement using a micromachined open tubular heterogeneous enzyme reactor (MOTHER)*. Microsystem Technologies, 1994. **1**(1): p. 48-50.
116. Watts, P. and S.J. Haswell, *The application of micro reactors for organic synthesis*. Chemical Society Reviews, 2005. **34**(3): p. 235-246.
117. El Achi, N., *Photochemical and photoredox reactions in continuous microreactors: application to cycloaddition, controlled polymerization and radical chemistry*. 2016, Lille 1.
118. Albin, A. and M. Fagnoni, *Handbook of synthetic photochemistry*. 2010: John Wiley & Sons.
119. Fukuyama, T., et al., *Adventures in inner space: Microflow systems for practical organic synthesis*. Synlett, 2008. **2008**(02): p. 151-163.
120. Jamali, A., et al., *A batch LED reactor for the photocatalytic degradation of phenol*. Chemical Engineering and Processing: Process Intensification, 2013. **71**: p. 43-50.
121. Su, Y., V. Hessel, and T. Noël, *A compact photomicroreactor design for kinetic studies of gas-liquid photocatalytic transformations*. AIChE Journal, 2015. **61**(7): p. 2215-2227.
122. Vasudevan, A., et al., *LOPHTOR: a convenient flow-based photochemical reactor*. Tetrahedron Letters, 2010. **51**(31): p. 4007-4009.

123. Lefebvre, Q., M. Jentsch, and M. Rueping, *Continuous flow photocyclization of stilbenes—scalable synthesis of functionalized phenanthrenes and helicenes*. Beilstein journal of organic chemistry, 2013. **9**(1): p. 1883-1890.
124. Talla, A., et al., *Metal-free photocatalytic aerobic oxidation of thiols to disulfides in batch and continuous-flow*. Advanced Synthesis & Catalysis, 2015. **357**(10): p. 2180-2186.
125. Straathof, N.J., et al., *Accelerated gas-liquid visible light photoredox catalysis with continuous-flow photochemical microreactors*. Nature protocols, 2016. **11**(1): p. 10-21.
126. Neumann, M. and K. Zeitler, *Application of microflow conditions to visible light photoredox catalysis*. Organic letters, 2012. **14**(11): p. 2658-2661.
127. Altwicker, E.R., *The chemistry of stable phenoxy radicals*. Chemical Reviews, 1967. **67**(5): p. 475-531.
128. Nonhebel, D.C. and J.C. Walton, *Free-radical chemistry: structure and mechanism*. 1974: CUP Archive.
129. Bhattacharjee, M. and M. Mahanti, *Kinetics of oxidative coupling of phenols: Oxidation of naphthols by alkaline hexacyanoferrate (III)*. International Journal of Chemical Kinetics, 1983. **15**(2): p. 197-203.
130. Penzkofer, A., A. Beidoun, and M. Daiber, *Intersystem-crossing and excited-state absorption in eosin Y solutions determined by picosecond double pulse transient absorption measurements*. Journal of luminescence, 1992. **51**(6): p. 297-314.
131. Penzkofer, A. and A. Beidoun, *Triplet-triplet absorption of eosin Y in methanol determined by nanosecond excimer laser excitation and picosecond light continuum probing*. Chemical physics, 1993. **177**(1): p. 203-216.
132. Hari, D.P. and B. König, *Eosin Y catalyzed visible light oxidative C–C and C–P bond formation*. Organic letters, 2011. **13**(15): p. 3852-3855.
133. Matsuura, T., K. Omura, and R. Nakashima, *Photo-induced reaction. II. The photo-sensitized oxidation of hindered phenols*. Bulletin of the Chemical Society of Japan, 1965. **38**(8): p. 1358-1362.
134. Mijs, W., et al., *The catalytic oxidation of 4-aryloxyphenols*. Tetrahedron, 1967. **23**(5): p. 2253-2264.
135. Mahadevan, V., et al., *Irreversible Reduction of Dioxygen by Simple Peralkylated Diamine–Copper (I) Complexes: Characterization and Thermal Stability of a [Cu<sub>2</sub> (μ-O)<sub>2</sub>] 2<sup>+</sup> Core*. Journal of the American Chemical Society, 1997. **119**(49): p. 11996-11997.
136. Higashimura, H., et al., *“Radical-controlled” oxidative polymerization of phenols. Substituent effect of phenol monomers on the reaction rate*. Polymers for Advanced Technologies, 2000. **11**(8-12): p. 733-738.
137. Boguta, G. and A. Dancewicz, *Formation of dityrosine in aqueous solution of tyrosine exposed to ionizing radiation*. Studia Biophysica, 1979. **73**(2): p. 149-156.
138. Boguta, G. and A.M. Dancewicz, *Radiation-induced dimerization of tyrosine and glycytyrosine in aqueous solutions*. International Journal of Radiation Biology and Related Studies in Physics, Chemistry and Medicine, 1981. **39**(2): p. 163-174.
139. Reid, L.O., et al., *A novel synthetic approach to tyrosine dimers based on pterin photosensitization*. Dyes and Pigments, 2017. **147**: p. 67-74.
140. Song, Q.-H. and K.C. Hwang, *Direct observation for photophysical and photochemical processes of folic acid in DMSO solution*. Journal of Photochemistry and Photobiology A: Chemistry, 2007. **185**(1): p. 51-56.
141. Dalsgaard, T.K., et al., *Dityrosine, 3, 4-dihydroxyphenylalanine (DOPA), and radical formation from tyrosine residues on milk proteins with globular and flexible structures as a result of riboflavin-mediated photo-oxidation*. Journal of agricultural and food chemistry, 2011. **59**(14): p. 7939-7947.
142. Silva, E. and J. Godoy, *Riboflavin sensitized photooxidation of tyrosine*. International Journal for Vitamin and Nutrition research. Internationale Zeitschrift für Vitamin-und Ernährungsforschung. Journal International de Vitaminologie et de Nutrition, 1994. **64**(4): p. 253-256.
143. Okkerse, C. and H. Van Bekkum, *From fossil to green*. Green Chemistry, 1999. **1**(2): p. 107-114.

144. Auvergne, R., et al., *Biobased thermosetting epoxy: present and future*. Chemical reviews, 2014. **114**(2): p. 1082-1115.
145. Lligadas, G., et al., *Renewable polymeric materials from vegetable oils: a perspective*. Materials today, 2013. **16**(9): p. 337-343.
146. Pandey, M.P. and C.S. Kim, *Lignin depolymerization and conversion: a review of thermochemical methods*. Chemical Engineering & Technology, 2011. **34**(1): p. 29-41.
147. Gundekari, S. and S. Kumar Karmee, *Recent Catalytic Approaches for the Production of Cycloalkane Intermediates from Lignin-Based Aromatic Compounds: A Review*. ChemistrySelect, 2021. **6**(7): p. 1715-1733.
148. del Río, J.C., et al., *Lignin monomers from beyond the canonical monolignol biosynthetic pathway: another brick in the wall*. ACS Sustainable Chemistry & Engineering, 2020. **8**(13): p. 4997-5012.
149. Grossman, A. and W. Vermeir, *Lignin-based polymers and nanomaterials*. Current opinion in biotechnology, 2019. **56**: p. 112-120.
150. Upton, B.M. and A.M. Kasko, *Strategies for the conversion of lignin to high-value polymeric materials: review and perspective*. Chemical reviews, 2016. **116**(4): p. 2275-2306.
151. Voxeur, A., Y. Wang, and R. Sibout, *Lignification: different mechanisms for a versatile polymer*. Current Opinion in Plant Biology, 2015. **23**: p. 83-90.
152. Krings, U., V. Esparan, and R.G. Berger, *The taste enhancer divanillin: a review on sources and enzymatic generation*. Flavour and Fragrance Journal, 2015. **30**(5): p. 362-365.
153. Jeon, J.-R. and Y.-S. Chang, *Laccase-mediated oxidation of small organics: bifunctional roles for versatile applications*. Trends in Biotechnology, 2013. **31**(6): p. 335-341.
154. Kobayashi, S., H. Uyama, and S. Kimura, *Enzymatic polymerization*. Chemical Reviews, 2001. **101**(12): p. 3793-3818.
155. Mita, N., et al., *Laccase-catalyzed oxidative polymerization of phenols*. Macromolecular Bioscience, 2003. **3**(5): p. 253-257.
156. Riva, S., *Laccases: blue enzymes for green chemistry*. TRENDS in Biotechnology, 2006. **24**(5): p. 219-226.
157. Solomon, E.I., U.M. Sundaram, and T.E. Machonkin, *Multicopper oxidases and oxygenases*. Chemical reviews, 1996. **96**(7): p. 2563-2606.
158. Pickel, B., et al., *An enantiocomplementary dirigent protein for the enantioselective laccase-catalyzed oxidative coupling of phenols*. Angewandte Chemie International Edition, 2010. **49**(1): p. 202-204.
159. Llevot, A., et al., *Selective laccase-catalyzed dimerization of phenolic compounds derived from lignin: Towards original symmetrical bio-based (bis) aromatic monomers*. Journal of Molecular Catalysis B: Enzymatic, 2016. **125**: p. 34-41.
160. Mikolasch, A. and F. Schauer, *Fungal laccases as tools for the synthesis of new hybrid molecules and biomaterials*. Applied microbiology and biotechnology, 2009. **82**: p. 605-624.
161. Chiang, H.C. and S.Y. Li, *Studies on the photodimerization of isoeugenol*. Journal of the Chinese Chemical Society, 1978. **25**(3): p. 141-147.
162. Cousin, H. and H. Herissey, *Oxidation de l'Isoeugenol. Sur la Dehydrodiisoeugenol*. CR hebd. Séances Acad. Sci.(France), 1908. **147**: p. 247.
163. Sarkanen, K.V. and A.F. Wallis, *Oxidative dimerizations of (E)-and (Z)-isoeugenol (2-methoxy-4-propenylphenol) and (E)-and (Z)-2, 6-dimethoxy-4-propenylphenol*. Journal of the Chemical Society, Perkin Transactions 1, 1973: p. 1869-1878.
164. Wu, G., M. Heitz, and E. Chornet, *Improved alkaline oxidation process for the production of aldehydes (vanillin and syringaldehyde) from steam-explosion hardwood lignin*. Industrial & engineering chemistry research, 1994. **33**(3): p. 718-723.
165. Bunzel, M., et al., *Sinapate dehydrodimers and sinapate-ferulate heterodimers in cereal dietary fiber*. Journal of Agricultural and Food Chemistry, 2003. **51**(5): p. 1427-1434.
166. Neudörffer, A., et al., *4-Hydroxycinnamic ethyl ester derivatives and related dehydrodimers: relationship between oxidation potential and protective effects against oxidation of low-density lipoproteins*. Journal of agricultural and food chemistry, 2004. **52**(7): p. 2084-2091.
167. Kumar, B.S., et al., *Synthesis of neolignans as microtubule stabilisers*. Bioorganic & Medicinal Chemistry, 2014. **22**(4): p. 1342-1354.

168. Damasceno, N.A., et al., *Scleral wound healing with cross-link technique using riboflavin and ultraviolet A on rabbit eyes*. *Clinical Ophthalmology*, 2017: p. 1265-1272.
169. Kwok, S.J., et al., *Flexible optical waveguides for uniform periscleral cross-linking*. *Investigative ophthalmology & visual science*, 2017. **58**(5): p. 2596-2602.
170. Insińska-Rak, M. and M. Sikorski, *Riboflavin interactions with oxygen—a survey from the photochemical perspective*. *Chemistry—A European Journal*, 2014. **20**(47): p. 15280-15291.
171. Ghosh, S. and M. Puranik, *Deep ultraviolet initiated excited state dynamics of riboflavin and flavin mononucleotide*. *Journal of Raman Spectroscopy*, 2018. **49**(10): p. 1628-1644.
172. Kowalczyk, R.M., et al., *The photoinduced triplet of flavins and its protonation states*. *Journal of the American Chemical Society*, 2004. **126**(36): p. 11393-11399.
173. Zaborniak, I. and P. Chmielarz, *Riboflavin-mediated radical polymerization—Outlook for eco-friendly synthesis of functional materials*. *European Polymer Journal*, 2021. **142**: p. 110152.
174. Suwannasom, N., et al., *Riboflavin: The health benefits of a forgotten natural vitamin*. *International Journal of Molecular Sciences*, 2020. **21**(3): p. 950.
175. Cardoso, D.R., S.H. Libardi, and L.H. Skibsted, *Riboflavin as a photosensitizer. Effects on human health and food quality*. *Food & Function*, 2012. **3**(5): p. 487-502.
176. Heelis, P., *The photophysical and photochemical properties of flavins (isoalloxazines)*. *Chemical Society Reviews*, 1982. **11**(1): p. 15-39.
177. Pattison, D.I., A.S. Rahmanto, and M.J. Davies, *Photo-oxidation of proteins*. *Photochemical & Photobiological Sciences*, 2012. **11**(1): p. 38-53.
178. Silva, E. and F.H. Quina, *Photoinduced processes in the eye lens: Do flavins really play a role?* *Flavins-Photochemistry and Photobiology*, 2006: p. 131-149.
179. Şahbaz, F. and G. Somer, *Photosensitized decomposition of ascorbic acid in the presence of riboflavin*. *Food chemistry*, 1993. **46**(2): p. 177-182.
180. Strauss, G. and W.J. Nickerson, *Photochemical cleavage of water by riboflavin. II. Role of activators*. *Journal of the American Chemical Society*, 1961. **83**(15): p. 3187-3191.
181. Smith, E.C. and D.E. Metzler, *The photochemical degradation of riboflavin*. *Journal of the American Chemical Society*, 1963. **85**(20): p. 3285-3288.
182. Karrer, P. and H. Meerwein, *Further studies of the decomposition of flavins in light*. *Helvetica Chimica Acta*, 1935. **18**: p. 1126-1130.
183. Moore, W.M., et al., *Photochemistry of riboflavin. I. The hydrogen transfer process in the anaerobic photobleaching of flavins*. *Journal of the American Chemical Society*, 1963. **85**(21): p. 3367-3372.
184. Silva, E., et al., *Riboflavin-induced Type 1 photo-oxidation of tryptophan using a high intensity 365 nm light emitting diode*. *Free Radical Biology and Medicine*, 2019. **131**: p. 133-143.
185. Garlets, Z.J., J.D. Nguyen, and C.R. Stephenson, *The development of visible-light photoredox catalysis in flow*. *Israel journal of chemistry*, 2014. **54**(4): p. 351-360.
186. Schuster, E.M. and P. Wipf, *Photochemical flow reactions*. *Israel Journal of Chemistry*, 2014. **54**(4): p. 361-370.
187. Su, Y., et al., *Photochemical transformations accelerated in continuous-flow reactors: basic concepts and applications*. *Chemistry—A European Journal*, 2014. **20**(34): p. 10562-10589.
188. Abe, K., et al., *Functional Group-Directed Photochemical Reactions of Aromatic Alcohols, Amines, and Thiols Triggered by Excited-State Hydrogen Detachment: Additive-free Oligomerization, Disulfidation, and C (sp<sup>2</sup>)–H Carboxylation with CO<sub>2</sub>*. *The Journal of Organic Chemistry*, 2020. **86**(1): p. 959-969.
189. Li, F., et al., *Aqueous-phase oxidation of syringic acid emitted from biomass burning: Formation of light-absorbing compounds*. *Science of The Total Environment*, 2021. **765**: p. 144239.
190. Siano, G., S. Crespi, and S.M. Bonesi, *Direct Irradiation of Phenol and Para-Substituted Phenols with a Laser Pulse (266 nm) in Homogeneous and Micro-heterogeneous Media. A Time-Resolved Spectroscopy Study*. *The Journal of Organic Chemistry*, 2020. **85**(21): p. 14012-14025.
191. Kholdeeva, O.A. and O.V. Zalomaeva, *Recent advances in transition-metal-catalyzed selective oxidation of substituted phenols and methoxyarenes with environmentally benign oxidants*. *Coordination Chemistry Reviews*, 2016. **306**: p. 302-330.

192. Munk, L., et al., *Can laccases catalyze bond cleavage in lignin?* Biotechnology advances, 2015. **33**(1): p. 13-24.
193. Bent, D. and E. Hayon, *Excited state chemistry of aromatic amino acids and related peptides. III. Tryptophan.* Journal of the American Chemical Society, 1975. **97**(10): p. 2612-2619.
194. Lu, C., et al., *Photophysical and photochemical processes of riboflavin (vitamin B 2) by means of the transient absorption spectra in aqueous solution.* Science in China Series B: Chemistry, 2001. **44**: p. 39-48.
195. Moonen, M.J., et al., *Flavoenzyme-catalyzed oxygenations and oxidations of phenolic compounds.* Advanced Synthesis & Catalysis, 2002. **344**(10): p. 1023-1035.
196. Areskogh, D., et al., *Oxidative polymerisation of models for phenolic lignin end-groups by laccase.* 2010.
197. Crestini, C., L. Jurasek, and D.S. Argyropoulos, *On the mechanism of the laccase–mediator system in the oxidation of lignin.* Chemistry—A European Journal, 2003. **9**(21): p. 5371-5378.
198. Martău, G.A., L.-F. Călinoiu, and D.C. Vodnar, *Bio-vanillin: Towards a sustainable industrial production.* Trends in Food Science & Technology, 2021. **109**: p. 579-592.
199. Havkin-Frenkel, D. and F.C. Belanger, *Biotechnological production of vanillin.* Biotechnology in flavor production, 2008. **3**: p. 83-98.
200. Fache, M., B. Boutevin, and S. Caillol, *Vanillin production from lignin and its use as a renewable chemical.* ACS sustainable chemistry & engineering, 2016. **4**(1): p. 35-46.
201. Wang, Y., et al., *Production of vanillin from lignin: The relationship between  $\beta$ -O-4 linkages and vanillin yield.* Industrial Crops and Products, 2018. **116**: p. 116-121.
202. Banerjee, G. and P. Chattopadhyay, *Vanillin biotechnology: the perspectives and future.* Journal of the Science of Food and Agriculture, 2019. **99**(2): p. 499-506.
203. Nishimura, R.T., C.H. Giammanco, and D.A. Vosburg, *Green, enzymatic syntheses of divanillin and diapocynin for the organic, biochemistry, or advanced general chemistry laboratory.* Journal of Chemical Education, 2010. **87**(5): p. 526-527.
204. Delomenède, M., et al., *Development of novel antiatherogenic biaryls: Design, synthesis, and reactivity.* Journal of medicinal chemistry, 2008. **51**(11): p. 3171-3181.
205. Reiss, I., et al., *Use of divanillin as a flavouring agent.* 2006, Google Patents.
206. Kunkel, R., et al., *Electrochemical synthesis of biobased polymers and polymer building blocks from vanillin.* RSC advances, 2021. **11**(15): p. 8970-8985.
207. Amarasekara, A.S. and M.A. Hasan, *Vanillin based polymers: III. Electrochemical dimerization of vanillin revisited and synthesis of hydrovanilloin–formaldehyde polymer.* Polymer Science Series B, 2016. **58**(3): p. 307-312.
208. Amarasekara, A.S., B. Wiredu, and A. Razzaq, *Vanillin based polymers: I. An electrochemical route to polyvanillin.* Green Chemistry, 2012. **14**(9): p. 2395-2397.
209. Soni, N.R., *Improve GC separations with derivatization for selective response and detection in novel matrices.* Journal of Environment and Life Sciences, 2016. **1**(1): p. 14-25.
210. Savonnet, E., et al., *Divanillin-based epoxy precursors as DGEBA substitutes for biobased epoxy thermosets.* ACS Sustainable Chemistry & Engineering, 2018. **6**(8): p. 11008-11017.
211. Perez, H.L. and C.A. Evans, *Chemical derivatization in bioanalysis.* 2015, Future Science. p. 2435-2437.
212. Ciriminna, R., et al., *Vanillin: the case for greener production driven by sustainability megatrend.* ChemistryOpen, 2019. **8**(6): p. 660-667.
213. Ramachandra Rao, S. and G.A. Ravishankar, *Vanilla flavour: production by conventional and biotechnological routes.* Journal of the Science of Food and Agriculture, 2000. **80**(3): p. 289-304.
214. Wong, Z., K. Chen, and J. Li, *Formation of vanillin and syringaldehyde in an oxygen delignification process.* Bioresources, 2010. **5**(3): p. 1509-1516.
215. da Silva, E.B., et al., *An integrated process to produce vanillin and lignin-based polyurethanes from Kraft lignin.* chemical engineering research and design, 2009. **87**(9): p. 1276-1292.
216. Maeda, M., et al., *Vanillin production from native softwood lignin in the presence of tetrabutylammonium ion.* Journal of Wood Science, 2018. **64**(6): p. 810-815.
217. Almeida, A.R., et al., *Volatility and thermodynamic stability of vanillin.* The Journal of Chemical Thermodynamics, 2019. **128**: p. 45-54.

218. Alijani, S., et al., *Influence of carbon support properties in the hydrodeoxygenation of vanillin as lignin model compound*. Catalysis today, 2021. **367**: p. 220-227.
219. Achyuthan, K.E., et al., *Supramolecular self-assembled chaos: polyphenolic lignin's barrier to cost-effective lignocellulosic biofuels*. Molecules, 2010. **15**(12): p. 8641-8688.
220. Katahira, R., et al., *Synthesis of  $\beta$ -O-4 type oligomeric lignin model compound by the nucleophilic addition of carbanion to the aldehyde group*. Journal of wood science, 2006. **52**(3): p. 255-260.
221. Mukhtar, A., et al., *Synthesis of lignin model compound containing a  $\beta$ -O-4 linkage*. Zeitschrift für Naturforschung B, 2017. **72**(2): p. 119-124.
222. Chen, H., *Synthesis of  $\beta$ -O-4 linkage containing lignin model compound*. 2020.
223. Stanzione III, J.F., et al., *Vanillin-based resin for use in composite applications*. Green Chemistry, 2012. **14**(8): p. 2346-2352.
224. Harvey, B.G., et al., *Cyanate Ester Composite Resins Derived from Renewable Polyphenol Sources*. 2011, NAVAL AIR WARFARE CENTER WEAPONS DIV CHINA LAKE CA.
225. Kubotava, A., et al., *Electrospray Ionization with High-Resolution Mass Spectrometry as a Tool for Lignomics: Lignin Mass Spectrum Deconvolution*.
226. Yamamoto, H., T. Hoshino, and T. Uchiyama, *Convenient preparation and quantification of 5, 5'-diferulic acid*. Bioscience, biotechnology, and biochemistry, 1999. **63**(2): p. 390-394.
227. Tiemann, F., *Ueber eine charakteristische Reaction des Vanillins*. Berichte der deutschen chemischen Gesellschaft, 1885. **18**(2): p. 3493-3496.
228. Kelly, D.R., et al., *Studies of nitrile oxide cycloadditions, and the phenolic oxidative coupling of vanillin aldoxime by Geobacillus sp. DDS012 from Italian rye grass silage*. Organic & Biomolecular Chemistry, 2008. **6**(4): p. 787-796.
229. Elbs, K. and H. Lerch, *Über dehydrodivanillin*. Journal für Praktische Chemie, 1916. **93**(1): p. 1-9.
230. Potineni, R. and D. Peterson, *Influence of thermal processing conditions on flavor stability in fluid milk: benzaldehyde*. Journal of dairy science, 2005. **88**(1): p. 1-6.
231. Antoniotti, S., et al., *Structural diversity of peroxidase-catalyzed oxidation products of o-methoxyphenols*. Organic Letters, 2004. **6**(12): p. 1975-1978.
232. Topal, Y., et al., *Horseradish peroxidase-catalyzed polymerization of ortho-imino-phenol: Synthesis, characterization, thermal stability and electrochemical properties*. Journal of Saudi Chemical Society, 2017. **21**(6): p. 731-740.
233. Hollmann, F. and I.W. Arends, *Enzyme initiated radical polymerizations*. Polymers, 2012. **4**(1): p. 759-793.
234. Uyama, H., *Enzymatic polymerization*, in *Future Directions in Biocatalysis*. 2007, Elsevier. p. 205-251.
235. Zhang, C., S.A. Madbouly, and M.R. Kessler, *Renewable polymers prepared from vanillin and its derivatives*. Macromolecular Chemistry and Physics, 2015. **216**(17): p. 1816-1822.
236. Lee, N., Y.T. Kim, and J. Lee, *Recent advances in renewable polymer production from lignin-derived aldehydes*. Polymers, 2021. **13**(3): p. 364.
237. Mohammed, I.A. and R.M. Hamidi, *Synthesis of new liquid crystalline diglycidyl ethers*. Molecules, 2012. **17**(1): p. 645-656.
238. Nanayakkara, S., et al., *Immobilized horseradish peroxidase (I-HRP) as biocatalyst for oxidative polymerization of 2, 6-dimethylphenol*. ACS Sustainable Chemistry & Engineering, 2014. **2**(8): p. 1947-1950.
239. Scaldaferrri, C.A., et al., *CO cleavage of diphenyl ether followed by CC coupling reactions over hydrophobized Pd/HY catalysts*. Applied Catalysis B: Environmental, 2019. **259**: p. 118081.
240. Nikulin, M. and V. Švedas, *Prospects of using biocatalysis for the synthesis and modification of polymers*. Molecules, 2021. **26**(9): p. 2750.
241. Nayak, P.L., *Enzyme-catalyzed polymerization: an opportunity for innovation*. Designed Monomers and Polymers, 1998. **1**(3): p. 259-284.
242. Akita, M., et al., *Structural change and catalytic activity of horseradish peroxidase in oxidative polymerization of phenol*. Bioscience, biotechnology, and biochemistry, 2001. **65**(7): p. 1581-1588.
243. Amarasekara, A. and A. Razzaq, *ISRN Polymer Science 2012*. 2012. **1**.

244. Fache, M., B. Boutevin, and S. Caillol, *Vanillin, a key-intermediate of biobased polymers*. European polymer journal, 2015. **68**: p. 488-502.
245. Almagro, L., et al., *Class III peroxidases in plant defence reactions*. Journal of experimental botany, 2009. **60**(2): p. 377-390.
246. Baynton, K.J., et al., *Inactivation of horseradish peroxidase by phenol and hydrogen peroxide: a kinetic investigation*. Biochimica et Biophysica Acta (BBA)-Protein Structure and Molecular Enzymology, 1994. **1206**(2): p. 272-278.
247. Malomo, S.O., et al., *Suicide inactivation of horseradish peroxidase by excess hydrogen peroxide: The effects of reaction pH, buffer ion concentration, and redox mediation*. Biokemistri, 2011. **23**(3).
248. Kim, H.S., et al., *Inactivation of Coprinus cinereus peroxidase during the oxidation of various phenolic compounds originated from lignin*. Enzyme and microbial technology, 2009. **45**(2): p. 150-155.
249. Huang, Q., et al., *Inactivation of horseradish peroxidase by phenoxyl radical attack*. Journal of the American Chemical Society, 2005. **127**(5): p. 1431-1437.
250. Gustafsson, M., et al.,  *$\beta$ -Fluoro-coniferyl alcohol does not inhibit lignin biosynthesis in suspension cultures of Picea abies (L.) Karst*. Phytochemistry, 2001. **58**(2): p. 243-248.
251. Poulos, T.L., *The stereochemistry of peroxidase catalysis*. 1980.
252. Derat, E. and S. Shaik, *The Poulos– Kraut mechanism of compound i formation in horseradish peroxidase: A QM/MM Study*. The Journal of Physical Chemistry B, 2006. **110**(21): p. 10526-10533.
253. Rodríguez-López, J.N., et al., *Mechanism of reaction of hydrogen peroxide with horseradish peroxidase: identification of intermediates in the catalytic cycle*. Journal of the American Chemical Society, 2001. **123**(48): p. 11838-11847.
254. Veitch, N.C., *Horseradish peroxidase: a modern view of a classic enzyme*. Phytochemistry, 2004. **65**(3): p. 249-259.
255. Guzik, U., K. Hupert-Kocurek, and D. Wojcieszńska, *Immobilization as a strategy for improving enzyme properties-application to oxidoreductases*. Molecules, 2014. **19**(7): p. 8995-9018.
256. Dunford, H. and J. Stillman, *On the function and mechanism of action of peroxidases*. Coordination chemistry reviews, 1976. **19**(3): p. 187-251.
257. Ibrahim, M., et al. *Optimization of the removal of phenol from wastewater catalyzed by Arthromyces ramosus peroxidase*. in *PROCEEDINGS OF THE CSCE ASCE ENVIRONMENTAL ENGINEERING CONFERENCE*. 1997. CANADIAN SOCIETY FOR CIVIL ENGINEERING.
258. Arnao, M., et al., *A kinetic study on the suicide inactivation of peroxidase by hydrogen peroxide*. Biochimica et Biophysica Acta (BBA)-Protein Structure and Molecular Enzymology, 1990. **1041**(1): p. 43-47.
259. Nazari, K., et al., *Suicide-peroxide inactivation of horseradish peroxidase in the presence of sodium n-dodecyl sulphate: a study of the enzyme deactivation kinetics*. Journal of Enzyme Inhibition and Medicinal Chemistry, 2005. **20**(3): p. 285-292.
260. Higashimoto, Y., et al., *The reactions of heme-and verdoheme-heme oxygenase-1 complexes with FMN-depleted NADPH-cytochrome P450 reductase: electrons required for verdoheme oxidation can be transferred through a pathway not involving FMN*. Journal of Biological Chemistry, 2006. **281**(42): p. 31659-31667.
261. Nwe, K. and M.W. Brechbiel, *Growing applications of “click chemistry” for bioconjugation in contemporary biomedical research*. Cancer Biotherapy and Radiopharmaceuticals, 2009. **24**(3): p. 289-302.
262. Wu, J.C.Y., et al., *Enhanced enzyme stability through site-directed covalent immobilization*. Journal of biotechnology, 2015. **193**: p. 83-90.
263. Rostovtsev, V.V., et al., *A stepwise Huisgen cycloaddition process: copper (I)-catalyzed regioselective “ligation” of azides and terminal alkynes*. Angewandte Chemie, 2002. **114**(14): p. 2708-2711.

264. Tornøe, C.W., C. Christensen, and M. Meldal, *Peptidotriazoles on solid phase:[1, 2, 3]-triazoles by regioselective copper (I)-catalyzed 1, 3-dipolar cycloadditions of terminal alkynes to azides*. The Journal of organic chemistry, 2002. **67**(9): p. 3057-3064.
265. Bock, V.D., H. Hiemstra, and J.H. Van Maarseveen, *CuI-catalyzed alkyne-azide "click" cycloadditions from a mechanistic and synthetic perspective*. European Journal of Organic Chemistry, 2006. **2006**(1): p. 51-68.
266. Presolski, S.I., V.P. Hong, and M. Finn, *Copper-catalyzed azide-alkyne click chemistry for bioconjugation*. Current protocols in chemical biology, 2011. **3**(4): p. 153-162.
267. Jiang, X., et al., *Recent applications of click chemistry in drug discovery*. Expert opinion on drug discovery, 2019. **14**(8): p. 779-789.
268. Best, M.D., *Click chemistry and bioorthogonal reactions: unprecedented selectivity in the labeling of biological molecules*. Biochemistry, 2009. **48**(28): p. 6571-6584.
269. Erde, J., R.R.O. Loo, and J.A. Loo, *Enhanced FASP (eFASP) to increase proteome coverage and sample recovery for quantitative proteomic experiments*. Journal of proteome research, 2014. **13**(4): p. 1885-1895.
270. Nakashima, S., et al., *A novel tag-free probe for targeting molecules interacting with a flavonoid catabolite*. Biochemistry and Biophysics Reports, 2016. **7**: p. 240-245.
271. Obaro-Best, O., et al., *Bismuth trichloride-mediated cleavage of phenolic methoxymethyl ethers*. Synthetic Communications, 2016. **46**(7): p. 586-593.
272. Eddarir, S., Z. Abdelhadi, and C. Rolando, *Fluorinated resveratrol and pterostilbene*. Tetrahedron Letters, 2001. **42**(52): p. 9127-9130.
273. Zhou, Y., et al., *Expanding APEX2 substrates for proximity-dependent labeling of nucleic acids and proteins in living cells*. Angewandte Chemie, 2019. **131**(34): p. 11889-11893.
274. Maza, J.C., et al., *Utilization of alkyne bioconjugations to modulate protein function*. Bioorganic & medicinal chemistry letters, 2017. **27**(1): p. 30-33.
275. Kiick, K.L., et al., *Incorporation of azides into recombinant proteins for chemoselective modification by the Staudinger ligation*. Proceedings of the National academy of Sciences, 2002. **99**(1): p. 19-24.
276. van Hest, J.C., K.L. Kiick, and D.A. Tirrell, *Efficient incorporation of unsaturated methionine analogues into proteins in vivo*. Journal of the American Chemical Society, 2000. **122**(7): p. 1282-1288.
277. Agard, N.J., et al., *A comparative study of bioorthogonal reactions with azides*. ACS chemical biology, 2006. **1**(10): p. 644-648.
278. Beatty, K.E., et al., *Fluorescence visualization of newly synthesized proteins in mammalian cells*. Angewandte Chemie, 2006. **118**(44): p. 7524-7527.
279. Dieterich, D.C., et al., *Selective identification of newly synthesized proteins in mammalian cells using bioorthogonal noncanonical amino acid tagging (BONCAT)*. Proceedings of the National Academy of Sciences, 2006. **103**(25): p. 9482-9487.
280. Hernandez-Ruiz, J., et al., *Catalase-like activity of horseradish peroxidase: relationship to enzyme inactivation by H<sub>2</sub>O<sub>2</sub>*. Biochemical Journal, 2001. **354**(1): p. 107-114.
281. Galende, P.P., et al., *Mechanism-based suicide inactivation of white Spanish broom (Cytisus multiflorus) peroxidase by excess hydrogen peroxide*. International journal of biological macromolecules, 2015. **81**: p. 975-979.
282. Tudela, J., et al., *Kinetic study in the transient phase of the suicide inactivation of frog epidermis tyrosinase*. Biophysical chemistry, 1988. **30**(3): p. 303-310.
283. Lopes, G.R., D.C. Pinto, and A.M. Silva, *Horseradish peroxidase (HRP) as a tool in green chemistry*. Rsc Advances, 2014. **4**(70): p. 37244-37265.
284. Maeda, Y., M. Fujihara, and I. Ikeda, *Spectroscopic study on structure of horseradish peroxidase in water and dimethyl sulfoxide mixture*. Biopolymers: Original Research on Biomolecules, 2002. **67**(2): p. 107-112.
285. Azevedo, A.M., et al., *Stability of free and immobilised peroxidase in aqueous-organic solvents mixtures*. Journal of Molecular Catalysis B: Enzymatic, 2001. **15**(4-6): p. 147-153.
286. Laurenti, E., et al., *Oxidation of 2, 4-dichlorophenol catalyzed by horseradish peroxidase: characterization of the reaction mechanism by UV-visible spectroscopy and mass spectrometry*. Journal of Inorganic Biochemistry, 2003. **95**(2-3): p. 171-176.

287. Monteiro, B., *Skin Cancer Recognition in Primary Care*. 2022.
288. Fiorino, S., et al., *SARS-CoV-2: lessons from both the history of medicine and from the biological behavior of other well-known viruses*. *Future Microbiology*, 2021. **16**(14): p. 1105-1133.
289. Seltsam, A. and T.H. Müller, *UVC irradiation for pathogen reduction of platelet concentrates and plasma*. *Transfusion medicine and hemotherapy*, 2011. **38**(1): p. 43-54.
290. Kuhn, H., S. Braslavsky, and R. Schmidt, *Chemical actinometry (IUPAC technical report)*. *Pure and Applied Chemistry*, 2004. **76**(12): p. 2105-2146.
291. Leighton, W.G. and G.S. Forbes, *Precision actinometry with uranyl oxalate*. *Journal of the American Chemical Society*, 1930. **52**(8): p. 3139-3152.
292. Volman, D. and J. Seed, *The photochemistry of uranyl oxalate*. *Journal of the American Chemical Society*, 1964. **86**(23): p. 5095-5098.
293. Hatchard, C. and C.A. Parker, *A new sensitive chemical actinometer-II. Potassium ferrioxalate as a standard chemical actinometer*. *Proceedings of the Royal Society of London. Series A. Mathematical and Physical Sciences*, 1956. **235**(1203): p. 518-536.
294. Lee, J. and H. Seliger, *Quantum yield of the ferrioxalate actinometer*. *The Journal of Chemical Physics*, 1964. **40**(2): p. 519-523.
295. Wegner, E.E. and A.W. Adamson, *Photochemistry of complex ions. III. Absolute quantum yields for the photolysis of some aqueous chromium (III) complexes. Chemical actinometry in the long wavelength visible region*. *Journal of the American Chemical Society*, 1966. **88**(3): p. 394-404.
296. Szychliński, J., et al., *Complementary study on the use of the potassium Reinecke's salt as a chemical actinometer*. *Analyst*, 1989. **114**(6): p. 739-741.
297. Montalti, M., et al., *Handbook of photochemistry*. 2006: CRC press.
298. Rau, H., *Spectroscopic properties of organic azo compounds*. *Angewandte Chemie International Edition in English*, 1973. **12**(3): p. 224-235.
299. Hartley, G.S., *The cis-form of azobenzene*. *Nature*, 1937. **140**(3537): p. 281-281.
300. El Achi, N., et al., *Rapid and facile chemical actinometric protocol for photo-microfluidic systems using azobenzene and NMR spectroscopy*. *RSC advances*, 2017. **7**(47): p. 29815-29820.
301. Roseau, M., et al., *Azobenzene: a Visible-Light Chemical Actinometer for the Characterization of Fluidic Photosystems*. *Helvetica Chimica Acta*, 2021. **104**(7): p. e2100071.
302. Zimmerman, G., L.-Y. Chow, and U.-J. Paik, *The photochemical isomerization of azobenzene I*. *Journal of the American Chemical Society*, 1958. **80**(14): p. 3528-3531.
303. Ahmed, Z., et al., *Controlling azobenzene photoswitching through combined ortho-fluorination and-amination*. *Chemical communications*, 2017. **53**(93): p. 12520-12523.
304. Brown, C., et al., *Differential azobenzene solubility increases equilibrium cis/trans ratio in water*. *Journal of Photochemistry and Photobiology A: Chemistry*, 2017. **336**: p. 140-145.
305. Hessel, V., H. Löwe, and S. Hardt, *Chemical micro process engineering: fundamentals, modelling and reactions*. Vol. 1. 2004: John Wiley & Sons.
306. Jähnisch, K., et al., *Chemistry in microstructured reactors*. *Angewandte Chemie International Edition*, 2004. **43**(4): p. 406-446.
307. de Souza, G.F., T.W. von Zuben, and A.G. Salles Jr, *A metal-catalyst-free oxidative coupling of anilines to aromatic azo compounds in water using bleach*. *Tetrahedron Letters*, 2018. **59**(42): p. 3753-3755.
308. Li, L., et al., *Smart azobenzene-containing tubular polymersomes: fabrication and multiple morphological tuning*. *Chemical Communications*, 2020. **56**(46): p. 6237-6240.
309. Dulin, D. and T. Mill, *Development and evaluation of sunlight actinometers*. *Environmental Science & Technology*, 1982. **16**(11): p. 815-820.
310. Laszakovits, J.R., et al., *p-Nitroanisole/pyridine and p-nitroacetophenone/pyridine actinometers revisited: Quantum yield in comparison to ferrioxalate*. *Environmental Science & Technology Letters*, 2017. **4**(1): p. 11-14.
311. Małkosza, M., *Reactions of nucleophiles with nitroarenes: multifacial and versatile electrophiles*. *Chemistry—A European Journal*, 2014. **20**(19): p. 5536-5545.